

University of Southampton Research Repository

Copyright © and Moral Rights for this thesis and, where applicable, any accompanying data are retained by the author and/or other copyright owners. A copy can be downloaded for personal non-commercial research or study, without prior permission or charge. This thesis and the accompanying data cannot be reproduced or quoted extensively from without first obtaining permission in writing from the copyright holder/s. The content of the thesis and accompanying research data (where applicable) must not be changed in any way or sold commercially in any format or medium without the formal permission of the copyright holder/s.

When referring to this thesis and any accompanying data, full bibliographic details must be given, e.g.

Thesis: Author (Year of Submission) "Full thesis title", University of Southampton, name of the University Faculty or School or Department, PhD Thesis, pagination.

Data: Author (Year) Title. URI [dataset]

University of Southampton

Faculty of Environmental and Life Sciences

School of Ocean and Earth Science

**Analysis of Expedited Chromatographic Separation Systems for Application to the
Decommissioning of Nuclear Facilities**

By

Alexander James Hately

ORCID ID: 0000-0003-4601-3168

Thesis for the degree of Doctor of Philosophy

December 2021

University of Southampton

Abstract

Faculty of Environmental and Life Sciences

Ocean and Earth Sciences

Doctor of Philosophy

Analysis of Expedited Chromatographic Separation Systems for Application to the
Decommissioning of Nuclear Facilities

By Alexander James Hately

To decrease cost and time for nuclear decommissioning, a move towards automation in the waste characterisation process has been the subject of increasing study in recent years. This thesis utilised an Automated Sequential Radionuclide Separator (ASRS) to investigate the effects of expediting the separation and purification of Sr, Pu, Th and U from concrete matrices. This benchtop separation system consists of 8 chromatographic columns with forced flow of solutions through the columns being achieved using peristaltic pumps.

Sr separation was found to be largely unaffected by increasing the flowrates up to those capable by the separator, and chemical recoveries of over 90 % were achieved. Pu, Th and U separation using three chromatographic materials demonstrated practically how different active site bonding method to the polymer support can affect uptake kinetics. The active site coated resin TEVA resin achieved equilibrium within 1 hour whereas Anion Exchange resin (that has the active site forming part of the polymer) took 2.5 hours.

A sample analysis method incorporating expedited chromatographic separation was tested using a simulated concrete digest. Purified fractions of U, Th, Pu and Sr were produced at elevated flow rates using a Sr-spec column as well as a series of TEVA and UTEVA columns. Chemical yields were found to be adequate and fully corrected measurements were accurate and precise. Separation times for the 4 analytes were significantly reduced, from over 2 hours 40 minutes to 25 minutes.

This thesis has proven the application of an expedited chromatographic separation system to the analysis of concrete samples for common radionuclides measured at nuclear facilities. The time savings, versatility, automation, and ability to be incorporated into fully shielded procedures make it an attractive prospect for both decommissioning organisations and multi-purpose laboratories.

Table of Contents

Table of Contents	i
List of Tables.....	v
List of Figures	vii
List of Equations	xi
Research Thesis: Declaration of Authorship	xiii
Acknowledgements	xv
Definitions and Abbreviations.....	xvii
Chapter 1 Introduction.....	1
1.1 Research context.....	1
1.2 Radionuclide origin and nature.....	3
1.3 Rationale and objectives	6
1.4 Quantification of column performance	10
1.4.1 Kinetic control on separation	13
Chapter 2 Expediting radionuclide separation and analysis.....	17
2.1 Introduction.....	17
2.2 Vacuum boxes	17
2.3 Pressurised injection	18
2.4 Flow injection analysis.....	19
2.5 Automated radionuclide separators	21
Chapter 3 Materials and instrumentation.....	27
3.1 Chromatographic materials.....	27
3.1.1 Strontium separation	27
3.1.1.1 Sr-Spec Resin	27
3.1.1.2 TK100.....	33
3.1.1.3 Cost effective Sr separation techniques.....	34
3.1.2 Separation of actinides.....	35
3.1.2.1 Anion exchange resin	35
3.1.2.2 TEVA resin.....	38

Table of Contents

3.1.2.3 UTEVA resin.....	40
3.2 Decay counting techniques.....	46
3.2.1 Liquid scintillation	46
3.2.2 Alpha Spectrometry	48
3.2.3 Gamma Spectrometry.....	53
3.3 ICP-QQQ-MS.....	55
3.3.1 Sample preparation for ICP-MS analysis.....	59
Chapter 4 Separation of Strontium-90 from cementitious matrices via extraction chromatography at higher flow rates	65
4.1 Introduction	65
4.1.1 Expediting strontium separation	66
4.1.2 Investigation into wider geochemical application.....	68
4.1.3 Experimental constraints	71
4.2 Experimental	73
4.2.1 Instrumentation	73
4.2.2 Reagents.....	73
4.2.3 Separation procedure	74
4.3 Method development.....	76
4.3.1 Concrete digestion	76
4.3.2 Batch uptake experiments.....	76
4.3.3 Repeatability	77
4.3.4 Effect of matrix	77
4.3.5 Flow rate effect on HETP	78
4.3.6 Effect of flow rate on Sr recovery	78
4.3.7 Effect of flow rate on decontamination	78
4.3.8 Column Reuse	79
4.3.9 Overall analytical performance.....	80
4.3.10 Sr isotope fractionation	83
4.4 Results and discussion	83
4.4.1 Batch Uptake.....	83

4.4.2 Repeatability	84
4.4.3 Effect of matrix.....	85
4.4.4 Flow rate effect on HETP.....	86
4.4.5 Effect of flow rate on Sr recovery in eluate fraction.....	87
4.4.6 Effect of flow rate on decontamination.....	89
4.4.7 Column reuse	93
4.4.8 Analytical performance of simulated sample	95
4.4.9 Sr isotope fractionation.....	96
4.5 Conclusions.....	98
Chapter 5 Kinetic control on uptake of major actinides and thorium on chromatographic materials	101
5.1 Introduction.....	101
5.2 Materials and Methodology.....	105
5.2.1 Instrumentation	105
5.2.2 Materials and reagents	105
5.2.3 Batch uptake of plutonium on anion exchange resin	106
5.2.4 Batch uptake of uranium and thorium on UTEVA, TEVA and anion exchange resin.....	107
5.2.5 HETP tests.....	107
5.2.6 Multi element tests	108
5.3 Results and discussion.....	109
5.3.1 Batch uptake experiments	109
5.3.2 HETP	115
5.3.3 Multi-element tests.....	119
5.4 Conclusions.....	121
Chapter 6 Development of a method for the rapid determination of multiple radionuclides from a single sample.....	123
6.1 Introduction.....	123
6.2 Materials and equipment.....	130
6.3 Method.....	131

Table of Contents

6.3.1 Radionuclide spiking	131
6.3.2 Composition of concrete sample	133
6.3.3 Chromatographic separation.....	136
6.3.4 Preparation for analysis	139
6.3.5 Analysis	139
6.4 Results and discussion	140
6.4.1 Uranium fractions	142
6.4.2 Thorium fractions.....	147
6.4.3 Plutonium fractions	151
6.4.4 Strontium fractions	153
6.5 Conclusions	155
Chapter 7 Conclusions and future work.....	157
Appendix A Determination of counting uncertainty	163
Combining uncertainties	163
Appendix B Zeta-score calculation	165
Appendix C ASRS configuration and control.....	167
List of References	169

List of Tables

Table 2.1. Table of expedited separation systems	26
Table 3.1. Summary table of chromatographic materials	45
Table 3.2. Common isobaric and polyatomic interferences	57
Table 4.1. Concentrations of bulk concrete trace element concentration	82
Table 4.2. Concentration of trace elements in samples	82
Table 4.3. Decontamination factors at 3 different flow rates	92
Table 4.4. Reuse decontamination factors with 3 uses of the column	94
Table 4.5. ^{85}Sr yield data	95
Table 4.6. Fully corrected ^{90}Sr measurement from simulated concrete separation	95
Table 4.7. Average $^{87}\text{Sr}/^{86}\text{Sr}$ values achieved from isocratic elution of Sr.....	98
Table 5.1. Th adsorption kinetics	113
Table 5.2. Pu adsorption kinetics on anion exchange resin.....	114
Table 5.3. U adsorption kinetics.....	114
Table 5.4. Retention and peak width of Th on anion exchange resin	119
Table 5.5. Retention and peak width of U on anion exchange resin.....	119
Table 6.1. Overview of digestion methods from Croudace et al., (2016).....	129
Table 6.2. Radionuclides added to concrete samples	133
Table 6.3. Major elemental composition of concrete sample used	134
Table 6.4. Uncorrected target radionuclide recoveries for concrete tests	140
Table 6.5. Accuracy and precision measurements for multiple separation technique	141
Table 6.6. ^{210}Po decontamination factors in uranium fractions	146

List of Tables

Table 6.7. Thorium spike alpha peak identification	150
Table 6.8. ^{238}U decontamination in thorium fractions	150
Table 6.9. ^{210}Po decontamination in thorium fractions	151
Table 6.10. ^{241}Am decontamination in plutonium fractions	152

List of Figures

Figure 1.1. Karlsruhe Chart of the Nuclides	4
Figure 1.2. Fission product chain yield curve for fissile U and Pu isotopes	5
Figure 1.3. Example of radionuclide production in a reactor (LWRs or AGRs)	6
Figure 1.4. Elution profile for isocratic elution of analyte	11
Figure 1.5. van Deemter Plot	12
Figure 1.6. Graph showing the two components of resistance to mass transfer.....	13
Figure 1.7. The relationship between K_d , HETP and elution profile	14
Figure 2.1. Pressurised injection schematic.....	18
Figure 2.2. Flow injection analysis schematic.....	21
Figure 2.3. Automated radionuclide separator schematic	24
Figure 3.1. Sr resin chemical structure	28
Figure 3.2. Sr resin acid dependency graphs	30
Figure 3.3. Polystyrene DVB structure	36
Figure 3.4. Anion exchange resin quaternary amines	37
Figure 3.5. Aliquat® 336 structure	38
Figure 3.6. TEVA resin acid dependency graphs	40
Figure 3.7. DAAP structure.....	41
Figure 3.8. UTEVA acid dependency graphs	43
Figure 3.9. Liquid scintillation counter schematic	48
Figure 3.10. Electron energy bands	49
Figure 3.11. Semiconductor diagram.....	51

List of Figures

Figure 3.12. Theoretical gamma spectrum.....	54
Figure 3.13. DDEM detector	59
Figure 3.14. ICP-MS calibration curve	60
Figure 4.1. Rb/Sr isochron	70
Figure 4.2. Flow chart of Sr separation on a Sr column	75
Figure 4.3. Sr uptake by Sr resin with time for batch uptake experiments.....	84
Figure 4.4. Sr repeat test elution profiles.....	85
Figure 4.5. Sr elution profiles with varying matrix mass	86
Figure 4.6. Isocratic elution of Sr from Sr column	87
Figure 4.7. Sr elution profiles at variable flow rates	88
Figure 4.8. Sr recovery versus flow rate	89
Figure 4.9. Profiles of contaminant washout and Sr elution at 5.1 mL/min	90
Figure 4.10. Cs washout profiles at 0.8, 2.5 and 5.1 mL/min.....	91
Figure 4.11. U washout profiles for 0.8, 2.5 and 5.1 mL/min.....	91
Figure 4.12. Sr elution profiles for the reuse of the same column at 5.1 mL/min.....	93
Figure 4.13. Variation of Sr isotope ratio with elution volume.....	97
Figure 5.1. Uptake curves for three different chromatographic materials.....	110
Figure 5.2. Isocratic elution of Th from anion exchange and TEVA resin.....	117
Figure 5.3. Isocratic elution of U from anion exchange and TEVA resin	118
Figure 5.4. HETP of U and Th on anion exchange and TEVA resin with increasing flow rates	118
Figure 5.5. Multi element elution on three different materials.....	120
Figure 6.1. Sample preparation flow chart.....	136

Figure 6.2. TEVA and UTEVA column separation system.....	138
Figure 6.3. Sr separation system.....	139
Figure 6.4. Alpha spectrum of uranium spike	144
Figure 6.5. Alpha spectrum of uranium fraction.....	144
Figure 6.6. Alpha spectrum of uranium from unspiked concrete.....	145
Figure 6.7. Alpha spectrum of thorium spike	148
Figure 6.8. Alpha spectrum of thorium fraction	148
Figure 6.9. ^{238}U decay chain	149
Figure 6.10. ^{232}Th decay chain.....	149
Figure 6.11. Alpha spectrum of plutonium fraction	152
Figure 6.12. ^{90}Y ingrowth to secular equilibrium for Test 1.....	154
Figure 7.1 Sample analysis schematic.....	159

List of Equations

Equation 1.1. Plate number equation	10
Equation 1.2. Chromatographic plate equation	10
Equation 1.3. van Deemter equation	11
Equation 1.4. Equation for distribution ratio	13
Equation 3.1. Equation for the uptake of U by DAAP	42
Equation 3.2. Uranium-238 hydride correction	62
Equation 4.1. Equation for ^{87}Sr ingrowth from ^{87}Rb	69
Equation 4.2. Decay constant equation	69
Equation 4.3. Equation for Rb/Sr isochron	70
Equation 4.4. Calculation of time from the gradient of the isochron	70
Equation 4.5. Decontamination factor equation	79
Equation 4.6. Limit of detection equations	96
Equation 5.1. Pseudo-first-order equation	111
Equation 5.2. Linear form of pseudo-first-order equation	112
Equation 5.3. Pseudo-second-order equation	112
Equation 5.4. Linear form of pseudo-second-order equation	112
Equation 6.1. Secular equilibrium equation	153

Research Thesis: Declaration of Authorship

Print name:

ALEXANDER HATELY

Title of thesis:

Analysis of Expedited Chromatographic Separation Systems for Application to the Decommissioning of Nuclear Facilities

I declare that this thesis and the work presented in it are my own and has been generated by me as the result of my own original research.

I confirm that:

1. This work was done wholly or mainly while in candidature for a research degree at this University;
2. Where any part of this thesis has previously been submitted for a degree or any other qualification at this University or any other institution, this has been clearly stated;
3. Where I have consulted the published work of others, this is always clearly attributed;
4. Where I have quoted from the work of others, the source is always given. With the exception of such quotations, this thesis is entirely my own work;
5. I have acknowledged all main sources of help;
6. Where the thesis is based on work done by myself jointly with others, I have made clear exactly what was done by others and what I have contributed myself;
7. None of this work has been published before submission

Signature:

Date: 20/12/2021

Acknowledgements

Firstly, I would like to thank my supervisors Phil Warwick and Ian Croudace for giving me the opportunity to complete this PhD studentship. I am very grateful for all the support, guidance and patience that has helped me to produce this thesis. I have grown in confidence due to their encouragement and greatly appreciate their expert advice during the more challenging aspects of the research.

I would like to thank everybody from the GAU. Their help, knowledge and advice during my lab work was invaluable. The GAU team made me feel welcome from the start and they have never made me feel an imposition, even though I know there are times when I must have been one. They have helped me develop my experimental design, aided in the analysis of my samples, and expanded my knowledge of the subject area. I would also like to thank Andy Milton, Mark James, Zilvinas Zacharauskas and Ben Russell for their help with regards to the ICP-MS analysis.

I am grateful for my friends and their support over the past 4 years. The world is a very different place compared to when I started my studentship, and their humour and positivity has helped me maintain perspective throughout challenging times.

Finally, I would like to thank my family and Ingrid for their constant, unwavering support during my PhD. They have never failed to make me feel encouraged and loved. Thank you to Dad for assistance in proofreading and to both my parents for the advice and help, especially during this last year. Thank you to Ingrid, for your patience and for always being able to lift my spirits. My family have facilitated my growth as scientist but also as a person, and for that I will be forever grateful.

Definitions and Abbreviations

AGR	Advanced Gas-cooled Reactor
ASRS	Automated Sequential Radionuclide Separator
Bq	Becquerel, a measurement of radioactivity equivalent to one disintegration per second
CPS	Counts per second
DAAP	Diamyl amylophosphonate
DF	Decontamination Factor
DTM	Difficult-to-measure (radionuclide)
DVB	Divinylbenzene
ETM	Easy-to-measure (radionuclide)
FCV	Free Column Volume to peak elution
HETP	Height Equivalent to a Theoretical Plate
HLW	High Level Waste
IAEA	International Atomic Energy Agency
ICP	Inductively Coupled Plasma
ICP-MS	Inductively Coupled Plasma – Mass Spectrometry
i.d.	Internal Diameter
ILW	Intermediate Level Waste
ICP-QQQ-MS	Inductively Coupled Plasma Triple Quadrupole Mass spectrometry
K'	Distribution ratio
K_d	Distribution coefficient at equilibrium
LLW	Low Level Waste
LOD	Limit of Detection

Definitions and Abbreviations

LSC	Liquid Scintillation Counting
LWR	Light Water Reactor
MAPEP	Mixed-Analyte Performance Evaluation Program
MARS	Modular Automated Radionuclide Separator
MC-ICP-MS	Multiple Collector – Inductively Coupled Plasma – Mass Spectrometry
MQ	Milli-q water, deionised, ultrapure water produced by Millipore water purification systems
NDA	Nuclear Decommissioning Authority (UK body)
NORM	Naturally Occurring Radioactive Material
ONR	Office for Nuclear Regulation
PFO	Pseudo-first-order
PSO	Pseudo-second-order
PUREX	Plutonium Uranium Reduction Extraction
RF	Radio Frequency
SF	Scaling Factor, also known as a waste fingerprint
TEVA	Tetravalent Actinide extraction chromatographic resin
TIMS	Thermal Ionization Mass Spectrometry
UTEVA	Uranium and Tetravalent Actinide extraction chromatographic resin
VLLW	Very Low Level Waste
WDXRF	Wavelength Dispersive X-ray Fluorescence
XRF	X-ray Fluorescence

Chapter 1 Introduction

1.1 Research context

In recent years, research into rapid and automated radionuclide separation has been focussed on assessing the extent of radionuclide contamination in the wake of a nuclear incident (Habibi et al., 2017; Kim et al., 2015; Maxwell et al., 2017; Sadi et al., 2018). Although these rapid techniques are extremely useful in the event of a major radioactive release, the major incidents for which these systems are designed are relatively rare with only one event rated 7 on the International Nuclear Event Scale (INES) occurring in the last 10 years (Fukushima Daiichi in 2011) (Wheatley et al., 2017). This means that for the majority of the time these techniques are applied only occasionally when they could, foreseeably, be utilised more regularly in environmental studies and potentially beyond. One major potential setting could be the nuclear decommissioning sector.

Decommissioning of nuclear reactor sites is an expensive task, with timescales spanning from decades to over a century at individual sites (European Commission, 2018; Nuclear Decommissioning Authority, 2017). European nuclear operators estimate that over the next 30 years, EUR 120 billion will be required for decommissioning activities (European Commission, 2018). Worldwide, there are 449 operational nuclear reactors, 54 reactors under construction and 176 reactors that have been permanently shut down (IAEA PRIS, 2019). Of the 176 permanently shut-down reactors, fewer than 10 have been fully decommissioned. In addition, countries may have plans to shut down a significant proportion of their operational reactors in the near future (Nuclear Decommissioning Authority, 2016). At the time of writing, nuclear power plants comprise a significant proportion of the UK grid's power supply (16.1% in 2020) (Martin, 2021). Presently, there are 13 nuclear power reactors in the UK (operated and owned by EDF Energy), which are all expected to be shut down by 2035 (EDF Energy, 2017; Nuclear Decommissioning Authority, 2016; Roberts, 2017). The Nuclear Decommissioning Authority (NDA) is currently responsible for overseeing the decommissioning of 17 historic nuclear sites across the UK (Nuclear Decommissioning Authority, 2016). The operations undertaken by the NDA require significant funding. In the 2020/21 financial year the NDA's expenditure was £3.059bn. Under a third of this (£0.612bn) was funded from income generated by the

Chapter 1

NDA's commercial operations, with the majority of NDA funding (£2.447bn) coming from the UK Government (Nuclear Decommissioning Authority, 2021). The UK Government, therefore, pays close attention to the NDA's expenditure in order to prevent unnecessary costs being incurred to the taxpayer. Cost-effective and efficient techniques are required to fulfil the NDA's requirements. The time-scales for clean-up after the reactor's shutdown are also important in cost consideration. The longer it takes to clean the sites, generally, the higher the cost incurred. According to the NDA, the 17 historic nuclear sites within its estates will require decommissioning activities for a period of over 100 years, with final site clearance of Sellafield and Capenhurst estimated to finish in 2120 (Nuclear Decommissioning Authority, 2017). In 2017 the budget requirement forecast for this clean-up was around £119bn, however, due to the uncertainty of forecasts the NDA acknowledges that the figure could range between £97bn and £222bn (Nuclear Decommissioning Authority, 2017). The cost and time implications faced by the NDA in the UK are comparable to the issues faced at nuclear facilities globally.

Waste characterisation is one of the first steps in the decommissioning of a nuclear facility. Over the lifetime of a nuclear reactor, radioactive contamination of building materials and equipment will occur. In addition to this, a small number of sites have experienced nuclear incidents which rank on the INES, which further complicate the decommissioning process (IAEA, 2001; Webb et al., 2006). Waste disposal and remediation techniques are chosen based upon the activity and the elemental composition. The highest activity waste, comprising 95% of the radioactive content in a nuclear facility, is taken for cooling and requires special shielding during transport and handling (Ewing et al., 1995). Intermediate level wastes (ILW) require shielding but not cooling and comprise 4% of the radioactive content (IAEA, 2011). Low-level wastes (LLW) are the least active, but the largest in volume. Waste repositories for LLW are generally less contained than for HLW and as a result they have lower activity limits. The radioactivity contained within them may not be of immediate concern, however they can contribute significantly to long term repository dose limits, so accurate characterisation of nuclear waste is crucial to prevent inappropriate waste disposal practices (Suslova et al., 2015).

The decommissioning process is broken down into several key stages:

1. Site shutdown and defueling
2. Post-operational cleanout
3. Ancillary building dismantlement
4. Reactor dismantlement
5. Land remediation

(Bond et al., 2004; International Atomic Energy Agency, 2000). Guidelines for each stage are published by regulatory bodies such as the International Atomic Energy Agency and governmental organisations in each territory. Adherence to the protocols and guidelines is often very strict in order to ensure safety of workers and efficacy of clean-up.

1.2 Radionuclide origin and nature

Radionuclides are unstable species of atoms, possessing excess nuclear energy, which undergo radioactive decay to achieve a more stable state. In doing so they emit alpha (α) or beta (β) particles. Gamma rays (γ) can be emitted alongside the alpha or beta particles, or they can be emitted as the primary manner of decay (Hanrahan, 2012). Emission of an alpha or beta particle changes the identity of the atom. An alpha particle consists of 2 protons and 2 neutrons (a helium nucleus) and a beta particle consists of either a positron or an electron (dependant on the type of beta decay occurring). Gamma rays are a form of electromagnetic radiation consisting of the shortest wavelength of electromagnetic waves. They have much higher frequency and consequently carry much more energy than that of other light waves (Reichardt and Bacchi, 2005). Alpha particles are the most ionising of these radiation methods, however they are the least penetrating, due to their size. Gamma radiation is the least ionising yet the most penetrating, requiring increased shielding using dense materials such as concrete or lead to protect workers.

Many radionuclides can be found naturally. Cosmogenic radionuclides are continuously produced through the bombardment of an atom with cosmic rays. This primarily happens in the Earth's atmosphere (National Research Council (US), 1999). Primordial radionuclides found on Earth have been synthesised before the formation of the Earth, during the big bang or ancient supernova explosions. Commonly, primordial radionuclides have half-lives on the order of the age of the Earth. The other natural radionuclides are comprised of the

Chapter 1

decay products of the primordial radionuclides (National Research Council (US), 1999).

Examples of naturally occurring radionuclides include ^{232}Th , ^{238}U , ^{40}K , and ^{14}C .

Generally, an atom is radioactive in nature if it contains too many protons, too many neutrons, or has a very large mass (>210 amu). Nuclides with excess protons and sufficient energy decay via beta plus decay, emitting a positron, while ones without sufficient energy decay via electron capture. Electron capture occurs when a proton-rich nucleus absorbs an inner atomic electron, prompting the changing of a proton to a neutron. This leads to the emission of an electron neutrino as well as x-rays and usually a gamma ray. Nuclides with excess neutrons decay via beta minus decay, emitting an electron. A field of stability exists between the beta minus and beta plus emitters. Alpha particles are generally emitted by heavier radionuclides; however, some exceptions exist (^8Be for example). A plot of each known nuclide and its decay mode was first constructed in 1958 by W. Seelmann-Eggebert and G. Pfennig (Normand et al., 2009). The chart shows the general trend of the decay modes as well as the field of stability. The chart of the nuclides is a useful tool for determining the likely components of a sample, showing the possible daughter products and decay chains that exist given the known presence of a radionuclide (Figure 1.1).

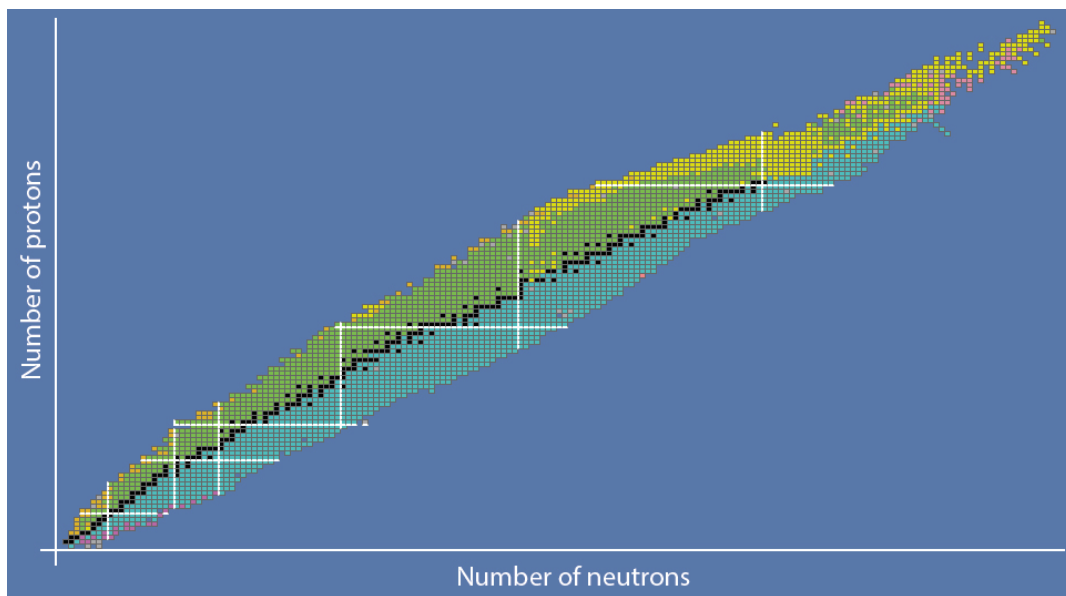


Figure 1.1.

Karlsruhe Chart of the Nuclides

Chart shows each known radionuclide and is colour coded for their major decay mode. Blue - β^- decay, Green - β^+ decay, Yellow - α decay, Black - Stable.

Some radionuclides are so unstable that they decay via fission, which splits the nuclide into two fragments. The dawn of the atomic era brought the creation of a range of radionuclides

associated with the fission of heavy elements. Splitting of fissile materials such as ^{235}U releases a large amount of energy and is useful for application to nuclear weapons and the production of electricity. Fission of these radionuclides is initiated on the addition of a neutron, and forms two lighter nuclides along with several free neutrons. The neutrons can then be absorbed by further fissile elements causing more fission reactions or by non-fissile elements, increasing their mass. The elements formed from the fission of the heavy nuclide are termed fission products, and the nuclides formed through the absorption of neutrons are called activation products.

Fission products are produced in a statistically predictable way. Masses of fission products at the extremes (the heaviest or the very lightest) and those close to half the mass of the fissile parent are the most unlikely (Koning and OECD Nuclear Energy Agency, 2006). Figure 1.2 shows the fission product yield for ^{235}U , ^{233}U , ^{239}Pu and ^{241}Pu with major yield peaks at around 140 and 100.

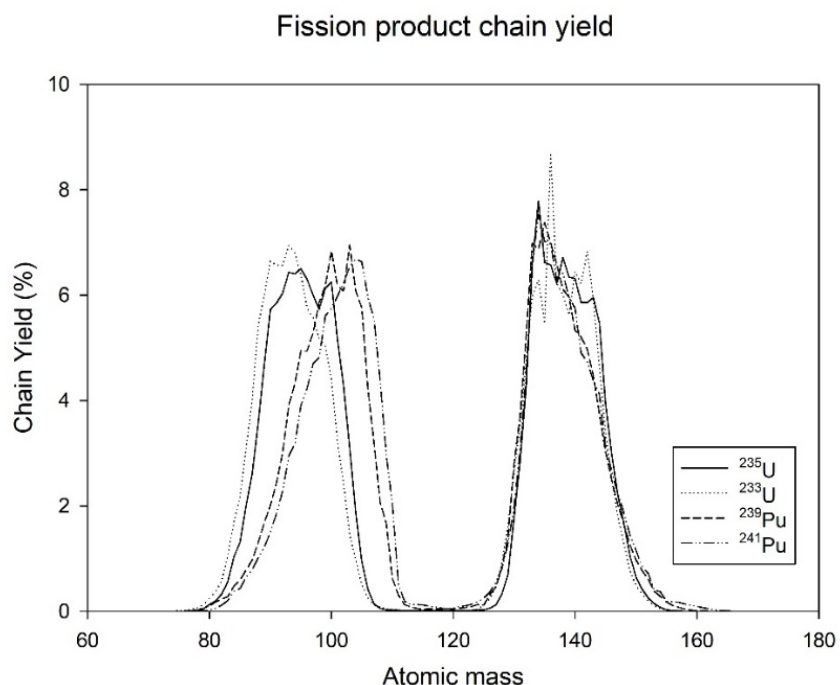


Figure 1.2.
Fission product chain yield curve for fissile U and Pu isotopes
Data from Koning and OECD Nuclear Energy Agency (2006)

Production of nuclear waste is unavoidable for nuclear facilities. The majority of the activity is contained in the fuel rods, however, contamination of other materials is commonplace and has to be accounted for during decommissioning. The nature of the contamination is dependent on the area within the facility, its use and history. Fission products and actinides

Chapter 1

can be present as contaminants in areas storing or exposed to fuel rods. Activation products can be formed through the absorption of neutrons by materials surrounding fuel, such as concrete shielding, steel structures and control rods. An example of radionuclide production in a reactor is shown in Figure 1.3.

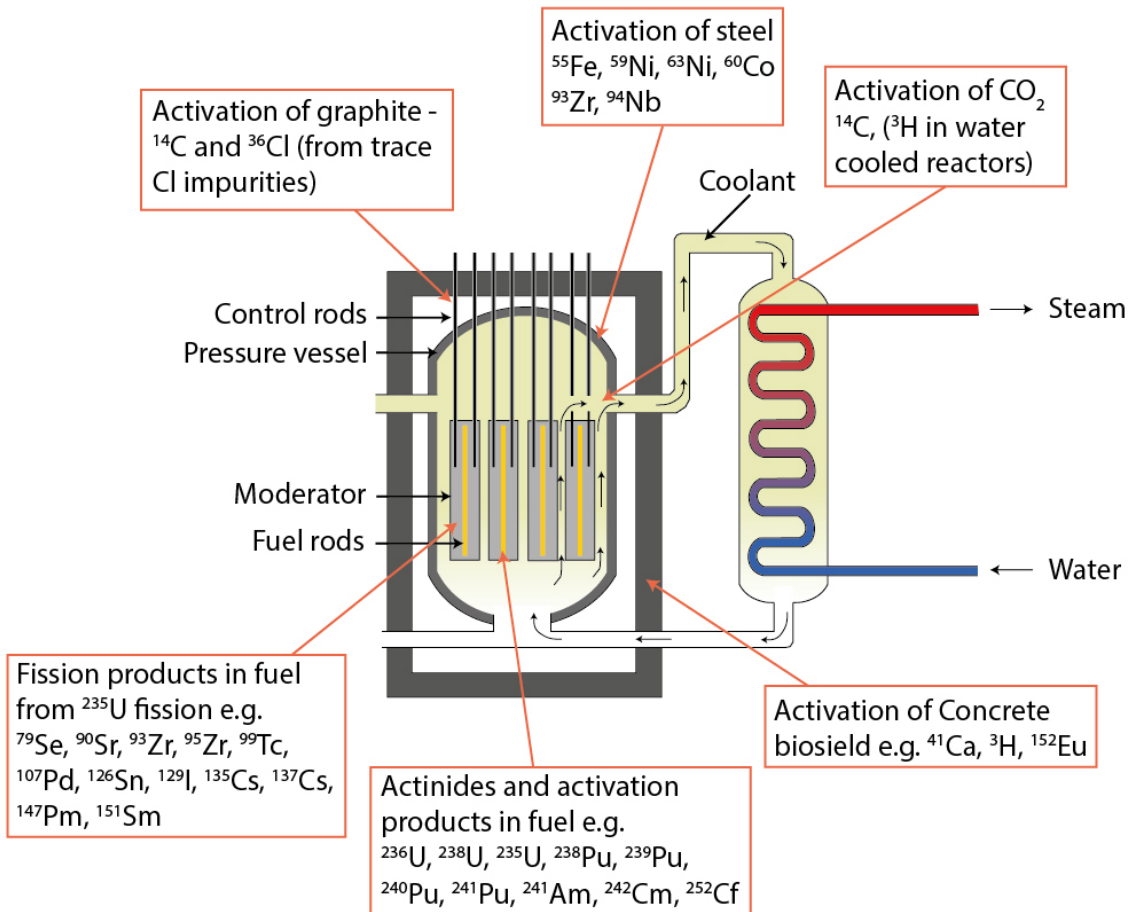


Figure 1.3. Example of radionuclide production in a reactor (LWRs or AGRs)

Adapted from Croudace et al., (2017)

Showing select radionuclide contamination from a reactor using ^{235}U as fuel

1.3 Rationale and objectives

As the current necessity for decommissioning activities is set to increase, so has the need for development of applicable technologies. Modular, remotely operated, automated systems have the potential to make the decommissioning process more efficient and safer for workers (European Commission, 2018). Nuclear waste characterisation is an essential component in waste sentencing during the cleanout, dismantlement and remediation stages. Understanding of a waste's radiological, chemical and physical properties are

crucial in determining the appropriate disposal, treatment or reuse of the material. A variety of technical procedures for radiological characterisation of waste are advised by the IAEA (International Atomic Energy Agency). Included in these are the removal of samples which are subsequently analysed with or without mechanical tools. These can be taken from various depths in order to attain a holistic understanding of a waste package. Analyses of the samples can be conducted on or off-site to attain alpha, beta and gamma activities either after radiochemical separation or to acquire gross alpha or beta measurements. *In-situ* measurements of dose rate and gross alpha/beta and gamma can be carried out. Additionally, a fully resolved gamma spectrum can be measured *in-situ* (Andrieu et al., 2013). The choice of measurement technique is based on historical records of the area within the site containing the waste package. This occurs during a planning phase of the implementation of radiological characterisation (Andrieu et al., 2013). Characterisation methods fall under one of two general classes – destructive and non-destructive. Destructive analysis provides the most accurate activity determination, which yield lower uncertainties than non-destructive techniques (International Atomic Energy Agency, 2007). Destructive analysis involves sampling, preparation of samples and chemical separation methods before analysis. Sample preparation often involves dissolution techniques which are dependent on the sample type. Chemical separation seeks to reduce or eliminate chemical or radiological interferences. Determination of radionuclide content is carried out by instrumental analysis, which may or may not be destructive in their own right, however when combined with the preparation and separation techniques undertaken prior lead to an overall destructive technique. These analyses include alpha or gamma spectrometry, liquid scintillation counting and mass spectrometry among others. Non-destructive techniques involve the observation of spontaneous or stimulated nuclear radiation. These measurements can be used to estimate the radionuclide content of waste without affecting the physical or chemical form. Non-destructive analysis includes gamma spectrometry (identifying gamma emitters), neutron methods (capturing neutrons emitted from spontaneous fission or nuclear reactions) or calorimetry (relying on specific heat to quantify activity) (International Atomic Energy Agency, 2007). Non-destructive analysis can be undertaken much more rapidly than destructive analysis however does require accurate calibration and relies much more heavily upon information gathered during the planning phase.

Chapter 1

Often the easiest, most time and cost-efficient method of characterising large waste volumes is to directly measure bulk or packed waste. However, many of the radionuclides important for long term waste management are difficult-to-measure (DTM) and cannot be measured directly (International Atomic Energy Agency, 2009). A common solution is to use Scaling Factors (SFs). Sometimes termed “waste fingerprinting”, this method utilises the relationship between easy-to-measure (ETM) nuclides and the DTM nuclides of interest. ETM nuclides are ones that can be determined by direct measurement of bulk or packed waste. This is completed by *in-situ* gamma spectrometric analysis which can fully resolve the gamma emissions present. If a correlation is apparent between a key ETM nuclide and a DTM nuclide of interest, the DTM content of a waste package can be estimated simply by measuring the ETM nuclides. The technique of ascertaining the radionuclide content using ETM nuclides is internationally recognised by the International Organisation for Standardisation (ISO Technical Committee: Nuclear installations, processes and technologies, 2007; Kashiwagi et al., 2007).

This method is commonly employed for the sentencing of low and intermediate level radioactive wastes. In the construction of SFs for use in this context, accurate and timely measurements of both ETM and DTM nuclides are required. Commonly, ETM nuclides are ones that can be determined via gamma counting, and DTM nuclides are pure alpha, pure beta, X-ray and low level gamma emitters (International Atomic Energy Agency, 2007). These DTM nuclides usually require chemical separation and pre-concentration techniques for accurate analysis.

Separation of radionuclides can be achieved by various techniques. Precipitative methods can be suitably fast and cheap, however they often lack the precise selectivity and require repeat precipitations to achieve adequate recoveries. Liquid-liquid extraction techniques have proven highly effective at separations on a large scale (PUREX process) however can be inefficient for use with multiple samples. Commonly, separation of DTM nuclides for accurate analysis is completed using column chromatography. This involves manually dripping digested sample and reagents through a chromatographic column, then collecting the fractions in glass beakers. A more eloquent and less time-consuming solution may be to automate the system, inducing forced flow of sample, and eluents through the column.

The high flow rates that can be achieved by automated systems significantly decrease overall radionuclide determination time. In addition, automation of the separation process can reduce labour costs and the risk of contamination through human error. Increasing flow rates, however, can have a negative effect on separation efficacy. The basic theory of chromatography is that there are 2 phases: a mobile phase and a stationary phase. Separation occurs due to sample component's different affinity for these phases. In column chromatography the stationary phase is the resin containing an active site and the mobile phase refers to the aqueous solution or reagents passing through the resin. Higher flow rates decrease the time allowed for interaction between the components of the mobile phase and the stationary phase. This has can cause the early elution of mobile phase elements, which affects the decontamination or recovery of the target radionuclide fraction.

The aim of the research presented in this thesis is to investigate the effects of increasing mobile phase velocity through chromatographic columns, facilitated by automated systems. Specific focus will be given to separations employed during the decommissioning of nuclear waste. Strontium separation will be analysed at increased flow rates using commercially available Sr-resin (Eichrom Technologies) in a chromatographic column. An investigation of actinide separation will be completed at expedited flow rates to compare the efficacy of different chromatographic materials (Anion Exchange resin, TEVA resin and UTEVA resin all supplied by Eichrom Technologies). Finally, a procedure will be analysed for the separation and measurement of multiple radionuclides from a single sample using expedited flow rates. Where appropriate, further application to other fields of study shall be investigated, with the aim of highlighting the versatility of automated systems for use in multi-purpose laboratories. Understanding of how a chromatographic material's characteristics affect their behaviour under increased flow rates will aid in further research of expedited separation systems using different materials. The investigation into the sorptive materials' behaviour under increased flow rates shall be used in the construction of the multi-separation procedure, aiming to separate and purify multiple radionuclides from a single sample. Efficacy of the separations shall be assessed using common performance quantifiers used in extraction chromatography, decontamination factors and by comparing limits of detection to internationally recognised guidelines on bulk waste activity limits.

1.4 Quantification of column performance

Height Equivalent to a Theoretical Plate (HETP) is often used when assessing chromatographic separation efficiency. Plate theory was first outlined by Martin and Synge in 1941. It divides a chromatographic column into multiple hypothetical layers. Each layer is defined as the distance through the column the mobile phase is required to travel before that portion of the mobile phase is in equilibrium with the solid phase (Martin and Synge, 1941; Stauffer et al., 2008). The solution issued from each layer is therefore in equilibrium with the mean concentration of solute in the solid phase throughout the layer. Chromatographic plate theory dictates that low HETP indicates the ability to achieve chromatographic separation with narrow elution peaks of constituents. HETP is calculated using the column length and the number of plates (Equation 1.2) (Ettre, 1993). The number of plates is obtained by analysing the elution profile of analyte using the same solvent. This is termed “isocratic elution” and produces an elution profile similar to that of Figure 1.4.

$$n = 5.545 \cdot \left(\frac{t_R}{W_h} \right)^2$$

Equation 1.1.

Plate number equation

n – number of plates, t_R – volume to peak elution, w_h – full width at half peak height

$$HETP = \frac{L}{n}$$

Equation 1.2.

Chromatographic plate equation

Following from Equation 1.1, HETP – Height Equivalent to Theoretical Plate, L - length of column, n - number of plates

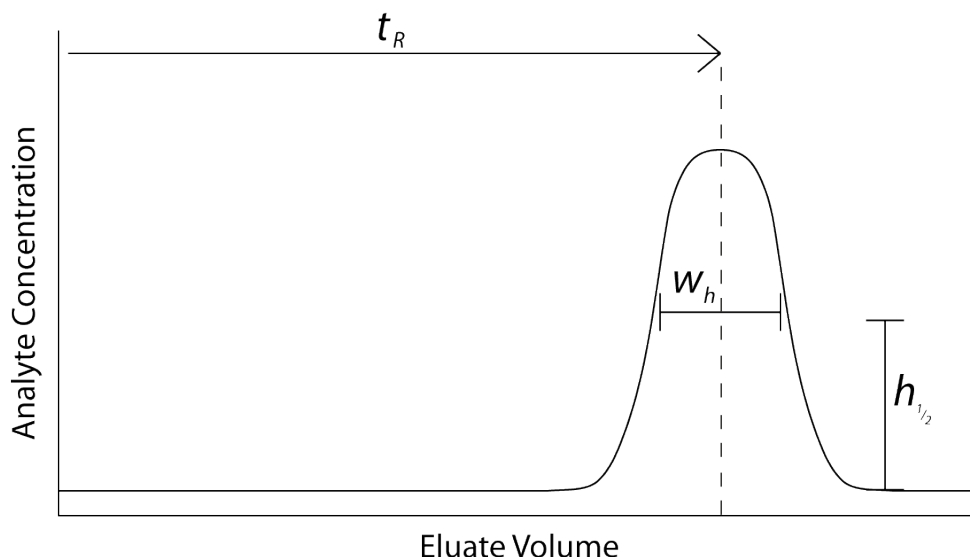
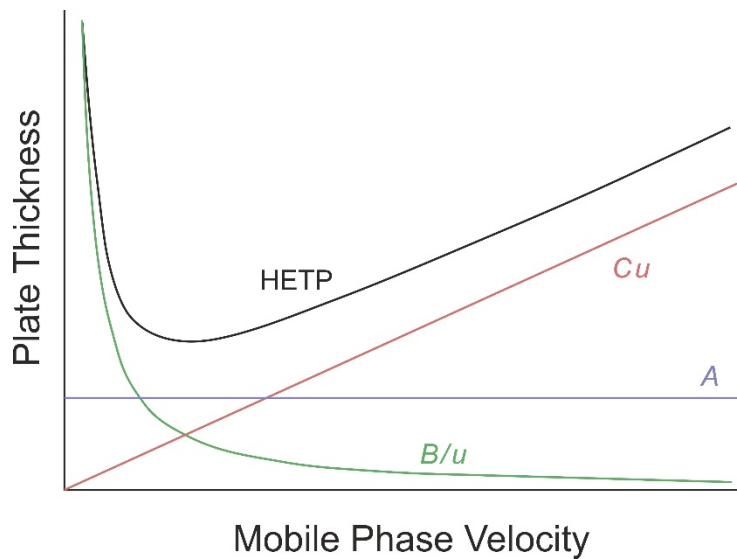


Figure 1.4.
Elution profile for isocratic elution of analyte
 W_h , t_R , analyte concentration and eluate volume

Dominant column conditions controlling HETP are related in the van Deemter equation (Equation 1.3). The eddy diffusion parameter (A) is independent of mobile phase velocity and is dependent only on the size of the stationary phase (resin diameter). For this reason, A is unaffected by increases in aqueous phase velocity and is constant for a given column. The longitudinal diffusion coefficient (B) quantifies the tendency for analyte molecules to redistribute from regions of high concentration via diffusion to regions of low concentration. This effect is greatly reduced as flow rate increases (Figure 1.5).

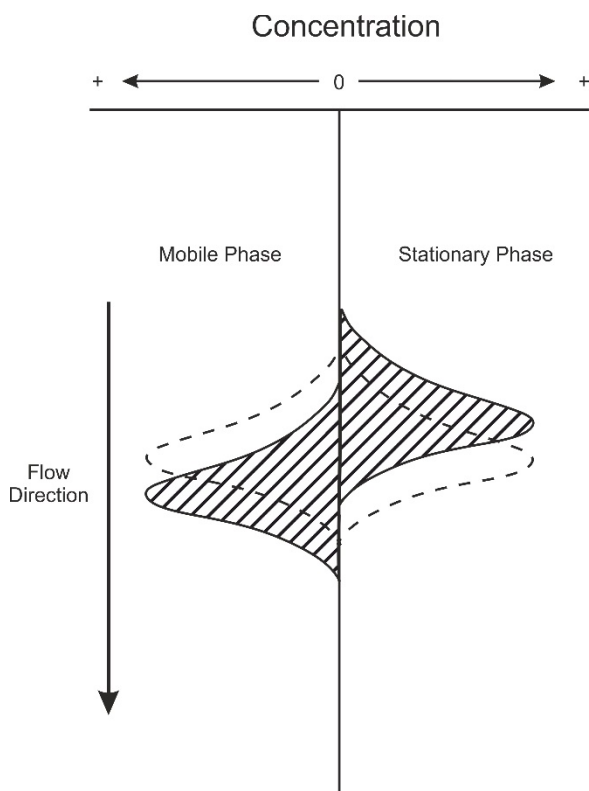
$$HETP = A + \frac{B}{u} + C u$$

Equation 1.3.
van Deemter equation
 Relating plate thickness and mobile phase velocity (u). C – resistance to mass transfer, B – longitudinal diffusion coefficient, A – eddy diffusion.

**Figure 1.5.****van Deemter Plot**

Effect of each individual constituent of the van Deemter equation on plate thickness

Resistance to mass transfer (C) refers to the non-instantaneous transfer of analyte between the mobile and stationary phases. It is comprised of two parts; analyte transfer from mobile phase to stationary phase and vice versa. For this reason, the term C in the van Deemter equation can be expanded to $C_s + C_m$. These two components have opposing effects on elution profiles as a delay from mobile phase to stationary phase causes mobile phase analyte profile to be in advance of the equilibrium position. A delay in transfer from stationary to mobile phases causes the stationary phase profile to be slightly behind the equilibrium position (Figure 1.6) (Poole, 2000). Increasing flow rate increases the disparity between the mobile and the stationary phase profiles individually and between both phase profiles and the equilibrium position. Elution peaks observed at higher flowrates will, therefore, be broadened.

**Figure 1.6.****Graph showing the two components of resistance to mass transfer**

The actual positions of the solute zones are depicted as solid outline with fill and the equilibrium position by the dashed line with no fill. Adapted from Poole., (2000).

1.4.1 Kinetic control on separation

Analyte uptake on the chromatographic material also affects the separation efficiency. This uptake is usually quantified as the ratio of analyte in the solid and liquid phases. For the purposes of this research, this shall be referred to as K' (Equation 1.4). When the ratio reaches an equilibrium state, maximum uptake of analyte by the resin has occurred. This is often termed “distribution coefficient” and referred to as K_d . Higher K_d ’s have the effect of retaining the analyte on the column for longer (Figure 1.7). If equilibrium (K_d) is not achieved due to shorter interaction times (caused by higher flow rates), analytes will elute from the column more rapidly, possibly during the elution of contaminants.

$$K' = \frac{\text{Analyte in solid phase}}{\text{Analyte in liquid phase}} \times \frac{\text{Mass of liquid phase}}{\text{Mass of solid phase}}$$

Equation 1.4.**Equation for distribution ratio**

Calculation of K' using masses of analyte in the solid phase and liquid phase and the masses each phase

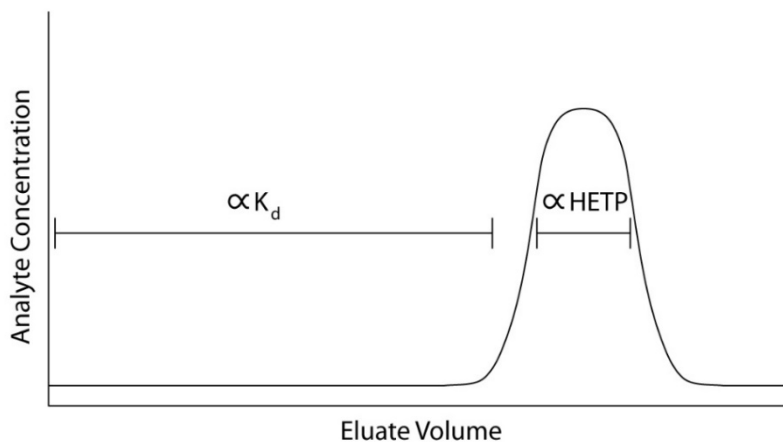


Figure 1.7.
The relationship between K_d , HETP and elution profile

In order to conduct this research, appropriate materials need to be utilised to ensure relevance to the nuclear sector. Traditional methods of radionuclide separation include liquid-liquid exchange, ion exchange chromatography and precipitation and these methods have been proven to be sufficient on a range of matrices (Butler, 1963; Kooi, 1958; Noshkin and Mott, 1967; Porter et al., 1967; Talvitie and Demint, 1965; Weiss and Shipman, 1957).

With plans for further nuclear power developments already on the horizon, advancement in radiochemical separation techniques will be focussed on, in order to decrease time and associated cost (BIS, 2013). The following thesis will evaluate the effect of increasing flow rate during the chromatographic separation of radionuclides commonly studied during nuclear waste characterisation. Strontium-90 separation will be investigated due to its high fission yield (Takagai et al., 2014). As a result, it is a significant constituent of waste containing fission products. In addition, it is a pure beta-emitter giving off no gamma radiation. This means it is also classed as a DTM radionuclide.

Uranium is commonly used as a nuclear fuel and the major isotopes of uranium decay via alpha decay. This can pose a risk to human health and the environment if contamination is significant. In addition, uranium has extensive decay chains which contain radioactive daughter isotopes as well as toxic heavy metals (e.g. polonium, lead) (Rožmarić et al., 2009). Analysis is of U is regularly undertaken, not just during decommissioning, but also during fuel reprocessing and disposal in order to assess the fissile content.

Thorium separation and purification will be assessed due to its presence as a decay product of nuclear fuels. Thorium poses a risk to environmental and human health if present in high quantities due to the decay mode of the most common isotopes (alpha decay) (Gad, 2014). Analysis of Th is carried out during reactor operation and decommissioning.

Plutonium is present as it is a common activation product in uranium fuelled reactors (especially ^{239}Pu). Because of its radiological and biological toxicity accurate determination of the Pu content of waste is required during decommissioning and fuel reprocessing (Rodriguez, 2014). Therefore, Pu separation and purification will also be analysed within the context of expedited chromatographic separation.

Chapter 1

Chapter 2 Expediting radionuclide separation and analysis

2.1 Introduction

Conventionally, gravity flow columns are used to perform anion exchange and extraction chromatography (Horwitz et al., 1992; Kołacińska et al., 2017). However, to expedite chromatographic separation, increases in flow rate can be induced in several ways.

2.2 Vacuum boxes

Most commonly, sample, reagent and eluent are drawn through using a vacuum box. Vacuum boxes can also be used to aid the preparation of chromatographic columns, commonly to ensure suitable packing of resin within the column (Habibi et al., 2017). Many studies have used vacuum systems to expedite the separation process, increasing flow rates through the columns (Grahek et al., 2018; Hurtado-Bermudez et al., 2017; Maxwell et al., 2017, 2016; Vajda and Kim, 2010). However, very little study exists on flow rate increases and its effect on separation efficiency. Vacuum boxes are an effective way of increasing flow rate, however study on flow rate effects using the vacuum systems may prove difficult because of the specific lack of control over the resulting flow rate. Flow rates may differ depending on size of resin bead, packing efficiency and effectiveness of sealing between the vacuum chamber and the ambient atmosphere. Studies such as Maxwell et al. (2016) that use vacuum systems in this way are only able to calculate the flow rates produced, not control the flow rate. Higher vacuums lead to increased flow rates, so only very rough control is possible but not precise control. Vacuum boxes are common for use in chromatographic separation procedures with methods existing for americium, neptunium, plutonium, thorium, curium, uranium and strontium using TEVA, TRU and Sr resins (Eichrom Technologies, LLC, 2006; Vajda and Kim, 2010). Vacuum box systems may help to reduce analytical time and overall labour costs with the ability to process multiple samples at once. However, manual handling and skilled workers are still required to add the sample and solutions to such systems.

2.3 Pressurised injection

Pressurised injection methods work by pressurising the vessel containing the sample and solvents with a gas, commonly N₂. The positive pressure forces the solutions through the column at increased flow rates (Figure 2.1). This method of injection can achieve high flow rates, can be utilised to work with more viscous solvents and can be set up at a relatively low cost. However, studies into this method of column introduction have shown that the separations completed are not easily repeated, again, due to the low level of control on flow rate (Guérin et al., 2013). The pressurised injection technique has been applied to the separation of actinides using TEVA and DGA resins as well as the separation of Sr using a silica based extraction chromatographic material, similar to that of Sr resin (Guérin et al., 2013; Zhang et al., 2008).

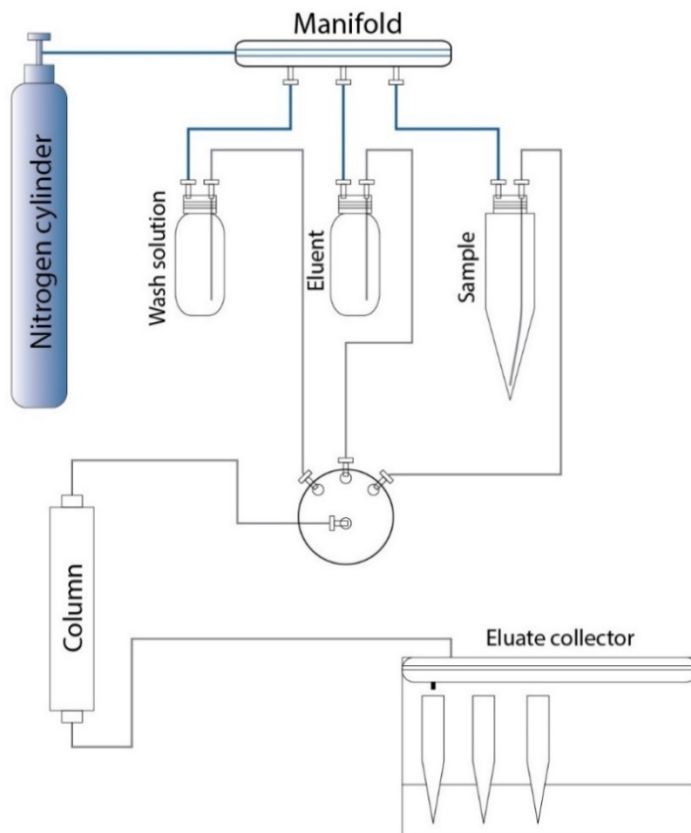


Figure 2.1.
Pressurised injection schematic
Pressurised injection of reagents and sample onto the column

2.4 Flow injection analysis

To advance techniques, automation of the separation processes could be beneficial in several ways. The system would reduce the need for skilled personnel, increase throughput (in comparison to gravity flow columns), reduce contamination risks, increase safety and also allow for controlled and consistent analytical protocols (Chung et al., 2015). Automated processes can also facilitate the expedition of the separation process, through reducing steps or using higher flow rates. Automated addition of sample and reagents is a key process that vacuum box systems generally do not possess and precise control of flow rates to allow repeatable separation is not possible with either vacuum box or pressurised injection systems.

One of the first examples of an automated system was a flow injection analysis system. It utilised a chromatographic column with injection of sample, reagent and eluent added by a pump system (Grate et al., 1996). An Sr-spec column was used in an on-line configuration, with liquid scintillation cocktail added to the eluate post-separation and liquid scintillation counting used as the detection method. The use of the Sr-spec column was as per Eichrom recommendation, with the columns prepared using 8 M HNO₃, and sample loaded and the column washed with more 8 M HNO₃ to remove interferences (including ⁹⁰Y) before elution with deionised water. In Grate et al.'s (1996) experiment, both washing and eluate were counted by LSC as the liquid scintillation counter used was a flow-through counter equipped with a 0.5 mL flow cell. The sample loading, washing and elution was carried out at a flow rate of 0.5 mL/min (controlled by a peristaltic pump). Column rinsing and wash cycle post-LSC were completed at a rate of 1 mL/min. Grate et al. showed that two distinct peaks in activity were apparent from the LSC. The first was the ⁹⁰Y (and other radioactive contaminants) elution during the column washing and the second being from the ⁹⁰Sr eluate. Grate et al. stated that the apparent delay from the end of the 8 M HNO₃ wash and the start of ⁹⁰Sr elution is due to Sr resin extracting HNO₃ from aqueous nitric acid solutions. The subsequent deionised water elution step will, for the first few millilitres, wash the nitric acid off the Sr resin until the column acidity drops to a sufficient level as to release the Sr. According to Grate et al., this occurs at a pH of less than 2. Grate et al. (1996) also tested the system with a larger flow cell (2.5 mL) and a longer residence time. This increased the number of counts detected and therefore improve the counting statistics. However, it is only possible do to this once the elution curve has been completely resolved using the

Chapter 2

smaller flow cell. This is because knowledge of the first radionuclide peak is required to avoid both washing and eluate activity being counted together. During the experiment with the larger flow cell, flow rate through the column was increased to 1 mL/min for the washing, but the elution step was kept at 0.5 mL/min. It is also mentioned that Ba is more strongly retained than that of most other potentially interfering species. This may present an issue in samples containing a significant amount of Ba (e.g. some concretes used in radiation shielding). However, the only Ba isotope likely to be present in nuclear waste is ¹⁴⁰Ba, which decays in 12.7 days and has a β^- energy double that of ⁹⁰Sr. Grate et al.'s study shows that automated techniques can be effective at preventing spills, minimising exposure to workers and increasing throughput.

Flow injection analytical techniques consist of the same general setup. The procedure utilises a relatively small volume of sample for measurement with preliminary steps designed to preconcentrate, purify or prepare target analytes for analysis. These steps are carried out on flow-through modules. The measurements are carried out on flow-through detectors which can allow for sequential analysis of different analytes using the same apparatus. In these cases the kinetic differences between the analytes in the preliminary stages allows for multicomponent determination (Trojanowicz and Kołacińska, 2016).

Several other flow injection techniques have been outlined in publications, most using an on-line arrangement (Mateos et al., 2000; O'Hara et al., 2009). O'Hara et al.'s and Mateos et al.'s systems utilise syringe pumps to induce forced flow meaning that the flow of aqueous phase through the column is stopped while the syringe pump is refilled. Systems employing peristaltic pumps to induce the flow through the system allowing for constant flow of sample and solutions (example of this in Figure 2.2).

These online systems, where separation leads directly to measurement may not be as attractive as offline or hyphenated systems. Online systems cannot easily be adapted for different separation procedures or measurement techniques, whereas offline or hyphenated systems can. These online systems can only separate one sample at a time. In addition, Grate et al. acknowledge that due to the lack of evidence or research into the viability of reusing Sr resin, the column has to be replaced after every sample. This increases handling operations and slows sample throughput. It is accepted that changing the columns is most likely required for all Sr separation procedures, however a system able to separate

multiple samples at once before a collective column change seems like a far more elegant and efficient solution.

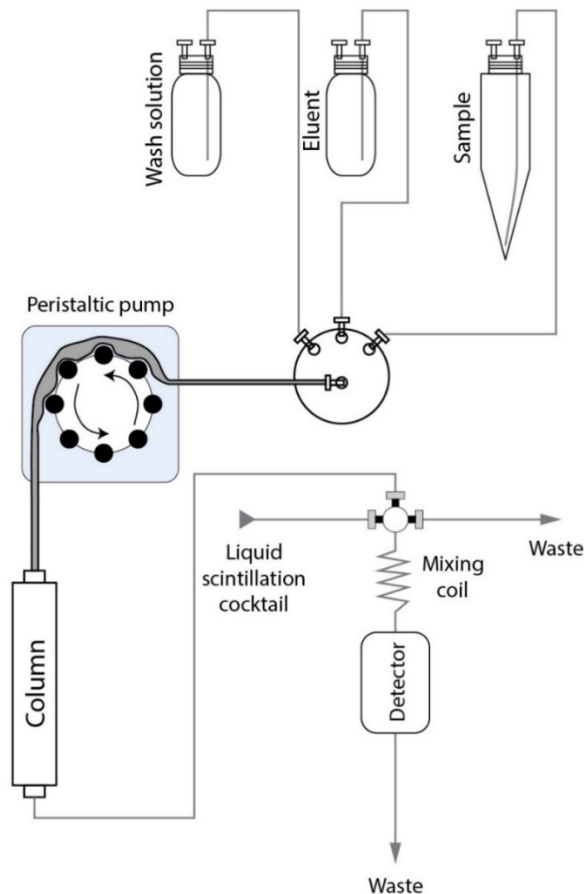


Figure 2.2.

Flow injection analysis schematic

Peristaltic pump used to induce flow, syringe pump can also be used

2.5 Automated radionuclide separators

In 2013 Chung et al. produced a paper outlining a novel automated radionuclide separator capable of separating ^{99}Tc from 4 groundwater samples at once. The modular automated radionuclide separator (MARS) utilised one peristaltic pump and multiple valves to direct reagent, sample and waste. The example outlined in the paper utilised 4 columns but Chung et al. (2013) stated that the system could be expanded to include up to 8 columns with the software installed (LabVIEW™). The testing of the MARS conducted by Chung et al. consisted of separating $^{99\text{m}}\text{Tc}$ tracer from five groundwater samples collected from Gyeongju City (Korea). Separation was completed using TEVA resin. Groundwater samples were acidified using HNO_3 and oxidised using H_2O_2 to ensure complete formation of

Chapter 2

pertechnetate ions (TcO_4^-). TEVA resin was packed into the columns on the MARS. The columns were conditioned with 0.1 M HNO_3 before the acidified (to pH 2) water samples containing TcO_4^- were loaded. The TEVA column was washed with 50 mL of 2 M HNO_3 and Tc was eluted with 20 mL 8 M HNO_3 . ^{99}Tc concentration was measured using ICP-MS after the eluate was evaporated and dissolved in 2% HNO_3 . Counting of the $^{99\text{m}}\text{Tc}$ tracer was completed using HPGe Gamma ray spectrometers to establish chemical yield. To produce elution curves GM (Geiger Müller) counters were employed at the base of the chromatographs. Elution curves were produced for 6 different elution flow rates (1.0, 1.5, 2.5, 3.0, 5.0 and 7.0 mL/min). Chung et al. (2013) stated the highest tailing of the elution curves occurred at the highest elution flow rates, and that the ideal elution flow rate was 1.5 mL/min. Even with the highest peak tailing, the baseline GM signal returned within 18 mL of eluent (8 M HNO_3). The loading, washing and rinsing steps were all undertaken at 5 mL/min, and Chung et al. made no comment over what effect altering the loading and wash steps would have on chemical recovery of ^{99}Tc . An average recovery of over 95% was achieved.

Chung et al. (2013) concluded that the MARS system, applied to the function of Tc separation using TEVA resin, successfully separated the target radionuclide from groundwater samples. They also stated that by altering the protocols, the MARS could be adapted to the separation of various other radionuclides from different matrices.

In 2015 two papers were published outlining the application of the MARS system from Chung et al. (2013) to the separation of radiostrontium from different matrices. Kim et al. (2015) outlined a procedure for separation of radiostrontium and plutonium from seawater. This was completed by using a sequential column setup. Sr and Pu in samples were concentrated by precipitation of PuCl_3 and SrCO_3 from the addition of $\text{FeCl}_3 \cdot 6\text{H}_2\text{O}$ and Na_2CO_3 . The filtered and dissolved precipitate (in conc. HNO_3) was loaded onto a TEVA resin chromatographic column in the MARS. The Sr was washed from the TEVA resin using 8 M HNO_3 , which was passed directly onto a Sr -spec column. The TEVA resin was washed with 1 M HNO_3 which was directed to waste and the Pu was eluted using 1 M HCl . The Sr on the Sr -spec column was washed with 8 M HNO_3 before elution with deionised water. All steps using the MARS were carried out at 2 mL/min apart from the elution of Pu from the TEVA column, which was carried out at 1 mL/min. Kim et al. (2015) found that recovery of Sr and Pu using this method was 87.8% and 62.5% respectively. They stated that when the Pu

purification steps on the MARS were isolated, Pu recovery was higher than 90%. This suggests that the lower values of recovery originally produced were due to losses of Pu from the concentration/precipitation step (prior to TEVA column loading).

Kim et al. (2015) concluded that although minimum detectable activity using this method was actually higher than that of background activity, the method described would be suitable in the case of an emergency, where Pu and radiostrontium concentrations in seawater are greatly increased. Kim et al.'s method demonstrated effective separation of multiple radionuclides from a sequence of chromatographic columns on the MARS.

The second paper using the MARS for radiostrontium separation was applied to milk matrices. Chung et al.'s (2015) procedure used Dowex resin to preconcentrate radiostrontium in milk samples that had been spiked with ^{89}Sr and ^{90}Sr . The resin was added to the milk sample, the supernatant solution discarded and then the resin was washed with deionised water. The resin was loaded into a column in the MARS and Sr, Ca and Ba were stripped from the resin using 4 M NaCl. The Sr Ca and Ba were then precipitated as a carbonate using Na_2CO_3 which was dissolved in 8 M HNO₃. The dissolved precipitate was then loaded onto a Sr-spec chromatograph in the MARS. Standard Sr separation procedure was followed, using an 8 M HNO₃ wash to remove Ca and Ba, and elution of Sr was completed using deionized water. Loading of sample was undertaken at 3 mL/min, washing at 2 mL/min and elution at 2 mL/min also. Counting of eluate was undertaken using liquid scintillation counters for beta and Cherenkov counting of ^{89}Sr , ^{90}Sr and ^{90}Y . Chemical recoveries were found to differ depending on the activity of the original milk sample. Higher activities yielded higher recoveries at an average of 87%, whereas lower activity samples had recovery yields of around 80% on average.

Chung et al. (2015) conclude by stating that their study proves another successful application of the automated radionuclide separator to the separation of radiostrontium from a matrix commonly investigated during the aftermath of a nuclear incident. The paper does not investigate the effects of higher flow rates however it does comment on the temporal difference between using a forced injection method in comparison to gravity flow columns.

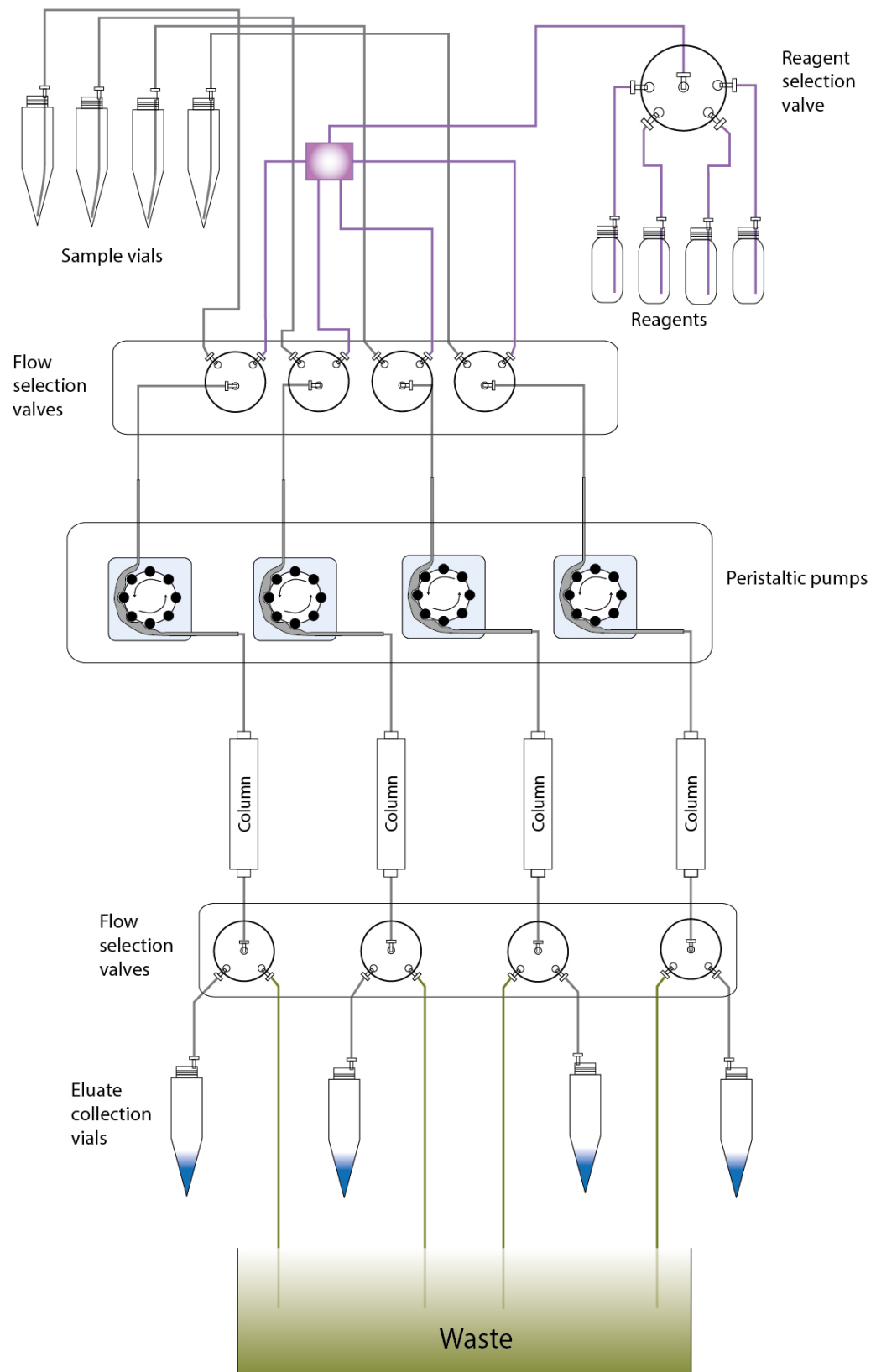


Figure 2.3.

Automated radionuclide separator schematic

Modular systems can increase number of selection valves, peristaltic pumps and eluate collection vials

Kim et al. (2015) and Chung et al. (2015) aimed to produce a safe and fast method of analysing environmental samples in the wake of a nuclear incident. As mentioned previously, these automated systems can potentially be beneficial not to only emergency situations but to regular analysis also. In this instant, the purpose of the analysis is to produce highly accurate characterisation of the radionuclide composition of a sample. Reduction of elapsed time and hence exposure of workers is of course of importance, but the efficiency of the separation must be paramount. For this reason, investigation into flow rate effects, matrix effects (mass as well as matrix composition) and repeatability must be tested. The application of the methods described by Kim et al. (2015) and Chung et al. (2015) were to samples which likely contained big increases of radionuclides in comparison to background, which would prove to be an immediate risk to the public, or any workers who might be exposed. In the nuclear decommissioning environment, overall concentrations may be relatively low, but long-term dose may be quite significant. A schematic of an automated radionuclide separator is shown in Figure 2.3. In comparison to flow injection analysis, pressurised injection and vacuum box systems, automated separators require larger numbers of components (e.g. pumps, columns, valves) which all have to be composed of materials resistant to chemical corrosion. This increases the cost of such systems. Comparison of the separation system is summarised in Table 2.1.

In addition, in the event of a nuclear incident, the types of matrix analysed are very different to those which may be analysed during an assessment of nuclear waste composition. Milk, grass and seawater are three matrices which have direct link to the human food chain. In nuclear facilities, the most common materials analysed are cement and steel, so investigation into these matrices and how flow rate and radionuclide interference affects their behaviour on chromatographic materials is key.

Method	Examples	Advantages	Disadvantages
Gravity flow columns	Kotacińska et al. (2017), Horwitz et al. (1992a)	Cheaper equipment costs.	Slow, labour intensive, high risk of contamination and exposure risk to workers.
Vacuum box	Grahek et al. (2018), Hurtado-Bermudez et al. (2017), Maxwell et al. (2017, 2016), Vajda and Kim (2010)	Higher flow rate, relatively cheap equipment costs, vacuum boxes can accommodate multiple columns and column packing can be homogenous.	Manual handling and skilled workers still required. Little control of overall flow rate.
Pressurised injection chromatography	Guerin et al., (2013) and Zhang et al., (2008)	High flow rates, relatively inexpensive and can accommodate more viscous solvent use.	Hazardous if a leak occurs due to the higher pressure. Has a low level of control on flow rate.
Injection analysis separators	O' Hara et al. (2009), Mateos et al. (2000), Grate et al. (1996)	Higher flow rates achieved and flow rates can be controlled more accurately. Worker exposure and contamination risks associated with manual handling are reduced.	Only one sample can be separated at once and subsequent samples have to wait for eluate to be analysed before they can be separated. Little adaptability to other separation systems.
Automated radionuclide separators	Chung et al. (2013), Kim et al. (2015), Chung et al. (2015)	Multiple simultaneous sample separation, higher flow rates and more flow rate control. Worker exposure minimized and protocols can be pre-installed to reduce the need for specialised workers. Contamination risk low in comparison to gravity flow and vacuum box methods.	Comparatively expensive.

Table 2.1.
Table of expedited separation systems

Chapter 3 Materials and instrumentation

3.1 Chromatographic materials

3.1.1 Strontium separation

3.1.1.1 Sr-Spec Resin

For accurate and precise determination of radiostrontium, it is crucial to separate active interferences for radiometric counting and the large quantities of inactive elements like calcium, which are often present in environmental, industrial and biological samples (Horwitz et al., 1991). Separation from radiometric interferences allows for accurate activity determination when using radiometric techniques, especially when analysing nuclear waste samples. Separation from matrix elements can reduce isobaric and polyatomic interferences for measurement of Sr by mass spectrometry. Additionally, other matrix components may affect Sr determination without being a direct measurement interference. Separation from calcium is important as residual calcium decreases the ionization efficiency of Sr and also causes the ion beam to become unstable when analysing samples by mass spectrometry (Pin and Bassin, 1992). Horwitz et al. (1991) recognized that the most common calcium-strontium separation depended on greater solubility of calcium nitrate in strong HNO_3 . A new method was sought to reduce steps in separation procedure and increase separation efficiency.

Precipitation techniques like precipitation of strontium sulphate (Fourie and Ghijssels, 1969) and strontium rhodizonate (Weiss and Shipman, 1957) have been reported, for which high strontium recoveries (>80%) were obtained. Ion exchange techniques have also been developed with the use of chelating agents (Noshkin and Mott, 1967; Porter et al., 1967), and liquid-liquid extraction techniques with organophosphorus acids used for milk matrices (Butler, 1963).

However, each of these techniques has shortcomings. For example, the precipitation techniques were still unable to separate calcium and strontium completely, even though their chemical Sr recoveries were most adequate. Ion exchange procedures worked with very tight pH ranges, so acidity control was often an issue, resulting in varying amounts of Ca present in the final samples, even from identical protocols (Horwitz et al., 1991).

Chapter 3

Developments in Sr separation from calcium utilised crown ether molecules, commonly in chloroform and showed more promising results (Kimura et al., 1977, 1979; Smułek and Łada, 1979). However, it was noted that these procedures proved ineffective at separating highly acidic samples. This is inadequate for many environmental samples as some materials necessitate a preliminary stage of digestion which requires the use acidic solutions of high molarity to dissolve the sample.

Horwitz et al. (1991) were able to overcome this by using the crown ether 4,4'-(5')-bis(tert-butylcyclohexano)-18-crown-6 (DtBuCH18C6) (Figure 3.1) in solvent 1-octanol, sorbed onto a purified, inert acrylic resin. This resin (referred to as Sr-spec material or Sr resin) was then transferred to a 10 cm glass Bio-Rad column to create a resin bed volume of 0.6 cm³. Rinsing of the resin was completed using 3 M nitric acid. Initial experiments showed that ideal loading solutions would consist of the Sr matrix in 3 M HNO₃. Sr separation from Ca would be most ideal at loading solutions of 2 M HNO₃ - 0.5 M Al(NO₃)₃. In this instance less than 1% of the Sr was lost during column washing and 99% of the Ca was removed before Sr elution.

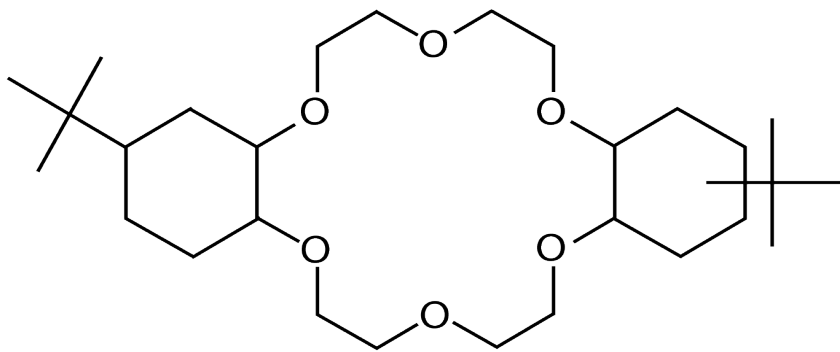


Figure 3.1.

Sr resin chemical structure

Crown ether DtBuCH18C6 structure

Horwitz et al. (1991) demonstrated the Sr resin's use for separating Sr from other radionuclides that are commonly present in nuclear waste. A 25-element solution (Ag, Al, Ba (2.1×10^{-4} M), Ca (1.4×10^{-3} M) Cd, Ce, Cr, Cu, Eu, Fe, La, Mg, Mn, Mo, Na, Nd, Ni, Pd, Pr, Rh, Ru, Sm, Sr (1.4×10^{-3}), Y, and Zr) was used to mimic that of a typical sample of nuclear waste. Horwitz et al. point out that although U, Th, Pu and Np would also be present, only tetravalent Np and Pu would be retained by Sr-spec resin. In practice, both of these would be removed by passing the waste solution through element-specific extraction

chromatographic columns prior to treatment with Sr-spec resin. Horwitz et al. (1991) conclude that the resin and methodology described could be applicable to any environmental, biological, industrial or geological sample that would be prepared by digestion or leaching with nitric acid.

Horwitz et al.'s 1992 paper describes the separation of Sr from HLW (High Level Nuclear Waste) containing a mixture of fission products and actinides. As described in Horwitz et al., (1991), Np and Pu are also retained by Sr-spec resin under normal operating acid concentrations. However, by complexing Np and Pu with oxalate ions (by using a load solution of 3 M HNO₃ - 0.05 M H₂C₂O₄), retention of these two actinides by Sr-spec resin can be effectively prevented with barely any effect on Sr retention. As shown in Horwitz et al.'s 1991 paper, recoveries of ⁹⁰Sr were around 99%.

The paper also notes the Sr-spec resin's retention of Pb. It is much higher than that of Sr in the operating HNO₃ concentrations. This is due to Pb²⁺'s similar cationic radius at coordination number 6. Pb²⁺ has an ionic radius of 1.19 Å and Sr²⁺ has an ionic radius of 1.18 Å (Burrows, 2013; Shannon, 1976). They therefore compete for space in the cavity of the crown ether. It is assumed that in a sample containing excess Pb in comparison to Sr, that Sr would be out-competed and would break through during sample loading. However, if Sr was present in excess, and the sample only contained trace Pb, Sr separation from Pb could be completed. Horwitz et al., (1992a) state that Sr elution could occur at low HNO₃ concentrations, whereas efficient Pb elution from Sr-spec resin requires dilute ammonium oxalate. Other radionuclides which can form ions of similar size can be disregarded due to their absence in HNO₃. Horwitz et al. (1992a) state that the capacity of Sr resin for strontium is 21 mg of Sr in a 2 mL column. One would assume, that due to the similar size of the Pb²⁺ ions and the relative atomic mass of Pb, Sr resin's capacity for Pb would be around 48 mg per 2 mL column.

The product literature also states that Sr chemical yield is significantly reduced at higher strontium concentrations (Triskem International, 2015a). It is stated that a significant reduction of ⁸⁹Sr chemical recovery was observed in a study using a 2 mL Sr-spec column and 8 mg of stable Sr carrier (Triskem International, 2015a).

Horwitz et al. (1992a) published data on the acid dependency of retention of alkali and alkaline earth metal ions as well as actinides and other selected possible interferences on

the Sr resin. It shows that selectivity for Sr over most alkali and alkaline earth metal ions (e.g. Ba^{2+} , K^+ , Ra^{2+}) increases with increasing HNO_3 molarity (Figure 3.2). Although this is not the case for Ca^{2+} ions the difference between the distribution coefficients of Sr^{2+} and Ca^{2+} is much larger than that of Sr^{2+} and Ba^{2+} , so selectivity for Sr over Ca is still much greater than for Ba.

One of the first studies to use Sr-spec resin was Pin and Bassin (1992) testing its effectiveness in the separation Sr from geological samples. Matrix effects were investigated for different in-house standards available to Pinn and Bassin, which aimed to cover a wide variety of elemental compositions. The matrices investigated were a peridotite, a basalt, a trachyandesite, a diorite and a granite. Chemical yields were assessed using ICP-AES (Inductively Coupled Plasma Atomic Emission Spectroscopy). All rock types except the peridotite yielded chemical recoveries of >96% (although this figure included dilution steps as well as the separation on the Sr-spec resin). The peridotite's lower recovery yield may be due to overloading the column with sample. The peridotite used had a much lower concentration of Sr in comparison to the other rock standards (at around 8.4 $\mu\text{g/g}$ compared to 165-780 $\mu\text{g/g}$) so more sample had to be used to provide a fair comparison.

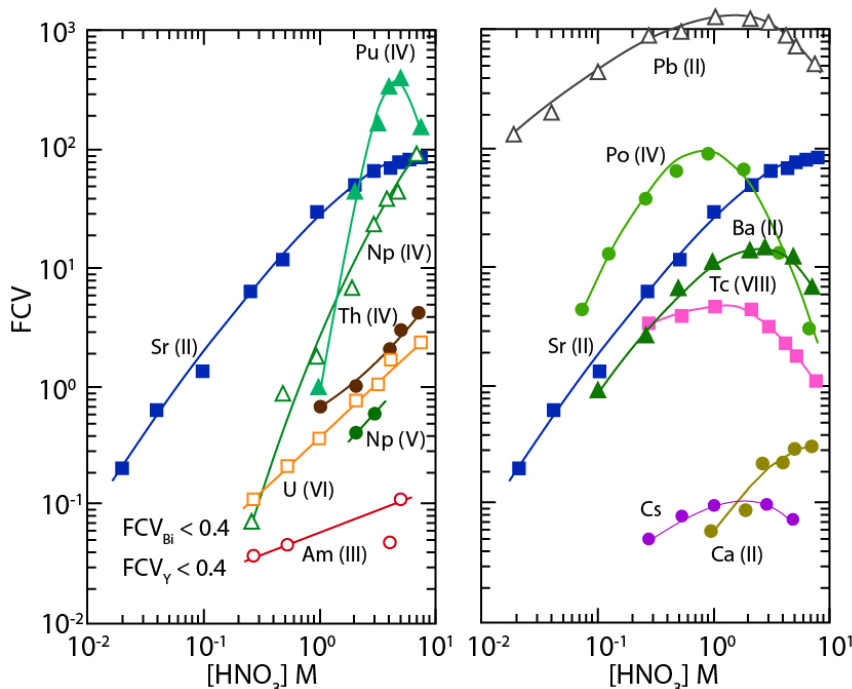


Figure 3.2.
Sr resin acid dependency graphs

Modified from Horwitz et al. (1992). Graphs show acid dependency for actinides and select elements on Sr resin (FCV) differs with nitric acid molarity. FCV – free column volume to peak elution

Pinn and Bassin (1992) stated that Sr-spec resin is capable of isolating Sr from most major and minor elements found in silicate rocks. However, Ba proves more difficult and is retained by the Sr resin more effectively. Barium affects sample ionization because it is easily ionized and so it decreases the electron work function of filament material which could, in turn, suppress Sr ionization (Pin and Bassin, 1992). Horwitz et al., (1991) identified this problem as well, stating that even by changing the load composition to 2 M HNO_3 - 0.5 M $\text{Al}(\text{NO}_3)_3$, some Ba would still remain unseparated from Sr. Horwitz et al.'s solution was to use a smaller mean particle diameter (75 μm), a load solution of 3 M HNO_3 and a larger volume of wash solution. Pin and Bassin also found that Ba separation could be achieved by using longer chromatographic columns or by washing the columns with 7 M instead of 3 M HNO_3 . The paper concludes that Horwitz et al.'s Sr-spec resin provides some distinct advantages over traditional ion exchange separation techniques; namely efficiency, simplicity and high chemical recovery. Its use during geological research is appropriate due to its exceptional separation of Sr from Rb and Ca.

Sr-spec resin was investigated in a nuclear context by Gjeçi (1996). Gjeçi stated that previous methods of Sr separation, specifically by precipitation, would take about 30 days. In the context of a nuclear incident, which causes the release of ^{90}Sr into the environment, this may be inadequate. Gjeçi noted that Horwitz et al.'s Sr-spec resin (which had been made commercially available at the time of Gjeçi's study) was, however, highly expensive in comparison to other techniques. Gjeçi used milk, bone, grass, soil and sediment matrices for his research. Preparation of matrices for Sr separation differed depending on matrix type, however each underwent a leaching or digestion process followed by a pre-concentration procedure using oxalic acid to form precipitates. As per Horwitz et al., (1991) each sample matrix, spiked with ^{90}Sr , was loaded into Sr-columns in 3 M HNO_3 . The columns were washed with 90 mL of 3 M HNO_3 to remove non-retained elements and complexes, before strontium elution with 30 mL of distilled water. The eluates were then counted by liquid scintillation counting (LSC) to ascertain ^{90}Sr recovery. The results proved that the separation of Sr by extraction chromatography from various matrices that would be investigated in immediate aftermath of a nuclear incident is highly efficient. In comparison to other methods, the use of Sr-spec resin and the associated processes described by Gjeçi take a much shorter time (less than a week).

Chapter 3

Maxwell et al., (2016) recognised that expedited methods for the determination of Sr in a variety of materials could potentially benefit the nuclear decommissioning sector. This increases the scope of use from just a pure emergency response. Maxwell et al.'s 2016 research used two extraction chromatographic materials; DGA resin (N,N,N',N'-tetraoctyldiglycolamide) and Sr-spec resin on concrete matrices. Both were used in 2 mL cartridges at a particle size of 50-100 μm . Samples of concrete were prepared by crushing and sieving before the radiotracer ^{90}Sr was added. In addition, Maxwell et al. also sought to test the removal of potential interfering radionuclides, namely ^{137}Cs , by adding MAPEP 32 soil (from Department of Energy Radiological and Environmental Sciences Laboratory) to the crushed concrete.

The method used to digest the concrete sample was fairly complex. Maxwell et al.'s method required fusion with NaOH, precipitation with $\text{Fe}(\text{OH})_2$ (added as $\text{Fe}(\text{NO}_3)_3$) and 3.2 M $(\text{NH}_4)_2\text{HPO}_4$ before dissolution of the solid in HCl. HF was used to precipitate CaF_2 (and therefore SrF_2) to remove Fe in the supernatant solution before final dissolution of Sr in HNO_3 . The final load solutions were formed of highly concentrated (8-9 M) HNO_3 . On Sr resin, Sr is retained on the columns at high HNO_3 concentrations, and elution was carried out using 0.05 M HNO_3 to prevent Pb elution.

The purpose of the DGA resin was to purify ^{90}Y after a period of ingrowth. It separated ^{90}Y from ^{89}Sr and ^{90}Sr . After Sr separation with Sr Resin, the eluate (in 0.05 M HNO_3) was transferred to planchets and evaporated to dryness. They were then counted for ^{89}Sr and ^{90}Sr on a gas flow proportional counter. After this, the yttrium carrier was added to the planchet and the planchet solids were dissolved in 8 M HNO_3 . This 8 M HNO_3 solution was then added to the DGA resin to purify the ^{90}Y , and ICP-MS was used to establish chemical yield.

The results of this study showed fairly inadequate Sr recoveries when using the sample preparation technique without phosphate addition during the initial precipitation step and passing through Sr-spec columns. Recoveries of around 50% were recorded for this method. Sr carrier yield was increased by over 10% to an average of around 65% yield on addition of PO_4^{3-} during the precipitation step. However, Maxwell et al. state that this yield is still inadequate for the purposes of their study. Additional HF was added in case, due to the excess Ca present in concrete, the HF amount was a limiting factor in SrF_2 precipitation.

This alteration to the method had little effect on recoveries, in fact the average yield decreased marginally. In response, Maxwell et al. added a larger quantity of phosphate in the precipitation step with Fe(OH)_2 . Sr recoveries were increased after this, with average yields of >75%.

A rapid method of collecting ^{90}Y was also described directly from the concrete sample. Concrete sample aliquots were loaded onto stacked TRU Resin and DGA Resin columns. Pu, U, Th and Bi were removed in the TRU column and the Y was separated from all other interferences using the DGA column. Y elution was performed using 0.25 M HCl. Maxwell noted that from the point of ^{90}Sr separation, the decay of ^{90}Y is roughly 1% per hour, however due to the rapidity of the separation process, counting can occur very soon after the removal of strontium. The test results show an 80% recovery efficiency. From this and using the precise time of measurement from Sr separation, ^{90}Sr concentration in the original concrete sample can be determined.

3.1.1.2 TK100

Surman et al. (2014) used Sr resin to create a selective chromatographic material for use at lower pHs. As mentioned previously Sr-resin consists of a 1 M 4,4'(5')-bis-t-butylcyclohexano-18-crown-6 (DtBuCH18C6) in a 1-octanol solution. Surman et al. (2014) exchanged this octanol for HDEHP (di(2-ethyl-hexyl)phosphoric acid). In this solution, the metal cation (Sr^{2+}) exchanges with the H^+ ion from the HDEHP to force the metal cation into the organic phase. HDEHP therefore binds strontium ions at environmental pHs and this molecule is separated by size exclusion on the 1M DtBuCH18C6 crown ether. Much like standard Sr resin, washing of the column to separate Sr from other radionuclides and interferences is optimal with 8 M HNO_3 . The binding of Sr to the TK100 resin was found to be lowest when using solutions of 2 M HCl, so it was concluded that this was the best reagent to use for elution (Triskem International, 2015b).

Surman et al. (2014) showed that a range of alkali and alkaline earth metals had a high affinity for the TK100, and like Sr resin, these were removed from the resin completely during the 8 M HNO_3 column washing. Uranium and lead were not detected in any of the washing or eluate solutions indicating that, like Pb on Sr resin, they are both strongly retained on TK100 resin. The design and manufacture of this resin is highly important to environmental study. It shows that Sr separation can be completed on environmental

Chapter 3

water samples without any pre-treatment, negating the need for acidification of samples prior to extraction chromatography. This shortens sample preparation time and lowers manual handling and exposure to workers. However, when investigating solid samples, pre-treatment digestion and dissolution processes must be completed, and these are often facilitated by acid leaching. Therefore, for the present study, TK100 will not be applicable when investigating Sr separation from materials such as concrete or steel.

3.1.1.3 Cost effective Sr separation techniques

Alternative separation techniques to the use of Sr resin was described by Yang et al (2017). This new method was investigated due to the high cost of Sr and DGA resins. Yang et al stated that alternative methods than that of extraction chromatography were still important and perhaps key to the cheap characterisation of radioactive wastes.

Samples of cement were leached and acidified in 1% HNO_3 before spiking with ^{90}Sr and ^{90}Y and a stable Y tracer. Y and Sr was then precipitated with the formation of hydrous titanium oxide (HTiO). After the precipitate was separated from the supernatant solution and re-dissolved in HCl, further precipitation was completed using concentrated HF to form YF_3 precipitate. The samples are then counted by Cherenkov counting. To ensure complete ^{90}Y ingrowth the leached cement solutions are kept for 2 weeks prior to measurement. ^{90}Sr is then calculated from this activity. Mean chemical recoveries of ^{90}Y were $86 \pm 8\%$.

Although cheaper processes are available, for the purpose of decommissioning, accurate activities must be attained to correctly characterise the waste present. Sr resin's high selectivity for Sr and the high chemical recoveries produced in much of the research using Sr resin, make it the primary candidate for use in the research to be undertaken. As shown by Maxwell et al (2016), the method of sample preparation is also key in producing good Sr recoveries. In order to ensure minimal losses during the digestion/dissolution stage, precipitation techniques are best avoided. It seems that the separation of the precipitate from the supernatant are the main cause of losses during these techniques. Using an aqua regia digest is the most promising method of digestion of cement. *Aqua regia* is effective at dissolving the calcium carbonate in the cement. However, the aggregate in the concrete is often composed, in large part, of quartz. Quartz is insoluble in *aqua regia* but due to the nature of the contamination, strontium is unlikely to penetrate the crystal structure (Broekmans and Jansen, 1998). Therefore, radiostrontium contamination will most likely

be surface contamination and digestion using aqua regia should still be adequate. The type of reagents used for sample preparation is also an important factor to consider in the design of a separation method. Acids like HF require extra care and training when used due to their hazardous nature, especially in comparison to *aqua regia*. This makes methods like Yang et al.'s less attractive, especially when trying to expedite the entire sample preparation process.

In order to remove organic matter that may have adverse effects on both sample preparation and analysis, the samples should be dry ashed. This is a relatively standard practice for non-volatile elemental analysis of samples that could contain organic matter (Mitra, 2003). For a 50 g sample of crushed concrete, ignition at 450 °C for 12 hours seems adequate as losses of Sr during ashing to remove organics are minimal for extended periods of time (Edward et al., 1990).

3.1.2 Separation of actinides

3.1.2.1 Anion exchange resin

Observation of ion exchange was first published by H.S. Thompson (1850), who found that ammonium sulphate was absorbed by soils and was not washed out by water. Thompson found that much of the ammonium sulphate had been converted to calcium sulphate (Sillanpää and Shestakova, 2017). This phenomenon was further explored by J.T. Way (1850) who demonstrated that the silicates in the soil supporting calcium were involved in an ion exchange mechanism whereby the ammonium ion substituted for the calcium forming ammonium soil compounds and calcium sulphate. This is of course a cationic exchange mechanism however it provided a basic understanding for the mechanism which takes place in ion exchange reactions. Initial large scale inorganic ion exchangers were successfully applied to water softening plants, replacing naturally occurring ion exchangers (zeolites) (Schubert and Nachod, 1956). The concept of polystyrene supported ion exchangers was developed in 1944 by D'Alelio whose resins were later improved allowing for greater capacity and mechanical stability (D'Alelio, 1944; Schubert and Nachod, 1956).

The production of ion exchangers is currently based around the polymerisation of styrene, with the addition of variable amounts of divinylbenzene. Divinylbenzene is used as a cross-linking agent, between the polystyrene chains (Figure 3.3). Generally, an increase in the

Chapter 3

divinylbenzene content of the resin leads to an increase in the capacity of the resin. Increased cross-linkages also increases the overall stability, density and resistance to deformation and particle breakage (Tooper and Wirth, 1956).

Early anion exchangers were prepared from aromatic amines and formaldehyde, and produced a weakly basic anion exchanger (Tooper and Wirth, 1956). Latter products containing aliphatic amines were more strongly basic, yet still only able to operate effectively in acidic conditions (Tooper and Wirth, 1956; Wheaton and Harrington, 1953). The development of anion exchangers utilising quaternary amines as an active site allowed for effective operation over a much wider pH range and allowed for complete deionisation of water when used in combination with cationic exchangers (Bajpai, 2018; Bauman and Robert, 1952; Mcburney, 1952).

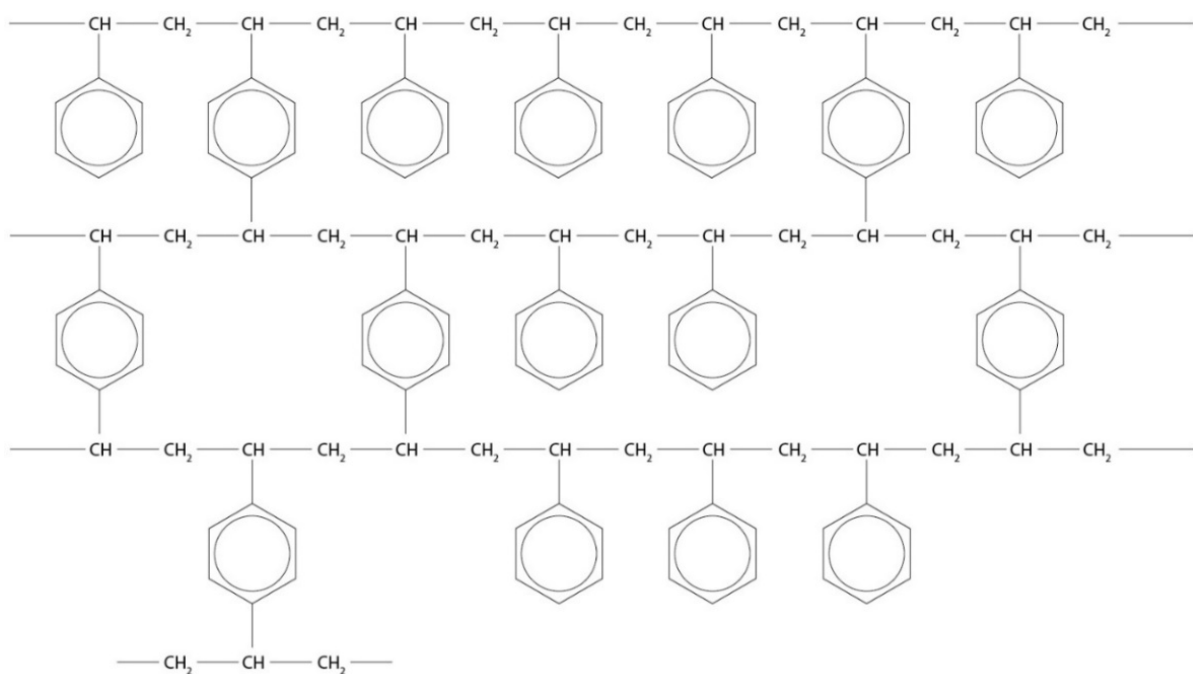


Figure 3.3.

Polystyrene DVB structure

Schematic showing polystyrene structure with divinylbenzene cross-linkages

Anion exchange resins have been utilised in a wide variety of contexts including protein purification, deionisation of water and inorganic purification of a variety of elements for radiological and stable elemental analysis (Carswell, 1957; Sillanpää and Shestakova, 2017; Sober and Peterson, 1954). For anion exchange resins, two quaternary amines are used as

the active sites; trimethylamine (Type I) and dimethylethanolamine (Type II) (Figure 3.4). They are formed by initial chloromethylation with methyl chloromethyl ether using a Friedel-Crafts type catalyst before amination with the desired amine (Tooper and Wirth, 1956).

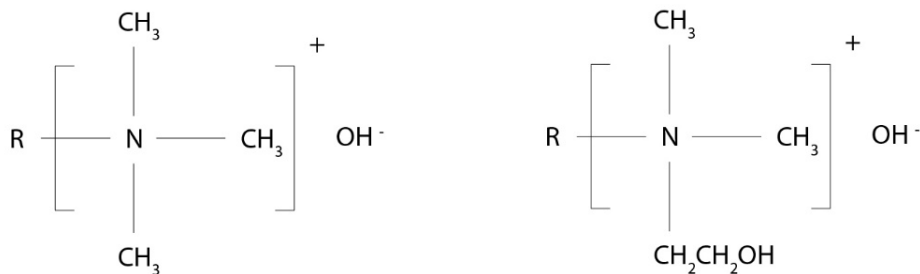


Figure 3.4.

Anion exchange resin quaternary amines

Type I and Type II anion exchange resin quaternary amines (left and right respectively)

The use of anion exchangers for the separation of actinides has been well documented. Separation of uranium and thorium nitrates were performed by Carswell et al., (1957) using strongly basic anion exchange resin De-Acidite FF (Naushad et al., 2013). Loading of thorium was achieved in 4 M HNO₃ from a solution of both uranium and thorium. Thorium sorbed to the resin, however the uranium passed straight through. Elution of the thorium was completed using water for collection in its own purified fraction.

Work by Ryan and Wheelwright (1959) showed that plutonium was adsorbed to anion exchange resin (Dowex 1 X-4) and yielded higher K_d values in calcium nitrate than in nitric acid solutions. However, Ryan and Wheelwright also stated that equilibrium in the calcium nitrate solution took significantly longer to be achieved than the nitric acid solution. Plutonium separation from uranium using anion exchange resin has been demonstrated by Navratil (1978). Thorium separation from plutonium can be achieved on an anion exchange column in hydrochloric acid as Th is not retained but plutonium is strongly adsorbed. Elution of plutonium can then be completed on addition of hydrobromic acid (Larsen and Oldham, 1975). The use of hydrobromic acid reduces the plutonium sorbed to the anion exchange resin from its (IV) form to (III) which is not retained on the resin. The use of ammonium iodide in hydrochloric acid has also been reported to reduce the plutonium on anion exchange in order to elute it (Warwick et al., 1999).

3.1.2.2 TEVA resin

TEVA resin was first synthesised by Horwitz et al., (1995) during a study into the use of tandem column arrangements where the eluate of one chromatographic column served as the load solution for subsequent columns. TEVA resin utilises a liquid anion exchanger sorbed onto an inert polymeric support. The liquid anion exchanger used is commonly known as Stark's Catalyst or Aliquat® 336 and consists of a mixture of trioctyl and tridecyl methyl ammonium chlorides with C₈ predominating (Horwitz et al., 1995; Litaiem and Dhahbi, 2015)(Figure 3.5). The polymeric support used was Amberchrom CG-71ms, a commercially available acrylic ester polymer. The method of adding the quaternary amine to the inert support is very similar to the method of bonding the crown ether of Sr resin to its inert support and is described in Horwitz et al., (1990). They took the polymeric support and washed it using water followed by methanol several times, drying the polymer under vacuum after each wash. The purified resin was then contacted with the liquid anion exchanger in methanol and thoroughly mixed during rotary evaporation of the methanol (Horwitz et al., 1990). This ensures homogenous coverage of the extractant on the polymer resin. It was found that re-suspension of the almost dry TEVA resin in a small amount of methanol before repeating the evaporation led to sufficiently homogenous extractant coverage (Horwitz et al., 1995).

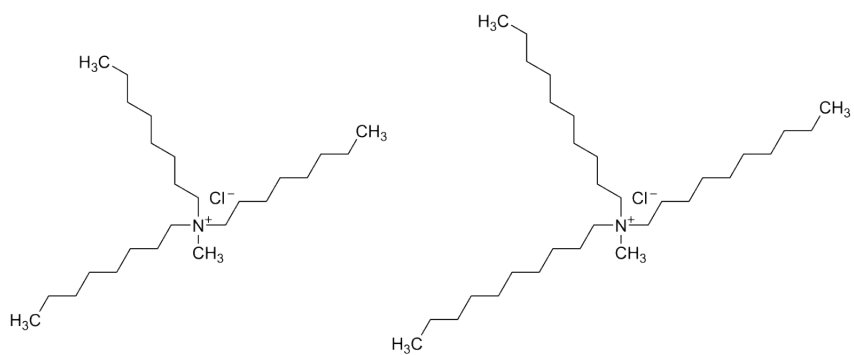


Figure 3.5.
Aliquat® 336 structure
 Trioctyl and tridecyl methyl ammonium chlorides

Horwitz et al., (1995) stated that an actinide adsorbing material, TRU resin had been synthesised in a similar fashion to TEVA resin, with the extractant being octyl(phenyl)-N,N-diisobutylcarbamoyl-methylphosphine oxide (CMPO) in tri-n-butyl phosphate (TBP). It was found that the separation of actinides from matrices and pre-concentration before

measurement yielded good recoveries and efficient results. However, the differences in elution behaviour between the actinides from the TRU resin were not sufficiently different as to permit single column purification of individual actinides (Horwitz et al., 1993). Horwitz et al., (1995) utilised previous work by Horwitz and Bloomquist (1974) which showed that tetravalent actinides had higher affinity for the liquid anion exchanger Aliquat® 336 than trivalent or hexavalent actinides did. This means that although both TRU and TEVA resins can effectively sorb actinides from nitric acid media, isolation of individual actinides is only possible when using TEVA resin.

Publication by Horwitz et al., (2005) detailed the synthesis of another actinide adsorbing extraction chromatographic material – DGA Resin. The resin is available in two forms; Normal and Branched depending on the diglycolamide molecule used. The molecules *N,N,N'N'*-tetra-n-octyldiglycolamide (TODGA) and *N,N,N'N'*-tetrakis-2-ethylhexyldiglycolamide (TEHDGA) were used to make Normal and Branched DGA resin respectively. The diglycolamide molecules were bonded to an inert support (Amberchrom CG-71) by a similar method to that of TEVA and Sr resins. Horwitz et al., (2005) show that the resins produced have a good uptake of tetravalent actinides as well as trivalent actinides (specifically Am (III)) in HNO₃. Other trivalent species adsorbed to DGA resin in nitric acid include yttrium, bismuth, europium and cerium (used as an analogue for actinium). The affinity for trivalent species as well as tetravalent make DGA resin's use more appropriate in conjunction with other chromatographic resins in series such as TEVA resin as suggested by Horwitz et al., (2005). The technical documentation for DGA resins (both Normal and Branched) state the main applications for DGA resin is for the separation of Actinium and Americium, not for the separation and purification of tetravalent actinides (Triskem International, 2015c). The analytical methods for DGA resin suggests the use of this chromatographic material in series with other chromatographic materials, for the separation and purification of actinides and radium (Triskem International, 2019a, 2019b, 2014). In the suggested methods for DGA resin, the separation and purification of Pu, Th and Np is achieved by using a TEVA resin cartridge.

The nitric acid dependencies calculated used the number of free column volumes to peak elution to represent retention on the column. In the product literature a conversion factor of 1.97 is provided in order to convert the free column volume to peak elution value to a distribution coefficient value (calculated using Equation 1.4) (Figure 3.6).

Chapter 3

TEVA resin has been used for the separation of actinides from a variety of matrices in combination with other resins (UTEVA, TRU, DGA) due to the high adsorption of Pu, Th and Np in nitric acid (Maxwell and Nichols, 1998; Maxwell III and Culligan, 2006; Maxwell et al., 2011a, 2014). Maxwell et al., (2011a) studied actinide separation from concrete and brick samples using a three column set up to separate Pu, U and Am for rapid analysis of these alongside Np and Cm. The study utilised a rapid fusion technique for total dissolution of sample before separation using TEVA, TRU and DGA columns and analysis by alpha spectroscopy. Tracer yields of around 90% and 77% were achieved for Pu and U respectively (Maxwell et al., 2011a).

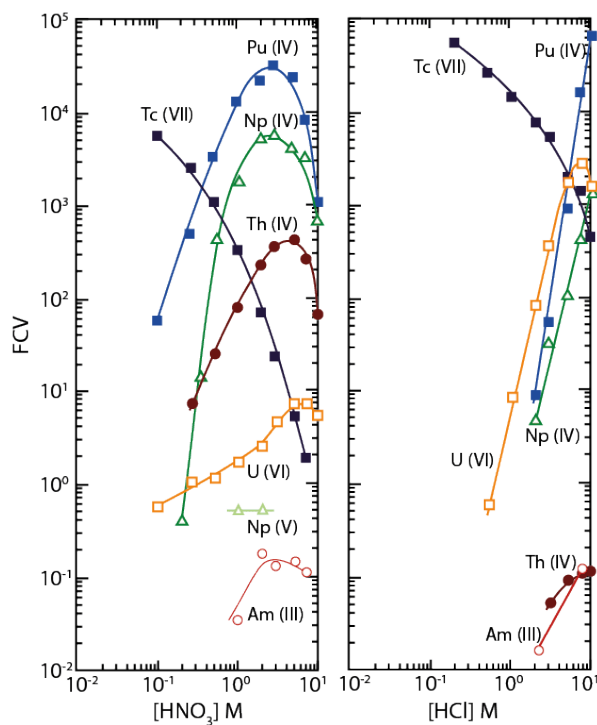


Figure 3.6.
TEVA resin acid dependency graphs

Acid dependency of select radionuclides in nitric and hydrochloric acid on TEVA resin. FCV – free column volume to peak elution.

3.1.2.3 UTEVA resin

Methods for the isolation and purification of uranium using solid phase chromatographic extractants initially focussed on the use of the organophosphorous extractant tri-*n*-butyl phosphate (TBP). This was due to ion-exchange's lack of specificity (Horwitz et al., 1992b). Warf, (1949) was the first to report extraction of uranyl nitrates by TBP. Hamlin et al., (1961) used powdered Kel-F (polychlorotrifluoroethylene) to support TBP, attaining

recoveries of uranium above 99%. Although uptake was very good, the TBP cannot separate U from other actinides from Pu and Th. Huff, (1965) published a method whereby an anion exchange column was used in conjunction with a TBP coated support for separation of Pu, Th and U for analysis of uranium alloys.

Development of a slightly different extractant based on TBP was undertaken by Mason and Griffin (1980). Their study showed that phosphorous based extractants which had a similar structure to that of TBP could be altered in order to enhance U extraction capabilities. One of the materials identified was diethyl amylphosphonate (DAAP) (Figure 3.7). It was found to function effectively in nitric acid solution allowing for use alongside other chromatographic materials if supported on a resin and used in a series of chromatographic columns (Horwitz et al., 1992b). The low U K_d 's at low acid concentrations allows for simple elution creating a purified uranium fraction that requires minimal pre-treatment before measurement. DAAP is insoluble in water which gives good stability on the column throughout the separation and leads to relatively inexpensive resin synthesis. All of these factors were taken into account when selecting the extractant for the UTEVA resin.

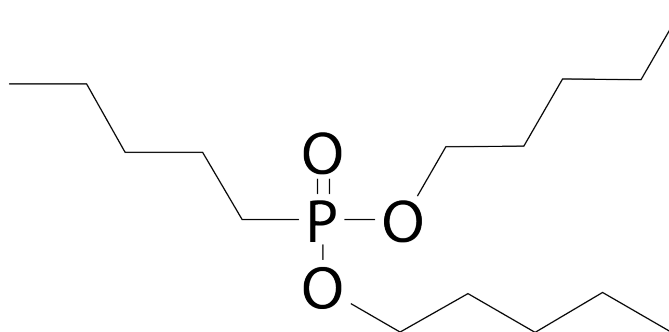


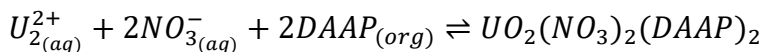
Figure 3.7.
DAAP structure
Diethyl amylphosphonate

Horwitz et al., (1992b) took DAAP and coated polymer resins Amberlite XAD-7 and Amberchrom CG-71ms in a similar fashion to the way Aliquat® 336 is supported in TEVA resin (Horwitz et al., 1990) (section 3.1.2.2). The selection of the two support materials (Amberchrom CG-71ms being Amberlite XAD-7's smaller particle size analogue) was based on a study comparing a variety of support materials including porous glass, polyethylene and styrene-DVB polymers (Warshawsky and Patchornik, 1978). The study concluded that Amberlite XAD-7 had high capacities for various extractants, especially Alamine 336 for

Chapter 3

which it had 3 times the capacity in comparison to porous glass and 23 times the capacity than a styrene 8% divinylbenzene copolymer. Horwitz et al., also stated that the Amberlite resin used was more stable during acid washing in comparison to other materials in the XAD series.

The work completed by Mason and Griffin (1980) showed that the uranium extraction by DAAP follows the equation:



Equation 3.1.

Equation for the uptake of U by DAAP

As indicated from the equation and as found by further study, U sorption to DAAP increases with increasing nitric acid concentration. This trend occurs up to around 4 M HNO₃ where the distribution ratio reduces. Mason and Griffin posit that this reduction in sorption is most likely due to a combination of activity effects, the formation of uranium nitro complexes in the aqueous phase and a reduction in free extractant concentration (Horwitz et al., 1992b; Mason and Griffin, 1980). Work done by Horwitz et al., (1992b) on the UTEVA resin in a column showed that peak sorption of uranium on the solid phase occurs at 6 M HNO₃ and significant sorption of uranium was achieved from nitric acid concentrations as low as 1 M (Figure 3.8). The performance of the UTEVA resin over this wide range of acid concentrations allows for uptake of U from a wide range of acid concentrations. Additionally, the low distribution ratios at dilute nitric acid concentrations (around 0.05 M) allow for simple elution of U after isolation on the column. Horwitz et al., (1992b) noted that the acid dependency of U on UTEVA made for a much simpler separation procedure than other U separation systems at the time, which often required the use of different eluents such as phosphoric acid, perchloric acid and hydrofluoric acid to strip U.

Study of the acid dependency of other actinides showed that Pu, Np and Th exhibit significant affinity for the UTEVA column. Pu shows the strongest affinity, with Np and Th affinities comparable to that of U. Thorium uptake is slightly lower than that of U, the most significant divergence occurring at 1 – 2 M HNO₃. This is demonstrated during isocratic elution of a solution of U and Th, whereby the Th is eluted significantly sooner than that of

U in a 2 M HNO_3 solution. Separation of U from Np on UTEVA requires oxalic acid, in which Np sorption to UTEVA is reduced significantly (Horwitz et al., 1992b).

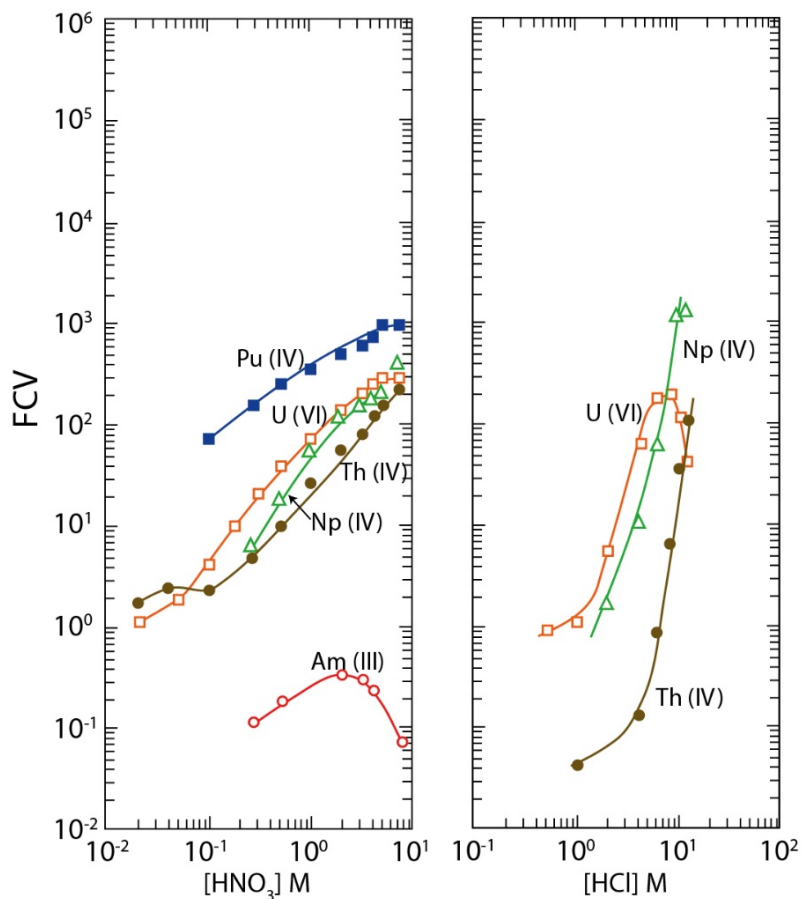


Figure 3.8.

UTEVA acid dependency graphs

Adapted from Horwitz et al., (1992b). FCV – free column volume to peak elution

Acid dependency in HCl shows U has good uptake, comparable to that of the maximum in HNO_3 at 7 M HCl. Uranium sorption declines more steeply with a reduction of HCl concentration in comparison to HNO_3 (Figure 3.8). The differences in sorption values between U and Np at 4 M HCl and between U and Th at 7 M HCl theoretically allow for sequential separation of these actinides on a single UTEVA spec column. However, due to the sensitivity of U sorption in HCl, acid concentrations must be tightly controlled in order to prevent simultaneous elution of the sorbed actinides (Horwitz et al., 1992b).

Initial use of UTEVA proved its applicability to the nuclear sector as two reports utilised it in studies relating to spent nuclear fuel. Smith et al., (1995) utilised UTEVA resin for the separation of uranium and lutetium, which UTEVA is also able to adsorb. Li et al., (1995) utilised UTEVA to recover uranium and plutonium from dissolved solutions containing

Chapter 3

fission products. Li et al., (1995) found that effective and rapid separation of uranium and plutonium was achievable through the use of UTEVA. Application of UTEVA to the separation of U from geological matrices by Carignan et al., (1995) proved its use in wider geochemical research.

Work by Croudace et al., (1998) utilised UTEVA resin in the development of a rapid procedure for U and Pu determination from soils and sediments. Uranium and plutonium separation and isolation was completed using two columns in series, the first being an anion exchange resin and the second being a UTEVA column. This two-column system was employed in order to remove plutonium from the load solution onto the anion resin, and allow uranium to pass onto the UTEVA column and sorb there. The use of two columns in this way was first reported by Warwick et al., (1999) for the separation of Pu and U from aqueous samples. Croudace et al., (1998) found that the system was able to effectively separate both Pu and U from a borate fusion digest yielding accurate and precise results. More recently, study into the use of TEVA and UTEVA resins for the measurement of ultra-trace levels of U and Pu has been undertaken. Metzger et al., (2019) analysed the U and Pu via HR-ICP-MS (high resolution inductively coupled mass spectrometry) and multi-collector-ICP-MS and was applied to the measurement of cotton swipe samples taken during environmental sampling. Measurements of isotopic ratios of selected certified reference materials agreed well with the certified values. The method developed by Metzger et al., (2019) was also reported to be significantly faster and reduced the use of certain reagents by 35%.

Chromatographic material	Active site	Elements selected	Useable conditions and uses	References
Sr-Spec Resin	Crown ether DtBuCH18C6	Sr, Pb	0.05 - 10 M HNO ₃ . For Sr separation from highly acidic matrices	(Horwitz et al., 1991)
TK100	Crown ether DtBuCH18C6 with HDEHP	Sr, Pb	Sr adsorbed in environmental pHs, with washing completed using 8 M HNO ₃ and elution using 2 M HCl. Primarily used for Sr isolation and pre-concentration from filtered raw or acidified water samples.	(Surman et al., 2014)
Anion exchange resin	Quaternary amines	Tetravalent actinides and Au in HNO ₃ . In HCl - a range of elements from periods 4-7 and groups 4-13 including PGEs and as well as Uranium	pH 0 – 14. Multiple uses including water purification, and separation of selected elements from acidic and basic solutions.	(Saito, 1984; Tropper and Wirth, 1956)
TEVA resin	Trioctyl and tridecyl methyl ammonium groups (long chain quaternary amines)	Tetravalent actinides in HNO ₃ , Pu, U, Np and Tc in HCl	0.05 - 10 M HNO ₃ and HCl. Separation of tetravalent actinides from highly acidic samples and digests.	(Horwitz et al., 1995)
UTEVA resin	Diamyl amylphosphonate	Tetravalent actinides and U(VI) in HNO ₃ . Np, U and Th in HCl	0.05 - 10 M HNO ₃ and 0.5 - 10 M HCl. For the separation of Uranium from acidic digests.	(Horwitz et al., 1992b)

Table 3.1. Summary table of chromatographic materials

Table includes TK100 which was not used in this research as it does not have specific relevance to highly acidic digest samples, like those used in the analysis of nuclear waste.

3.2 Decay counting techniques

Recently, there has been interest in the quantification of longer-lived radionuclides in nuclear waste. The activity of all radionuclides is inversely proportional to their half-life. As such, longer-lived radionuclides require more sensitive analytical techniques than their shorter-lived counterparts. Their activity may not be of key importance during the working lifetime of a nuclear facility, however, due to the time spent in waste repositories, longer-lived radionuclides contribute significantly to the dose estimates post-decommissioning. Although ^{90}Sr does not have a significantly long half-life, in comparison to other fission products its specific activity is low, and its abundance in materials present at nuclear facilities make it important to decommissioning processes. Beta counters are often unable to resolve all spectral interferences so other radionuclides that are present may produce significant masking interferences for the measurement of ^{90}Sr . For this reason, even when measuring by radiometric analysis, it is important to separate Sr (and, therefore, the ingrowing Y) from other radionuclides in the sample. Generally, in radiochemical studies of nuclear waste, the radiostrontium isotope of interest is ^{90}Sr . Also measured is ^{90}Y ingrowth from ^{90}Sr decay. Isotopes of uranium, thorium and plutonium that are present in nuclear wastes are often alpha emitters and often occur in conjunction with other alpha emitting contaminants. This can make resolution of alpha spectra and determination of individual activities difficult or even impossible from an unseparated sample. Measurement by mass spectrometric techniques are also aided by separation and isolation as elements of similar mass can disrupt quantification of target radionuclides. Here, the measurement techniques used for the research are explained in order to provide insight into the reasons for their selection.

3.2.1 Liquid scintillation

Liquid scintillation is commonly used for detection and quantification of low energy beta emitters but can be used for high energy beta emitters as well as alpha and occasionally gamma emitters (Vitkus et al., 2021). The sample is placed in a scintillation vial along with scintillation cocktail. The energy from the decay of the radionuclide within the sample is transferred to the molecules of the scintillation cocktail which then produce photons of light. The photons travel away from the scintillation cocktail molecule isotropically and are detected by photomultiplier tubes. Often a liquid scintillation detector will have two or

more photomultiplier tubes. These photomultiplier tubes function by collecting the photons using a photocathode and emitting electrons, which are then accelerated and multiplied by a series of dynodes. The detection and photomultiplication happens simultaneously in each photomultiplier tube for a single decay event. The electrical pulses produced by the photomultipliers are sent to a coincidence unit which then decides whether it has received two simultaneous pulses or only one pulse from the photomultipliers. If only one pulse is detected, the pulse is ignored. If two simultaneous pulses are received, they travel onto a multichannel analyser which sorts the pulses onto channels depending on the pulse energy. An amplification phase then takes place before the pulse is counted (Figure 3.9). The number of pulses is proportional to the amount of the radionuclide in the sample and the energy channel is proportional to the energy of the decay itself (Kramar, 2017; Vitkus et al., 2021).

Another use for liquid scintillation counters is Cherenkov counting. Cherenkov counting does not use a scintillation cocktail. It relies on light produced from high energy beta particles making pulses of light from the interaction with the solution that the radionuclide is contained in, if that medium is dielectric (L'Annunziata, 2003). If the beta particles move through the medium faster than the speed of light in that medium, the spherical wavefronts of the photons emitted from the medium overlap. The constructive interference resulting creates a cone of light called Cherenkov light. Counting efficiency for Cherenkov counting is 40%, however the background levels are exceptionally low due to the unusual way light pulses are created (Vajda and Kim, 2010). Cherenkov counting of ^{90}Y is a common technique used for ^{90}Sr analysis, as it is ^{90}Sr 's daughter isotope and it is a high energy beta emitter. Repeated measurements to observe ^{90}Y ingrowth can be used to increase confidence of chemical purity of the sample (Hou and Roos, 2008). In this thesis, Perkin Elmer 1220 Quantulus Ultra Low Level Liquid Scintillation detectors were used.

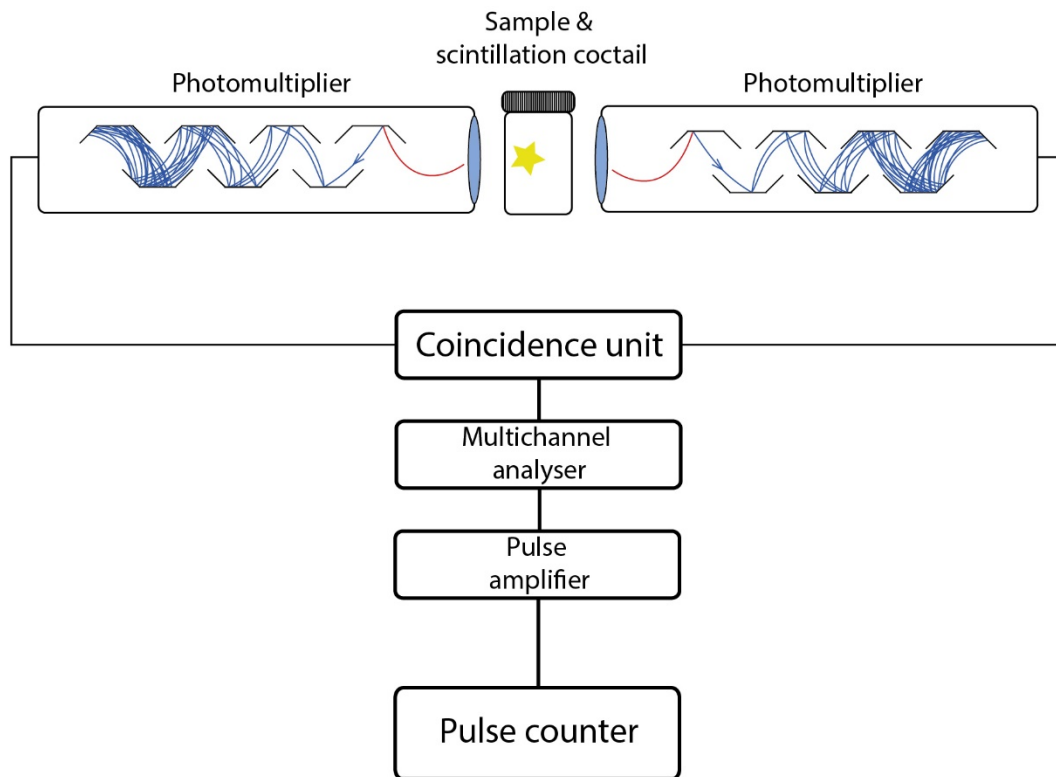


Figure 3.9.
Liquid scintillation counter schematic

3.2.2 Alpha Spectrometry

The alpha spectrometers used during this work were Canberra alpha analysts. These systems utilise PIPS (passivated implanted planar silicon) detectors, a type of semiconducting detector. In order to understand the workings of a semiconductor, it is first essential to understand the concept of the band structure of solids. In a free atom, electrons are arranged into distinct energy levels (orbitals). However, in solids which contain many atoms these energy levels are broadened into bands order to satisfy Pauli's Exclusion Principle. Pauli's Exclusion Principle states that no two electrons can have the same four quantum numbers (number used to describe the movement and trajectories of an electron). This also explains why electrons that share the same orbital must have opposing spins. The bands are separated by energy regions in which electrons cannot exist (termed the forbidden energy gap). The uppermost band in which electrons sit is termed the valence band (inhabited by valence electrons) (Gilmore, 2008). It is possible for electrons to move from one atom to another atom. However, to do this they must move to a higher energy level than the valence band. This is termed the conduction band.

Different materials have different gaps between the valence band the conduction band. Materials which have a large forbidden energy gap and a full valence band are insulating materials. Here, the energy required to move a valence electron into the conduction band is too great to move it all the way through the forbidden energy gap, so it remains in the valence band. Materials which have no forbidden energy gap and an unfilled valence band have a conduction band which overlaps the valence band. Here the electrons freely move in and out of the conduction band. If an external voltage is applied to the material an electric current will flow (Figure 3.10). These materials are conductors. Semiconducting materials, like insulators have a full valence band but the forbidden energy gap is very small. This means that under certain conditions, if an electron were to gain extra energy it could move into the conduction band and the material will be able to conduct electricity.

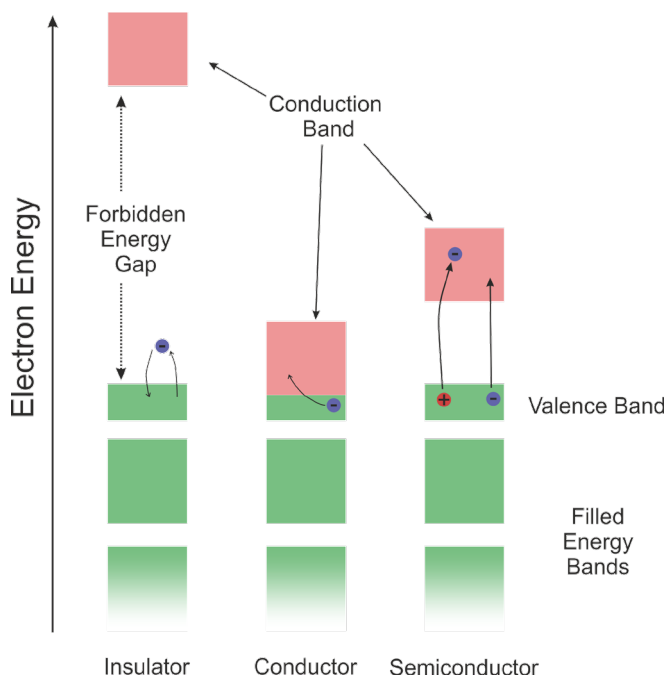


Figure 3.10.
Electron energy bands

Semiconductor detectors are composed of semiconducting materials. Silicon and germanium are two examples of such materials; however, they require different conditions in order to exhibit their semiconducting behaviour (room temperature for silicon and 80 K for Ge). As previously described, a material's semiconducting nature is due to the energy required to move the valence electrons into the conduction band. Silicon's valence electrons require roughly 1.115 eV at 293K. This intrinsic conductivity can be initiated by nuclear radiation, providing a valence electron with the energy required to move it into the

Chapter 3

conduction band. It is important to note however, that some energy is lost due to crystal excitation. The liberated electron (in the conduction band) leaves behind a positively charged Si ion which is termed a “hole”. Each liberation of an electron from a semiconductor atom creates an electron-hole pair. Both electrons and holes diffuse through the semiconductor transferring charge from atom to atom. If an electric bias is applied across the semiconductor, the electrons will flow toward the anode and the holes will flow towards the cathode.

To enhance the semiconductor, donor and acceptor atoms are added to the crystal. These are elements which substitute for Si in the crystal matrix. The donor elements have an excess of electrons which are weakly bound, much more so than silicon's valence electrons, allowing them to easily pass into the conduction band. Common examples of donor materials are phosphorous and arsenic. Doping with a donor element creates an *n-type* extrinsic semiconductor. Acceptor materials are ones which have fewer valence electrons than the surrounding material. This causes a vacant site to form in the crystal as the semiconductor (Si) has fewer electrons to bond with and therefore an incomplete octet structure. Electrons moving in the conduction band interact with the vacant sites and fill them in. This causes an excess of holes to form within Si-Si bonds and these outnumber the electrons in the conduction band. Examples of acceptor materials are boron, indium or gallium. Semiconductors doped with acceptor materials are termed *p-type* extrinsic semiconductors.

It is important to note that although the dopant provides an excess of either holes or electrons, the overall charge on the crystal irrespective of type is still neutral. This is easiest to understand by considering the following example. The dopant phosphorous in a silicon crystal provides one extra conduction band electron per atom. This extra electron travels through the crystal transferring from one Si atom to another. The charge of this excess electron however, is counter balanced by the positive charge which phosphorous now has due to losing the electron. The net effect on the n-type crystal charge is that it is neutral. In terms of net charge, the same is true for the p-type material. Each acceptor atom creates a hole by taking a silicon electron, but the acceptor atom itself becomes negatively charged. Therefore, the net crystal charge is neutral.

Juxtaposing these two types of semiconductor material so that they are contained within the same crystal brings about the most useful property of a semiconductor (Figure 3.11). The contact between the p and n-type contact is termed the *p-n junction*. In the area around this, a few holes migrate from the p to the n-type material and a few electrons migrate from the n to the p-type material. In doing so the migrated electrons then combine with the resident holes in the p-type material and destroy each other and the same for the migrated holes and resident electrons in the n-type material. This area is usually a few microns thick and is termed the *depletion layer*. As the layer is depleted in terms of electrons and holes the charges on the dopant atoms are revealed. This makes it difficult for diffusion of holes and electrons from one material to another. As an electron from the n-type material migrates across the p-n junction it is repelled by the negatively charged acceptor atoms of the p-type material and is forced back into the n-type. The same is true for the holes, they are repelled by the positively charged donor atoms. This means the depletion layer acts as an area of resistivity and charge carriers are required a certain energy (voltage) if they are to make it across the depletion layer. This energy is termed *barrier potential*.

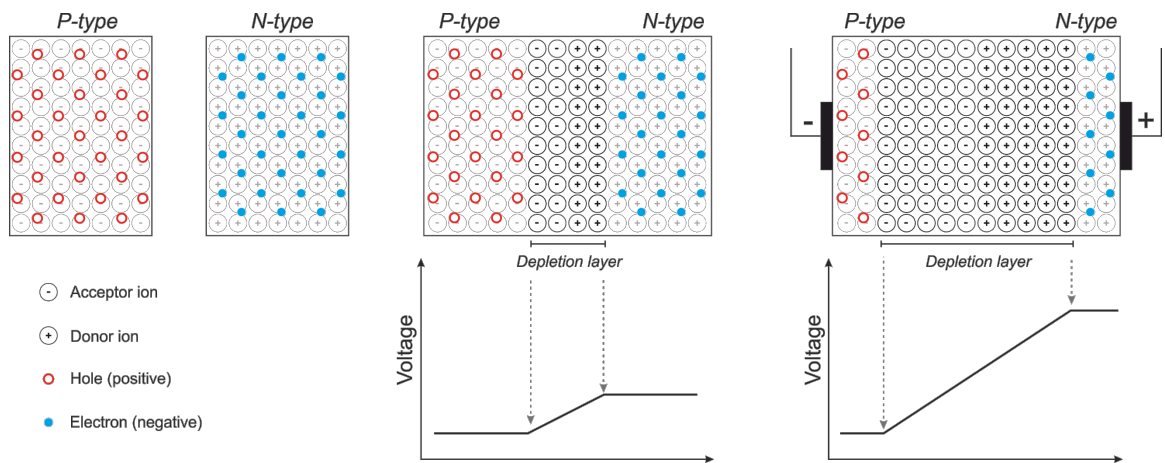


Figure 3.11.
Semiconductor diagram

To utilise this property effectively for radionuclide measurement, a reversed bias external voltage is applied across the crystal. The negative terminal connecting to the p-type material has the effect of attracting the holes (positive charges) and pulls them away from the p-n junction. The positive terminal connected to the n-type material has the same effect on the electrons. This causes an increase in depletion layer size. The size of the

Chapter 3

increase is directly proportional to the voltage applied across the semiconductor. If a 1 V is applied then the barrier potential increases by 1 V, effectively increasing the resistivity.

When an electron-hole pair is created in the depletion layer, they are each accelerated towards the opposing electrode and a current can be detected in the external circuit. If the depleted layer is exposed to ionising radiation, an electron from a Si atom is liberated and an electron-hole pair is formed. The higher the energy of the radiation, the more energy it will impart to the electron. This electron can then go on to liberate more electrons initiating a cascade-like production of electrons and holes and causing an even larger current to flow in the external circuit. Therefore, the current is directly proportional to the energy of the radiation.

Alpha spectrometers are usually surface barrier detectors, which are composed of a doped silicon diode wafer with a very thin depletion layer. The silicon is n-type with the exposed surface etched with gold ($\sim 40 \mu\text{g}/\text{cm}^2$) and the other coated in an equally thin layer of aluminium. These surfaces provide the electrical contact and are used to create a reversed biased semiconductor. The gold is used as the anode, and a voltage is set up across the silicon wafer to the aluminium cathode. As a result, a thin depletion layer is created in the silicon at and around the area of the etched gold layer. Alpha and beta particles can penetrate through the gold layer into the depleted silicon and liberate Si electrons creating electron-hole pairs which are collected at the electrodes.

In this study, samples are electroplated onto a stainless-steel disc and placed within 5mm of the detector. During measurement a vacuum is placed between the sample and detector as α energy is easily absorbed and will cause a reduction in measurement if a vacuum is not maintained. Counting efficiency is at most 50% as only one surface of the disc is exposed to the detector. Radiation emanating in the opposite direction or at angles acute to the disc on the exposed side do not interact with the detector and are not counted.

Alpha spectrometry is a commonly used analytical technique for alpha detection due to its relatively low cost, high sensitivity and simplicity (Hou and Roos, 2008). Measurement of Pu, Th and U is routine using alpha spectrometry, however separation of the actinides may be required to ensure most efficient counting (Thakur, 2017).

3.2.3 Gamma Spectrometry

The gamma spectrometers used for this research were High Purity Germanium (HPGe) semiconductor detectors. The theory behind the semiconductor is much the same as in the alpha spectrometers detailed in section 3.2.2. Electrons are liberated from the material of the detector through interaction with gamma rays produced by the radionuclide. The spectrum produced by a gamma spectrometer is very different to that of an alpha spectrum due to the way in which gamma rays (high energy photons) interact with the materials of the detector and its surroundings.

A theoretical spectrum (Figure 3.12) shows the signal on a gamma spectrum from a single gamma emitting radionuclide. Each individual peak is created from an interaction between the incident photon (carrying the gamma energy). The most basic interaction is the photoelectric effect, whereby the incident photon carrying energy E_γ , interacts with an electron in the material imparting all of its energy. This ejects the electron which carries a kinetic energy equal to that of E_γ minus the energy required to liberate the electron (known as the binding energy). The photoelectric effect usually occurs at low photon energies (<200 keV) (Mirion Technologies, 2021). When detected, the electron causes a count in the full energy peak region.

For photons carrying gamma energies of 200 to 2000 keV, the primary mechanism of interaction is Compton Scattering. This occurs when the incident photon interacts with an electron of the material it's travelling through and imparts less than 100% of its energy. The electron is ejected from the electron shell (as a "recoil electron"). However, the kinetic energy it has is less than E_γ minus the binding energy ($K.E. < (E_\gamma - E_{bind})$). The energy not imparted to the electron remains in the photon which is scattered. The angle at which the reduced-energy photon is scattered is based on the initial gamma energy and is predictable, with higher energy photons scattering in the forward direction. A gamma ray that enters the detector, undergoes multiple Compton interactions and ends up initiating a photoelectric event and a count is observed in the full energy region. If a gamma ray interacts via the Compton effect only once, there is a maximum energy that is detected. This is equivalent to the energy imparted by the photon at an angle of 180°. Lesser energies created by Compton interactions occurring at < 180° generate counts below the maximum Compton energy. This effect manifests as a Compton continuum on a gamma spectrum,

Chapter 3

with the maximum Compton energy resulting in a feature termed the Compton Edge (Figure 3.12). Incident rays which undergo multiple Compton interactions will have energies that sum above the energy of the Compton edge and create counts between that of the Compton edge and the full energy region (Mirion Technologies, 2021).

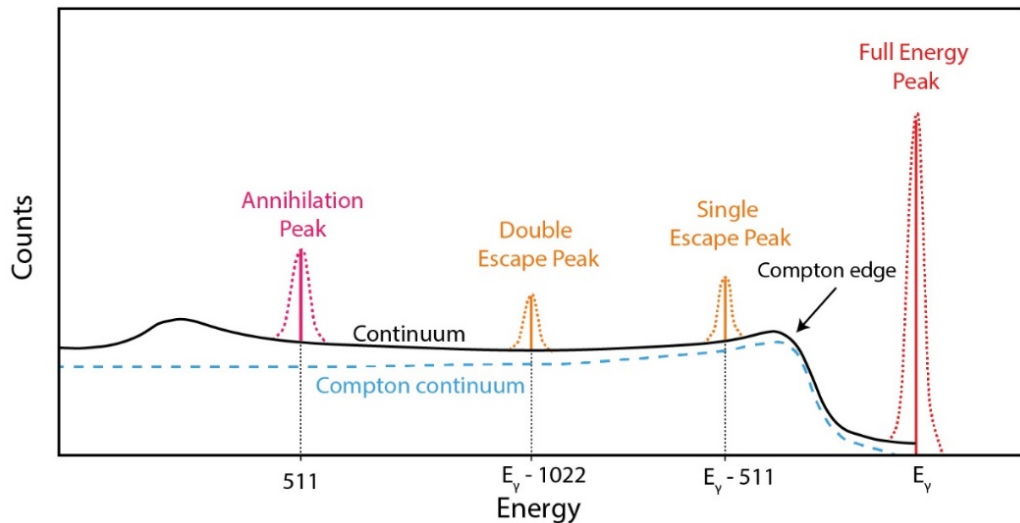


Figure 3.12.
Theoretical gamma spectrum

Adapted from International Atomic Agency (2021)

The final interaction occurs during the interaction of high energy gamma rays (usually >2000 keV, but certainly above 1022 keV). The incident photon passes through the material, within the vicinity of an atomic nucleus. This initiates the conversion of the electromagnetic energy to matter, producing a positron and an electron. The positron and electron each have a rest mass equivalent to 511 keV, which is why the incident photon must have an energy of at least twice that (1022 keV) in order to produce the pair. The electron continues to travel through the material with kinetic energy equivalent to $\frac{1}{2} E_\gamma$ minus the rest mass of the electron (511 keV). Secondary ionisation of other atoms in the detector material resulting from the kinetic energy of the electron produced will always be captured by the detector and represents the lowest energy captured in the interaction.

The positron travels until it meets an electron, annihilating themselves in the process. Two photons are produced by this interaction, each with an energy equivalent to the rest mass of an electron or positron (511 keV). It is possible that one or both of these annihilation photons escape the detector without further interaction with the material. If this happens, the full energy of the initial incident gamma ray will not be deposited within the detector.

If both annihilation photons react and deposit 100% of their energy within the material of the detector, they will produce a count within the full energy region of the spectrum. If one of the annihilation photons leaves the detector without further interaction and all of the other's imparted energy is fully contained within the material of the detector, a count will be produced with an energy of full energy peak – 511 keV. Once a significant number of single annihilation photon escapes occur, a peak in the gamma spectrum forms called a Single Escape Peak. If both annihilation photons escape the detector without further interaction with the rest of the energy fully contained a count with an energy of full peak energy – 1022 keV will be produced. Significant occurrence of this can result in the formation of a Double Escape Peak in the spectrum (Figure 3.12). Finally, if either annihilation photon undergoes Compton scattering, before leaving the detector, an indiscete amount of energy is deposited within the detector. This produces counts which contribute towards the Compton continuum (International Atomic Energy Agency, 2021; Mirion Technologies, 2021).

Use of gamma spectrometry in this study is primarily for measurement of ^{85}Sr which is used as a chemical yield tracer. Use of gamma spectrometry for Sr yield monitoring is a well-established technique and takes advantage of the gamma energy released during ^{85}Sr 's decay to ^{85}Rb (551 keV) (Be et al., 2004; Chen et al., 2002; Vesterlund et al., 2009).

3.3 ICP-QQQ-MS

An Agilent 8800 - an Inductively Coupled Plasma Triple Quadrupole Mass Spectrometer (ICP-QQQ-MS) was used to analyse stable element solutions. Mass spectrometers rely on ionised sample components being separated according to their mass-to-charge ratio (m/z) before reaching the detector. The number of counts detected in a certain time is proportional to the concentration of the isotope in the sample.

The samples in this study were solutions, introduced into the ICP via a nebulizer forming an aerosol and a spray chamber ensuring homogenous droplet size. Solid samples can be directly introduced without the need for dissolution by using Electrothermal Vaporisation (ETV) or Laser ablation (LA) (Carey and Caruso, 1992; Gray, 1985). Solutions were pumped into the nebuliser using a peristaltic pump and samples were selected using an autosampler.

Chapter 3

ICP-MS's utilise an argon plasma to ionise sample components. The plasma is created at the end of a quartz torch. The torch in the Agilent 8800 used consisted of three concentric tubes in once piece in an arrangement called a Fassel-type ICP torch (Thomas, 2004). The nebulizer gas which carries the droplets of sample from the spray chamber travels through the torch and into the plasma. Surrounding the end of the plasma torch is the radio frequency (RF) generator coil, which controls the movement of electrons in the plasma. The plasma is induced when a high voltage spark is applied across the plasma gas as it flows through the torch. This introduces free-moving electrons into the gas stream by stripping them from Ar atoms. The free electrons are then accelerated by the electromagnetic field set up by the RF coil.

The energy required to strip an electron from an Ar atom is 15.8 eV (first ionisation potential (M^+) given in electron volts). As this is the energy required to ionize the plasma gas, any element in the sample with an ionisation potential of less than 15.8 eV is likely to be ionised. Argon has the fourth highest first ionisation potential of all the elements in the periodic table whose ionisation potentials are known. There are multiple elements whose first and second ionisation potential are less than 15.8 eV. In this instance it is likely that doubly charged ions will be formed (M^{++}). This will cause a halving of the m/z and the ion will be detected as half its actual mass. This can cause an interference if an off-mass analyte within the sample has a mass of double the analyte of interest (Thomas, 2004).

The ions then travel from the plasma, through an interface zone and into the ion focussing zone. The ion beam is then purified and focussed using a series of lenses. In the case of the Agilent 8800, removal of photons, particulates and neutral species is completed using an off-axis omega lens. This method for the removal of undesirable particles and particulates from the ion beam is commonly termed a "Chicane design". After the omega lens, the ion beam is narrowed and focussed using an Einzel lens (Agilent Technologies Inc., 2015; Thomas, 2004).

The Agilent 8800 has two quadrupole mass filters in series with an octopole reaction/collision cell in between, giving the ability to remove isobaric and polyatomic interferences after sample uptake (Warwick et al., 2019). The mass filters consist of 4 molybdenum or stainless-steel rods set parallel to each other. Each opposing rod has a direct current (DC) and an alternating current (AC) placed on them creating an

electromagnetic field which steers the ions through the quadrupole. The ratio of AC/DC determines which m/z ratio will be electrostatically steered through the quadrupole, with all others being ejected from the ion beam, passing through the spaces between the rods (Somogyi, 2008; Thomas, 2004).

It is not uncommon for the plasma gas and sample matrix components to cause spectral interferences as their mass may be the same as the analyte of interest. In addition to these isobaric interferences, plasma gas derivatives and matrix components may form polyatomic compounds whose mass equates to the analytes. Some examples of these are given in Table 3.2. To try and reduce these, a cold plasma condition can be applied in order to reduce the formation of argon containing interferences. However, in many cases for reduction in matrix component interferences it is common to place a collision/reaction cell before the analyser mass filter. In the case of an ICP-QQQ-MS, this is between the first and second quadrupoles. The collision/reaction cell in the Agilent 8800 is an octopole, operated in RF mode as to not separate the masses inside the ion beam. Instead it acts as a focussing element, ensuring the ions are in the optimal position in order to interact with the collision/reaction gas.

Analyte	Polyatomic/Isobaric interference
^{56}Fe	$^{40}\text{Ar}^{16}\text{O}^+$
^{40}Ca	$^{40}\text{Ar}^+$
^{39}K	$^{38}\text{Ar}^1\text{H}^+$
^{51}V	$^{35}\text{Cl}^{16}\text{O}^+$
^{80}Se	$^{40}\text{Ar}_2^+$
^{52}Cr	$^{40}\text{Ar}^{12}\text{C}^+$
^{75}As	$^{40}\text{Ar}^{15}\text{Cl}^+$
^{55}Mn	$^{40}\text{Ar}^{14}\text{N}^1\text{H}^+$

Table 3.2.
Common isobaric and polyatomic interferences
 (Longbottom et al., 1994; Thomas, 2004)

Chapter 3

Using the octopole, the ion beam collides with the reaction/collision gas, with the ions interacting in different ways in order to remove the interference. Either the interfering isobaric or polyatomic ions will interact with the gas, altering them to a non-interfering species, or the analyte will interact and be converted to another species which does not have an interference.

The Agilent 8800 second quadrupole filters out all interferences from the reaction/collision cell and directs the ion beam towards the detector. The detector used in the 8800 is a dual-mode, Discrete Dynode Electron Multiplier (DDEM). This type of detector allows for high and low ion concentrations to be analysed in one scan (hence “dual mode”). The DDEM (Figure 3.13) operates off-axis and utilises individual dynodes to perform the electron multiplication. The off-axis position further lowers detector background noise originating from stray radiation and any neutral species still in the ion beam. Analyte ions interact with the first dynode liberating secondary electrons, which are accelerated towards the second dynode, liberating more secondary electrons. This process is repeated until the mid-point dynode. If a high enough concentration of analyte has entered the detector and reached a threshold number of counts at this mid-point, the signal is processed through analogue circuitry. If the threshold has not been reached, the signal cascade continues through the rest of the dynodes. The signal is then processed as a pulse signal. The range for pulse mode circuitry is usually $0 - 10^6$ cps, and for analogue the range is $10^4 - 10^9$ cps. This method of detection allows for both high and low concentrations of analyte to be processed without prior knowledge of the solution concentration and without losing information during analysis of transient, short-lived peaks (Agilent Technologies Inc., 2015; Thomas, 2004).

In order to fully utilise the DDEM capabilities, an accurate calibration needs to be established, especially in the overlap between pulse and analogue count regions. This decreases the likelihood of an inconsistent count vs concentration relationship over a large range of concentrations. If a suitable calibration can be established counts of $0 - 10^9$ cps can be accurately detected in one scan.

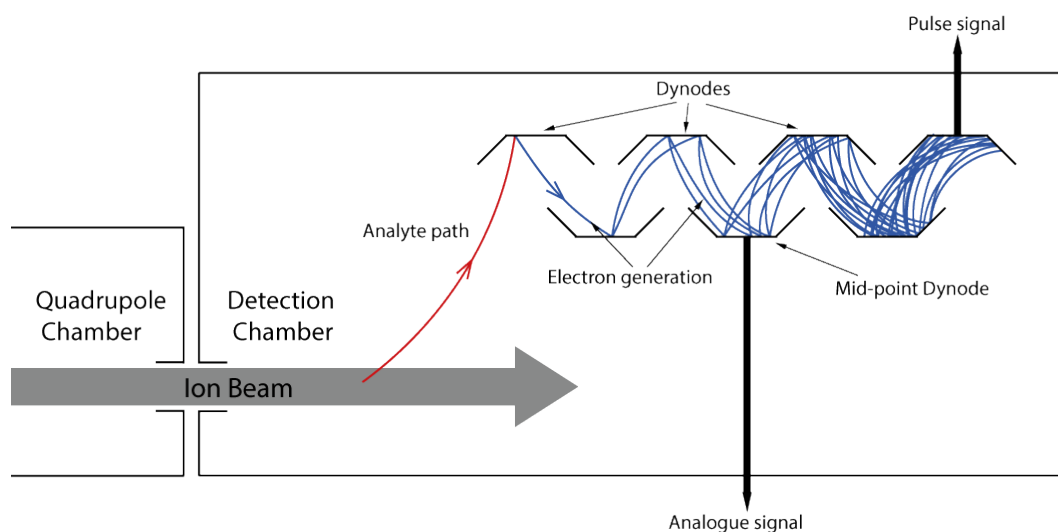


Figure 3.13.
DDEM detector
 Discrete Dynode Electron Multiplier

3.3.1 Sample preparation for ICP-MS analysis

The ICP-QQQ-MS system utilised requires all samples and calibrations to be introduced in a solution of 2% HNO_3 . In addition, calibrations must be created which span the expected concentration range of the samples. This is done using laboratory standards of known concentrations of the analytes used. They are diluted to form solutions at the desired concentrations in 2% HNO_3 . These are then run together with the samples. A linear calibration curve is then constructed relating the known concentrations of analyte to their corresponding CPS measurement. When a sample is measured, its analyte concentration can be calculated using the calibration curve (Figure 3.14). This can be done either by the data analysis software that comes with the Agilent 8800 or offline. To save time between sample preparation and running on the ICP-MS, this data analysis was completed offline.

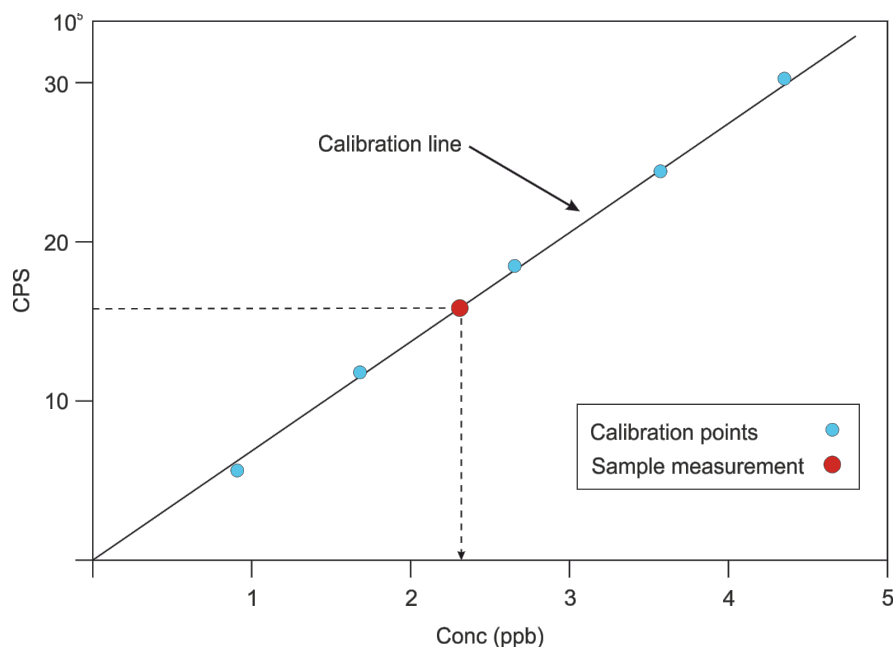


Figure 3.14.
ICP-MS calibration curve

For the Agilent 8800 utilised in this study, concentrations were kept below 100 ppb as the mass spectrometer is commonly used for trace metal analysis in low matrix samples. In order to ensure this, prior knowledge of the approximate concentration of analyte in the sample is required. If a sample of completely unknown concentration was to be measured, dip tests were performed whereby the sample is sequentially diluted by 10 or 100 times each dilution. This is done to ensure adequate dilution is achieved so as not to cause blockages in the system or overload the detector. The theoretical lowest concentration is then analysed first, and if the counts detected are below the range of the calibration, the next highest dilution in the sequence is run. Once an accurate concentration is measured within the calibration range, the concentration of the original sample can be calculated.

Occasionally, inconsistencies and faults can occur during analysis. There are many causes of these, some examples are alterations in sample flow speed, a change in plasma power or change in detector sensitivity. These can cause inaccuracies in measurement. In order to recognise these an internal standard is used. This is an element, or series of elements which are kept at the same concentration in all measured samples. If an inconsistency occurs (e.g. flow rate suddenly decreases due to a fault in the peristaltic pump), analyte signal will be significantly reduced. Without an internal standard, the reduction in signal could be interpreted as lower analyte concentration in the sample. However, if internal

standard signal was lower also, the user would be able to recognise the fault and either apply a correction or find the source of the inconsistency and re-run the affected samples.

For the ICP-MS runs completed, In and Re were selected as the internal standards due to their range of masses. The majority of the analysis was completed under No-Gas mode, meaning no collision/reaction gas was introduced to the ion beam when it passed through the octopole.

Mass spectrometric techniques offer faster analysis times (Bu et al., 2016). Study on mass spectrometric analysis of ^{90}Sr has so far concluded that LODs are much lower for radiometric analysis. Taylor et al. (2006) describe an expedited technique for analysis of Sr in river water samples. Spiked river water samples were pre-concentrated on cation exchange resin before being acidified and separated from Sr on Sr-spec columns. Taylor et al. (2006) then analysed the eluate on both an ICP-MS and by Cherenkov counting. Removal of isobaric ^{90}Zr was achieved by the separation protocol before ICP-MS analysis, but further suppression of ^{90}Zr was achieved by addition of O_2 in the reaction cell of the mass spectrometer. Zr forms the oxide more easily on reaction with O_2 in comparison to Sr. By introducing O_2 to the reaction cell, Zr forms the oxide and is filtered out by a mass filter prior to hitting the detector. Taylor et al. (2006) were able to achieve limits of detection of 0.5 Bq g^{-1} , 0.2 Bq g^{-1} and 5 Bq g^{-1} for sediment, plant and water samples respectively.

Feuerstein et al. (2008) were able to achieve LODs of 0.02 Bq g^{-1} in sample solutions containing no Zr. In soil samples, again separated using Sr-spec columns, detection limits of 1 Bq g^{-1} were achieved. Both Taylor et al. and Feuerstein et al. conclude by stating that although the method of using ICP-MS is an expedited analysis method in comparison to radiometric techniques, limits of detection are still far off what can be achieved by gamma spec, LSC and Cherenkov counting. Lower LODs have subsequently been achieved by other studies utilising ICP-MS with O_2 reaction cell gas. Takagai et al., (2014) achieved LODs of 2.34 Bq L^{-1} from aqueous solution and 3.91 Bq Kg^{-1} from soil samples.

Feuerstein et al., (2008) also state that peak tailing of ^{88}Sr can affect ^{90}Sr measurement due to the much higher abundance of ^{88}Sr in samples. This occurs when the defocussing forces of the quadrupole are too small to cause rejection of the off mass ions within the transit time (Feuerstein et al., 2008). This then causes counts to occur at m/z 90 from ions of m/z 88.

Chapter 3

Tumey et al. (2008) utilised an accelerator mass spectrometer (AMS) to analyse Sr concentrations. A minimum background of 75mBq was achieved this way. However, AMS is very expensive and the time saved during analysis is often outweighed by the time it takes to set up an AMS for a specific analyte.

More recent study by Russell et al. (2017) utilises a ICP-QQQ-MS system. Unfortunately, this study did not achieve lower LODs than previously but did, however, point out that the addition of O₂ in the reaction cell significantly increased the detection limits. Under no gas mode ⁹⁰Sr LOD was 0.9 Bq g⁻¹ and if both mass filters were used this increased marginally to 1.2 Bq g⁻¹. However, under gas mode ⁹⁰Sr LOD increased dramatically. An optimal flow rate of O₂ was found to be at 0.2 - 0.3 mL/min. If soil samples were leached using *aqua regia*, separated by hydroxide and carbonate precipitation and then separated using Sr resin, a limit of detection of 6.4 Bq g⁻¹ could be achieved on the ICP-QQQ-MS.

Measurement of plutonium has also been reported on an ICP-MS. Wang et al., (2018) separated and isolated plutonium on a TEVA column followed by a DGA column from a concrete digest. The digest procedure utilised perchloric acid and hydrofluoric acid for full opening out of the concrete matrix. Uranium-233 was used as an internal standard during the ICP-MS measurement. Plutonium-239, ²⁴⁰Pu and ²⁴¹Pu were measured as analytes and ²⁴²Pu was measured to establish chemical recovery yield. Uranium-238 was also measured. The hydride that forms (²³⁸UH⁺) and the peak tailing from the ²³⁸U signal itself are the main interferences for ²³⁹Pu measurement. Correction for this interference is achieved through the application of a subtractive equation (Equation 3.2).

$$^{239}\text{Pu}^+ \text{ signal} = \text{Raw } m/z 239 \text{ signal} - ((^{238}\text{UH}^+ / ^{238}\text{U}^+) \cdot (^{238}\text{U}^+ \text{ signal}))$$

Equation 3.2.

Uranium-238 hydride correction

Study of this subtractive equation has shown that (²³⁸UH⁺ / ²³⁸U⁺) does not remain constant when overall ²³⁸U concentration varies (Zheng and Yamada, 2006). If ²³⁸U⁺ signal is significantly higher than that of ²³⁹Pu, separate measurement of ²³⁸U and ²³⁸UH⁺ may have to be completed using a purified uranium source. This is done in order to establish hydride formation at the ²³⁸U concentration measured in the Pu sample. The calculated hydride ratio can then be applied to the Pu sample. For the study completed by Wang et al., (2018)

U decontamination factors through the use of extraction chromatography were significantly high enough to reduce the ^{238}U interference to operational blank level. Wang et al., (2018) reported high chemical recoveries for 22 samples analysed (57-93%) and accurate determination of $^{240}\text{Pu}/^{239}\text{Pu}$ ratios for two standard reference materials (SRMs). Warwick et al., (2019) stated that $^{238}\text{UH}^+$ interference on ^{239}Pu can be further reduced by addition of O_2 gas within the reaction cell.

Schramel et al., (1997) produced a method for the determination of U and Th concentration from urine matrices using an ICP-MS. Limits of detection (LODs) were found to be 0.5 ng/L in aqueous solutions and 1 ng/L for urine samples. Accuracy of the measurements was carried out by comparison to alpha spectrometry analysis, and adequate recoveries were achieved. Shi et al., (2013) found that adequate uranium isotope analysis from human urine samples can be achieved using ICP-MS, but they note that TIMS multi-collector analysis will always be more accurate. The benefits of analysing samples using an ICP-MS lay in the reduced sample preparation time for analysis in comparison to TIMS.

Thorium determination by ICP-MS is a well-established technique, and given the appropriate sample digestion procedure offers low detection limits and fast analysis times as well as offering accurate Th isotopic data (Holmes, 2001).

Chapter 3

Chapter 4 Separation of Strontium-90 from cementitious matrices via extraction chromatography at higher flow rates

4.1 Introduction

As previously mentioned, large scale bulk waste determination is completed by rapid in-situ measurement and application of scaling factors (SFs). The development of these SFs is reliant on accurate determination of the radionuclide content of small sample of the waste, specifically the relationship between the ETM and DTM radionuclides.

One difficult-to-measure (DTM) nuclide is the radiotoxic strontium isotope ^{90}Sr . Strontium-90 has a half-life of 28.8 years and is a pure beta emitter (546 keV). Chemical separation of the analyte from the sample matrix and any potential interferences is required for accurate activity determination. Strontium-90 has isobaric (e.g. $^{90}\text{Zr}^+$, $^{90}\text{Y}^+$, $^{180}\text{Hf}^{++}$), polyatomic (CrAr^+ , MnCl^+ , YH^+) and peak tailing (from ^{88}Sr) interferences if measured by ICP-MS. It also has radiometric interferences (e.g. ^{234}Pa , ^{137}Cs) if measured by liquid scintillation or via Cherenkov counting ^{90}Y that are prevalent in decommissioning wastes. Strontium-90 constitutes around 6% of the ^{235}U fission yield and 2% of the ^{239}Pu fission yield (Takagai et al., 2014). During routine operation it is likely that construction materials in the immediate vicinity of the reactor will be contaminated with fission products. The level of contamination can be exacerbated if the site has a history of nuclear incidents (Grahek et al., 2018; Wallace et al., 2012). In addition, other processes related to power production also cause contamination of materials with fission products. Storage ponds for spent nuclear fuel contain large amounts of fission products and fragments of the fuel itself (Parry et al., 2011). These fission products contaminate the walls of the ponds. Nuclear fuel reprocessing produces a large amount of radioactive waste. Fission products constitute a significant quantity of these wastes, which are vitrified in order to immobilise harmful radionuclides (Gin et al., 2013). Post irradiation examination (PIE) can also lead to exposure of construction materials to fission product releases, especially if the fuel pin has been subject to damage.

Chapter 4

Concrete is widely used to construct the buildings and other crucial structures (such as storage ponds and bioshields) on these sites. The United Kingdom Radioactive Waste & Materials Inventory states that concrete constitutes a significant volume of ILW (12%) and LLW (31%) and the majority of VLLW (88%) (DEFRA, 2002; Department for Business, Energy and Industrial Strategy, 2019). The volumes for the waste categories increase with decreasing activity, so LLW and VLLW wastes represent the majority of waste on a nuclear site (~90%). Therefore, it is one of the most voluminous materials disposed of during decommissioning (Basu et al., 2013). Accurate determination of activities is crucial in order to direct a package of waste to the correct method of disposal. Because of the enormous quantities of concrete wastes produced (50 – 55 million tonnes per nuclear power plant), time saving techniques in the measurement of the radionuclide content of concrete wastes represent a huge cost-saving opportunity.

4.1.1 Expediting strontium separation

Early strontium separation was chiefly used to establish nuclear weapons' yield and investigate weapon fallout (Andrews, 1955; Crocker, 1963; Freiling, 1961). Separation techniques from this time used ferric hydroxide and barium chromate to separate the strontium from natural and artificial radionuclides (Bowen, 1970). Strontium's yield determination from this separation was made gravimetrically. However, calcium's similar chemical behaviour meant that the final precipitate of Sr was often contaminated with Ca (Goldin et al., 1959). To overcome this, Sr and Ca were separated using a selective nitrate precipitation from fuming nitric acid. This step resulted in a precipitate of pure strontium nitrate (Bowen, 1970; Budnitz, 1974).

Another common method of Sr separation was through the use of ion exchange chromatography. Porter and Kahn (1964) described the use of Dowex 50W-X8 to determine ⁹⁰Sr activity in milk by measuring ingrown ⁹⁰Y, separated from alkali earth metals present in milk. Noshkin and Mott (1967) reported a more direct measurement of ⁹⁰Sr in seawater. This was achieved by complexation with cyclohexanediaminetetra-acetic acid (CyDTA) and sorption to Dowex 50-X12 cation exchange resin. Separation from Ca required careful control of pH, achieved through altering NH⁺ concentrations.

The mid to late 1980's saw an increase in the use of crown ethers in the separation of Sr from various matrices (Blasius et al., 1985; Mohite and Khopkar, 1987; Suzuki et al., 1987;

Wai and Du, 1990). Crown ethers effectively separated Sr from a wide range of elements with fewer preparatory steps, avoided the use of hazardous fuming nitric acid, and hence were more rapid than the ion exchange methods of the time (Kimura et al., 1979). This was due to their method of extraction which was based on size exclusion of Sr ions from the other matrix components.

Horwitz et al., (1991) produced a crown ether loaded resin which allowed for Sr separation in highly acidic solutions. This resin consisted of (4,4'(5')-bis(t-butylcyclohexano)-18-crown-6) bonded to an inert polymeric support. Typically, Sr analysis is performed on samples which require a preliminary digestion or leaching stage, using nitric acid or *aqua regia*, producing a highly acidic solution. The crown ether-based resin showed high selectivity for Sr in acidic media (K_d 's of 87-200 at 2-10 M HNO_3) and good separation from a wide variety of metal ions (Horwitz et al., 1992a). Sr resin can effectively separate Sr from Pb, Cs, Ca, and U. This resin is commonly used today for separation of strontium and has a variety of applications (Horwitz et al., 1992a).

Traditional chromatographic separation techniques using gravity flow columns can be time consuming, resulting in delays in obtaining ^{90}Sr measurement. Recently, there has been much interest into the automation of column separation procedures. Work by Chung et al., (2015), Kim et al., (2015) and Chung et al., (2013) has demonstrated the application of an automated radionuclide separator to be advantageous for use in emergency situations. These circumstances require rapid screening of samples of unknown activity. Accidents like Chernobyl and Fukushima have driven research into expedited separation techniques, focussing on nuclides posing a risk to the environment and human health. Applying these techniques to routine analysis and for use in the nuclear decommissioning sector specifically, has been largely overlooked. Characterisation of samples is required throughout the lifecycle of a nuclear facility. Radiometric analysis is commonly undertaken by independent radiochemical laboratories, who may receive samples from a variety of different sites. Facilities such as these may also analyse samples from other fields of industry or research. Use of automated separation systems in laboratories such as this allow for a higher throughput of samples and has the potential to reduce labour costs. Encasing systems in appropriate shielding can increase worker safety while providing precise, repeatable separations for analysis.

Chapter 4

The automated systems described in the above studies utilise peristaltic pumps to force solutions through separation columns at higher, more controlled flow rates than that of conventional gravity flow columns. The high flow rates that can be achieved by automated separators significantly decrease the time taken for ^{90}Sr determination. In addition, automation of the separation process can reduce labour costs and the risk of contamination through human error.

However, increasing flow rates can have a negative effect on separation efficacy. Chromatographic separation efficiency is governed by the Height Equivalent to a Theoretical Plate (HETP) and column residence time. Good chromatographic separation is achieved by narrow elution peaks of both analyte and contaminant and significant differences in uptake.

4.1.2 Investigation into wider geochemical application

Expedited chromatographic separations not only have implications for the nuclear industry, but for wider scientific research as well. Research into expediting these processes can impact any laboratory's productivity, and for research facilities looking to expedite separation processes, expediting chromatographic separations may be of interest.

Many areas of geochemistry require chromatographic separations. Specifically, the separation of strontium is required in isotope geochemistry to radiometrically date ancient crustal rocks. Rubidium-strontium dating is a commonly used technique and utilises ^{87}Rb 's long, 48.8 Ga half-life. Rubidium, although not forming any minerals independently, often replaces K due to its similar ionic radius (Attendorn and Bowen, 2012). This substitution can occur in all K-bearing minerals. Rubidium-87 decays via β - decay to ^{87}Sr with a β - energy of 282 KeV (Huang et al., 2021). The only other Rb isotope found in nature is ^{85}Rb , which is stable, has an abundance of 72.172% (Attendorn and Bowen, 2012; Takács et al., 2019).

Strontium is a reactive metal, sharing similar chemical characteristics to Ca. As a result, strontium can replace Ca in many calcium-bearing minerals. However, due to Sr's larger ionic radius, it is not able to substitute for Ca in all Ca-bearing minerals. Strontium substitution for Ca occurs more commonly at eight-fold coordination sites, whereas Ca ions can fill both eight and six-fold coordination sites.

Strontium has four isotopes found in nature, all of which are stable. Strontium-86 has a natural abundance of 9.861%. Even though ^{86}Sr is produced by the decay of ^{86}Rb , the half-life of ^{86}Rb is short (18.6 days) in comparison to ^{87}Rb and is not found naturally. Therefore, ^{86}Sr concentration does not change and can be regarded as a constant. Strontium-87 is another Sr isotope present naturally and has an abundance of 7.001% (Huang et al., 2021). Strontium-87 is radiogenic, being produced from the decay of ^{87}Rb . The concentration of ^{87}Sr increases over time in a mineral enriched with Rb. The growth of ^{87}Sr is directly proportional to the half-life of ^{87}Rb (Equation 4.1 and Equation 4.2).

$$^{87}\text{Sr}_t = ^{87}\text{Sr}_0 + ^{87}\text{Rb} (e^{-\lambda t} - 1)$$

Equation 4.1.

Equation for ^{87}Sr ingrowth from ^{87}Rb

$^{87}\text{Sr}_t$ is the total number of strontium-87 atoms in the mineral sample at time t , ^{87}Rb is the number of rubidium-87 atoms in the mineral sample at time t , and $^{87}\text{Sr}_0$ is the number of ^{87}Sr atoms present in the mineral sample at the date of crystallisation (time = 0). λ is the decay constant for of ^{87}Rb .

$$\lambda = \frac{\ln 2}{t_{1/2}}$$

Equation 4.2.

Decay constant equation

Where $t_{1/2}$ is the half-life, calculated in a unit of time consistent with t from Equation 4.1.

Strontium-86 is used as a constant to produce ratios allowing for relative ^{87}Sr and ^{87}Rb determination. For the most accurate age determination, several measurements of different crystals from the same rock sample must be taken. Multiple crystals are analysed because differing initial $^{87}\text{Rb}/^{86}\text{Sr}$ ratios are required. This is possible because different minerals are composed of differing amounts of Ca or K. Therefore, the substitution of these for their respective replacements (Sr and Rb) during crystal formation will lead to different initial $^{87}\text{Rb}/^{86}\text{Sr}$ ratios. As time progresses, ^{87}Rb decays to ^{87}Sr , but ^{86}Sr remains constant and thus the $^{87}\text{Rb}/^{86}\text{Sr}$ ratio decreases. Likewise, as the ^{87}Rb decays, the ^{87}Sr concentration increases, so the $^{87}\text{Sr}/^{86}\text{Sr}$ ratio increases. These are then used to construct an isochron (Figure 4.1).

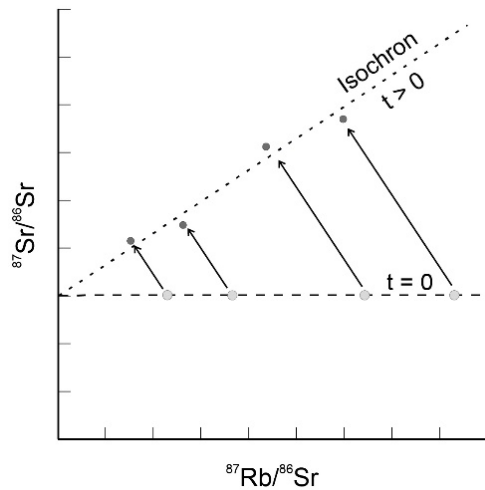


Figure 4.1.

Rb/Sr isochron

Ratios of $^{87}\text{Sr}/^{86}\text{Sr}$ and $^{87}\text{Rb}/^{86}\text{Sr}$ measured and the isochron constructed from their measurements

The dark grey points represent measurable data at time t . If the samples measured were formed concurrently, they should lay on the same line of best fit (isochron). The light grey points represent the initial ratio values at the time of crystallisation. The intercept of the isochron represents the value of $^{87}\text{Sr}/^{86}\text{Sr}$ if no rubidium was present at crystallisation, and therefore, the initial $^{87}\text{Sr}/^{86}\text{Sr}$ value. The equation for the isochron:

$$\frac{^{87}\text{Sr}}{^{86}\text{Sr}_t} = \left(\frac{^{87}\text{Sr}}{^{86}\text{Sr}_0} \right) + \frac{^{87}\text{Rb}}{^{86}\text{Sr}} (e^{-\lambda t} - 1)$$

Equation 4.3.

Equation for Rb/Sr isochron

This involves the ^{86}Sr component in Equation 4.1 and takes the form of a straight line ($y = mx + c$). The gradient of the line is therefore proportional to time which can then be calculated:

$$t = -\frac{\ln (\nabla + 1)}{\lambda}$$

Equation 4.4.

Calculation of time from the gradient of the isochron

The gradient (∇) is taken from the isochron constructed from the data. Time t is calculated in the same unit time as the time function used to calculate λ .

For an accurate elapsed time to be calculated, precise measurement of the Sr and Rb isotopes is required. To do this, mass spectrometry is used. Commonly, multi-collectors are used, the two main types being MC-ICP-MS (multi-collector inductively coupled plasma mass spectrometry) or TIMS (thermal ionisation mass spectrometry). For these techniques, Sr and Rb must be separated before measurement. This is because these mass spectrometers only distinguish between different masses and cannot easily resolve isobars. Preparative chemistry is therefore required to separate Sr from Rb. These fractions are then measured separately.

It is therefore of upmost importance that the sample's isotopic ratios are not altered during the preparation for measurement. The use of Sr resin in this context has been demonstrated (Dong et al., 2018; S. Li et al., 2019). Chromatographic separations in other systems are known to cause fractionation of isotopes based on their mass (W. Li et al., 2019; Misra and Froelich, 2009; Russell and Papanastassiou, 1978; Sonoda et al., 2008). Efforts to minimise this are employed to attain the most accurate results. If mass fractionation were to occur, it would most likely be exacerbated if the chromatographic system were under higher flow rates. Consequently, for a forced flow chromatographic system to be applicable to Sr separation for Rb-Sr dating, it needs to exhibit minimal mass fractionation. Therefore, investigation into this mass fractionation under these conditions is required for application to preparative chemistry in geochemical analysis.

4.1.3 Experimental constraints

Horwitz reports that Sr is most strongly bound to Sr resin (has the highest K_d) in an 8 M HNO_3 solution. This study will therefore use 8 M HNO_3 as the load solution for the matrix digests.

Sample masses and contaminant concentration also affect strontium separation by Sr resin. Increasing the ionic content of the load solution leads to higher competition for crown ether binding sites. Sr resin has a high selectivity for cations with a similar ionic radius to Sr^{2+} . Increasing the concentration of ions with a similar ionic radius to Sr^{2+} will lead to higher competition for binding sites. This could also lead to peak broadening of the Sr or contaminant elution peak, decreasing the efficiency of ^{90}Sr separation. One potential competing ion is Pb^{2+} which has an ionic radius of 1.19 Å which is comparable to Sr^{2+} (1.18 Å) and is prevalent in many environmental samples and industrial materials (Shannon,

Chapter 4

1976). The K_d for Pb is >800 in 8 M HNO₃ compared to Sr which is 200. Increased sample mass and contaminant concentration has the potential to affect Sr separation at any flow rate.

The IAEA (International Atomic Energy Agency) state that solid material is considered radioactive waste if (a) it contains more than 1 Bq/g ⁹⁰Sr or (b) it contains multiple radionuclides with A/B ratios summing to >1 . In this instance “A” is the activity concentration of the nuclide in the material analysed. Term “B” is the activity concentration of that nuclide required to class the material as radioactive waste if that nuclide was present exclusively. In the case of Sr, “B” would be 1 Bq/g.

The main aim of this research is to demonstrate the applicability of rapid and cost-effective Sr separation techniques to the determination of ⁹⁰Sr in cementitious waste for waste classification and fingerprinting. This will be achieved by determining the following:

- The effect of increasing flow rate on Sr separation from concrete matrices by assessing:
 - a. Strontium elution profiles and HETP values
 - b. Decontamination of interferences from the Sr fraction
 - c. Precision of separation over multiple runs with high levels of contamination
- The effect of increasing sample mass on Sr separation efficiency
- The effect of reusing columns for multiple sample separations on Sr separation

To fully demonstrate this applicability, the system has to deliver sufficient resolution. Considering the guidelines, regulations and ⁹⁰Sr’s prevalence in nuclear waste, it is proposed that the limit of detection is 0.1 Bq/g ⁹⁰Sr (i.e. 10% of the Environmental Permitting Regulations, 2016).

Isotopic analysis of Sr profiles will determine if any Sr isotope fractionation effects occur at higher flowrates on Sr resin. This will demonstrate whether or not expedited separation systems can be applied to the separation of Sr from geological samples for accurate age determination.

4.2 Experimental

4.2.1 Instrumentation

An Automated Sequential Radionuclide Separator (ASRS) (Hanjin Eni Co., LTD., Daejeon, Republic of Korea) was utilised to separate the samples. The system uses 8 peristaltic pumps to perform simultaneous separations on 8 individual chromatographic columns or, when used in series, perform a 2-stage separation on 4 samples simultaneously. Loading, washing and elution can be completed at a flow rate of up to 6 mL/min. The ASRS can adjust flow rate in 0.5 mL/min increments and uses a LabVIEW program to control the hardware. A schematic of the ASRS and the LabVIEW control panel can be found in Appendix C. A Canberra p-type High Purity Germanium well detector GCW4523 (Mirion Technologies (Canberra UK), San Ramon, CA, USA) was used for the determination of ^{85}Sr activity. Stable ^{88}Sr concentrations were measured using a Triple Quadrupole Inductively Coupled Plasma Mass Spectrometer 8800 ICP-QQQ- MS (Agilent, Santa Clara, CA, USA). Strontium-90 and ^{90}Y were measured on a PerkinElmer 1220 Ultra Low-Level Liquid Scintillation Spectrometer (PerkinElmer, Waltham, MA, USA). For the purposes of this study, ^{85}Sr may be utilised as a radiostrontium tracer, in which case gamma spectroscopy may also be employed, along with LSC for work with ^{90}Sr radiotracers. Single sample analysis for gamma spectrometry can take upwards of 2 hours and LSC of ^{90}Sr up to half an hour. Due to the photoluminescence phenomenon, UV and visible light energy has to be dissipated from samples prior to LSC. This is a passive process and can be achieved by storing samples in the dark, away from any sources of white light (Chapon et al., 2016). Once this time is factored in, a single sample run of LSC can be up to 2.5 hours.

4.2.2 Reagents

All reagents were of analytical grade unless otherwise stated. Nitric acid solutions were produced from a 70% (weight) concentrate (Fisher Scientific, Loughborough, England). HCl solutions were produced from a 37% (weight) concentrate for analysis (Fisher Scientific, Loughborough, England). For analysis by ICP-QQQ-MS, 2% nitric acid solutions were prepared from PrimarPlus-Trace analysis grade (>68% by weight) (Fisher Scientific, Loughborough, England). High purity water was generated using a Q-POD Milli-Q Advantage A10 Water Purification System (Merck, Darmstadt, Germany). A bulk concrete

Chapter 4

sample sourced from an ex-residential demolition site in central London was used to prepare a matrix-relevant digest for the majority of the method development. A second, active concrete sample was used as a base matrix to create a worst-case-scenario matrix. This was obtained from a sample of bioshield concrete from the Steam Generating Heavy Water Reactor (SGHWR), a research reactor at the Magnox Winfrith site in Dorset, U.K., (Warwick et al., 2009). Stable strontium standard was produced from strontium chloride (May & Baker, UK). Strontium-85 standard solutions (ID: 2016-1838 and 2017-1686) were sourced from Physikalisch-Technische Bundesanstalt (Germany). Strontium-90 standard solution (ID: SIZ64) was obtained from AEA Technology (now Ricardo-AEA, Harwell, UK). Working dilutions of the radiotracers were prepared by gravimetric dilution. Gold Star Multi-Purpose Liquid Scintillation Cocktail (Meridian Biotechnologies, Tadworth, England) was used for the counting of ^{90}Sr via liquid scintillation counting.

Whatman 40 ashless filters were used for filtering concrete digestions. For rapid, small volume filtrations Millex[®]GP 0.22 μm PTFE syringe filters were used. Sr Resin (Triskem International, Bruz, France) of size 100-150 μm was used to separate Sr from the matrix solution. Sr Resin was packed into columns as a slurry to a bed of dimension 40 \times 6.6 mm (i.d.) in a glass chromatographic column (Omnifit[®] Chromatography Column, Diba Industries, Danbury, CT, USA).

4.2.3 Separation procedure

The ASRS separation procedure uses a 40 \times 6.6 mm Sr-spec column and the procedure described in Figure 4.2. Pb retention on Sr resin is high, even at very low HNO_3 concentrations. To further avoid co-elution of Pb and associated ^{210}Pb which may interfere with radiometric measurement of ^{90}Sr via ingrowth of its ^{210}Bi daughter, Sr was selectively eluted with 0.05 M HNO_3 . The dead volume of tubing in the ASRS between sample vials/reagent containers and the columns was calculated to be 1.5 mL. Before use, the column was also washed with MQ and 0.05 M HNO_3 to ensure any removal of any residues prior to conditioning and loading with nitric acid. Low concentration 0.05 M HNO_3 was used to increase the solubility of potential residues present on the resin before separation.

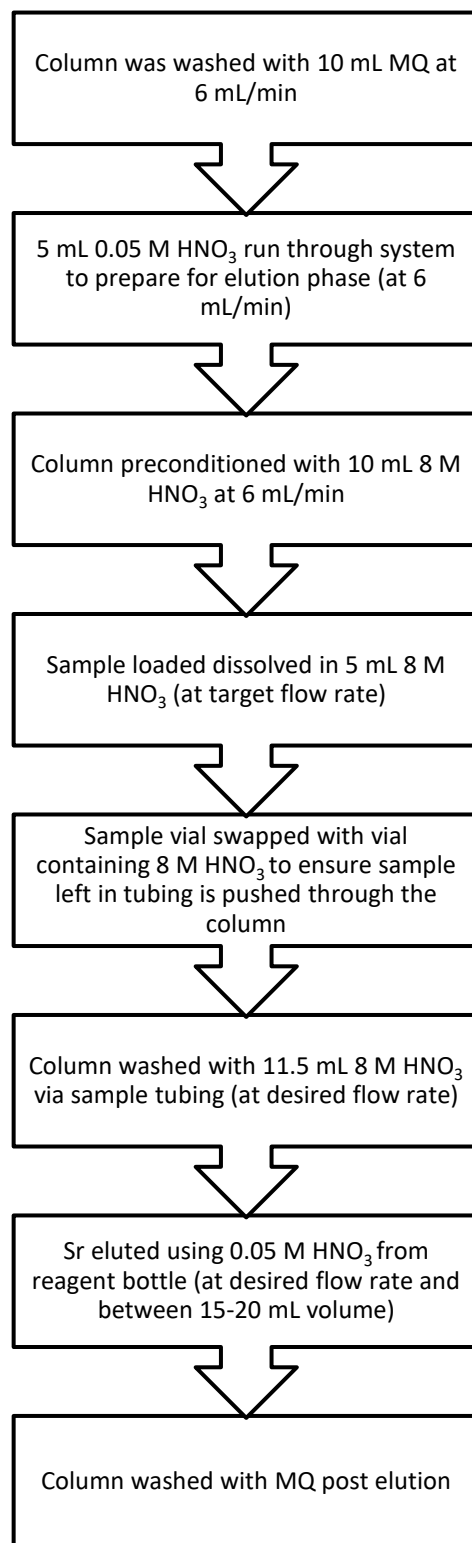


Figure 4.2.
Flow chart of Sr separation on a Sr column

4.3 Method development

4.3.1 Concrete digestion

The concrete matrix digest was prepared from the bulk concrete sample. Fifty grams of powdered concrete was digested with 500 mL *aqua regia* for at least 2 hours on a hotplate at 90°C. The mixture was then filtered using a Whatman 40 ashless filter into a second beaker. The filter was washed with 6 M HCl and MQ (Milli-Q) water, washings were transferred to the second beaker and evaporated to dryness. The filter paper containing the digest residue was transferred to a Pyrex beaker, dried on a hotplate and ignited at 460°C for 13 hours. This was treated again with 500 mL *aqua regia*, for at least 2 hours before being filtered as described previously, and added to the first digest. For active concrete samples, this second filter was retained for further digestion if required. The digests were evaporated to dryness. The resulting residue was then dissolved in 250 mL 8 M HNO₃ to produce a concrete digest equivalent to 1 g of concrete: 5 mL solution (0.2 g/mL). For testing with active concrete samples, much smaller masses of powdered concrete were used. The ratio of *aqua regia* volume to sample mass was 0.5 g : 20 mL for the active concrete digestion. The final residue was dissolved in 20 mL 8 M HNO₃.

4.3.2 Batch uptake experiments

Batch uptake experiments were undertaken to determine the rate at which Sr reached equilibrium with Sr resin and how ionic interference affects this. Additionally, these tests enable comparison of Sr resin performance between this study and previous work (Horwitz et al., 1992a). Strontium in a solution of HNO₃ with and without 0.5 g concrete matrix was studied. Dry Sr resin (0.1 g) was added to 5 mL 8 M HNO₃ or concrete digest in 8 M HNO₃, along with 21 Bq of an ⁸⁵Sr tracer. Samples were placed on a roller mixer for a range of times (1, 2, 5, 10, 20 and 60 minutes and 2, 4, 7 and 24 hours). Solid and aqueous phases were separated using a syringe filter. Strontium-85 activity in the aqueous phase was then determined using gamma spectrometry. Aqueous phase activities were compared to the initial activity of the aqueous phase to determine the uptake of Sr by the Sr resin.

To quantify Sr resin uptake, the ratio of Sr in the solid and liquid phase (K') was calculated (Equation 1.4). At equilibrium the K' is equal to the K_d, where maximum uptake of Sr by the

resin occurs. Faster equilibration times lead to thinner HETP and sharper chromatographic resolution.

4.3.3 Repeatability

The Sr separation repeatability from a concrete digest was assessed by determining chemical recovery and elution profiles for 4 replicate separations. A solution consisting of 2.5 mL matrix solution and 2.5 mL 8 M HNO₃ was spiked with ⁹⁰Sr to mimic a 5 mL solution containing 0.5 g of concrete. The sample loading, washing and elution were performed at 1 mL/min. The eluate was collected in 1 ± 0.09 mL fractions to permit construction of an elution profile. The ⁹⁰Sr activity concentration of each fraction was measured using gamma spectrometry. The cumulative ⁹⁰Sr activity in all eluate fractions was used to calculate the chemical recovery. Each separation was performed using a fresh slurry of Sr resin. The column was emptied and washed with 5% HNO₃ after each sample was run.

4.3.4 Effect of matrix

The most likely component present in concrete digest is likely to be calcium. Stable calcium can undergo neutron activation to produce radioactive isotopes (most commonly ⁴¹Ca and ⁴⁵Ca). However, these are not of concern regarding measurement interferences with ⁹⁰Sr due to their differing decay modes (in the case of ⁴¹Ca) and lower decay energy (in the case of ⁴⁵Ca) compared to ⁹⁰Sr or ⁹⁰Y. However, historical Sr separation techniques suffered as a result of Sr and Ca's similar chemical behaviour, especially when the final Sr precipitate recovery was determined gravimetrically (Goldin et al., 1959). To assess if Ca concentration affects Sr uptake, samples with differing concrete matrix concentration were separated. This effectively changed the Ca concentration. WDXRF analysis of the solid concrete sample showed the CaO composition to be 39%. The concrete digest solution (0.2 g : 1 mL) was then diluted to 0.1 g : 1 mL and 0.05 g : 1 mL in order to assess Sr separation with changing Ca concentration. Solution volumes of 5 mL were used and results were given in terms of solid mass equivalent (0.25, 0.5 and 1 grams per separation). These were loaded in 8 M HNO₃ and 0.05 M HNO₃ was used as the eluent. In addition, increasing the mass of concrete per sample decreases the limit of detection of ⁹⁰Sr per gram of solid sample.

4.3.5 Flow rate effect on HETP

HETP is often used to assess and quantify column performance. To attain HETP values, isocratic elution of analytes is required. This was done using a 15 ppm stable Sr solution in 8 M HNO₃ in a 5 mL load solution and using clean 8 M HNO₃ to elute the Sr. Aliquots of Sr were taken at regular intervals, diluted to 1/10th and their concentrations analysed via ICP-QQQ-MS. Three flow rates were tested, and elution profiles of the Sr eluate concentration were produced. The graphs were smoothed using sigma plot's 2D data smooth function. Peak width at half maximum was calculated using sigma plot's transform tool. Plate number and HETP was then calculated using Equation 1.1 and Equation 1.2 .

4.3.6 Effect of flow rate on Sr recovery

Column separations under gravity flow achieved flow rates of 0.60 ± 0.14 mL/min. Tests to investigate ⁹⁰Sr peak broadening with flow rate increase were performed at 1 mL/min intervals from 1 - 6 mL/min using the ASRS system. Digests equivalent to 0.5 g concrete were used for each separation. Sample loading, washing and elution was completed at the same flow rate during each test. Sample load volume was 5 mL, column wash consisted of 11.5 mL of 8 M HNO₃ and elution of Sr was achieved using 20 mL 0.05 M HNO₃. Strontium-90 was used as a radiotracer and measurement was performed using liquid scintillation counting. Aliquots of the Sr fraction were collected as 1 mL fractions. Both total recoveries and elution profiles were used to assess the effect of flow rate on Sr adsorption on the Sr resin column.

4.3.7 Effect of flow rate on decontamination

A synthetic solution was produced to represent the most likely contaminants present in a concrete matrix. The elements identified were Fe, Co, Ni, Sr, Cs, Eu, Pb and U. Iron, cobalt and nickel are likely to be present if the concrete is reinforced with rebar and could contaminate concrete samples. Their inclusion is not meant to demonstrate the effect of dissolving a sample of rebar, merely minor contamination of a concrete sample. Prominent long lived activation products that are likely to be present in concrete are ¹⁵²Eu, ¹⁵⁴Eu, ⁶⁰Co and ¹³⁴Cs (Carroll, 2001). Uranium sorption to components of cementitious matrices has been previously demonstrated (Altenhein-Haese et al., 1994; Wellman et al., 2007). Pb is a

commonly found trace metal which may prove to be an interesting contaminant to study due to its high K_d .

Stable solutions of Fe, Co, Ni, Sr, Cs, Eu, Pb and U were added (by mass) to a cleaned 20 mL scintillation vial in the volumes and concentrations. The solution was then evaporated on a hotplate at 60°C to a dry residue. Twenty millilitres of 8 M HNO₃ was then added to dissolve the residue and produce the final synthetic solution. Fe, Sr and Pb were made to 100 ppm and Co, Ni, Cs, Eu and U were made to 10 ppm in the final solution. The concentrations of contaminants were dictated by the stable standards available. The solution was then used to complete a column separation using the same volumes and procedure as the flow rate tests. The final Sr fraction was collected as on 20 mL aliquot, then analysed via ICP-MS to determine contaminant concentrations.

The degree of decontamination is quantified as a decontamination factor (DF) calculated in Equation 4.5.

$$DF = \frac{\text{Mass in load solution}}{\text{Mass in Sr fraction}}$$

Equation 4.5.
Decontamination factor equation

The elution profile of these contaminants in the load and wash phases was also examined to determine the optimum wash volumes required to effectively remove the contaminant prior to Sr elution.

4.3.8 Column Reuse

Reuse of columns has the potential to reduce analytical cost and time as one of the most time-consuming processes during the Sr separation is the preparation of the columns. By reusing columns, the need for preparation of fresh columns is reduced. Column preparation can be replaced by an extra column wash, which is far less time consuming - especially when conducted at higher flow rates. However, column degradation could occur with multiple uses so for the reuse of columns to be appropriate, they would need to show

Chapter 4

consistent performance over multiple runs. Degradation may be the result of the physical action of the reagents through the column, chemical decomposition by strong acids or a combination of both causing leaching of the organic extractant from the resin. The column must be adequately washed between uses so that separations are not contaminated from previous separations, potentially resulting in cross contamination between samples and false positive results. To test this, Sr-spec columns were used to separate ^{90}Sr from 5×0.5 g concrete samples, run sequentially with a 20 mL MQ wash between each elution and the following separation's procedure. Column reuse tests were conducted at 1, 3 and 6 mL/min to assess the impact of flow rate on column degradation and analyte separation. Decontamination factors for key interferences was determined using the methodology described in 4.3.7. The columns were reused 3 times at 1, 3 and 6 mL/min flow rates. The variation in Sr recoveries and DFs were calculated to assess performance.

4.3.9 Overall analytical performance

The performance over the entire analytical procedure (sample preparation, digestion, separation, and measurement) for the separation of ^{90}Sr was evaluated. Concrete composition varies significantly, dependant on the type of concrete required and the source of the raw materials. The expedited technique must therefore be applicable to a wide range of concrete compositions. To do this a worst-case-scenario type matrix was produced. A bulk concrete sample was acquired and spiked with known masses of trace elements to create a digest with high concentrations of all contaminants. This eliminated the need for a large range of samples. Various concrete compositions from the literature were compiled (Table 4.1), with a list of the major and minor components (Evans et al., 1984; Harms and Gilligan, 2010; Shin et al., 2002; Warwick et al., 2009). Major component composition such as Al_2O_3 , SiO_2 , and CaO was obtained from the bulk sample of bioshield concrete from the Steam Generating Heavy Water Reactor (SGHWR). Trace element compositions of the SGHWR concrete were altered to resemble the highest concentrations found in the literature. To do this, stable trace element standards were added to the powdered SGHWR sample before digestion. Concentration of trace element in bulk sample was calculated using the mass of element standard added and the mass of dry sample used (0.5 g).

Trace element concentrations were taken from data for the SGHWR bioshield bulk sample which was used as a base for the digest (Warwick et al., 2009). Samples of 0.5 g of the SGHWR concrete were spiked with stable standards of Ba, Ce, Ni, Pb, Sr, Th, U (depleted) and Mn. The theoretical concentrations of the spiked elements in the solid sample were calculated (Table 4.2).

Assessment of the entire analytical procedure was achieved through replicate analysis of the spiked bioshield concrete. A known activity of ^{90}Sr was added to each replicate. Strontium-85 tracer was added to assess losses during the procedure and overall recoveries. Inherent ^{90}Sr and ^{85}Sr in the bioshield concrete had been assessed in a previous study and reported as below the detection limit. Six replicates were processed using the digestion method described in 4.3.1 and the separation method in 4.2.3. The samples were eluted in 20 mL 0.05 M HNO_3 . Three of these replicates were spiked with stable Sr to assess the impact of Sr concentration in chemical recovery. The measured ^{90}Sr in the eluate of each replicate was compared to the known activity added to assess the accuracy of the technique. Inter-replicate variability was used to assess the precision of the technique.

The column capacity for Sr was calculated at 8 mg Sr/g resin (using estimate from Horwitz et al., 1992). The capacity for Pb would be over double this (19 mg) due to Pb's higher atomic mass. From the concentrations in the solid sample calculated, the mass of Pb in the replicates was 0.31 mg and the mass of Sr was 0.08 mg in the non-spiked and 0.6 mg in the spiked replicates. These masses are well within the maximum capacity of the column; however, this is the only test presented in the study which analyses Sr mass effect on separation efficiency.

Each 20 mL replicate solution was measured by gamma spectrometry to determine ^{85}Sr activity relative to the original spike activity and losses during digestion. The 20 mL sample was then transferred to a centrifuge tube prior to loading into the separation system. The separation procedure was performed at a flow rate of 5.1 mL/min to evaluate separation at maximum flow rate capacity of the system. The total 20 mL solution was loaded onto the column and washed with 10 mL 8 M HNO_3 . Strontium was eluted with 2×10 mL 0.05 M HNO_3 , with each eluate fraction collected separately.

Trace Element	Study Name and Concentration (ppm)			
	Harms and Gilligan, 2010 (NPL)	Evans et al., 1984 (US Regulatory commission)	Warwick et al., 2009	Max concentrations from literature
As	2.5		2.3	2.5
Ba	610	7060	48	7060
Cd	5.0		0.0	5.0
Ce	12.5	52.0	28.2	52.0
Co	2.5	31.0	16.7	31.0
Cr	20.1	540.0	315.0	540.0
La	8.0	28.0	2.0	28.0
Ni	150	87	1244	1244
Pb		560.0	16.0	600.0
Sr	720	940	151	1000
Th	1.0	120.0	7.0	120.0
U	1.7	4.4	3.5	4.4
V	17.7		14.6	17.7
Zn	17	340	15	340
Mn		990	150	990

Table 4.1.**Concentrations of bulk concrete trace element concentration**

(Evans et al., 1984; Harms and Gilligan, 2010; Warwick et al., 2009)

Element	RCW 1	RCW 2	RCW 3	RCW 4	RCW 5	RCW 6
Ba (ppm)	7300	7500	7500	7400	7500	7400
Ce (ppm)	80	85	85	80	85	85
Ni (ppm)	1400	1400	1400	1400	1400	1400
Pb (ppm)	600	630	630	630	630	630
Sr (ppm)	1200	1200	1200	150	150	150
Th (ppm)	130	130	130	130	130	130
U (depleted) (ppm)	4.5	4.6	4.5	4.5	4.6	4.6
Mn (ppm)	1200	1200	1200	1200	1200	1200

Table 4.2.**Concentration of trace elements in samples**

4.3.10 Sr isotope fractionation

As previously discussed, isotopic fractionation must be minimised during preparative chemistry during the analysis of Sr isotopes when dating geochemical samples via Rb-Sr dating. To test this a stable Sr ICP-MS standard was used to produce a 15 ppm Sr solution in 8 M HNO₃. Isocratic elution of this solution was then performed through a 1.3 mL column at three different flow rates, and aliquots of the eluate were taken at regular intervals. These aliquots were diluted to the same concentration and then analysed via MC-ICP-MS. The aliquots' ⁸⁷Sr/⁸⁶Sr ratios were compared to a dilute of the unseparated solution. Elution curves of ⁸⁷Sr/⁸⁶Sr ratios were also produced to identify fractionation trends if present.

It is noted that when purifying Sr samples using Sr resin, gradient elution is used to strip the Sr from the column after washing, producing a relatively small volume of eluate. However, isocratic elution in 8 M HNO₃ will highlight fractionation effects as Sr is not taken up by Sr resin in low concentrations of HNO₃. In addition, larger eluate volumes will magnify any fractionation effects present.

4.4 Results and discussion

4.4.1 Batch Uptake

The distribution coefficient (K_d) was found to be 250 in 8 M HNO₃. Distribution coefficient for the 0.5 g concrete digest in 8 M HNO₃ was significantly lower at 100. Both 8 M HNO₃ and the concrete digest reached equilibrium within 20 minutes (Figure 4.3).

Horwitz et al., (1992a) defined uptake of Sr and other ions by a “volume to peak elution” value (V_p). A conversion factor ($K_d / V_p = 2.17$) allows for K_d to be calculated from the volume to peak elution (Triskem International, 2015a). Horwitz et al., (1992a) reported K_d 's of 200 for Sr in 8 M HNO₃, through gravity flow columns which is comparable to the K_d of 250 measured in this study. Using this K_d and the reported conversion factor Sr break through is estimated to occur after the addition of 178 mL 8 M HNO₃ and 75 mL of 0.5 g concrete matrix through 5 mm \varnothing \times 40 mm gravity flow columns. These volumes are significantly greater than the actual load volumes used and breakthrough of Sr during sample loading is, therefore, not considered likely even at increased flow rates. The difference in K_d between 8 M HNO₃ and cement digest is due to suppression of Sr uptake because of matrix

derived species. These may directly compete for space in the Sr binding sites of the crown ether (e.g. Pb) or through non-specific interference caused by high concentrations of matrix elements (e.g. Ca). Non-specific interferences can decrease Sr uptake by complexation with the analyte (Sr) or by changing the solubility.

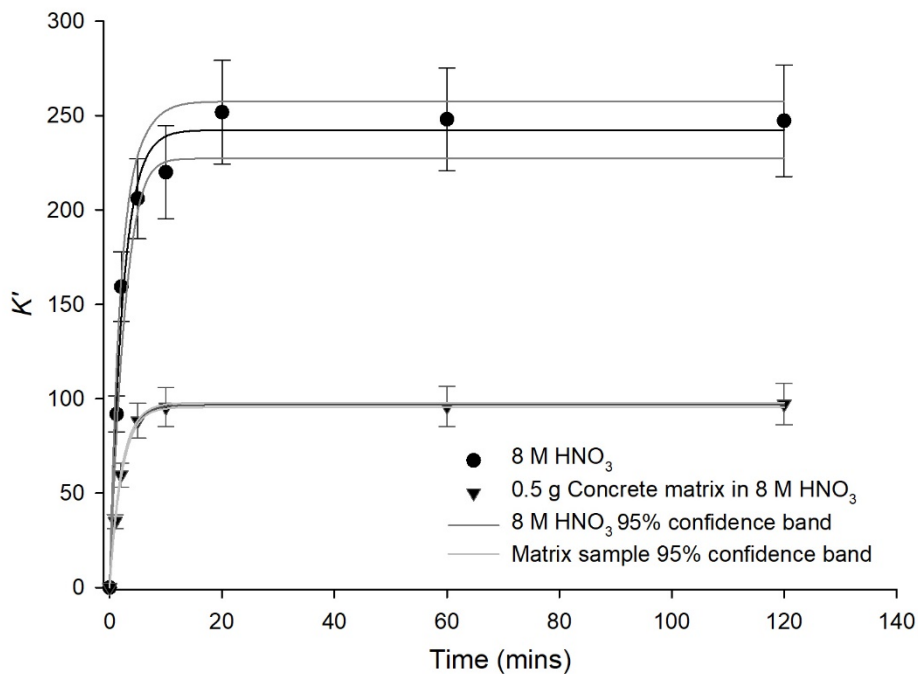
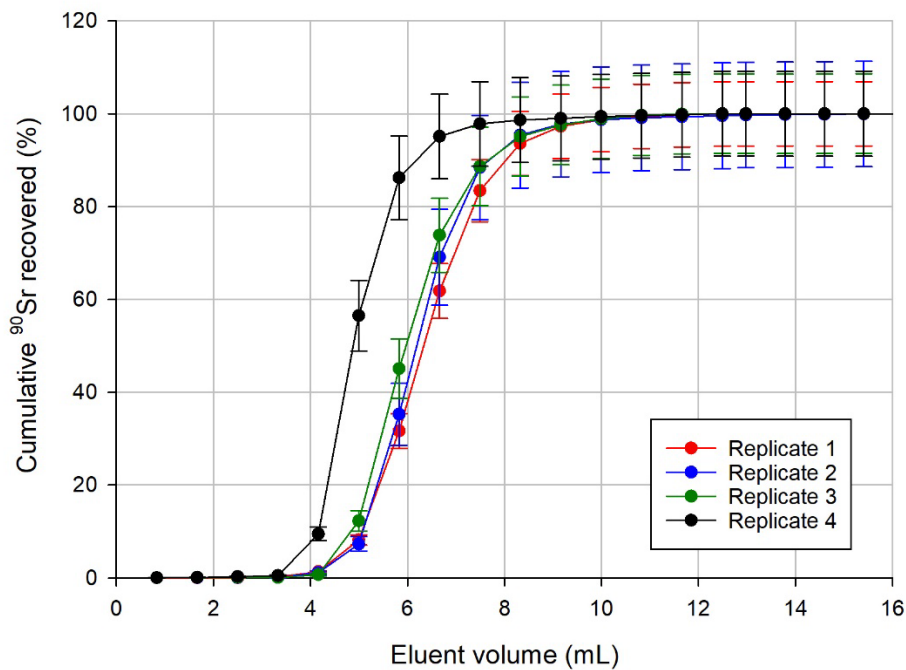


Figure 4.3.
Sr uptake by Sr resin with time for batch uptake experiments

From two different solutions; nitric acid and concrete matrix in nitric acid

4.4.2 Repeatability

Peak elution occurs on addition of 6-9 mL of 0.05 M HNO₃ (Figure 4.4). Elution of ⁹⁰Sr is completed within 13 mL for a flow rate of 1 mL/min. Recoveries of ⁹⁰Sr were >95% for three replicates. There is slight variability between runs. Replicate 4 shows faster Sr elution initially, reaching 10% elution before commencement of elution for replicates 1 - 3. Replicate 1 shows the slowest elution, however 100% elution is still achieved on addition of 10 mL. Variability between the runs is most likely due to packing effects of the Sr columns.

**Figure 4.4.****Sr repeat test elution profiles**

Procedure completed at 1 mL/min on 3 fresh columns from a 0.5 g loading mass

4.4.3 Effect of matrix

For concrete masses of 0.25 g, 0.5 g and 1 g, Sr elution occurs between 4 – 13 mL (Figure 4.5). Recoveries were above 90% for all three masses. This data shows no variation on Sr elution or recovery with increasing concrete mass. FWHM for 0.25 g, 0.5 g and 1 g were 1.3 mm, 1.3 mm and 1.0 mm respectively. The variation between the 3 masses analysed were within the variation seen in the repeatability tests (section 4.4.2). Given the K_d values established in 4.4.1, it is reasonable to expect variation in elution profiles between samples containing varying concentrations of matrix elements. However, because the elution of Sr in the matrix experiments was gradient elution, Sr was stripped and eluted from the column sooner than it would if isocratic elution in 8 M HNO₃ was utilised. This makes observation of elution profile variation with increasing matrix mass more difficult, especially given the resolution. This experiment demonstrated that for the separation procedure described in 4.2.3 and the column system used here, Sr elution and recovery is not notably affected by increases in matrix concentration up to 1g per 5 mL sample.

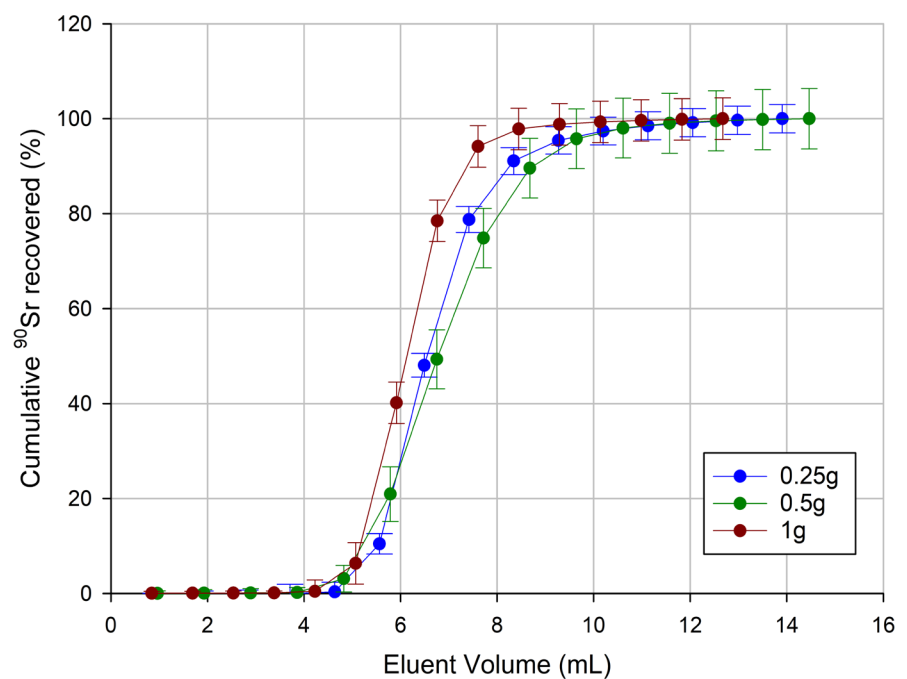


Figure 4.5.
Sr elution profiles with varying matrix mass

4.4.4 Flow rate effect on HETP

Over the flow rates tested, peak width increased with increasing flow rates (Figure 4.6). This is reflected in the HETP values which also increase with flow rate. The HETP values were 0.53, 1.4 and 2.7 cm for flow rates of 0.8, 2.3 and 4.5 mL/min respectively. The elution profiles show at the higher flow rates, breakthrough of Sr occurs more quickly. The Van Deemter equation (Equation 1.3) describes the effect of increasing flow rates on chromatographic separation characteristics. As the flow velocity of the mobile phase through the chromatograph increases, the exchange of analyte molecules between mobile and solid phases must be fast enough to maintain equilibrium (Stauffer et al., 2008). If this exchange is not fast enough a broadening of Sr peaks occurs. The two other controls on separation efficiency defined in the Van Deemter equation are eddy diffusion and longitudinal diffusion. Eddy diffusion does not change with flow rate and longitudinal diffusion effects are usually negligible in liquid chromatography (Nicoud, 2015). Additionally, it is important to note that if longitudinal diffusion was significant, increasing flow rate would decrease peak broadening (Stauffer et al., 2008). HETP values obtained from these experiments are comparable to that of results obtained by Horwitz et al., (1992a) and Grahek et al., (2006). Horwitz et al., (1992a) attained a HETP value of 0.59 cm

for a column of length 10.1 cm and diameter 0.27 cm, with 3.2 M HNO₃ at a flow rate of 1-2 mL/min. Horwitz et al., (1992a) also tested a finer particle size (50-100 μ m), and achieved a much thinner HETP (0.11 cm). Grahek et al., (2006) used a 14.2 cm long column of diameter 1 cm, a HNO₃ concentration of 3 M and a flow rate of 1 mL/min. HETP values of 0.71 and 0.15 cm were obtained using Sr resin particle sizes of 100-150 μ m and 50-100 μ m respectively.

Given the significant changes in HETP with increasing flow rate, investigation into Sr recovery is required to assess the separation performance at increasing flow rates. It is noted that previous study into Sr separation at higher flow rates was able to delay breakthrough by using significantly larger columns (Chung et al., 2015).

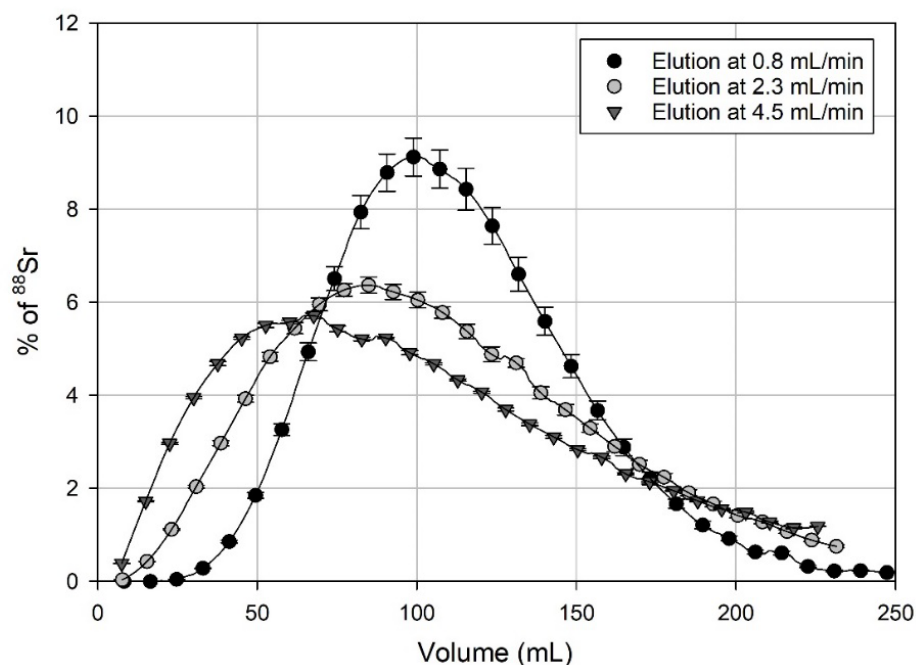


Figure 4.6.
Isocratic elution of Sr from Sr column

4.4.5 Effect of flow rate on Sr recovery in eluate fraction

Elution curves for ⁹⁰Sr elution were corrected for activity of sample during test and for overall recovery (Figure 4.7). Elution profiles for each flow rate remain largely unchanged and > 95% elution occurs within 18 mL for all flow rates. Slight variation in Sr elution is apparent after the addition of 8 mL of eluent. Flow rates of 0.8, 1.6 and 2.5 mL/min show 90% elution of Sr on addition of 8 mL of eluent. Flow rates of 3.4 – 5.1 mL/min show a

Chapter 4

slightly slower elution, with 90% achieved between 8 – 10 mL eluent addition. Volume to 50% elution for all flow rates occurs at 7 mL eluent addition. Maximum recovery of 105% ($\pm 7\%$) at 1 mL/min contrasts to the 94% ($\pm 7\%$) recovery at 5.1 mL/min (Figure 4.8). Although these recoveries are comparable within uncertainty, there is an apparent trend of decreasing recovery with increasing flow rate.

Strontium-90 elution curves also show that at the highest flow rates, Sr elutes from the column earlier than at the lowest flow rates. The overall effect of this peak broadening can be seen in the ^{90}Sr recovery data (Figure 4.8). Although uncertainty is high for these recovery values, a negative correlation between Sr recovery and flow rate is observed. Selection of an appropriate volume of eluent (>18 mL) can minimise any variation in Sr recovery. Variations that remain can be corrected for by use of a strontium radiotracer (e.g. ^{85}Sr). It must be noted, however, that changes in elution characteristics (specifically fwhm) which are observed with changing flow rate are less significant than inter-run variability.

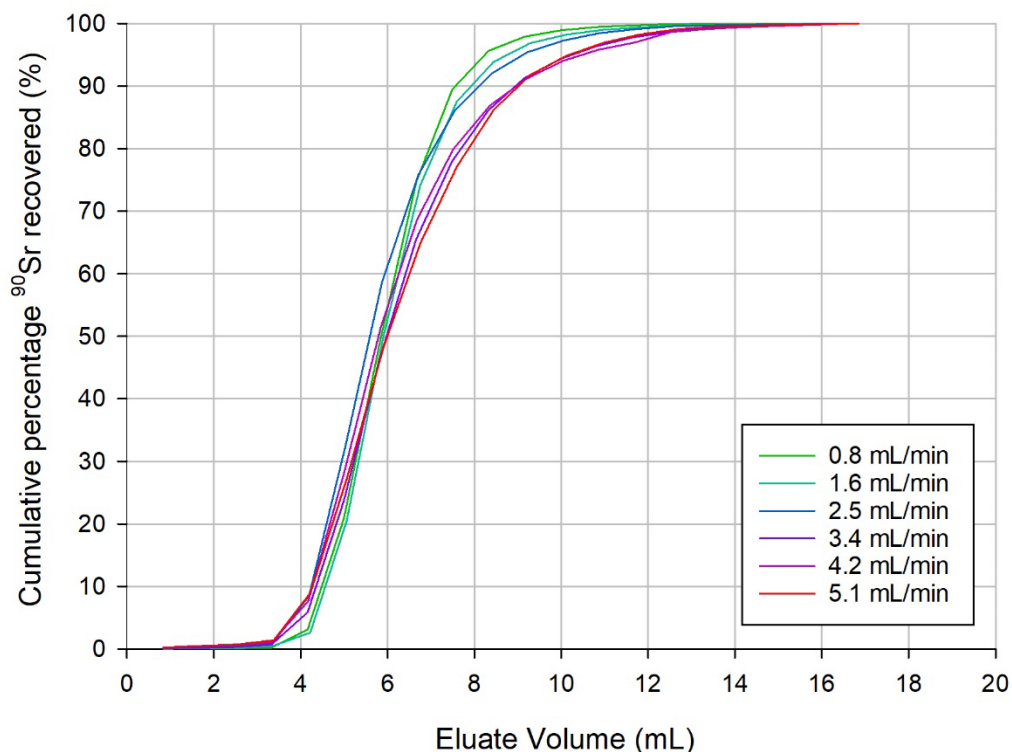
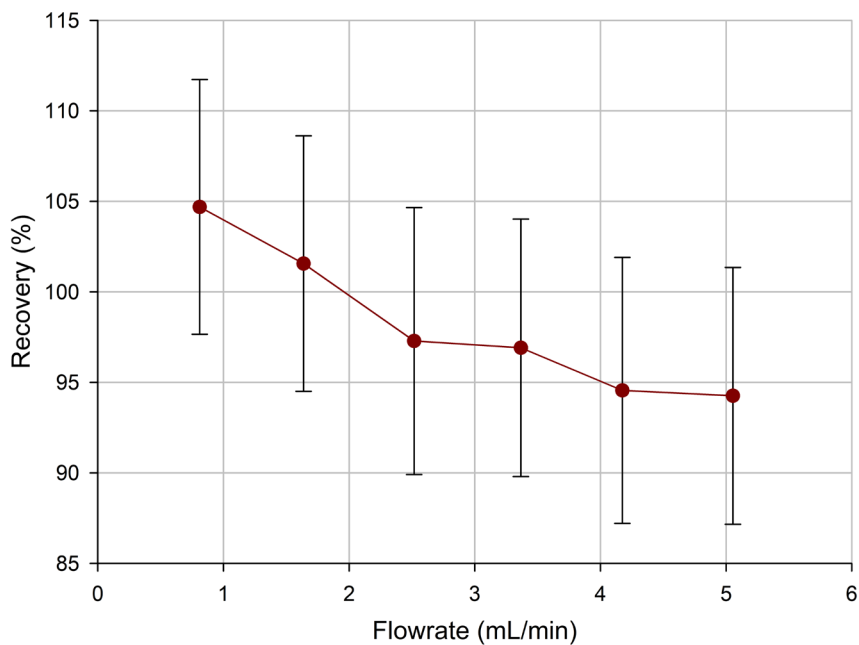


Figure 4.7.
Sr elution profiles at variable flow rates

**Figure 4.8.****Sr recovery versus flow rate**

Graph shows how recovery decreases with increasing flow rate

4.4.6 Effect of flow rate on decontamination

The elution data of contaminants at 5.1 mL/min shows that Co, Ni, Cs, U, Fe and Eu are washed from the column after 11.5 mL wash (Figure 4.9). During the load and wash phases of Sr separation there are three distinct behaviours of contaminants. The first behaviour is of Co, Ni, Cs, Eu, and Fe all of which show distinct peaks after roughly 2 mL of wash (as represented by Cs – Figure 4.10), followed by a steep decline in wash concentrations with contaminant elution completing within a total elution volume of 7 mL. This behaviour is consistent over all three flow rates tested. Additionally, Cs, Ni, Co, Eu and Fe decontamination factors were all similar. A systematic decrease in DF with increasing flow rate, is observed for all elements tested (Table 4.3). Horwitz et al did not publish uptake data for Co, Ni, Eu, or Fe. It is expected that their K_d 's are much lower than for U because of the similarity in their elution profiles compared to Cs. The second behaviour was that of U. Uranium profiles at all flow rates show some retention with an associated slower elution from the column at higher flow rates. This is demonstrated by the broader peaks of the U profile in the wash phase (Figure 4.9 and Figure 4.11). The DFs for U decrease with increasing flow rate from 1000 to 80 (Table 4.3). Horwitz et al., (1992) reported K_d for U at

Chapter 4

8 M HNO₃ of 5.5. Although this distribution coefficient for U is much lower than that of Sr, it is over an order of magnitude higher than that of Cs ($K_d = 0.15$). The third contaminant behaviour was that of Pb. Lead's DFs are much higher than that of all other elements studied here. This is due to Pb's much higher affinity for Sr resin. The K_d for Pb is > 1000 at 8 M HNO₃ and remains high at low HNO₃ concentrations (430 at 0.05 M HNO₃) (Horwitz et al., 1992a). Lead, although retained with Sr, is not subsequently co-eluted. This could have implications for reuse of columns where Pb build-up may occur causing bleed of both Pb and Sr. Lead's decontamination factor also decreased with increasing flowrate, from 50,000 to 1000 at the highest flow rate (Table 4.3).

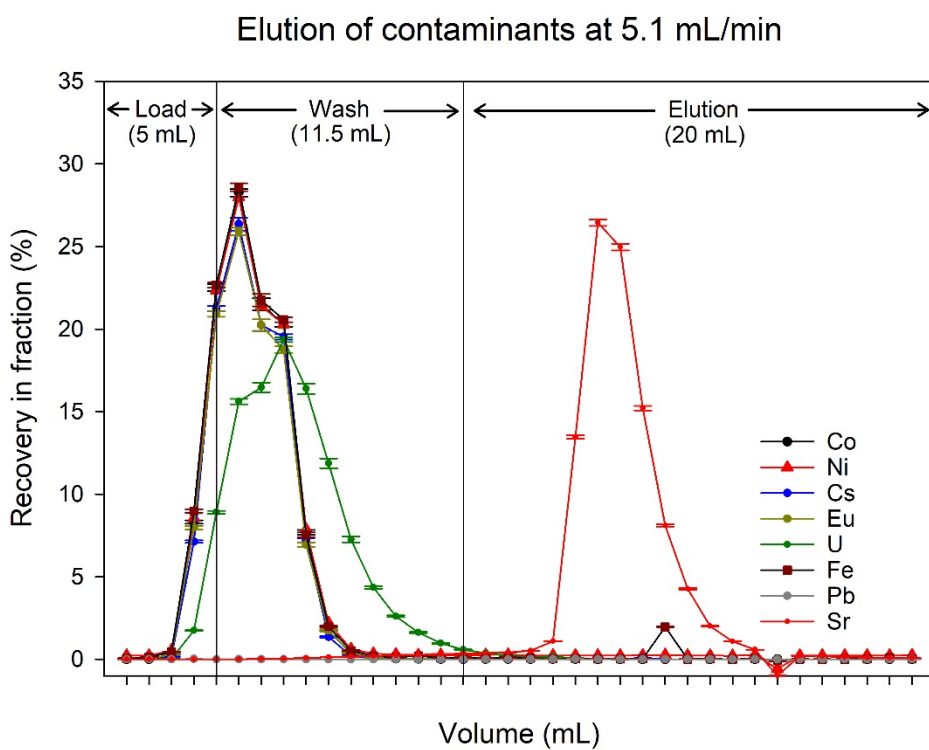


Figure 4.9.
Profiles of contaminant washout and Sr elution at 5.1 mL/min

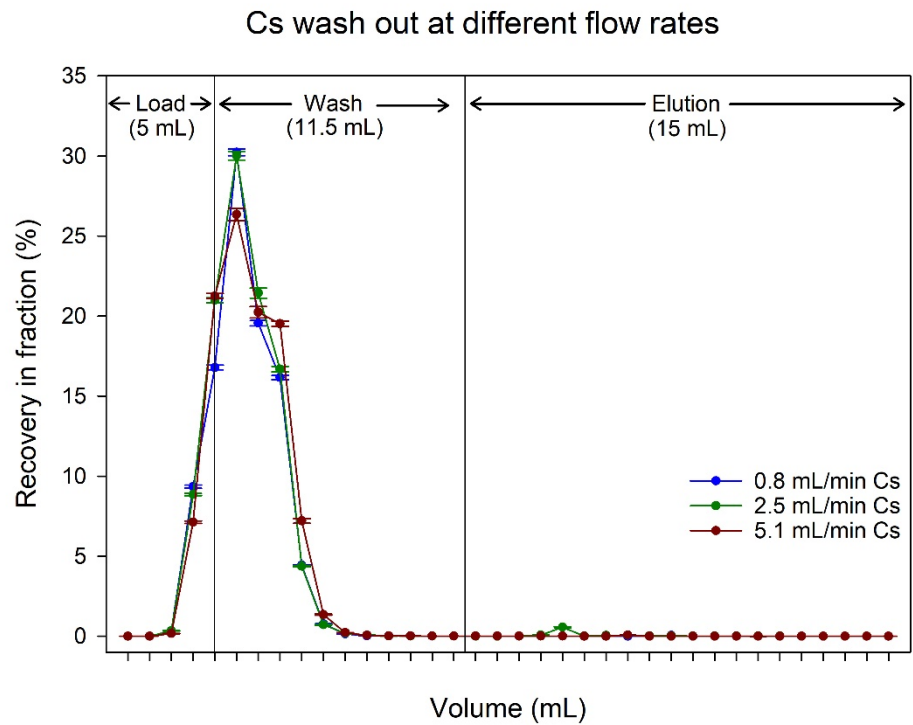


Figure 4.10.
Cs washout profiles at 0.8, 2.5 and 5.1 mL/min

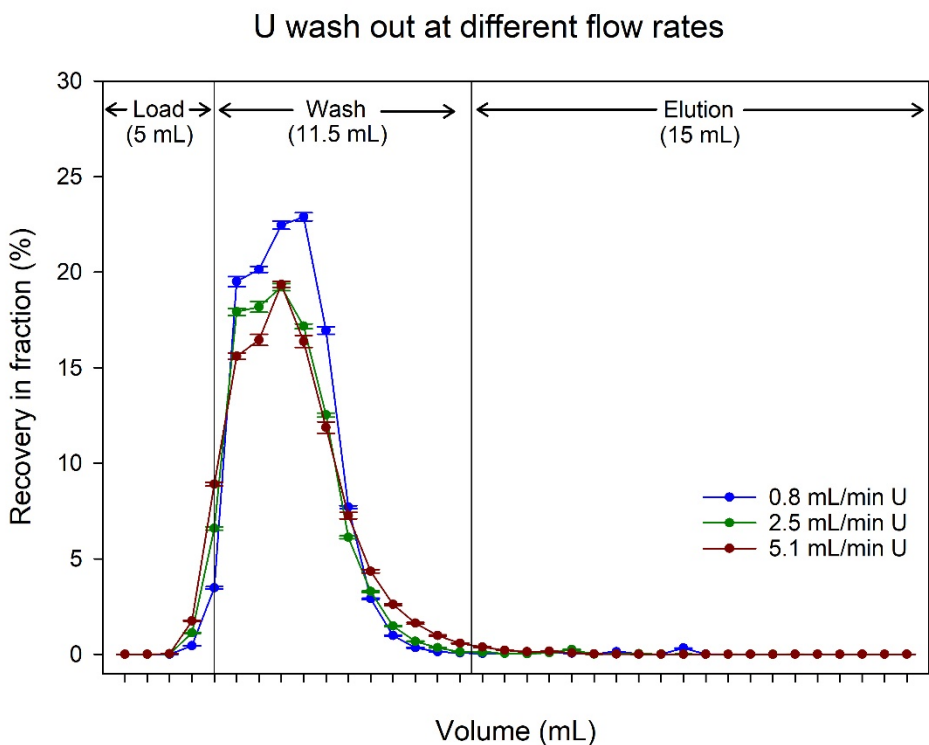


Figure 4.11.
U washout profiles for 0.8, 2.5 and 5.1 mL/min

Element	Fe	Co	Ni	Cs	Eu	Pb	U
DF at 0.8 mL/min	3×10^3	5×10^5	1×10^3				
DF at 2.5 mL/min	1×10^3	2×10^3	2×10^3	2×10^3	2×10^3	4×10^4	3×10^2
DF at 5.1 mL/min	1×10^3	90					

Table 4.3.
Decontamination factors at 3 different flow rates

The behaviour of U at the highest flow rate could, if present in large enough quantities, be present in the Sr fraction causing contamination of the purified Sr. Another consideration is that of the uranium-238 decay product ^{234m}Pa , (from ^{234}Th decay) which has a similar beta decay energy to ^{90}Y (2.3MeV). If ^{238}U is present in significant quantities compared to ^{90}Sr and ^{234m}Pa is allowed sufficient time for ingrowth the measurement of ^{90}Sr by Cherenkov counting ^{90}Y may be affected. As previously discussed, measurement L_D (limit of detection) of 0.1 Bq/g for ^{90}Sr would be adequate for the waste sentencing of concrete. Typically, to determine ^{90}Sr via ^{90}Y ingrowth, the sample must be stored for 14 days, for the ^{90}Y to reach secular equilibrium. The concentration of uranium present in the original sample to cause 0.1 Bq/g ^{234m}Pa contamination after 14 days must be determined. In addition, it is important to assess the worst-case scenario: if ^{234m}Pa is allowed an ingrowth time long enough to reach equilibrium with ^{238}U . A period of 1 year was assumed adequate enough time to allow for equilibrium to be reached between ^{238}U and ^{234m}Pa . Secular equilibrium was assumed for ^{234m}Pa ingrowth from ^{234}Th owing to the short half-life of ^{234m}Pa (1.17 minutes). Given a decontamination factor of 90 (Table 4.3), to produce an activity equivalent to 0.1 Bq/g of ^{234m}Pa after 14 days of ingrowth, an activity concentration of over 24 Bq/g of U is required in the original bulk material. If the eluate was left for sufficient time for equilibria to be established between ^{238}U and ^{234m}Pa , then over 8 Bq U/g is required in the original concrete sample. These values of ^{238}U are far higher than the maximum 1 Bq/g activity concentration given by EPR and IAEA required for exclusion from radioactive waste legislation or exemption and clearance from regulatory control based on the materials activity (Department for Business, Energy and Industrial Strategy, 2018; International Atomic Energy Agency, 2012; Internationale Atomenergie-Organisation, 2005). Thus, any concrete with a high enough ^{238}U concentration to affect the determination of ^{90}Sr would be classed as radioactive due to its ^{238}U content.

4.4.7 Column reuse

Slight variation in elution profiles became apparent with column reuse (Figure 4.12). Although overall recoveries decrease slightly with use (from 96.5% in Test 1 to 92.3% in Test 5) elution profiles and recovery data show effective removal of Sr from cementitious matrix even after 5 uses of the same column at 5.1 mL/min. Washing of the column after each elution was also deemed effective as elution of Sr began on addition of similar volumes of eluent (4 mL). As with previous test conducted in this present study, elution of Sr from the column ceased before 18 mL of eluent had been washed through the column.

Reduction in Sr resin efficacy over the five runs may be down to one of two factors, or a combination of both. Firstly, uptake of Sr on the crown ethers may be inhibited by Pb ions present in the cement matrix. As the columns were washed with MQ, the majority of Pb would not have been washed off the Sr resin (due to Pb's high K_d) and could prevent Sr take up in subsequent sample runs. Secondly, the Sr resin may be degraded as a proportion of the crown ether extractant may be removed from the solid phase during each elution cycle or degraded via chemical oxidation by the 8 M HNO_3 .

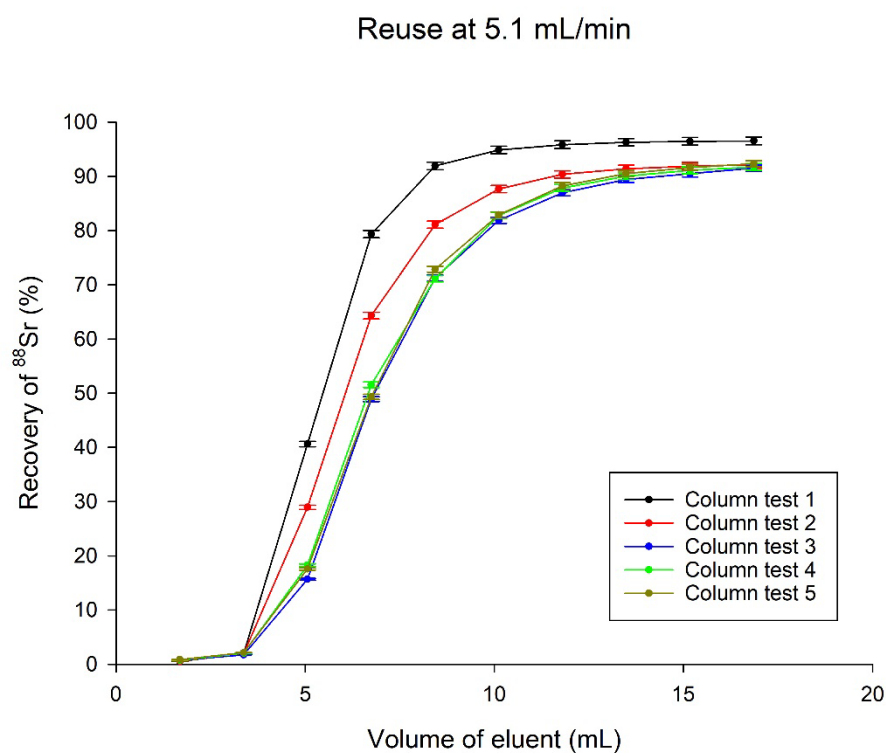


Figure 4.12.
Sr elution profiles for the reuse of the same column at 5.1 mL/min

Chapter 4

The decontamination of samples with multiple uses of the column shows no trend in terms of decontamination factor for Fe, Co, Ni, Cs and Eu (Table 4.4). Uranium showed a slight systematic decrease with reuse of columns, especially at flow rates of more than 0.8 mL/min, and Pb shows a marked decrease in DF with reuse at all flow rates. This is most likely due to Pb and U not being adequately washed from the column during the wash phase in between each run. This is due to Pb's very high K_d in 8 M HNO₃ and it only being removed from Sr resin upon the addition of 6 M HCl. Uranium's behaviour is similar however, it has a much lower K_d so the relative decrease in its DF with reuse is not as pronounced than Pb's.

Decontamination factor								
Flow rate	Repeat #	Fe	Co	Ni	Cs	Eu	Pb	U
0.8	1	2×10^3	6×10^5	6×10^2				
	2	1×10^3	2×10^3	4×10^2				
	3	2×10^3	53	5×10^2				
2.5	1	2×10^3	4×10^4	4×10^2				
	2	2×10^3	60	2×10^2				
	3	2×10^3	30	1×10^2				
5.1	1	1×10^3	90					
	2	1×10^3	2×10^3	2×10^3	2×10^3	1×10^3	50	60
	3	2×10^3	3×10^3	2×10^3	3×10^3	3×10^3	30	50

Table 4.4.
Reuse decontamination factors with 3 uses of the column

As stated in 4.3.9, the column capacity for Pb is 19 mg. During the reuse decontamination experiments 380 μ g Pb were added per run; a total of 1.1 mg over the 3 uses. Although this is significantly less than the 19 mg capacity of the column, a reduction in available binding sites in the column for Pb is the likely cause for the considerable decrease in decontamination factor. In addition, the crown ether binding sites occupied with Pb would be unable to retain Sr during the load and wash phases, further decreasing the separation efficiency of the column. Fewer crown ether binding sites means Sr sample has to travel further down the column before reaching K_d , increasing its HETP. Because of this, it is proposed that flow rate compounds the HETP increase during reuse of columns.

4.4.8 Analytical performance of simulated sample

Gamma analysis of the digest samples indicated < 10% losses of Sr from the digest procedure (Table 4.5). An average of < 10% of Sr breaks through the column during the load and wash phases. The average ⁹⁰Sr activity concentrations (corrected for chemical recovery using ⁸⁵Sr), shows a negative deviation between the expected ⁹⁰Sr activity in the sample and the fully corrected measured activity concentration from the purified fraction (Table 4.6). There was little difference at high Sr concentrations (RCW 1, 2 and 3).

Test	RCW 1	RCW 2	RCW 3	RCW 4	RCW 5	RCW 6
⁸⁵ Sr Activity added to concrete bulk (Bq)	10.8 ± 0.6	10.9 ± 0.6	11.0 ± 0.6	11.1 ± 0.6	11.1 ± 0.6	11.2 ± 0.6
⁸⁵ Sr Activity measured in sample after digestion (Bq)	11.2 ± 0.8	10.9 ± 0.7	10.8 ± 0.7	11.0 ± 0.7	11.2 ± 0.7	11.4 ± 0.8
⁸⁵ Sr Activity measured in eluate (Bq)	10.0 ± 0.7	9.9 ± 0.5	10.1 ± 0.6	10.2 ± 0.6	9.8 ± 0.7	10.2 ± 0.5
⁸⁵ Sr recovery (%)	93.5	91.7	91.8	91.9	88.3	91.1

Table 4.5.
⁸⁵Sr yield data

Test	RCW 1	RCW 2	RCW 3	RCW 4	RCW 5	RCW 6
Activity added concrete sample (Bq/g)	21.4 ± 2.4	22.2 ± 2.4	22.0 ± 2.4	21.9 ± 2.4	22.0 ± 2.4	21.9 ± 2.4
Measured activity concentration post separation (Bq/g)	20.1 ± 1.8	21.1 ± 1.5	20.1 ± 1.7	20.5 ± 1.7	22.3 ± 1.9	21.3 ± 1.7
Deviation (%)	-6.1	-5.0	-8.6	-6.4	1.4	-2.7

Table 4.6.
Fully corrected ⁹⁰Sr measurement from simulated concrete separation

Chapter 4

Due to the elution of Sr occurring from a change in HNO_3 concentration, the matrix of the solution in which ^{90}Y is measured is different to that which the Cherenkov counters are calibrated. Cherenkov counting efficiency was calibrated in a matrix of MQ. The Sr fraction of eluate is composed of 8 M and 0.05M HNO_3 , different to the calibration matrix. To investigate the quenching effect this different composition would cause, aliquots of ^{90}Sr tracer in equilibrium with ^{90}Y were added to a solution of MQ and to 8 M HNO_3 . Counting efficiency in 8 M HNO_3 and exact activity concentration of the ^{90}Sr tracer was established. The counting efficiency in 8M HNO_3 was found to be around 90% of that in MQ. This was included in the propagated method uncertainty budget.

The limit of detection (L_D) for the process was $0.060 \pm 0.008 \text{ Bq } ^{90}\text{Sr/g}$ of concrete (Equation 4.6, (Hurtgen et al., 2000)). This is below the target of 0.1 Bq/g discussed in 4.1.3.

$$L_D(\text{counts}) = 2.86 + 4.78\sqrt{(B + 1.36)}$$

$$L_D(\text{Bq/g}) = \frac{L_D(\text{counts})}{60 \times t} \times \frac{100}{E} \times \frac{100}{P} \times \frac{100}{R} \times \frac{1}{M}$$

Equation 4.6.

Limit of detection equations

B = total background counts, t = count time in minutes, E = counting efficiency, P = probability of emission, R = chemical recovery, M = mass in grams

4.4.9 Sr isotope fractionation

Accurate determination of Sr isotopes can reveal the age of a rock's formation, through analysis of different minerals within the geological sample. The precision of the age derived from Sr/Rb isotope analysis is dependent upon (i) the number of points used to construct the isochron, (ii) the variation in $^{87}\text{Rb}/^{86}\text{Sr}$, (iii) the degree to which the phase formed in isotopic equilibrium and (iv) the error on the individual measurements of Rb and Sr isotope measurements. Depending on analytical capability, varying magnitudes of Sr isotope composition can be measured. Generally, large variations in Sr isotope ratios result from older samples. Subtler variations among whole rocks or mineral phases can be measured by more sensitive techniques (MC-ICP-MS or TIMS), commonly to the fifth decimal place (i.e. 0.0000X) (Nakai et al., 1993; Nebel, 2014).

The Sr standard's $^{87}\text{Sr}/^{86}\text{Sr}$ was measured as $0.707510 (\pm 2.4 \times 10^{-5})$. At the average $^{87}\text{Sr}/^{86}\text{Sr}$ ratios were calculated for each flow rate (Table 4.7). Isocratic elution of the stable Sr solution in 8 M HNO₃ showed no trend of fractionation of the Sr isotopes. At the highest flow rate tested (4.5 mL/min) major variations in isotope ratio were observed (Figure 4.13). However, as these fluctuations were seemingly random, it is unlikely that the fluctuations were caused by mass fractionation during elution. As gradient elution is used during normal operation, it is unlikely that the fluctuations observed during isocratic elution of Sr would manifest any notable effect on $^{87}\text{Sr}/^{86}\text{Sr}$ ratios. The uncertainties on the average $^{87}\text{Sr}/^{86}\text{Sr}$ ratios were between 1.1×10^{-4} and 2.4×10^{-5} which are comparable to uncertainties on $^{87}\text{Sr}/^{86}\text{Sr}$ measurements used in geochemical studies (Brannon et al., 1992; Creaser et al., 2004; Nakai et al., 1993; Zack and Hogmalm, 2016).

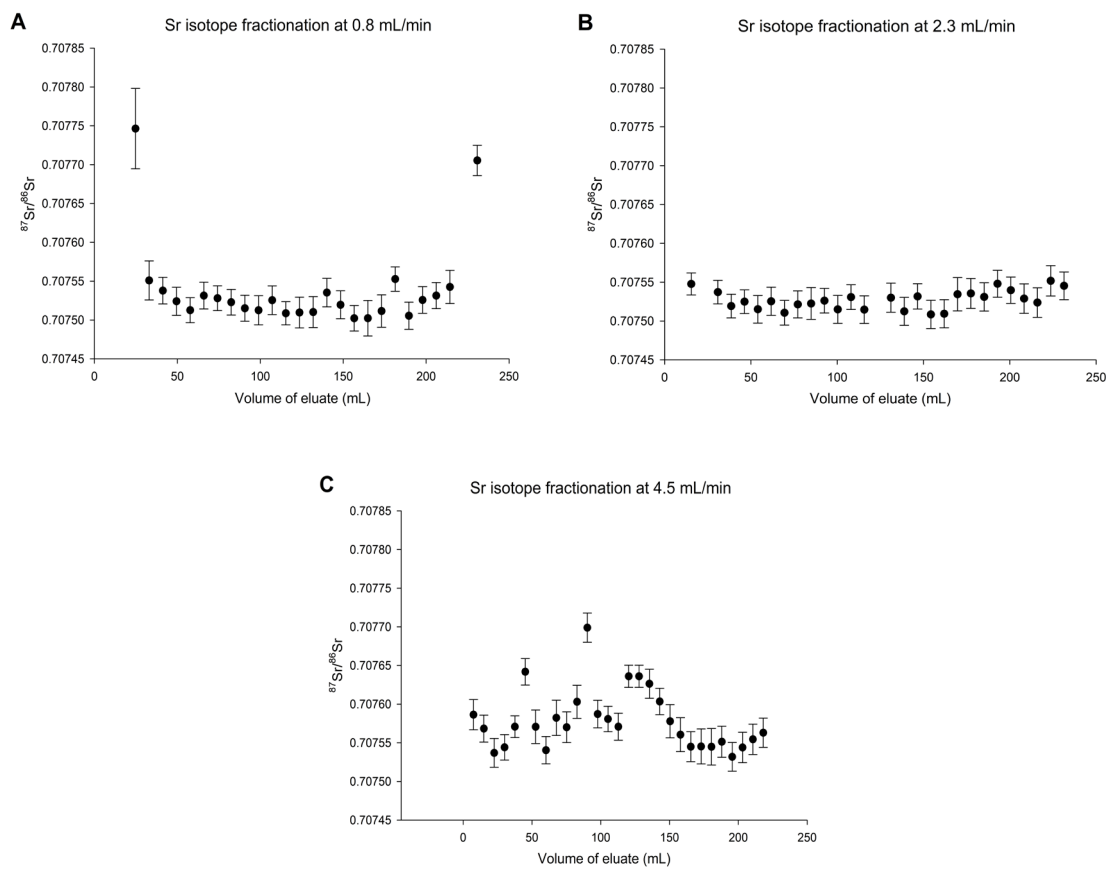


Figure 4.13.
Variation of Sr isotope ratio with elution volume
A – at 0.5 mL/min, B – 2.3 mL/min, C 4.5 mL/min

Flow rate (mL/min)	Average $^{87}\text{Sr}/^{86}\text{Sr}$	2 s.d.
0.8	0.707539	1.1×10^{-4}
2.3	0.707527	2.4×10^{-5}
4.5	0.707578	7.7×10^{-5}

Table 4.7. Average $^{87}\text{Sr}/^{86}\text{Sr}$ values achieved from isocratic elution of Sr in 8 M HNO_3 at varying flow rates

4.5 Conclusions

This study has shown that Sr resin can be used to effectively separate Sr from concrete matrices when used in a chromatographic column at high flow rates. High recoveries can be achieved (90% on average) at significantly higher flow rates than that achievable on gravity flow columns. Study of uptake kinetics shows that Sr resin can achieve equilibrium with Sr in solution in under 20 minutes. Comparison of HETP values during isocratic elution of Sr shows peak broadening occurring with increasing flow rate. Subsequent experiments utilised gradient elution to strip Sr from the column. This was done to initiate Sr elution prematurely and to contain Sr eluate in a smaller volume for analysis. During gradient elution, peak broadening occurs again as flow rate increases, however, compared to inter-test variability the increase observed is not significant. Elution profiles of Sr and washout profiles of contaminants indicate that higher flow rates have little effect on Sr separation from cement matrices.

Decontamination factors calculated from multi-elemental samples showed a systematic decline in decontamination capability for all elements tested when flow rate was increased. However, the lowest decontamination factor for all but one element, was on the order of 10^3 . Uranium decontamination was decreased to 80 at the highest flow rate tested. This behaviour is due to its slight retention on Sr resin in high HNO_3 concentrations.

This study has also demonstrated the efficacy of using the same chromatographic column for the separation of strontium from two or more samples. Peak broadening did increase with use and the efficacy is dependent on Pb concentration in the samples. Samples with

high Pb concentrations may cause a more rapid decline in Sr separation efficiency due to Pb and Sr's direct competition for resin active sites.

Separation of ^{90}Sr from a concrete matrix formed from an acid digest yielded accurate and precise measurements with average recoveries of $91.4\% \pm 3.4$. Limits of detection for the entire method were suitable for characterisation of solid waste using IAEA and UK guidelines. For the separation procedure described in 4.2.3, a conventional gravity flow separation (at 0.6 mL/min) using the same materials, reagents and column size would take at least 1.5 hours. The flow rates used in this study (6 mL/min) completed the separation procedure in under 10 minutes. This represents a significant time saving whilst achieving adequate recovery, good ^{90}Sr measurement and using similar volumes of materials and reagents than conventional techniques.

Although the procedure described in section 4.3.1 is fit for purpose, it is suggested that the following alteration is made based on the results gained from the method development. Due to slower washout of U from the column in comparison to other elements present it is advised that if high U are expected, a precipitative step of U using iron hydroxide is performed prior to sample loading on the Sr-spec column. This would greatly reduce the U present in the sample and likely reduce the likelihood of $^{234\text{m}}\text{Pa}$ disrupting ^{90}Sr determination in high U samples. Gamma spectrometry can be used to determine $^{234\text{m}}\text{Pa}$ activity concentration. This can be done prior to digestion or before or after ^{90}Y measurement in the eluate.

This study has taken the first step to validate the use of higher flow rates when separating Sr for application to geochemical study. Strontium isotope ratios commonly used in radiometric dating ($^{87}\text{Sr}/^{86}\text{Sr}$) were found to vary over the course of isocratic elution however average ratios calculated attained uncertainty values similar to that used in geochemical study. Use of gradient elution (as is common during normal Sr separation procedures) would further reduce the possibility of isotope fractionation effects in the final purified Sr fraction.

To fully develop this method, a range of geological matrices should be tested at the higher flow rates. Investigation into specific and non-specific interferences and their effects on Sr isotope fractionation at higher flow rates should be undertaken. Additionally, increasing

Chapter 4

the column length would make any fractionation effect more obvious. This should be considered if longer columns are required for separations.

Chapter 5 Kinetic control on uptake of major actinides and thorium on chromatographic materials

5.1 Introduction

Measurement of thorium, uranium and plutonium is routinely carried out throughout the life of a nuclear power plant to ensure safety and compliance. In addition, accidental release of these elements from nuclear facilities can lead to more extensive and expensive decommissioning processes. Determination of these actinides is crucial in ensuring the safety of the site after decommissioning activities have finished. Chromatographic separation of thorium, uranium and plutonium from industrial and environmental samples is often done to ascertain relative and absolute concentrations. These elements are often found in nuclear facilities due to their use as fuels and reactants or due to formation by neutron activation. Work done to expedite the concentration and purification of these has focussed mainly on use in emergency situations, most commonly after nuclear accidents (Maxwell et al., 2011b; Qiao, 2011). Isotopes of these actinides pose a threat to the environment and human health if they are unsafely released.

Thorium is over three times more abundant than uranium in Earth's crust and about as abundant as lead. Thorium is present as both a decay product of fuel elements and can be used as fuel itself. Thorium-232 can be used to create ^{233}U , a fissile element (Wickleder et al., 2006). Activation of ^{232}Th forms ^{233}Th which decays via beta decay to ^{233}Pa and then to ^{233}U . Thorium can be used for ^{233}U fuel production either *in-situ* or the Pa produced can be separated during fuel reprocessing for use in recycled fuel. There are no stable isotopes of Th and Th build-up in nuclear reactors occurs as a consequence of its presence in the decay chains of fuel radionuclides such as ^{238}U and ^{235}U . Significant quantities of Th can pose a risk to the environment and human health due to their method of decay (^{227}Th , ^{228}Th , ^{229}Th , ^{230}Th , and ^{232}Th via alpha decay) (Gad, 2014). Analysis of spent fuels and waste may be performed to assess Th content during reprocessing or disposal. Additionally, thorium's presence in nuclear fuels presents an issue of interference when trying to measure other radionuclides.

Chapter 5

Uranium is a naturally occurring radioactive element, isotopes of which can also be produced synthetically. Two uranium isotopes (^{233}U and ^{235}U) are fissile. It is the fissile nature of the two isotopes which has resulted in uranium's main use: as nuclear fuel. Natural uranium consists of three isotopes; ^{234}U , ^{235}U and ^{238}U , present in abundances of 0.0054, 0.7204 and 99.2742% respectively (Kondev et al., 2021). Natural uranium is enriched in order to achieve a higher proportion of ^{235}U , the only fissile U isotope found in nature. This is achieved by converting concentrated, purified uranium to uranium hexafluoride (UF_6), which is gaseous at relatively low temperatures. The gaseous UF_6 is then fed into a gas centrifuge – a cylindrical device that spins at high speed in a vacuum. Uranium-238 migrates to the outer edges of the cylinder, leaving the ^{235}U containing compounds in the centre, which are then extracted (Harding, 2016). The other fissile U isotope, ^{233}U , is synthesised from ^{232}Th . Uranium isotopes used in nuclear reactors decay via alpha decay, and this presents a significant radiological hazard when found in high concentrations. Because of the long half-lives of uranium and the radioactive nature of many of the daughter isotopes, knowledge of U content of nuclear wastes is crucial in order to prevent human exposure and environmental damage (Rožmarić et al., 2009).

Plutonium's most predominantly monitored isotopes are ^{238}Pu , ^{239}Pu , ^{240}Pu and ^{241}Pu with half-lives of 87.7 years, 24110 years, 6561 years and 14.3 years respectively (Qiao et al., 2009). Plutonium is rarely found in the natural environment as it requires specific conditions for synthesis (Rodriguez, 2014). Plutonium-239 is the most predominant Pu isotope created. This is because of the common use of uranium fuel in nuclear reactors. The most abundant isotope of uranium, ^{238}U , is activated by a neutron (emitted during fission) to form ^{239}U , which decays via beta decay (with a $t_{1/2}$ of 23.5 minutes) to ^{239}Np and then to ^{239}Pu (with a $t_{1/2}$ of 2.4 days). The formation of Plutonium during nuclear power production poses a challenge during standard operation as well as during the decommissioning of a nuclear facility, due to its highly radiological and biological toxicity (Rodriguez, 2014). Evaluation of Pu abundance in samples is required during assessment of samples for fuel reprocessing and waste disposal.

Separation and purification of these radionuclides is often required for accurate quantification due to their measurement interferences. Plutonium and uranium isotopes can prove to be isobaric and polyatomic interferences (e.g. $^{236}\text{U}^+$ with $^{236}\text{Pu}^+$ and $^{238}\text{UH}^+$ with $^{239}\text{Pu}^+$) when measured via ICP-MS and analysis via alpha spectrometry of all three

radioactive elements often requires separation due to spectral overlaps. Ion exchange and extraction chromatography are commonly employed to carry out these separations. Recent work looking into expediting sample preparation has highlighted the advantages of forced flow over gravity flow columns. However, in order for these new techniques to be applicable, their efficacy when used at higher flow rates must be analysed and modelled. Streamlining and expediting Pu, Th and U separations in the context of nuclear decommissioning first requires preparative work to establish materials' suitability. This study seeks to establish how the chromatographic materials typically used in actinide separation perform when mobile phase velocity is increased. Three commercially available materials were studied; anion exchange resin, TEVA resin and UTEVA resin.

The use of anion exchange chromatography for the separation of U, Th and Pu has been a long established technique (Carswell, 1957; Korkisch and Tera, 1961). Modern anion exchangers can be bonded to a solid support to allow for a robust, streamlined separation technique with simpler waste disposal. Eichrom, Bio-Rad and Dowex all produce anion exchange resins in which the functional group, a quaternary amine, is bonded directly to the monomer from which the polymer is synthesised, producing a polyelectrolyte (Budd, 1989). The physical properties of the resins (density, porosity and water retention capacity) are affected by the number of cross-linkages between the polymer chains. Ion exchangers with higher degrees of cross-linkages have lower pore spaces, higher exchange capacity but can only adsorb smaller anionic complexes. Ion exchangers with lower amounts of cross-linkages have a higher porosity and can adsorb larger anion molecules (Kunin and Myers, 1949; Tooper and Wirth, 1956). The functional group dictates the conditions that the resin is capable of performing in. Strongly basic functional groups allow for the resin to be used over the whole pH range. Weakly basic functional groups only allow for use in acidic media. The same is true for cationic exchangers - the more strongly acidic the functional groups are, the better they perform in acidic media. This in turn affects its separation capabilities. Type I and Type II anion exchange resins (described in 3.1.2.1) are available commercially (Bio-Rad Laboratories, 2021).

TEVA resin was first synthesised in 1994 by Horwitz et al., (1995). Its separation characteristics are reported to be very similar to that of a strongly basic anion exchange resin (Horwitz et al., 1995; Saito, 1984). This is due to TEVA having a quaternary amine as its functional group. TEVA resin's method of production however differs to anion exchange

Chapter 5

resin, as it does not contain the functional group chemically bound to the polymer of the resin. TEVA resin consists of a liquid mixture of trioctyl and tridecyl methyl ammonium chloride (commercially available and known as Aliquat® 336) sorbed to an inert acrylic ester polymer (Amberchrom CG-71ms) (Horwitz et al., 1995). The resin is formed by cleaning the inert support material in methanol, then mixing the extractant (Aliquat® 336) mixture with the clean support and additional methanol. The methanol is then removed by slow rotary evaporation in order to ensure homogenous distribution of the extractant on the support. Physical properties of the resin such as pore diameter, surface area of the resin and amount of swelling are governed by the properties of the Amberchrom CG-71ms support. Therefore, the capacity of the resin is governed by the inert support used, as resin beads with higher pore diameter or larger overall surface area will allow for larger coverage of the extractant. Increased coverage of extractant per resin bead means there are a larger number of functional groups available to the anions in the liquid phase.

UTEVA resin is the only resin of the three studied which is used for the separation and purification of uranium. It is an extraction chromatographic material, first synthesised by Horwitz et al., (1992). Similar to TEVA resin, UTEVA resin consists of an extractant sorbed to an inert support (Horwitz et al., 1992b). The extractant used is diethyl amylphosphonate (DAAP) and the process of sorbing it to the support material is the same as for TEVA resin. The inert support material used was Amberchrom CG-71 or Amberlite XAD-7, dependant on the resin diameter. Horwitz stated that the two support materials were essentially the same, differing only in particle size. The resulting material was termed UTEVA resin due to its ability to adsorb uranium as well as other tetravalent actinides, provided they were in the tetravalent form (Horwitz et al., 1992b). The resin was able to effectively sorb uranium from solutions of varying nitric or hydrochloric acid concentrations (0.5 - 10 M for HNO₃ and 6 - 12 M for HCl). Its ability to function in highly acidic conditions make it suitable for use in uranium purification from nuclear waste samples.

The use of UTEVA in series with another chromatographic column is common for the isolation and purification of multiple actinides including uranium (Croudace et al., 1998; Metzger et al., 2019; Warwick et al., 1999). Often the anion exchanger (be it TEVA or anion exchange resin) is used to isolate the Pu, Th and other actinides, with the wash being transferred to the UTEVA resin.

The aim of this research is to assess the applicability of Anion exchange, TEVA and UTEVA resins to expedited separations using increased flow rates. This will be done in preparation for an expedited separation method for U, Th and Pu. In addition, the characteristics of the extractant and its effect on the sorption of target species will be evaluated. This will be achieved by assessing the following:

- Resin uptake kinetics
- The elution behaviour of sorbed species during isocratic elution
- Elution behaviour of contaminants

Comparison of two chromatographic materials with similar active sites (TEVA resin and Anion exchange resin) will aid in the understanding of how active site and their bonding method to the polymeric support affects uptake kinetics.

5.2 Materials and Methodology

5.2.1 Instrumentation

Alpha spectrometric analysis utilised an AMETEK® ORTEC® Alpha Analyst (Berwyn, Pennsylvania, U.S.). Alpha samples were electrodeposited onto stainless steel planchet counting trays (27 mm diameter) provided by Nuclear Supplies Ltd. ICP-MS measurement was conducted using an Agilent 8800, an ICP-QQQ-MS, supplied by Agilent (Santa Clara, California, USA).

An Automated Sequential Radionuclide Separator (ASRS) (Hanjin Eni Co., LTD., Daejeon, Republic of Korea) was utilised for the column experiments. Instrument control utilised a custom programme created using LabVIEW provided with the ASRS. Actual flow rates for each experiment were calculated gravimetrically from the elute produced.

5.2.2 Materials and reagents

Elemental solutions of U, Th and contaminants in multi-element tests were produced from ICP-MS solutions. The ^{239}Pu radiotracer was produced from dilutes of purified isotope solutions from the National Physical Laboratory (Teddington, UK) (ID: R24-01). The ^{242}Pu radiotracer was sourced from AEA Technology (now Ricardo-AEA, Harwell, UK) (ID: PRP10020). Working dilutions of the radiotracers were prepared by gravimetric dilution.

Chapter 5

All reagents were of analytical grade unless otherwise stated. Nitric acid solutions were produced from a 70% (weight) concentrate (Fisher Scientific, Loughborough, England). HCl solutions were produced from a 37% (weight) concentrate for analysis (Fisher Scientific, Loughborough, England). For ICP-QQQ-MS analysis, 2% nitric acid solutions were prepared from PrimarPlus-Trace analysis grade (>68% by weight) (Fisher Scientific, Loughborough, England). High purity water obtained using a Q-POD Milli-Q Advantage A10 Water Purification System (Merck, Darmstadt, Germany).

Anion exchange resin 1x8 in chloride form, 100-200 mesh (75 – 150 µm) was supplied by Eichrom Technologies (IL, USA). TEVA and UTEVA resins (100 – 150 µm) were supplied by Triskem Intl. (Bruz, France).

For rapid, small volume filtrations Millex®GP 0.22 µm PTFE syringe filters were used. Resins in column test were packed into columns as a slurry to a bed of dimension 40 × 6.6 mm (i.d.) in a glass chromatographic column (Omnifit® Chromatography Column, Diba Industries, Danbury, CT, USA).

5.2.3 Batch uptake of plutonium on anion exchange resin

Mass of 0.1 g Anion exchange resin was taken and mixed with a 10 mL solution of ^{239}Pu in 8 M HNO₃. Eight samples were prepared in this manner and the anion exchange resin was exposed to the Pu for different time intervals per sample. The time intervals were 1, 5, 10 and 30 minutes, 1, 4, 7 and 24 hours. During this time the samples were left on a vial tumbler in order to ensure constant mixing of resin and sample solution. After the elapsed time the solution and resin were separated using a syringe filter. A known activity (50 mBq) Plutonium-242 was added to each sample as a tracer for the electrodeposition stage. The filtrate was evaporated to dryness with 5 – 6 drops of Na₂SO₄ to ensure efficient dissolution of Pu. The Pu was dissolved in 1 mL of 1.2 M HCl, 5 mL of 4% ammonium nitrate was added and the solution transferred to an electrodeposition cell along with washings. The plutonium was deposited onto a stainless steel disc by passing a 400 mA current through the solution, using the stainless steel disc as the cathode. After 1.5 hours the cell solution was neutralised with a few drops of concentrated ammonia solution before dismantling the cell. The steel disc was lightly rinsed with MQ and set to dry on a hot plate. Once dried, the disc was counted on an Alpha detector for >100,000 seconds.

Plutonium uptake was only tested on anion exchange resin in order for comparison to published data. Published uptake data for Pu on TEVA and anion exchange resin showed stronger adsorption than Th. Given that both Pu and Th adsorb to the materials in the same way, Th was used as an analogue for Pu uptake during the study of uptake kinetics between TEVA and anion exchange resins.

5.2.4 Batch uptake of uranium and thorium on UTEVA, TEVA and anion exchange resin

Method of exposure of the resin to the analyte (U or Th) was similar to that described in 5.2.3. Mass of 0.1 g of either TEVA or UTEVA was taken and mixed with 10 mL of 1 ppm solution of U or Th in 8 M HNO₃. Eight samples of each analyte and for each chromatographic material were prepared and mixed for the same time intervals as for Pu on anion exchange resin. After the respective time interval had elapsed the solution and chromatographic material was separated using a syringe filter. The filtrate was then diluted by 100 times in preparation for analysis by ICP-MS. The solution diluted to around 3% HNO₃ and indium and rhenium was added to give a concentration of 5 ppb for use as an internal standard. The diluted filtrate was analysed via ICP-QQQ-MS using a 7-point concentration calibration curve.

The ratio of analyte in the stationary and mobile phase (K') and the distribution coefficients (K_d) were calculated using Equation 1.4.

5.2.5 HETP tests

HETP values for two chromatographic materials were determined; TEVA resin and Anion Exchange resin. Because of their similar active site, an analysis of their HETP will further demonstrate the uptake differences between the two materials. Solutions of analyte in 8 M HNO₃ were produced and loaded onto columns of TEVA and Anion Exchange. For anion exchange, a 1 ppm solution of U and 33 ppm solution of Th were produced and for TEVA resin, 700 ppb of U and 40 ppm of Th were produced as the load solutions. The concentrations of analyte were varied based on literature data and the results from the batch uptake analysis. Load concentrations were selected to permit measurement of the eluent without the need for serial sample dilution.

Chapter 5

A 5 mL load solution was used and isocratic elution of the analyte was completed using further volumes of 8 M HNO₃. Fractions of eluate were collected and their mass recorded to establish precise flow rates and eluate volumes during each test. Eluate fractions were diluted in the sample collection vessel using 2.5% HNO₃ with 5 ppb In/Re as internal standard. The analyte concentration of each fraction was then measured by ICP-MS using a 6-point concentration calibration curve.

5.2.6 Multi element tests

Stable multi element solutions were made using Fe, Co, Cs, Pb, Eu, Ni, U and Th of concentrations of 100 – 500 ppb. These elements were chosen due to their common presence in rebar reinforced samples and because of their occurrence due to activation of some elements in concrete. This was done to examine the behaviour of different elements on anion exchange, TEVA and UTEVA resin at 3 flow rates. Gradient elution was used to elute the different analytes to simulate the fractions collected during a separation procedure. For all materials, the load solution containing the elements was 8 M HNO₃. For anion exchange and TEVA resins the wash phase consisted of 8 M HNO₃ and the elution phase was 0.05 M HNO₃. The procedure for UTEVA resin was altered to assess its ability to separate both U and Th into their own fractions. The wash phase after loading used 8 M HNO₃ to elute the contaminants with both Th and U remaining sorbed to the resin. The Th was then eluted in 6 M HCl. Under these conditions U should remain sorbed to UTEVA (Horwitz et al., 1992b). Uranium elution was completed using MQ.

Aliquots were collected at regular intervals (1.5 mL). Each aliquot was evaporated to dryness with the addition of a few drops of 2% NaSO₄ to aid redissolution. The dried sample was redissolved in 2% HNO₃ containing 5 ppb In/Re. Analysis was performed by ICP-MS using a 6-point calibration created using an aliquot of the bulk sample solution used for each test.

5.3 Results and discussion

5.3.1 Batch uptake experiments

Uptake tests show that in 8 M HNO₃, Pu and Th are taken up on to anion exchange resin and yield distribution coefficients (average of 4300 and 270 respectively). Uranium on the other hand, is not taken up as well by anion exchange resin (Figure 5.1, top). The average distribution coefficient value for U on anion exchange was 10. The distribution coefficient (K_d) data correlates with published data for Pu, Th and U uptake in nitric acid (Faris and Buchanan, 1964). Maximum uptake (K_d) of Pu and Th on anion exchange resin is achieved after ~2.5 hrs.

UTEVA resin exhibited the fastest reaction kinetics, with both Th and U reaching equilibrium by 10 minutes. UTEVA resin also yielded the highest distribution coefficients of the three materials investigated. Average UTEVA distribution coefficient values were 750 and 900 for U and Th respectively. These values are slightly higher than those reported in the product literature for UTEVA resin (500 and 420 for U (VI) and Th (IV) once a conversion factor of 1.67 is used). Repeat experiments show higher K_d values for Th on UTEVA than U (Horwitz et al., 1992b).

For Th uptake on TEVA resin, equilibrium was achieved after 30 – 60 minutes. Uranium uptake on TEVA resin, much like anion exchange resin, was low. Average distribution coefficients for Th and U on TEVA were found to be 550 and 50 respectively aligning with the 600 and 15 previously reported (Horwitz et al., 1995). Previous study found that uptake of Th and U on TEVA and UTEVA respectively reached equilibrium by 10 minutes (Horwitz et al., 1995). This time for TEVA resin is slightly faster and may be due to the smaller particle size used in the Horwitz study (50 – 100 µm). Plutonium distribution coefficients on TEVA and UTEVA resin are reported in their technical documentation. In 8 M HNO₃ K_d's for Pu are ~10,000 and ~2,000 for TEVA and UTEVA respectively (Horwitz et al., 1995, 1992b).

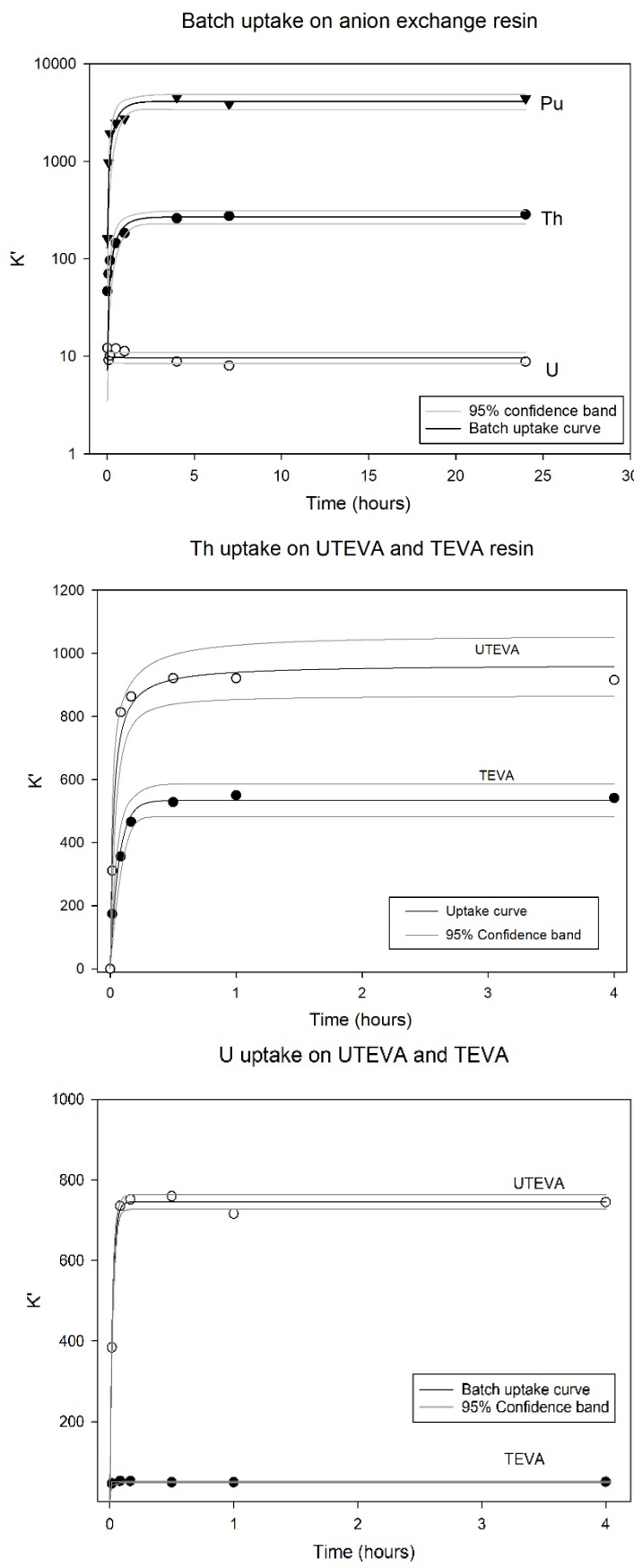


Figure 5.1.

Uptake curves for three different chromatographic materials

Pu, U and Th on anion exchange resin (top), Th on UTEVA and TEVA (Middle) and U on UTEVA and TEVA (bottom)

The adsorption of an analyte from mobile phase to stationary phase is governed by a combination of different stages (Ho et al., 2000; Hristovski and Markovski, 2017; Sahoo and Prelot, 2020):

1. Diffusion of the analyte from the bulk solution to the liquid film surrounding the absorbent
2. External diffusion of the analyte across the surface liquid film
3. Intraparticle diffusion of the analyte from the liquid film to the surface via pore diffusion or surface diffusion
4. Interaction of the analyte with the active sites via physi- or chemisorption and in the case of reversible systems, desorption of analyte from the active site

Kinetic models can aid in the description of adsorption. The kinetic model determines the time taken for equilibrium to be reached. Datasets for the analytes exhibiting significant sorption to the chromatographic materials were characterised to further pinpoint the control on uptake for each system. Pseudo-first-order and pseudo-second-order kinetic models are most commonly applied to chromatographic system kinetics. Both of these kinetic models have numerous non-linear forms which can be converted to linear forms. The analysis here was performed using the two most commonly used linear forms and assessing goodness of fit to the linear regression of each model.

The pseudo-first-order (PFO) model is a kinetic model based on the assumption that the rate of change of analyte adsorption with time is directly proportional to the concentration of analyte at saturation, and the amount of analyte uptake with time. The Lagergren equation is commonly used to describe the PFO kinetics (Lagergren, 1907)(Equation 5.1).

$$\frac{dq_t}{dt} = k_1(q_e - q_t)$$

Equation 5.1.

Pseudo-first-order equation

t (min) is time, k_1 (L min^{-1}) is the rate coefficient of PFO adsorption q_e and q_t (mg g^{-1}) are the stationary phase concentrations of analyte at time t and at equilibrium respectively

Chapter 5

To convert to the linear form, the Lagergren equation is integrated using boundary conditions of $q_t = 0$ at $t = 0$ and $q_t = q_e$ at $t = t$:

$$\log(q_e - q_t) = \log(q_e) - \left(\frac{k_1}{2.303}\right)t$$

Equation 5.2.

Linear form of pseudo-first-order equation

If $\log(q_e - q_t)$ is plotted against t a system following the PFO kinetic model would have points lying on the straight line with the y-intercept being the \log of the experimentally determined q_e . Pseudo-first-order describes systems where analyte adsorption occurs through diffusion of the solid-liquid interface (Sahoo and Prelot, 2020).

The pseudo-second-order (PSO) model differential equation is given by:

$$\frac{dq_t}{dt} = k_2(q_e - q_t)^2$$

Equation 5.3.

Pseudo-second-order equation

k_2 is the equilibrium rate constant for pseudo-second-order sorption (g/mg min)

Which after mathematical development, applying the same boundary conditions and the PFO model is expressed in its linear form:

$$\frac{t}{q_t} = \frac{1}{k_2 q_e^2} + \frac{t}{q_e}$$

Equation 5.4.

Linear form of pseudo-second-order equation

Plotting t/q_t vs t should yield a straight line if the system follows the PSO kinetic model. The slope of the line gives $1/q_e$ and the y-intercept gives $1/k_2 q_e^2$. From this k_2 can be determined. Additionally, q_e (mass of analyte adsorbed at equilibrium) can be calculated. The q_e calculated here gives a useful check as the value calculated from the PSO linear equation can be compared to the data collected at equilibrium. This is not possible with the PFO linear equation as the experimental q_e value is required in order to construct the plot. Systems following the pseudo-second-order kinetic model are assumed to have

chemisorption as the rate determining step (Ghaedi et al., 2011; Sahoo and Prelot, 2020). Additionally, the model is suitable to predict behaviour over the whole range of adsorption of analyte onto the resin. In PSO kinetics, adsorption rate is proportional to adsorption capacity (number of active sites occupied) and not on the concentration of active sites available.

For the data analysed here the same time periods were assessed for all analytes on the three different materials. Time periods for sorption data collection were not evenly spaced but increasing with time, and the maximum time period analysed was 7 hours (420 minutes). Seven hours was more than adequate to include the entire range of adsorption up to equilibrium for all materials and analytes. All sorption data was converted to mass in mg. SigmaPlot's polynomial linear regression analysis tool was used to assess goodness of fit via the R^2 value as well as providing the equation for the linear relationship.

All systems exhibit pseudo-second-order adsorption kinetics (Table 5.1, Table 5.2 and Table 5.3). The R^2 values show that deviation from linearity of the PFO was more severe than for PSO. The larger deviation from linearity causes more inaccurate q_e values for PFO fits. The calculated q_e values or the PSO model fits are much closer. The modelling of the batch uptake data to the two kinetic models shows that for all 3 materials and for all adsorbed species that chemisorption is the rate-limiting step.

Th adsorbent	q_e (exp.)	Pseudo-first-order model			Pseudo-second-order model		
		R^2	q_e (calc.)	k_1	R^2	q_e (calc.)	k_2
Anion exchange	0.0875	0.699	2.90×10^{-2}	3.22×10^{-3}	0.9995	0.092	1.54
TEVA	0.0525	0.823	7.21×10^{-3}	1.77×10^{-2}	0.9997	0.052	189.3
UTEVA	0.0521	0.018	3.86×10^{-3}	6.91×10^{-4}	0.9956	0.050	20.1

Table 5.1.
Th adsorption kinetics

Chapter 5

Pu adsorbent	q_e (exp.)	Pseudo-first-order model			Pseudo-second-order model		
		R^2	q_e (calc.)	k_1	R^2	q_e (calc.)	k_2
Anion exchange	1.89×10^{-7}	0.576	4.12×10^{-8}	7.83×10^{-3}	0.9919	1.86×10^{-7}	5.26×10^6

Table 5.2.
Pu adsorption kinetics on anion exchange resin

U adsorbent	q_e (exp.)	Pseudo-first-order model			Pseudo-second-order model		
		R^2	q_e (calc.)	k_1	R^2	q_e (calc.)	k_2
UTEVA	0.0545	0.3565	2.49×10^{-3}	5.99×10^{-3}	0.9999	0.0535	-36.054

Table 5.3.
U adsorption kinetics

The adsorption mechanism for tetravalent actinides is similar given the comparable functional group chemistry (Horwitz et al., 1995; Tooper and Wirth, 1956). The difference in uptake kinetics between TEVA resin and anion exchange resin could be due to the manner by which the extractant is bonded to the resin bead. TEVA resin has the liquid anion exchanger (Aliquat 336[®]) coated to the outside of an inert support material, Amberchrom CG-71M (Horwitz et al., 1995, 1990). Anion exchange resin has the quaternary amine groups (trimethylamine) bonded to the styrene molecules. One of the stipulations of chemical collision theory is that reactions may only occur if the orientation of the molecules at the point of collision is such that the atoms involved in the sharing or transfer of electrons come into contact with each other (Moeller et al., 1980). It is suggested that the faster kinetics for TEVA are because the quaternary amines are more freely moving when coated to the surface of the inert support than when they are part of the forming structure (as is the case with anion exchange resin). This allows the functional sites of the TEVA resin to orient themselves around the target anions more effectively and could be the mechanism leading to TEVA resin's faster uptake.

Another possibility is that there are more active sites contained by the TEVA resin. More exchanger molecules in the resin bead would lead to a much larger probability of interaction between quaternary amine and analyte. The number of useable active sites on the bead of both materials would be proportional to the capacity of the resins. The materials' capacities are available in product literature and show that TEVA resin has a

capacity for Th (IV) of 24.5 mg mL^{-1} (given a capacity of 70 mg Th per gram of resin and a bead density of 0.35 g mL^{-1}) and anion exchange has a capacity for Th (IV) of 69 mg mL^{-1} (given a quoted capacity of 1.2 meq mL^{-1}). Therefore, the faster reaction kinetics exhibited by TEVA are not due to its higher capacity.

The differences between the active sites of the two resins may also play a part in uptake kinetics. TEVA's exchangers – trioctyl and tridecyl methyl ammonium chloride – contain significantly longer chain alkyl groups bonded to the nitrogen atom in comparison to the 3 methyl groups in the anion exchange's quaternary amine. However, research into uptake of pertechnetate ions using anion exchange molecules demonstrated that longer chain alkyl- amine groups actually slow the exchange kinetics (Bonnesen et al., 2000; Gu et al., 2000). It is suggested that the quaternary amines of the TEVA resin should result in slower kinetics in comparison to the quaternary amines of the anion exchange resin used. Longer chain quaternary amines are required for the production of TEVA resin as shorter chain quaternary amines are soluble in water and would therefore be washed from the inert support in aqueous solutions (data from PubChem database (Kirk et al., 1978; Yalkowsky et al., 2019; Yalkowsky and Dannenfelser, 1992)). As the quaternary amines are bonded to the polymer support in anion exchanger resin, ones with shorter alkyl groups can be utilised. The slower kinetics of the longer chained alkyl-amines strengthens the argument in favour of active site bonding method to the support material being the cause of the faster kinetics.

UTEVA's uptake kinetics are faster in comparison to both TEVA and anion exchange resin. However, due to lack of a suitable comparison, it is not possible to tell if the kinetics of uptake are due to the method of DAAP bonding to the inert support, the extractant's own kinetics, or both.

5.3.2 HETP

Analysis of the isocratic elution is aided by the calculation of HETP. This is done using Equation 1.1 and Equation 1.2. Thorium elution characteristics at variable flow rates differ markedly between the TEVA and anion exchange resin. On TEVA resin, as flow rate increases, elution peaks broaden. On anion exchange resin, the elution peaks sharpen (Figure 5.2). The explanation for the difference in elution behaviour lies in the difference between the two uptake kinetics for the resins. For TEVA resin, higher flow rate leads to an

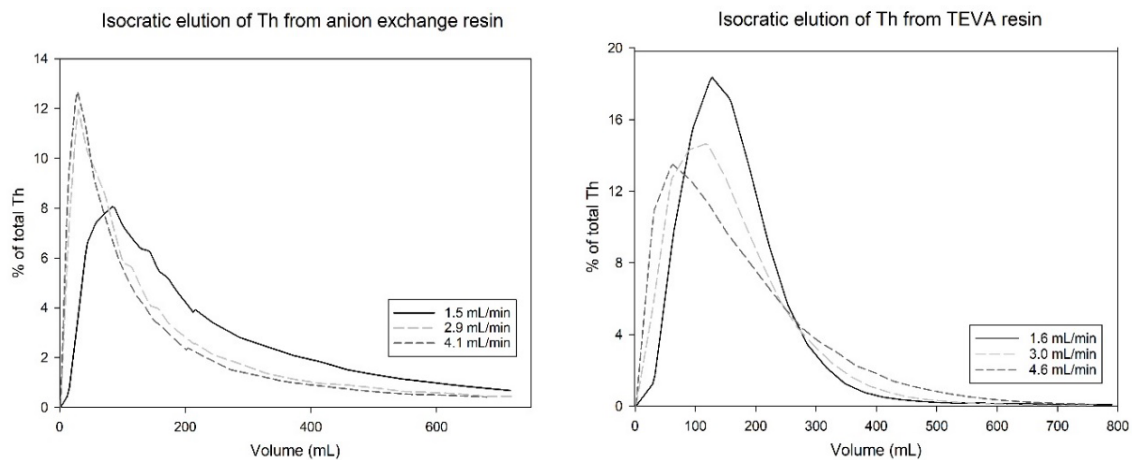
Chapter 5

increase in the HETP. The HETP calculated at the highest flow rates tested (4.6 mL min^{-1}) is actually greater than the length of the column (HETP of 5.7 cm for a column length of 4 cm). This elution behaviour is predictable for a system where significant mass transfer between stationary and mobile phase takes place. In terms of the van Deemter equation, the C term is the term governing the HETP. As C is increased, the HETP increases also.

For anion exchange resin, increasing flow rate leads to increasing HETP. However, unlike TEVA resin, the elution peaks sharpen with increasing flow rate. Despite the distribution coefficient of Th on anion exchange being relatively high ($K_d = 550$), as flow rate increases there is insufficient time for the Th to achieve equilibrium. This difference in elution behaviour from TEVA resin is due to the slower uptake (data from 5.3.1), as anion exchange resin takes a significantly longer time to equilibrate than TEVA resin.

At the lowest flow rate tested (1.5 mL/min), the Th^{4+} is allowed adequate time to equilibrate with the anion exchange resin before reaching the end of the column. However, at higher flow rates, the Th cannot equilibrate at all. The increased mobile phase velocity moves the vast majority of thorium anions through the column before they have time to interact and sorb to the exchanger. Mass transfer between mobile and stationary phase still takes place, but the majority of the Th stays in the mobile phase. The resultant elution profile has an earlier, sharper peak. This is apparent in the values of full peak width at half maximum height (W_h) and the volume to peak elution (t_r) (Table 5.4). In the van Deemter equation (Equation 1.3) the C term, which refers to resistance to mass transfer between the mobile phase and stationary phase, increases with increasing flow rate. As mass transfer between mobile and stationary phase still occurs, the C term has the majority of the influence over the HETP values at the higher flow rates. This results in HETP values larger than the length of the column (5.8 and 5.4 cm for 2.9 and 4.1 mL min^{-1} respectively) while the elution peaks become sharper.

Differences are also apparent in the elution of U from the two materials. Uranium elution profiles from anion exchange resin exhibit sharper peaks with increasing flow rate, whereas U peaks from TEVA resin broaden with increasing flow rate (Figure 5.3). This elution behaviour is similar to thorium's elution from the two materials. The HETP values for U on TEVA resin increase with increasing flow rate, remaining significantly thinner than the length of the column (0.71 cm at the maximum flow rate tested: 4.3 mL min^{-1}).

**Figure 5.2.****Isocratic elution of Th from anion exchange and TEVA resin**

Performed at 3 different flow rates, Left – Anion exchange resin, Right – TEVA resin

Uranium elution from anion exchange resin yields decreasing HETP values with increasing flow rates. This is disparate from Th elution from anion exchange resin, where increasing flow rate leads to increasing HETP despite peak sharpening. This difference in elution behaviour is due to uranium's especially low uptake on anion exchange resin even at equilibrium. Given sufficient time Th will yield a K_d of 550 on anion exchange resin, whereas U will only achieve a K_d of 10. Therefore, for uranium on anion exchange resin, the C term (mass transfer term) in the van Deemter equation is so small that it only has a minor influence on the value of HETP. The term governing the HETP trend in this instance becomes the B term, longitudinal diffusion, which decreases plate thickness with increasing flow rate.

As the uranium anions in the mobile phase flow through the anion exchange column, there is barely any interaction between them and the anion exchange resin. At the lower flow rates, U is able to diffuse along the column, ahead of the peak. As the flow rate increases, the U diffusion in front of the peak occurs at the same rate (given constant temperature and pressure conditions). The increased velocity of the mobile phase, however, reduces the time between initial U elution and peak U elution and thus reduces peak fronting. Diffusion in the opposite direction to mobile phase flow is also reduced at higher flow rates, as U trailing the peak is forced along the column more rapidly. These cause an overall sharpening of the elution peak.

Although the uranium distribution coefficient for TEVA resin was of the same order of magnitude as U on anion exchange resin, it is slightly higher (50 to anion exchange's 10).

This coupled with the much faster uptake kinetics of the TEVA resin means that although uptake is low, adequate mass transfer between mobile and stationary phase occurs to cause broadening of the elution peak. Similar to the anion exchange resin, U on TEVA columns exhibit reduced peak fronting at higher flow rates. However, because of the increased mass transfer on TEVA, a minor amount of U is sorbed to the resin, delaying its elution leading to increased peak tailing. The HETP is therefore governed by the C term thus, the plates thicken with increasing flow rate.

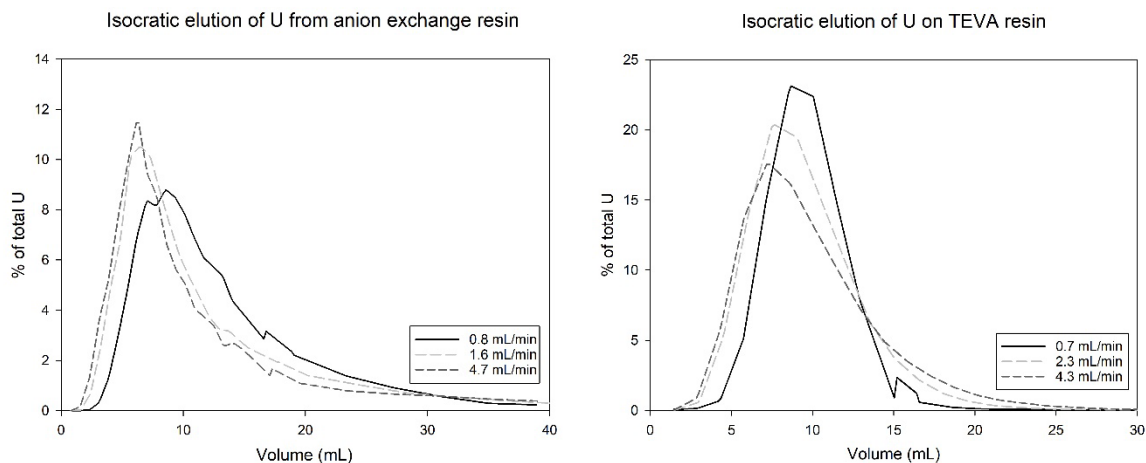


Figure 5.3.
Isocratic elution of U from anion exchange and TEVA resin
 Performed at 3 different flow rates left – anion exchange resin, right – TEVA resin

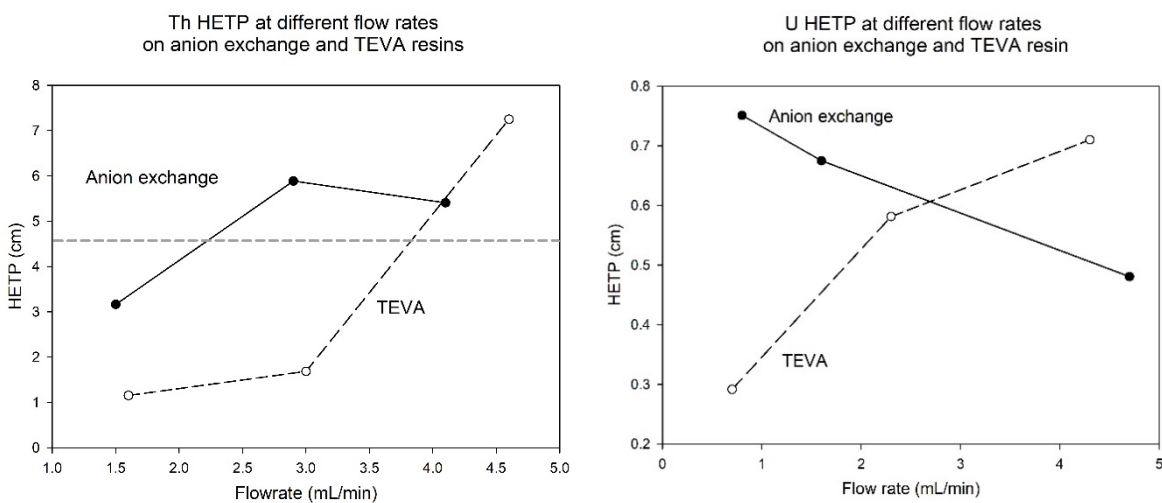


Figure 5.4.
HETP of U and Th on anion exchange and TEVA resin with increasing flow rates
 Left – thorium, right – uranium. Dotted line indicated column length

	1.5 mL min ⁻¹	2.9 mL min ⁻¹	4.1 mL min ⁻¹
t _r	83.7	30.1	28.5
W _h	175.3	86.1	78.0

Table 5.4.**Retention and peak width of Th on anion exchange resin**t_r – volume to peak elution (mL), W_h – peak width and half peak height

	1.5 mL min ⁻¹	2.9 mL min ⁻¹	4.1 mL min ⁻¹
t _r	8.6	6.5	6.3
W _h	8.8	6.3	5.2

Table 5.5.**Retention and peak width of U on anion exchange resin**

5.3.3 Multi-element tests

Tests to establish washout and decontamination are important for application of resins to the separation of U, Th and Pu. This is a three stage separation and requires the washing of sample and decontamination of a Pu, Th and U fraction.

On all three materials, the selected contaminants added were washed from the column very rapidly (within 12 mL). On TEVA and anion exchange resin U was treated as a contaminant. However, due to its very slight uptake on the two materials, its elution from the column during the wash phase was slightly delayed (Figure 5.5). The washout of U on TEVA and anion exchange with variable flow rate follows the same trend as seen in the HETP experiments, with the U peak sharpening on anion exchange resin and broadening on TEVA resin. Elution of Th between the two resins is also significantly different. The eluate (low concentration HNO₃) was able to produce a much sharper elution peak of Th on TEVA resin than on anion exchange resin. The start of the elution was marginally different, however the tailing of the Th elution peaks are much more pronounced from anion exchange resin than from TEVA resin. This elution behaviour is again most likely due to binding of the chemical exchangers to the resin. The liquid anion exchanger allows for easier orientation of incoming ionic groups which either replace the target anion groups already bound to the resin or interact with them, changing their coordination, causing their desorption from the resin.

Chapter 5

UTEVA proved more effective at separating Th, U and the selected contaminants by use of elution of Th from UTEVA with 6 M HCl. Uranium is effectively retained on UTEVA resin under these conditions. As the flow rate increases, the elution peak of Th in 6 M HCl becomes broader, whereas the elution of the contaminants becomes sharper. This reflects the differences in affinity for UTEVA resin. As the contaminants do not sorb to the resin at all their elution profile is governed by lateral diffusion through the column, (just like U on anion exchange). Thorium's K_d is very low in 6 M HCl. However, peak broadening occurs because of the desorption initiated by the ionic gradient set up as HCl replaces HNO₃ as the mobile phase. This test showed that even under changing column conditions (HNO₃ to HCl) U remains strongly sorbed to UTEVA resin.

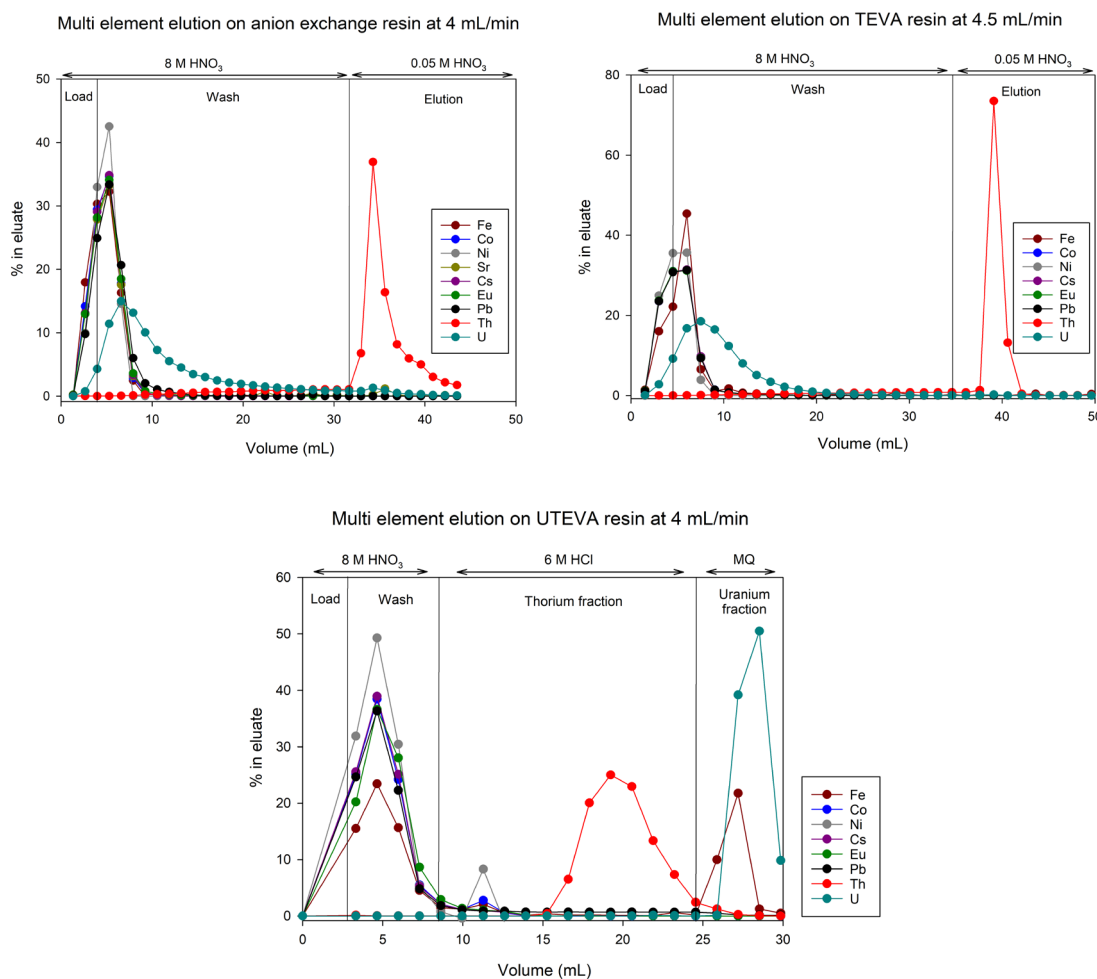


Figure 5.5.

Multi element elution on three different materials

Performed at 4-5 mL/min, left – anion exchange resin, light – TEVA resin, below – UTEVA resin.

5.4 Conclusions

This study has found that the efficacy of a chromatographic material is greatly affected by the way in which the extractant is supported on the resin. Investigation of the kinetics of uptake for Th on TEVA and anion exchange resin has shown that extractant bonded to the polymer chain exhibits slower uptake of species in comparison to extractant-coated resin. It is suggested that this is due to extractant molecules having the ability to orient themselves independently. This may also explain the fast uptake kinetics displayed by UTEVA resin. For expedited separation systems using chromatographic resins, having an insoluble extractant coated to the outside of the polymer support will yield faster uptake of sorbed species than resins with the same active site bonded to the polymer of the resin. Extractant coating allows the active sites to orient themselves around the sorbed species, increasing the uptake kinetics.

This research has also laid the groundwork for the development of an expedited separation system to isolate Pu, Th and U from a single sample. Thorium's isocratic elution using 8 M HNO_3 from TEVA column showed longer retention than thorium on an anion exchange column. Uranium's elution under the same conditions was marginally more delayed on TEVA resin and peak broadening was more significant on TEVA resin also. However, the faster uptake kinetics and longer retention of Th on TEVA resin outweigh the peak broadening effects of U. Due to TEVA's inability to effectively sorb U, a second column consisting of UTEVA resin is required for uranium purification.

The multi-element tests on TEVA resin showed strong retention of Th throughout the load and wash phases, and effective decontamination of U at the highest flow rates. UTEVA column multi-element tests showed strong retention of U at the highest flow rate even under changing column conditions. A notable omission from the multi-elemental tests was that of calcium. Calcium is a major component in cementitious matrices. Although calcium is not adsorbed to either anion exchange resin or TEVA resin its presence as a non-competing interference should be investigated.

For expedited chromatographic separation of Pu, Th and U a setup of a TEVA column above a UTEVA column will yield the most efficient separation and purification of the target elements. Strong U retention on UTEVA is of vital importance to the proposed column separation scheme in which the UTEVA load phase is comprised of both the sample load

Chapter 5

and column wash from the TEVA column. The UTEVA column itself is then washed, to ensure decontamination of matrix components before U elution in its purified fraction.

Further study could be undertaken to analyse the desorption of Th and from TEVA resin in HCl conditions. However, given the efficiency of desorption of Th from the UTEVA column in this study along with the reported K_d values of Th on TEVA resin it can be assumed that Th desorption from TEVA resin is similarly as efficient (Horwitz et al., 1995).

To prove relevance to the nuclear decommissioning sector, separation and purification of these actinides must be performed from materials commonly found in nuclear facilities. Investigation into expedited separation of these actinides from concrete matrices will aid in the understanding of whether non-competing species (Ca for example) from real samples will affect separation efficiency or recoveries.

Chapter 6 Development of a method for the rapid determination of multiple radionuclides from a single sample

6.1 Introduction

The decommissioning of nuclear facilities, both commercial and civil, creates a large volume of waste. A significant proportion of these wastes are contaminated with a variety of different radionuclides dependent on the location's use and the material itself. The management and disposal of these wastes is dependent on their physical and chemical characteristics and the criteria by which each country classifies radioactive wastes. Concrete represents one of the largest material types used in nuclear facilities. It is not only used in the shielding of reactors but also extensively in the construction of ancillary building across the site (Hohmann et al., 2012). The accurate and timely determination of the radionuclide content of such materials can expedite the decommissioning process, lowering costs. The use of nuclear waste scaling factors is widely accepted practice by many facility operators and requires the accurate determination of radionuclide content in several subsamples of the bulk material (International Atomic Energy Agency, 2009). Characterisation of nuclear waste is essential in order to ensure public safety, limit environmental damage and minimise the amount of material requiring costly processing and storage. For characterisation of wastes on a nuclear site, a safe, quick method of radionuclide purification is required. The radionuclides of interest are isolated in order to determine their concentration accurately, whilst minimising interferences from associated radionuclides and matrix elements. Expediting this separation and purification process can have a knock-on effect on the whole procedure, allowing for much more rapid sample turnaround.

Chromatographic techniques are commonly used to separate, preconcentrate and purify radionuclides before analysis. The use of an automated radionuclide separator for expedited chromatographic separations has several advantages over manual preparative techniques. One of the features of these separation systems is the ability to function at controlled flow rates. Research so far has focussed on chromatographic material's ability

Chapter 6

to function at higher flowrates than achievable using gravimetric flow. However, for application to the nuclear decommissioning sector, a full separation using real or simulated material must be demonstrated. The development of a rapid, highly precise separation system must have the ability to purify and concentrate multiple target radionuclides from a single sample. This allows for a reduction in the total number of solid samples processed, optimising technicians' time and reducing the total activity passing through the laboratory. This chapter will focus on the development and testing of a multi-stage preparative technique, incorporating an automated radionuclide separator in the measurement of multiple radionuclides from a single simulated sample.

The actinides uranium, plutonium and thorium along with ^{90}Sr were selected as target radionuclides as they are often associated with concretes following reactor operations and their characterisation typically involves radiochemical separation followed by radiometric or mass spectrometric techniques (Abe and Asakura, 2012; Brown et al., 2015; Joyce, 2018). Strontium-90 was chosen as it is a major fission product and a difficult-to-measure nuclide (International Atomic Energy Agency, 2009). The IAEA and the UK's Department for Business, Energy and Industrial Strategy (BEIS) both class bulk solid waste as radioactive with regards to its Sr-90 content if it contains more than 1 Bq/g of ^{90}Sr (Department for Business, Energy and Industrial Strategy, 2018; International Atomic Energy Agency, 2017). Previous study in this body of work has shown that separation of Sr at higher flow rates than that achievable with gravimetric systems can yield good results when using a Sr-spec column. The previous work also showed that Sr can be effectively leached from a concrete digest (Russell et al., 2017). However, in many instances, a simple acid leach digestion is not thorough enough to liberate some key radionuclides (Braysher et al., 2019).

Uranium-238 was chosen due to its presence in nuclear fuel and cheap availability as an ICP-MS standard. Uranium-238 comprises the majority of the nuclear fuel in a uranium reactor (Chenoweth and Pool, 2003). Thorium can be present as a decay product of nuclear fuel, or it can be used in the production of nuclear fuels, through the activation of ^{232}Th . Significant quantities of Th can pose a risk to the environment and human health due to their method of decay (alpha emission) (Gad, 2014). For ^{232}Th and ^{238}U in secular equilibrium with their daughter nuclides, UK BEIS department classifies was solid material as radioactive waste if it contains more than 0.01 Bq/g. Plutonium-239 is produced in uranium reactors through the neutron activation of ^{238}U to ^{239}U which decays via beta

decay to ^{239}Np and then to ^{239}Pu . The IAEA and UK's BEIS department class bulk solid waste as radioactive with respect to its ^{239}Pu or ^{242}Pu content if it contains more than 100 mBq/g (Department for Business, Energy and Industrial Strategy, 2018; International Atomic Energy Agency, 2004).

Extensive research into sample preparation methods for plutonium and uranium determination has been carried out. The use of acids to completely dissolve the sample matrix has been well documented and utilised (International Atomic Energy Agency, 1989). Sample leaching using acids such as HCl or HNO₃ can permit high sample throughput, but often yield unsatisfactory results (Jia et al., 1989; Parsa, 1992). Dissolution of refractory radionuclide compounds often requires a more intense method of sample attack. Complete dissolution of sample matrices is required to ensure none of the radionuclides of interest remain in the sample matrix, especially in silicate minerals (Emerson and Young, 1995; Galindo et al., 2007). For silica rich materials, hydrofluoric acid is often employed alongside nitric and hydrochloric acid to ensure complete dissolution of both Pu and U. Using HF for complete opening-out of sample matrices is, however, both time-consuming and hazardous for the worker (Braysher et al., 2019). Additionally, the significant quantities of dissolved silica present in concrete and other materials' digests can present issues during column chromatography, as there is a tendency for the silica gel to precipitate on anion exchange columns (Croudace et al., 1998).

Alternative techniques to completely open up silica rich matrices have been successfully developed (Braysher et al., 2019; Cook, 2021; Croudace et al., 1998; Jäggi et al., 2019; Sáez-Muñoz et al., 2020). These techniques allow for complete dissolution of sample. Fusion techniques are commonly utilised in geochemical study and employ high temperatures. The heated sample is dissolved in a solvent or flux. Generally, fusion techniques are only used on small sample sizes (up to 5 g) (Braysher et al., 2019; Suran et al., 2018). Although fusion techniques are more effective at dissolving refractory matrices, the process of fusion is generally more labour-intensive and volatile radionuclides like tritium or ^{14}C will be lost during sample preparation. Therefore other techniques will be required in order to preserve and analyse these before fusion of the sample (Braysher et al., 2019). Various fusion techniques have been developed using different fluxes.

Chapter 6

Sodium hydroxide fusions require temperatures of 600 °C and methods have been developed for samples of up to 2 g (Maxwell et al., 2015; U.S. Environmental Protection Agency, 2014). Sodium peroxide fusions have been developed for sediment and soil samples in order to dissolve actinides in sample sizes of 1 g (Galindo et al., 2007). Fluxless fusions have been developed in order to form a glass bead, which is subsequently analysed by X-ray fluorescence (XRF) or ICP-MS analysis using laser ablation as the sample introduction method. This has been successfully applied to the analysis of 1.5 g geochemical references, and uranium ores and their concentrates (Reading et al., 2017). A summary of sample digestion methods is available in Table 6.1.

The use of lithium borate fusions has been used in a variety of contexts for complete opening out of sample matrices (Braysher et al., 2019; Croudace et al., 1998). Lithium and sodium borate fluxes are effective at dissolving silicate, carbonate and sulphate minerals in addition to a whole host of oxide compounds. This method of fusion can be completed relatively quickly (5-10 mins) at temperatures in excess of 1000 °C. The molten flux can be poured into an XRF bead mould to produce an homogenous glass bead suitable for XRF determination (Braysher et al., 2019; Croudace et al., 1998). The first lithium borate fusion used in a radioanalytical context was by Croudace et al., (1998). Their method employed a mixture of lithium metaborate (80%) with lithium tetraborate (20%). Higher proportions of lithium tetraborate ($\text{Li}_2\text{B}_4\text{O}_7$) are used when producing beads for XRF analysis as it produces a clearer bead than lithium metaborate (LiBO_2) (Braysher et al., 2019). Additionally, tetraborate fluxes are lower cost (Croudace et al., 1998). The use of lithium metaborate is preferred due to the higher solubility of most elements in pure LiBO_2 (Braysher et al., 2019). The procedure was used to determine the Pu and U content of internationally referenced soil and sediment samples.

Dry ignited soil sample masses of 5 g were mixed with 7 g of borate flux before heating to 1200 °C for 30 minutes. Afterwards, the samples were quenched in MQ the mixture was acidified with concentrated nitric acid before heating to 40 °C and stirring for more than 4 hours. It was found that although the borate fusion was able to open up the sample and dissolve the actinides of interest from the soil sample, significant quantities of silica remained in the mixture (Croudace et al., 1998). This is unlike hydrofluoric acid techniques which react with the silicates to produce volatile SiF_4 . On reduction of temperature the silica and boric acid form a gelatinous precipitate which is filtered from the sample and

washed with excess nitric acid. Croudace et al., states that some of the silica remains in solution in colloidal form and can precipitate during column chemistry, blocking the columns. Croudace et al., used polyethylene glycol (PEG-2000) to flocculate the colloidal silica by adding 1 mL of a 0.2 M solution to the nitric acid used to digest the glass after fusion. After 4 hours this was then filtered again to remove the silica. The removal of colloidal silica can also be achieved by centrifugation and may be a quicker method (L. L. Smith et al., 1995). The resulting supernatant solution should contain the actinides of interest.

The use of parallel column setups for separation of radionuclides from a single sample has been previously studied (Maxwell et al., 2010; Solatie et al., 2002). The separation of Sr from actinides has also been studied, however many of these processes focus on using chemical precipitation in order to purify the Sr fraction (Buesseler et al., 1990; LaRosa et al., 1992; Lee et al., 2000; O'Donnell et al., 1997). All of these studies separate Sr from the sample digest prior to purification steps, using either precipitation or a chromatographic based technique. The most common method of separating the actinides from Sr is by using a hydroxide precipitation. Ageyev et al., (2005) reports the use of Fe(OH)_3 with NH_4OH to form a precipitate entraining Pu, Am, Cm, Ce, Pm, Eu, Y and La with Sr remaining in solution. Lee et al., (2000) uses a sodium carbonate precipitation for initial actinide/strontium separation and then goes on to use Fe(OH)_3 to ensure complete removal of the actinides. However, once in separate fraction further purification is required to isolate the desired elements.

The purpose of this study is to show how the expedited separation using an automated radionuclide separator is applicable to the separation of multiple radionuclides from a single sample. This seeks to optimise laboratory worker's time and reduce the need for large sample sizes, which in turn can reduce exposure. It also increases sample throughput and reduces lead times for analysis which is commercially important and attractive to decommissioning project managers. The separation techniques examined so far in this thesis have analysed the performance of Sr resin (Triskem International, Bruz, France), 1X8 anion exchange resin (Eichrom Technologies IL, USA), UTEVA and TEVA resin (Triskem Intl. Bruz, France). Use of Sr resin for the separation of Sr from a variety of matrices has proven to be highly effective and is used not just in the context of analysing nuclear wastes and fallout but also to wider geochemical study (Chung et al., 2013; Kim et al., 2015; S. Li et al.,

Chapter 6

2019; Schneider et al., 2007). This study has shown that effective Sr purification from a partially opened out concrete matrix can be achieved at constant flowrates above those achievable in gravity flow columns. From study of separation systems in this report and from the literature, the use of two columns in series seems to be the most effective way to purify U, Th and Pu from the same sample (Metzger et al., 2019). Due to the faster kinetics of TEVA resin over anion exchange resin discussed here, this chapter will focus on the use of TEVA in series with UTEVA to purify target actinides in parallel with Sr resin to purify Sr. These column separations will be undertaken after full opening out of a concrete sample and subsequent precipitation steps with an iron carrier to remove the actinides from the strontium fraction.

The objective of this chapter is to investigate whether separation of U, Th, Pu and Sr at high flow rates from a concrete matrix is adequate for activity determination in line with solid waste exclusion guidelines published by the International Atomic Energy Agency (2004) and the UK's Department for Business, Energy and Industrial Strategy (2018). This will be achieved by assessing the following for each purified fraction:

- Chemical recovery
- Decontamination of radionuclides present
- Accuracy of results
- Precision of repeat tests
- Limit of detection for the whole procedure

Comparison of this system to conventional techniques will be drawn in order to assess whether an automated system operating at expedited flow rates can be applied to the separation of multiple elements from concrete matrices.

Digestion method	Problems / comments	Silicates	Oxides	Sulphates	Carbonates	Borates	Phosphates	Metals Carbides, Silicides*	References
Borate fusion +/- acid digestion	Flexible method with no problems. Effectively digests all materials and is ideal for many elemental and isotopic analysis purposes. High purity lithium borate fluxes used to ensure low analytical blanks. Sample size can vary from 0.1–10 g. Sample: flux ratios from 1:1 upward. Pt-Au crucibles used which are easily cleaned. Typical fusion temperature <1000–1200°C. Possible volatility issues with: Cs, Tc, Ru, I, Hg, Pb Po & Tl.	X	X	X	X	X	X	X	(Croudace et al., 1998)
Flux free fusion +/- acid digestion	Small sample volumes treatable. Conducted in inert Ar atmosphere. Typical fusion temperature >1300°C. May require addition of SiO ₂ and MgO if silicate poor to help glass formation. Possible volatility issues with Cs, Hg, Pb & Tl.	X	X	X	X			X	(Fedorowich et al., 1993)
HCl, HNO ₃	Microwave digestion, heating in PTFE or PFA pressure vessels may be effective. Full recovery of analytes potentially low. Oxidation of sample may be required to prevent volatilisation. Difficult to achieve full dissolution. Possible volatility issues with: As, Ge, Po, S, Sb, Se, Tc.				X	X		X	(Bock, 1979)
HF / HClO ₄ Acid mix	Only small sample masses readily treatable. HF needs to be removed prior to analysis. Insoluble fluoride precipitates in large sample volumes. Perchlorates potentially explosive. Frequently requires the use of HCl and/or HNO ₃ . Possible volatility issues with: As, B, Ge, Po, Sb, Tc.	X	X		X	X	X	X	(Parsa, 1992)
HF / H ₂ SO ₄ Acid mix	Small sample volumes treatable. HF needs to be removed prior to analysis. Many evaporation stages.							X	(Bock, 1979)
Alkali fluoride with pyrosulphate	Hazardous as HF produced; requires treatment with pyrosulphate to remove fluorides. Will attack Pt hardware.	X			X				(Sill et al., 1974)
NaCO ₃ fusion	Opens out mineral lattices but requires lengthy treatment. Dissolution of Pt hardware possible. Elevated Pb or Fe(II) will alloy with Pt hardware. Possible volatility issues with: As, Hg, Po, Tc, Tl, Se.	X			X	X		X	(Fisher and Kunin, 1957)
NaOH fusion	Opens out mineral lattices but requires lengthy post fusion treatment. Dissolution of Pt hardware possible.	X			X			X	(U.S. Environmental Protection Agency, 2014)
Na ₂ O ₂ fusion or sinter with acid digestion	Attack of Pt hardware possible. Typical fusion temperature of 250–500°C. Small sample volumes treatable. Time intensive procedure to dissolve the alkaline fusion cake. Possible volatility issues with Au & Ru.	X						X	(Galindo et al., 2007)

Table 6.1. Overview of digestion methods from Croudace et al., (2016)

* use of oxidants or nitric acid digestion may be required

6.2 Materials and equipment

For the measurement of samples via alpha spectrometry an AMETEK® ORTEC® Alpha analyst was used (Berwyn, Pennsylvania, U.S.). Samples for alpha spectrometry were electrodeposited onto stainless steel Planchet counting trays provided by Nuclear Supplies Ltd. For the analysis of ⁹⁰Y via Cherenkov counting, a 1220 Quantulus Ultra Low Level Liquid Scintillation was used. Gamma analysis was conducted using a Canberra p-type High Purity Germanium well detector (Mirion Technologies (Canberra UK), San Ramon, CA, USA). Detectors were calibrated against a mixed radionuclide standard solution. The standard was used to prepare a source of near-identical geometry to that of the samples. Gamma spectra were analysed and individual radionuclides quantified using Fitzpeaks spectral deconvolution software (JF Computing Services). The geometries used for gamma spectrometry were produced and are used commercially by a UKAS accredited laboratory (GAU-Radioanalytical Laboratories (GAU), Southampton, UK) certified to ISO/IEC 17025:2017. Height corrections for each sample were calculated using previously established data as the counting efficiency of the well detector is altered when the sample is not completely filled (Croudace, 2012).

An Automated Sequential Radionuclide Separator (ASRS) (Hanjin Eni Co., LTD., Daejeon, Republic of Korea) was utilised to separate the samples. It uses 8 peristaltic pumps to perform simultaneous separations on 8 individual chromatographic columns or, when used in series, perform a 2-stage separation on 4 samples simultaneously. Loading, washing and elution can be completed at a flow rate of up to 6 mL/min. Calibration of the system is performed using MQ from the reagent bottles, however significant differences in flowrate were attained when loading the columns from the sample bottles. This may be due to the differences in size of tubing and the valves used to control the direction of the samples/reagents to the column. As a result, flowrates were set to 6 mL/min on the instrument control programme (using a custom LabVIEW programme provided with the ASRS) and actual flow rets for each experiment were calculated gravimetrically from the elute produced.

The reagents used were of analytical grade unless otherwise stated. Nitric acid solutions were produced from a 70% (weight) concentrate (Fisher Scientific, Loughborough, England). HCl solutions were produced from a 37% (weight) concentrate for analysis (Fisher

Scientific, Loughborough, England). For ICP-QQQ-MS analysis, 2% nitric acid solutions were prepared from PrimarPlus-Trace analysis grade (>68% by weight) (Fisher Scientific, Loughborough, England). High purity water obtained using a Q-POD Milli-Q Advantage A10 Water Purification System (Merck, Darmstadt, Germany). For Pu elution a solution of 0.1 M NH₄I in 9 M HCl was prepared using 1.4 g solid ammonium iodide, dissolved first in 25 mL MQ then diluted by 75 mL concentrated HCl (37% w/w). This ammonium iodide solution was prepared the day of use as the reagent degrades over time.

Sr-spec, TEVA and UTEVA resins (100 – 150 µm) were all supplied by Triskem Intl. (Bruz, France). Resins were packed into columns as a slurry to a bed of dimension 40 × 6.6 mm (i.d.) in a glass chromatographic column (Omnifit® Chromatography Column, Diba Industries, Danbury, CT, USA).

6.3 Method

This study focusses on the chromatographic separation of actinides from cementitious matrices. For this reason, both target radionuclides, their tracers and contaminants were added after sample dissolution. The preparation of the sample for the column chemistry was included in the analysis as this is a relevant step in the separation process.

6.3.1 Radionuclide spiking

For these tests, an activity of 10 Bq of ⁹⁰Sr was added to each sample giving a simulated Sr activity concentration of 20 Bq/g. Limit of detection was calculated to assess whether the technique is suitable for determining if the sample would fall under the exemption criteria. Strontium-85 was used as a strontium tracer as it is a gamma emitter and easy to measure. This allowed for relatively simple, non-destructive measurements that could be undertaken at various points in the separation process. Strontium-85 standard solutions (ID: 2016-1838 and 2017-1686) were sourced from Physikalisch-Technische Bundesanstalt (Germany). Strontium-90 standard solution (ID: SIZ64) was obtained from AEA Technology (now Ricardo-AEA, Harwell, UK).

The ²³⁸U standard was a depleted uranium ICP-MS standard and contained ²³⁴U and trace ²³⁵U. Uranium-236 was used as a radiotracer and sourced from AEA Technology (Ricardo-AEA, Harwell, UK) (ID: UFP10030). A uranium standard was made to assess the

Chapter 6

concentration of these isotopes in the standards used. Likewise, ^{232}Th was used from an ICP-MS standard due to the ease of use and cost effectiveness with ^{229}Th as a tracer. Thorium-229 radiotracer was obtained from NPL (National Physical Laboratory, Teddington, UK) (ID: R26-01). These thorium isotopes were plated in isolation and counted in order to establish precise activities. Both uranium and thorium activities were set at 50 mBq per sample (100 mBq/g). Activities were calculated using the specific activities of ^{238}U and ^{232}Th (12,440 and 4,100 Bq/g respectively).

Plutonium isotopes ^{239}Pu and ^{242}Pu were used. Plutonium-242 was used as a yield monitor. The ^{239}Pu radiotracer was produced from dilutes of purified isotope solutions from the National Physical Laboratory (Teddington, UK) (ID: R24-01). The ^{242}Pu radiotracer was sourced from AEA Technology (Ricardo-AEA, Harwell, UK) (ID: PRP10020). Each sample was spiked with 50 mBq of ^{239}Pu and ^{242}Pu .

A range of gamma emitting radionuclides indicative of interfering species were added in order to assess decontamination from the Sr fraction. These included ^{210}Pb and a mixed gamma source containing ^{241}Am , ^{109}Cd , ^{60}Co , ^{137}Cs , ^{54}Mn and ^{65}Zn (Table 6.2). All samples were analysed via gamma analysis before the separation procedure to ascertain both ^{85}Sr activities and gamma emitter activities.

Radionuclide	Activity to be in 0.5 g sample (Bq)
Strontium	
⁹⁰ Sr Target	10
⁸⁵ Sr Tracer	10
Uranium	
²³⁸ U Target	0.05
²³⁶ U Tracer	0.05
Thorium	
²³² Th Target	0.05
²²⁹ Th Tracer	0.05
Plutonium	
²³⁹ Pu Target	0.05
²⁴² Pu Tracer	0.05
Contaminants	
Lead	
²¹⁰ Pb	10
Mixed γ source	
²⁴¹ Am	8
¹⁰⁹ Cd	3
¹³⁷ Cs	8
⁵⁴ Mn	0.1
⁶⁵ Zn	0.1
⁶⁰ Co	5

Table 6.2.
Radionuclides added to concrete samples

6.3.2 Composition of concrete sample

An inactive concrete powder taken from a non-nuclear site was sourced. This was used as the base for the simulated concrete digest. Wavelength Dispersive X-ray fluorescence (WDXRF) analysis of the powder was undertaken to establish the precise composition of the material. Analysis of the concrete sample was carried out at the University of Leeds School of Earth and Environment and utilised a Rigaku ZSX Primus II WDXRF spectrometer. Major elemental compositions were determined on fused glass beads prepared from dried powders with a sample to flux ratio of 1:10. The flux consisted of 66% lithium tetraborate and 34% lithium metaborate. Major elemental composition shows SiO_2 as being the major constituent, with CaO and Al_2O_3 substantial constituents as would be expected in a concrete sample (Table 6.3).

Compound	Mass%
SiO ₂	64.170
TiO ₂	0.451
Al ₂ O ₃	7.195
Fe ₂ O ₃	2.635
MnO	0.080
MgO	1.060
CaO	9.830
Na ₂ O	1.420
K ₂ O	1.126
P ₂ O ₅	0.073
Cr ₂ O ₃	<0.010
LOI	9.390
Total	97.436

Table 6.3.
Major elemental composition of concrete sample used

Semi-quantitative analysis of the powdered concrete was also carried out. The sample was mixed with a CEREOX binder in a ratio of 4:1, pressed at a force of 10 tons to form a pellet of 32 mm in diameter. This was then analysed using the Rigaku ZSX Primus II using a pre-calibrated EZ-scan semi-quant program which covered elements F – U. Simultaneous, repeat analysis of 2 certified reference standards was also carried out with the concrete sample (MRG-1 and STM-1) (Faye and Sutarno, 1976; Franklin and Knauss, 1992).

Five grams of concrete powder was taken. Two, 2.5 g subsamples of the concrete powder were fused with 6 g of lithium metaborate flux at 1100 °C for 15 minutes to ensure total dissolution. Samples were removed from the furnace and immediately quenched in excess MQ water. Samples were drained and the solid was dissolved in 150 mL 8 M HNO₃. The samples were set to dissolve on a stirring hotplate at 90 °C for two hours. After this the hotplate was turned off and the samples left to cool while stirring for 10 hours. During cooling and mixing, a fine precipitate formed. This solution was filtered through a Whatman 40 filter supported on a glass fibre filter using a vacuum filter. The solution was retained and the precipitate disposed of. The solutions were combined to ensure homogeneity of the digest and then weighed.

A calculated mass (1/10) of the bulk solution was taken equivalent to 0.5 g of solid concrete powder. The radionuclide spikes and radiotracers were then added to the digest. An FeCl₃

carrier was added in excess (> 20 mg Fe) to co-precipitate actinides from the spikes digest solution. Ammonia solution (NH₄OH) was added dropwise until Fe(OH)₃ precipitate formed at pH >4. At this point the actinides co-precipitate with the Fe(OH)₃. The precipitate was separated from the supernatant by centrifuging the solution and pouring the supernatant out. The supernatant was set aside whilst the Fe hydroxide precipitate was redissolved in concentrated HNO₃ and diluted. A second precipitation with NH₄OH of Fe hydroxide with actinides was performed in order to liberate as much Sr from the precipitate as possible. The Fe(OH)₃ precipitate was dissolved in concentrated HNO₃ and set to evaporate on a hotplate. Once evaporated to dryness the solid was dissolved in 5 mL 8 M HNO₃. In order to ensure Pu was in the tetravalent state, a small mass of NaNO₂ (~0.2 g) was added to act as an oxidising agent. Once the solution had reacted with the NaNO₂ this sample was taken for loading on the TEVA/UTEVA columns.

The supernatant from the iron hydroxide precipitation was evaporated and the resulting solid left was dissolved in 8 M HNO₃. The volume of HNO₃ required to dissolve the solid was so large that the concentration of Sr would have been far too low to permit a load volume of 5 mL. As a result, an oxalate precipitation was performed to pre-concentrate the Sr before loading onto the column. The precipitation of Sr as an oxalate is used in many of the preparative chemistry reported (Ageyev et al., 2005; Lee et al., 2000; Maxwell et al., 2010; Solatie et al., 2002). The use of calcium oxalate to preconcentrate actinides is also a well reported procedure (Ageyev et al., 2005; Solatie et al., 2002). Actinides left in solution should be incorporated into the oxalate precipitate. One millilitre of 2 M CaCl₂ was added to the nitric acid solution, followed by 50 mL of ammonium oxalate and 3 drops of bromocresol green to act as an indicator. Ammonia solution was added to adjust the pH until a pH of > 4 is achieved (bromocresol indicator turns blue). At this pH both calcium and strontium oxalate precipitate. The solutions were left on a hot plate at 60 °C to settle. The oxalate precipitate was filtered under vacuum onto cellulose nitrate filters. The precipitate on the cellulose filter was then ignited at 450 °C for over 10 hours to decompose the oxalate. The solid remaining was dissolved in 1 mL of concentrated HNO₃ and set to evaporate to dryness and ignited at 450 °C once more for 2 hours. After the sample cooled, the residue was dissolved in 5 mL 8 M HNO₃ in preparation or loading onto the column.

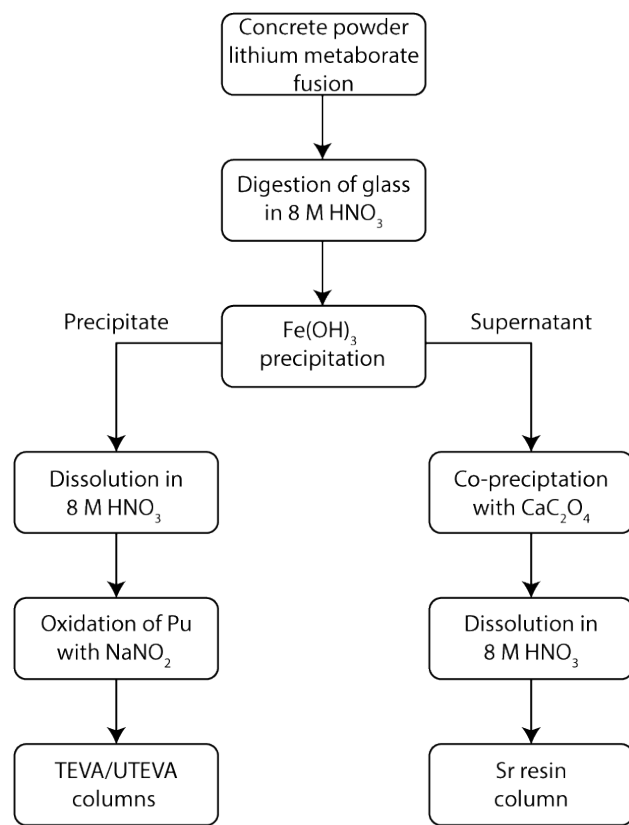


Figure 6.1.
Sample preparation flow chart

6.3.3 Chromatographic separation

For the separation of the actinides, a two column system was employed on an automated sequential radionuclide separator (ASRS). This system utilises peristaltic pumps to induce a forced flow of solution through chromatographic columns and the flow rates through the system can be roughly calibrated. The solution containing the actinides (formed from the Fe(OH)₃ precipitate) was loaded onto the TEVA column. The eluate from this was then passed onto the UTEVA column. TEVA and UTEVA resins were used due to previous study on their kinetic behaviour and UTEVA was selected based on its ability to sorb U. All column separations were conducted at the highest flow rate possible (4.5 mL/min). This flow rate had also been tested in previous experiments.

Two columns were prepared, one TEVA and one UTEVA column. Both measured 0.66 cm in diameter and 4 cm in height (1.37 cm³). Each column was rinsed with 10 mL MQ followed by 10 mL 0.05 M HNO₃. The columns were then prepared with 15 mL 8 M HNO₃ prior to sample loading.

The separation system is summarised in Figure 6.2. The load solution containing the actinides and any contaminants still present after the preparative chemistry were loaded into TEVA resin in 8 M HNO₃. U should not sorb to the TEVA under these conditions and flow through to the UTEVA column. The TEVA column was then washed with 20 mL of 8 M HNO₃ to elute U, with the washings from the TEVA resin flowing through to the UTEVA resin. After this the columns were separated so the eluate from the TEVA resin was no longer loaded onto the UTEVA column. The TEVA resin was treated with 15 mL 9 M HCl in order to elute the thorium. The eluate was collected and set aside in preparation for the electrodeposition step.

For complete elution of the plutonium from the TEVA column, reduction to Pu (III) from Pu (IV) is required. This is done using a solution of 0.1 M NH₄I in 9 M HCl. For each separation 20 mL of this ammonium iodide solution was used for the elution of Pu.

The UTEVA column containing the load and washings from the TEVA column was washed with a further 15 mL 8 M HNO₃ to remove any contaminants. The uranium was then stripped from the column using 20 mL 0.05 M HNO₃.

Each eluate had concentrated HNO₃ added, along with 1 mL 2% Na₂SO₄ solution to aid redissolution of actinides. They were then evaporated to dryness.

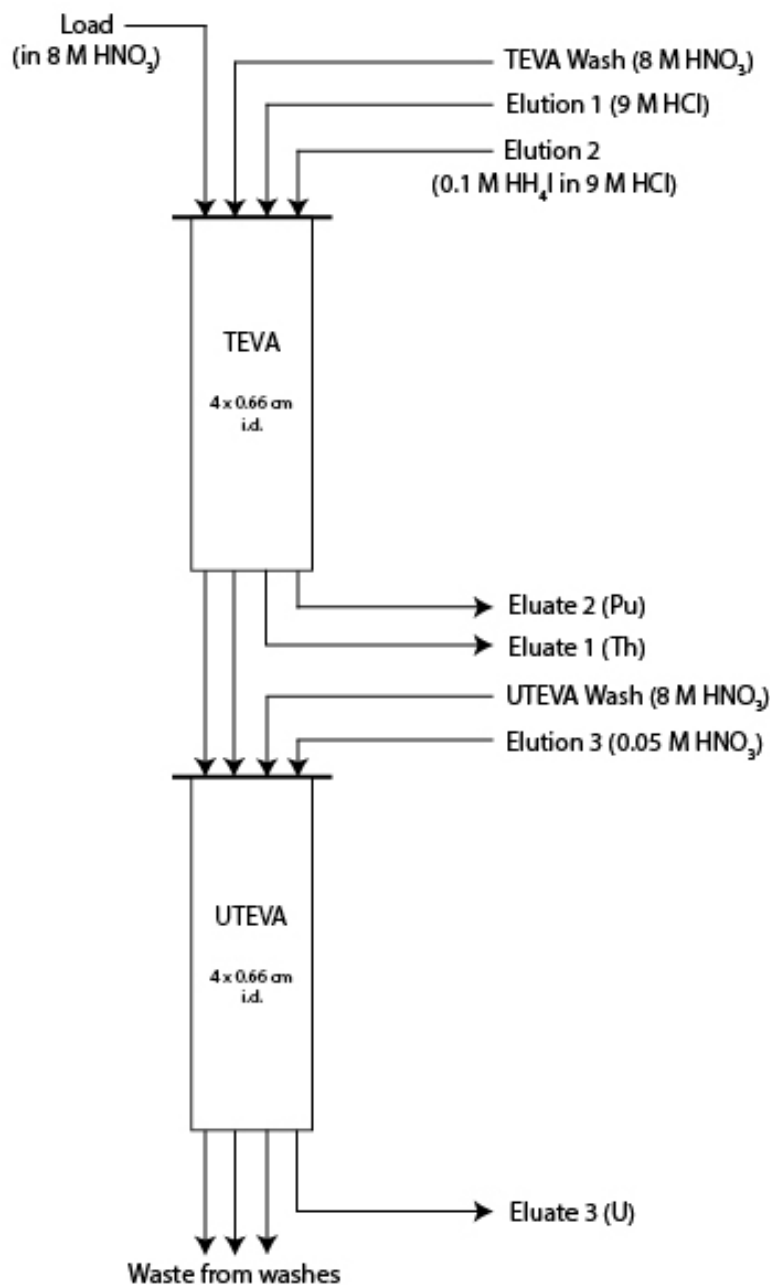


Figure 6.2.
TEVA and UTEVA column separation system

For the Sr separation, a Sr-spec column was employed, 4 cm in height and 0.66 cm in diameter. The 5 mL sample was loaded onto the column in 8 M HNO₃. The column was then washed with 15 mL 8 M HNO₃ and elution of Sr was achieved upon addition of 20 mL 0.05 M HNO₃. Strontium elution using 0.05 M HNO₃ was completed in order to ensure retention of Pb on the Sr column, preventing Pb contamination of the Sr fraction (Figure 6.3).

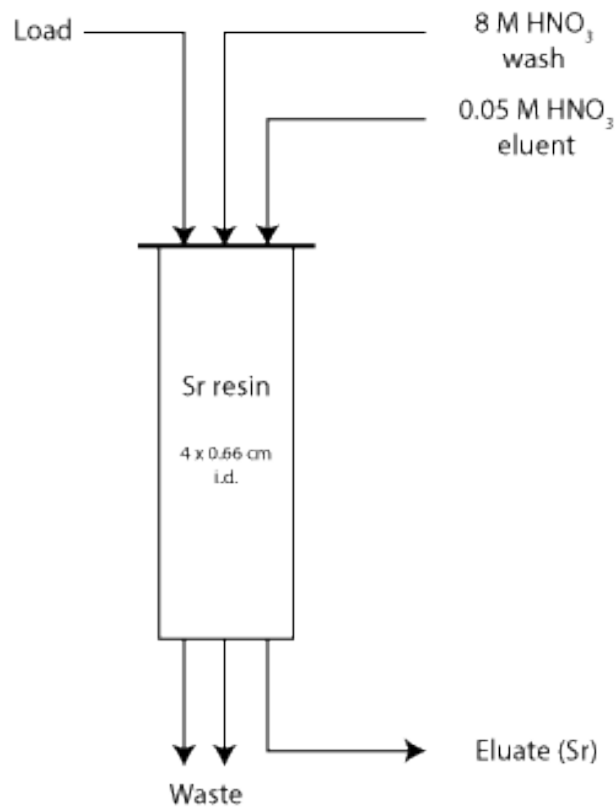


Figure 6.3.
Sr separation system

6.3.4 Preparation for analysis

The three fractions from the TEVA/UTEVA separations are taken and their residues are dissolved in 1 mL 1.2 M HCl, followed by 5 mL 4% ammonium oxalate solution. Each fraction is warmed gently and electrodeposited onto a stainless steel disc which acts as a cathode and a platinum wire is used as an anode. A current of 400 mA is used for 1.5 hours. Before the plating is stopped, 0.5 mL NH₄OH is added to neutralise the solution. The disc is rinsed with MQ and left to dry.

The Sr fraction was transferred to a scintillation vial for direct measurement.

6.3.5 Analysis

The Th, U and Pu fractions electrodeposited to the stainless steel discs were counted via alpha spectrometry. Each fraction was counted for >100,000 seconds. Procedural blanks for each fraction were created for both the preparation for measurement procedures as well as an unspiked sample that taken through the whole separation procedure. Spectra

Chapter 6

were analysed using Maestro (Ortec) and spectral peaks were identified using 8th Edition of table of isotopes (Firestone and Baglin, 1999). Regions of interest were selected manually and the area of the peak represents the alpha counts detected. Calibration standards of known activity are used regularly to determine detector efficiencies. Tracer activities are measured simultaneously and are used to correct for losses during preparative chemistry, source attenuation and detector efficiency.

Measurement of the Sr fraction is completed using two measurement techniques. Strontium-85, which is used as a yield tracer, is measured by gamma spectrometry as it decays via electron capture with associated gamma emission. Additionally, the gamma analysis is used to assess the decontamination of the contaminants added (²¹⁰Pb and radionuclides present in the mixed gamma source). The ⁹⁰Sr activity is determined by measuring ⁹⁰Y via Cherenkov counting after a period of 14 days is left to ensure sufficient ingrowth of ⁹⁰Y reaches from ⁹⁰Sr. Instrumental background contributions were corrected for using a blank consisting of 20 mL MQ.

6.4 Results and discussion

Radiometric analysis shows good yield of target nuclides (Table 6.4) and high accuracies once corrected for tracer recovery. Five tests were completed and an average was calculated. Radionuclide fractions were collected and analysed separately. Fully corrected target radionuclide accuracies were calculated and are presented in Table 6.5. for accuracy measurements zeta score was used for each measurement (Appendix B). Comparison of the ζ -score to ± 2.576 (corresponding to significance levels of $\alpha = 0.01$) determines whether the values are in agreement. Measurements yielding values of ζ -scores outside of ± 2.576 are regarded as not in agreement with one another, and the result is questionable (Analytical Methods Committee, 2016).

	²³⁹ Pu yield	²³² Th yield	²³⁸ U yield	⁹⁰ Sr yield
Test 1	100.4	60.7	44.4	83.2
Test 2	96.5	66.4	51.2	83.1
Test 3	100.0	76.5	78.0	84.7
Test 4	94.1	64.7	69.5	84.6
Test 5	96.2	44.5	59.3	83.5

Table 6.4.
Uncorrected target radionuclide recoveries for concrete tests
As a percentage of the activity added

²³⁹ Pu		²³² Th		²³⁸ U		⁹⁰ Sr	
Activity added (mBq)	Activity measured (mBq)	Activity added (mBq)	Activity measured (mBq)	Activity added (mBq)	Activity measured (mBq)	Activity added (Bq)	Activity measured (Bq)
Test 1 activities	51.5 ± 1.0	51.7 ± 4.5	64.1 ± 2.8	65.9 ± 3.0	63.7 ± 2.6	63.9 ± 5.1	9.95 ± 0.05 9.67 ± 0.73
Deviation	0.42%	2.86%		0.28%		-2.77%	
ζ -score	0.046	0.446		0.031		-0.378	
Test 2 activities	51.7 ± 1.0	52.5 ± 3.8	64.1 ± 2.8	64.4 ± 2.8	64.1 ± 2.6	63.3 ± 3.0	9.95 ± 0.05 10.04 ± 0.76
Deviation	1.69%	0.34%		-1.34%		0.88%	
ζ -score	0.218	0.055		-0.215		0.116	
Test 3 activities	51.9 ± 1.0	53.7 ± 3.2	63.3 ± 2.8	64.6 ± 2.7	63.7 ± 2.6	59.2 ± 1.9	9.94 ± 0.05 9.65 ± 0.71
Deviation	3.48%	2.11%		-6.97%		-2.93%	
ζ -score	0.532	0.344		-1.373		-0.406	
Test 4 activities	51.7 ± 1.0	50.5 ± 2.9	64.5 ± 2.8	64.7 ± 2.9	64.0 ± 2.6	64.3 ± 2.9	9.98 ± 0.05 10.69 ± 0.76
Deviation	-2.33%	0.34%		0.40%		7.14%	
ζ -score	-0.390	0.055		0.066		0.931	
Test 5 activities	51.6 ± 1.0	51.4 ± 3.7	64.6 ± 2.8	64.3 ± 3.0	63.7 ± 2.6	60.9 ± 2.1	9.96 ± 0.05 9.4 ± 0.71
Deviation	-0.42%	-0.36%		-4.35%		-5.57%	
ζ -score	-0.056	-0.055		-0.834		-0.774	

Table 6.5. Accuracy and precision measurements for multiple separation technique

Activities measured in mBq for actinides and Bq for ⁹⁰Sr. Percentage deviation from the expected value was calculated for each test to assess precision and ζ -score used to assess accuracy.

6.4.1 Uranium fractions

Measurement of the uranium standards used was completed to establish the precise activity of the ^{238}U standard produced from dilution of a 1000 ppm ICP-MS solution. Uranium-236 was used as a tracer to establish chemical recovery during the plating of the standard. The ^{236}U standard was of known activity and the ^{238}U ICP-MS standard was a depleted uranium source from Spex CertiPrep (Metuchen, NJ, USA). A mass of each standard equivalent to 50 mBq activity was taken, plated and counted for 200,000 seconds. The spectrum produced showed 3 significant peaks (Figure 6.4). Uranium-238 and ^{236}U were the most significant peaks present, however there was also a small peak for ^{234}U . Activities for these three radionuclides were calculated using predetermined counter efficiencies. It was found that the yield from the electrodeposition of the uranium standards from a clean solution was very high ($102.8 \pm 5.8\%$). Activity concentrations of the standards were calculated in addition to the activity ratio of ^{234}U to ^{238}U . As the ^{236}U standard only contains ^{236}U , the source of the ^{234}U and ^{238}U in the spike is the depleted U ICP-MS standard. The abundance of both ^{238}U and ^{234}U in the standard was calculated from the activities measured. The $^{234}\text{U}/^{238}\text{U}$ activity ratio for the ICP-MS standard was 0.13. Uranium-234 was found to comprise 0.0007% of the measured uranium, much lower than that found naturally (0.005%) which is to be expected for a depleted source.

Analysis of sample uranium fractions found significantly higher $^{234}\text{U}/^{238}\text{U}$ activity ratios than that established from the standard analysis (Figure 6.5) (0.24 - 0.30). It was assumed that the concrete itself contained some U that was then being recovered during the separations. This was further confirmed by ^{238}U recoveries, which were in excess of 100% once tracer corrected. In order to establish the ^{238}U content of the concrete digest, ICP-MS analysis of an unspiked dilute of the digest was carried out, using a 7-point calibration created from the depleted U ICP-MS standard used for spiking the digest. The ^{238}U concentration of the unspiked concrete was found to be 19.8 ppb – equivalent to an activity concentration of 0.24 mBq g⁻¹, which given a digest mass of ~ 47.5 g can lead to a significant contribution to the final ^{238}U activity. This excess ^{238}U was then taken into account during the calculation of recoveries.

Calculation of the ^{234}U content of the digest was more difficult because of its low abundance. Due to the requirement for dilution of the digest, the ^{234}U concentration in the

sample analysed by ICP-MS would have been too low for effective quantification. However, because of the much shorter half-life of ^{234}U (2.455×10^5 years) in comparison to ^{238}U (4.468×10^9 years), analysis of the U content of the unspiked digest via alpha spectrometry was completed. Unspiked concrete digest was subject to a TEVA/UTEVA separation with fractions collected for Th, Pu and U. The U fraction was counted on the alpha spectrometer without yield tracer. The ratio of $^{234}\text{U}/^{238}\text{U}$ activities in the concrete was 1.004 ± 0.14 . Percentage abundances of uranium isotopes in the digest were calculated. Uranium-234 was found to comprise $0.0055\% \pm 0.0015$ of the Uranium present in the unspiked digest. This value is comparable the value for the natural abundance of ^{234}U (0.005%).

From the concentration of ^{238}U in digest and added in the spike, and the activity ratios calculated, theoretical $^{234}\text{U}/^{238}\text{U}$ activity ratios can be calculated for each sample. Activity ratios for unseparated concrete $^{234}\text{U}/^{238}\text{U}$ ratios were 0.291 ± 0.001 . These values correlated well with the measure activity ratios in the uranium fractions for each spiked sample (0.272 ± 0.033).

Accuracy of the measurements was achieved by analysing the activity added to the fully corrected measurement of the sample (Table 6.5). A ζ -score (zeta score) was calculated for each radionuclide in each separation. All values of the ζ -score were inside ± 2.576 (between 0.066 and -1.373). Zeta scores increase as either deviation from the expected value increases or the uncertainty decreases. Large ζ -scores indicate large error or underestimated uncertainty. Precision of the measurement was completed using percentage deviation between activity added and fully corrected measurement. Percentage deviations from the expected value ranged from 0.40% to -6.97%.

Limit of detection for uranium was calculated using Equation 4.6. LOD for the separation of ^{238}U from the concrete matrix was found to be 0.57 ± 0.22 mBq/g. This is much lower than the 10 mBq/g required for classification of solid waste as radioactive due to its ^{238}U content (Department for Business, Energy and Industrial Strategy, 2018).

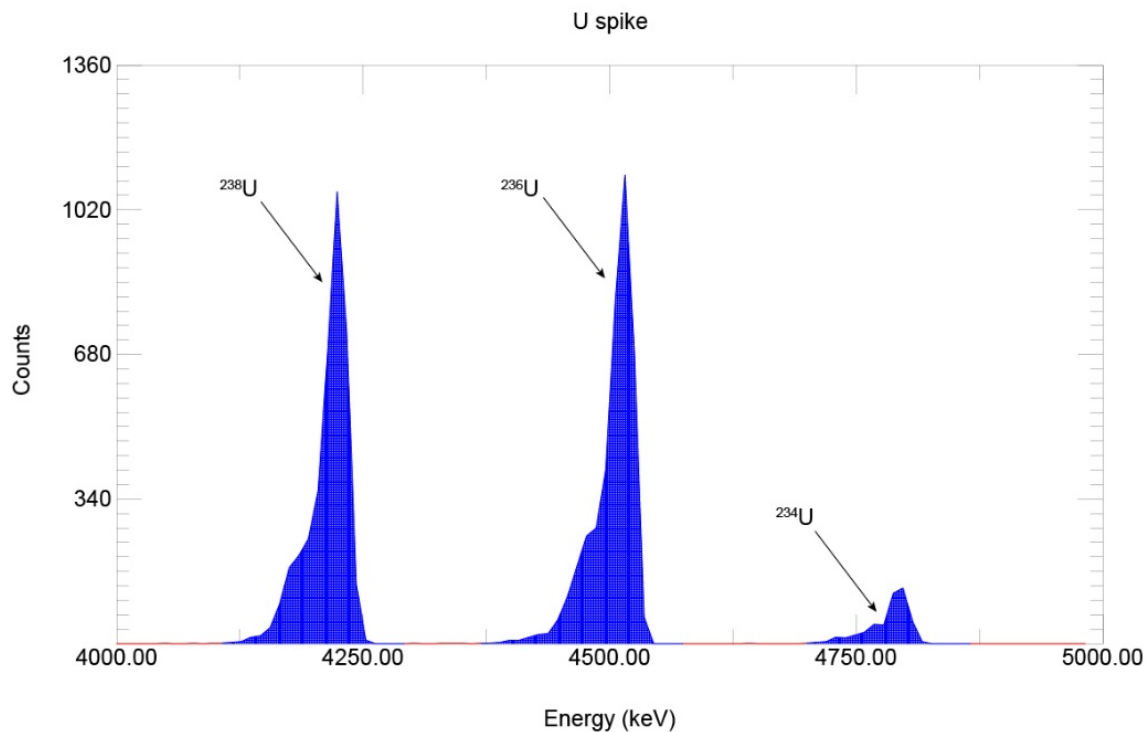


Figure 6.4.
Alpha spectrum of uranium spike

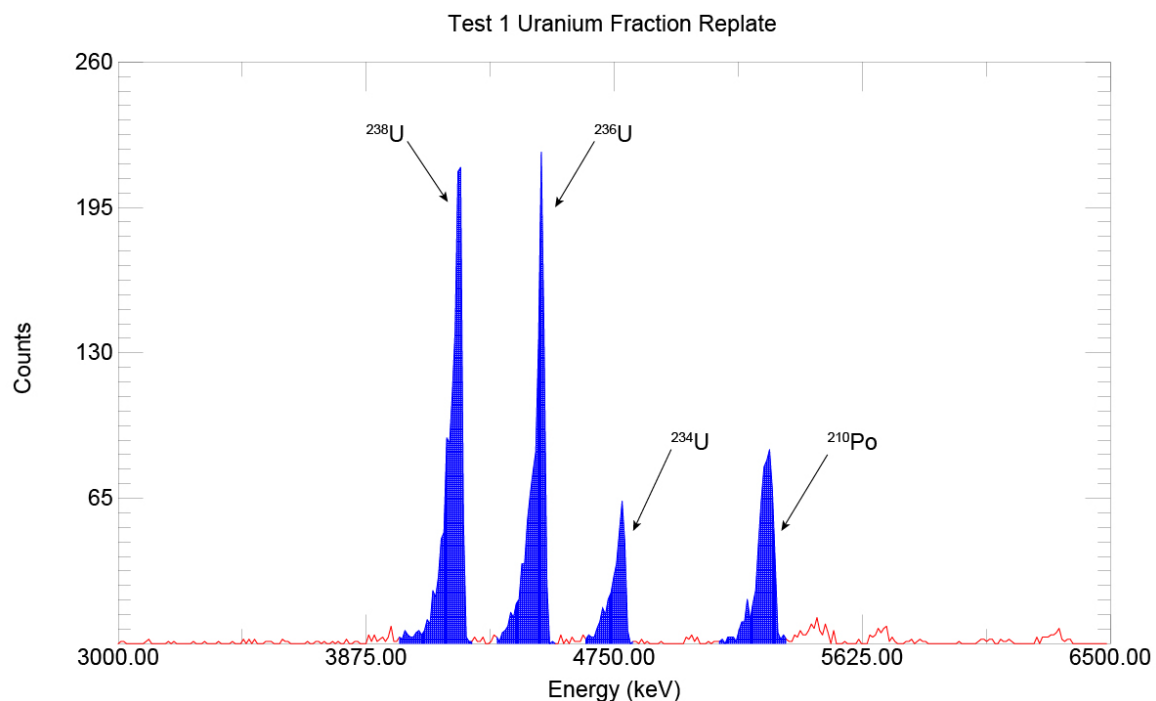


Figure 6.5.
Alpha spectrum of uranium fraction
Test 1 representative of U fractions from all tests

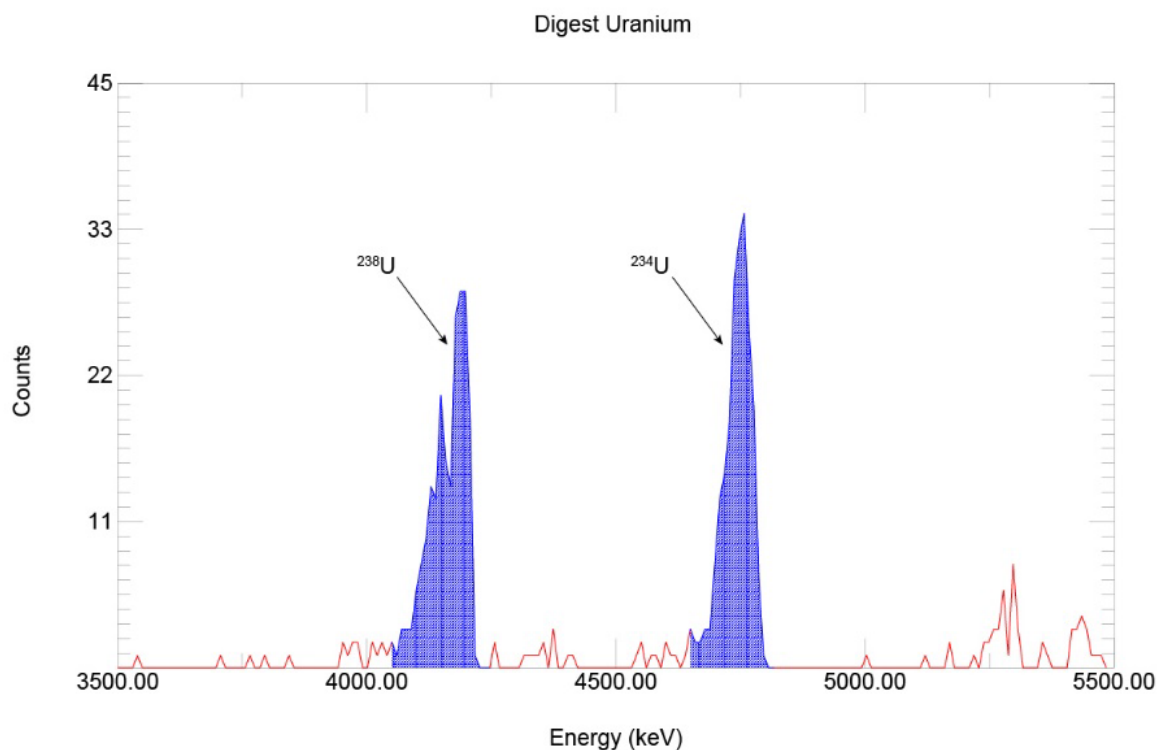


Figure 6.6.
Alpha spectrum of uranium from unspiked concrete

In addition to uranium, polonium-210 was also found in significant quantities in some of the uranium fractions (Figure 6.5). The origin of the ^{210}Po was a product of the decay of ^{210}Bi from the ^{210}Pb added as a contaminant to each sample. Due to the varying amounts of ^{210}Po measured, calculation of ^{210}Po added to each sample was completed in order to ascertain decontamination factors. Bismuth-210 and ^{210}Po half-lives (5 days and 138 days respectively) are much shorter than that of ^{210}Pb (22.3 years). It was assumed that secular equilibrium between ^{210}Po and ^{210}Pb had been achieved given the length of time that had elapsed from the creation of the ^{210}Pb source (18 years)

The decontamination of ^{210}Po is in the order of 10^2 - 10^3 (Table 6.6). Slight retention of the Po on UTEVA in 8 M HNO_3 may be occurring causing minor contamination of the uranium fractions. The decontamination of polonium is adequate for U measurement via alpha spectrometry as their alpha decay energies are significantly different and the masses are significantly different as well, so they can be resolved for during measurement via ICP-MS.

	Test 1	Test 2	Test 3	Test 4	Test 5
^{210}Po added (Bq)	14.12	12.98	12.15	11.84	12.98
^{210}Po present in U fraction (Bq)	0.0244	0.0119	0.0081	0.0192	0.0049
Decontamination factor in U fraction	580 ± 220	1090 ± 440	1500 ± 620	620 ± 220	2640 ± 930

Table 6.6.
 ^{210}Po decontamination factors in uranium fractions

During the measurement of the U fractions, initial recoveries were especially low (<30%). Analysis of the Th, Pu and wash fractions showed minimal contamination with U. The aqueous portion of the uranium fraction had been saved after the plating process. This solution was evaporated to dryness and treated with concentrated HNO_3 . This was then evaporated to dryness again before the electrodeposition process was repeated once more, onto a new stainless steel disc. Analysis of the re-plating of the uranium fractions showed significantly higher U activities than the first plating. The first plating was kept and was not dissolved and added back to the original solution. The activities of the two uranium discs produced were added to produce the final U activity and achieved recoveries of 60.4% \pm 27.1. the uranium yield achieved in this study was slightly lower than from a similar study undertaken by Zapata-García and Wershofen (2017) (around 70% U recovery)

The low electrodeposition efficacy of U is most likely due to the presence of the extractant in the uranium eluate. Dipentyl pentyphosphate (DP[PP]) is thought to slowly bleed from the column during elution, and this residual extractant can affect the plating of U. In order for more efficient U plating and measurement, treatment of the uranium fractions with *aqua regia*, hydrogen peroxide in nitric acid or perchloric acid should be used to decompose any organic species. The resulting solution can then be evaporated to dryness and the plating procedure can be carried out. Treatment of the eluate with strong acids, specifically nitric and perchloric acids is advised in the literature pertaining to the electrodeposition of actinides on stainless steel planchets for alpha spectrometry (Talvitie, 1972). The issues experienced in this study may be due to the age of the resin, the temperature of the eluate solutions (18 °C) or the eluate itself.

6.4.2 Thorium fractions

Alpha spectrometric analysis of the thorium spike (both ^{232}Th and ^{229}Th) show the significant presence of the daughter nuclides of the Th decay (Figure 6.7). The daughter radionuclides of Th are more apparent than the daughter radionuclides of the ^{238}U spike because of their shorter half-lives. Even though ^{232}Th has a longer half-life than ^{238}U (1.4×10^{10} years compared to 4.47×10^9 years) a similar activity of Th was present in the sample after spiking (Kondev et al., 2021). The decay products of ^{238}U (specifically ^{234}U , ^{230}Th and ^{226}Ra) in the decay chain have significantly longer half-lives than the decay products of ^{232}Th (Figure 6.9 and Figure 6.10). This results in higher activities of ^{232}Th daughter nuclides in the sample spike. It is noted that the ^{238}U initial decay products ^{234}Th and $^{234\text{m}}\text{Pa}$ have short half-lives but as these are beta emitters, they are not present in the alpha spectra. Each peak in the Th spike alpha spectrum was resolved and matched to the corresponding radionuclide (Table 6.7) (Firestone and Baglin, 1999).

Average thorium yields were $63\% \pm 23$. The variation in yields may be due to a similar issue to that of U yields. Although the kinetics of the TEVA resin are superior to that of anion exchange resin, active site leaching may occur more from TEVA resin given the method of active site attachment to the polymer support. Thorium fractions were not re-plated because all of the tests achieved yields above 30%. Thorium measurement accuracy yielded good ζ -scores (between 0.446 and -0.055), indicating good alignment with expected values. Percentage deviation from expected activity for all ^{232}Th measurements was within 2.86% and -0.36% indicating good precision over the 5 tests. Limit of detection for the separation of ^{232}Th from the concrete matrix was $0.48 \pm 0.18 \text{ mBq/g}$, significantly lower than the 10 mBq/g required to classify waste as radioactive based on its ^{232}Th content.

The alpha spectra of the Th fractions show the presence of ^{238}U and ^{236}U as well as ^{210}Po from the ^{210}Pb spike. Decontamination factors for uranium and polonium were calculated for U and Po in the Th fraction (Table 6.8 and Table 6.9 respectively). The average decontamination factors for uranium and polonium in the thorium factors were 64 and 95 respectively. The variation in decontamination factors of ^{210}Po in the thorium fraction bears little correlation to the decontamination of ^{210}Po in the uranium fractions. Due to the high activities of ^{210}Po added in comparison to U and Th activities the contamination in the Th fraction is most likely due to incomplete washing from the column. Study of Po has shown

Chapter 6

slight retention on TEVA resin in 8 M HNO₃ and 9 M HCl (Johansson, 2008). The changing of mobile phase during the elution of Th may have initiated the elution of Po when the Th eluent (9 M HCl) is added. The low decontamination factors for U are due to the slight retention exhibited by U on TEVA resin and incomplete washing of U from the resin. Despite this, decontamination factors were adequate enough to permit measurement of ²³²Th and ²²⁹Th via alpha spectrometry without spectral interference.

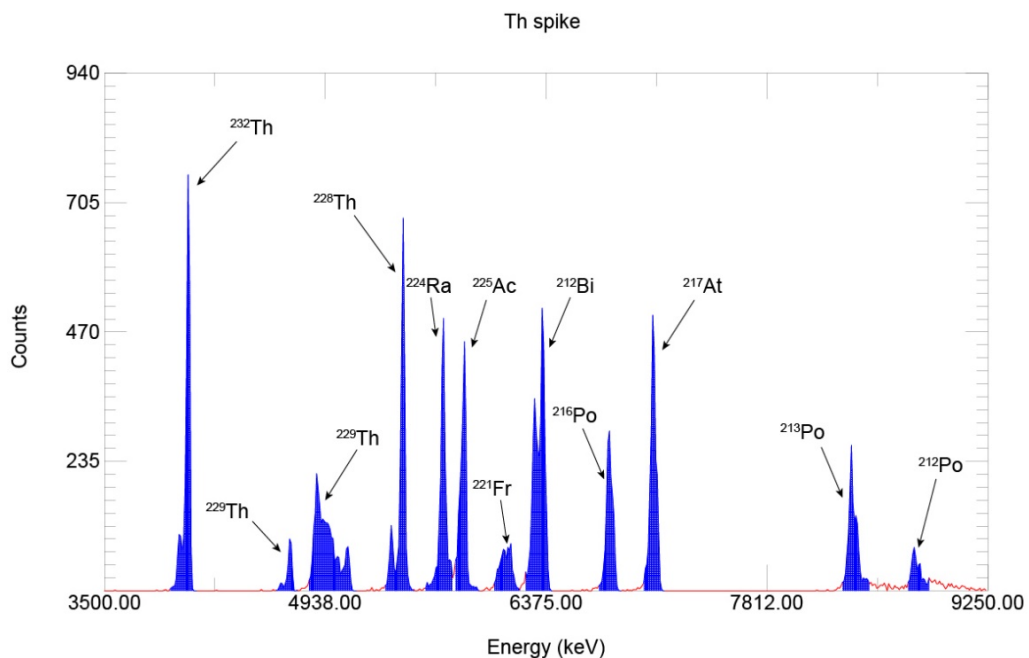


Figure 6.7.
Alpha spectrum of thorium spike

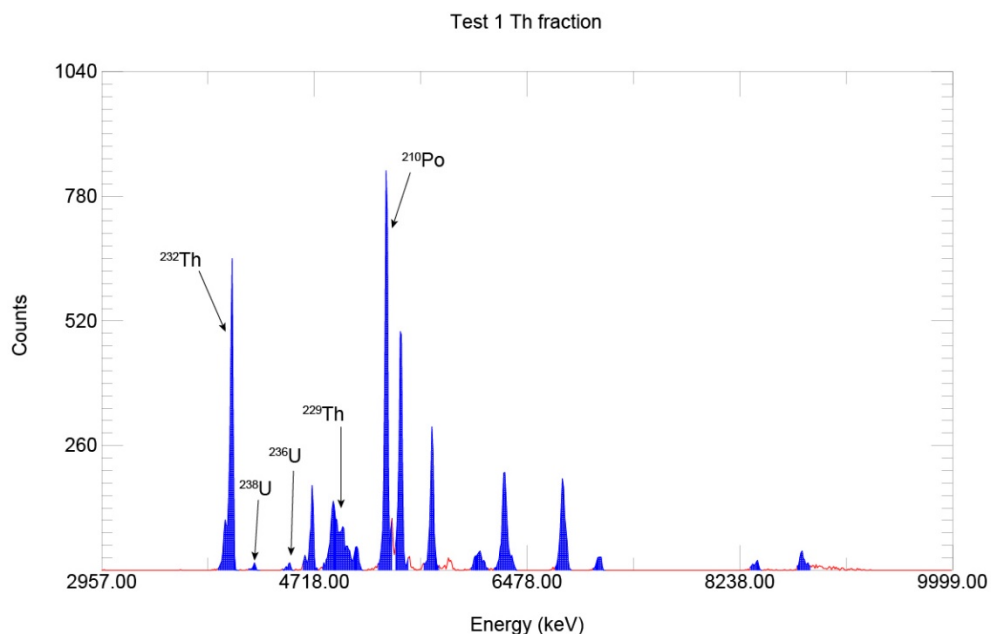


Figure 6.8.
Alpha spectrum of thorium fraction

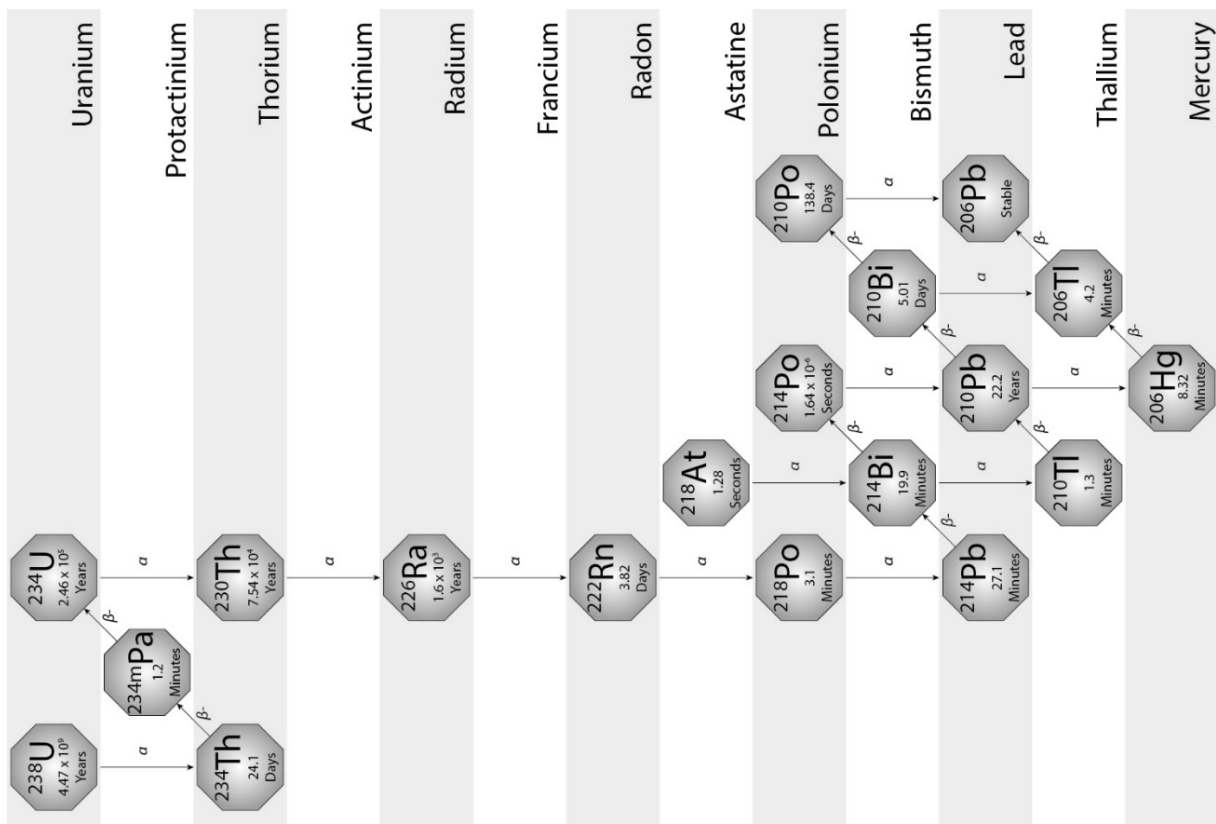


Figure 6.9.
 ^{238}U decay chain

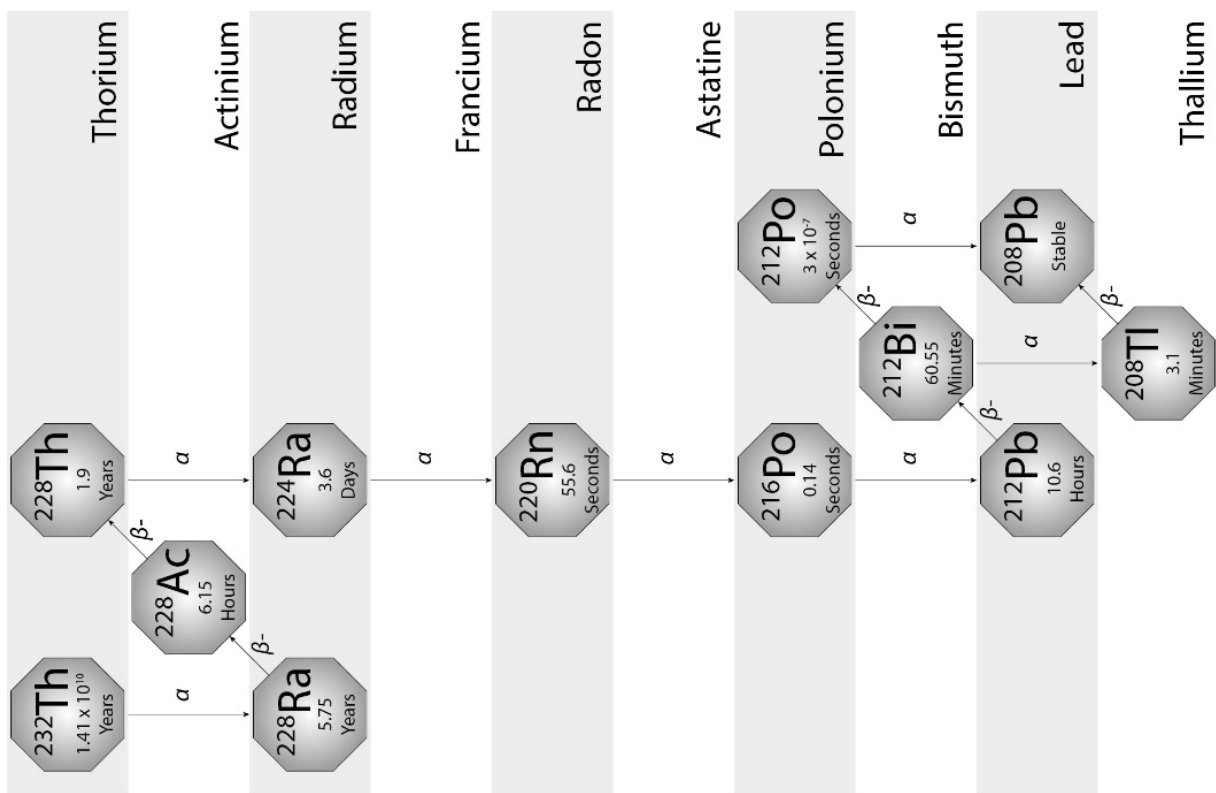


Figure 6.10.
 ^{232}Th decay chain

Peak Energy (KeV)	Nuclide	Origin
4025	^{232}Th	Target nuclide added
4700	^{230}Th	Abundant naturally (present in ICP-MS standard)
4875	^{229}Th	Tracer nuclide added
5350	^{228}Th	^{232}Th decay chain
5440	^{228}Th	^{232}Th decay chain
5700	^{224}Ra	^{232}Th decay chain
5835	^{225}Ac	^{229}Th decay product
6090	^{212}Bi	^{232}Th decay chain
6140	^{221}Fr	^{229}Th decay product
6290	^{212}Bi	^{232}Th decay chain
6340	$^{212}\text{Bi} + ^{221}\text{Fr}$	^{232}Th decay chain and ^{229}Th decay product respectively
6780	^{216}Po	^{232}Th decay chain
7060	^{217}At	^{229}Th decay product
8360	^{213}Po	^{229}Th decay product
8760	^{212}Po	^{232}Th decay chain

Table 6.7.
Thorium spike alpha peak identification

	Test 1	Test 2	Test 3	Test 4	Test 5
^{238}U added (Bq)	0.063739	0.064113	0.063668	0.064034	0.063707
^{238}U present in Th fraction (Bq)	0.000797	0.001047	0.001524	0.001377	0.000696
Decontamination factor in Th fraction	80 ± 24	60 ± 16	40 ± 9	45 ± 11	90 ± 28

Table 6.8.
 ^{238}U decontamination in thorium fractions

	Test 1	Test 2	Test 3	Test 4	Test 5
^{210}Po added (Bq)	14.12	12.98	12.15	11.84	12.98
^{210}Po present in Th fraction (Bq)	0.044	0.16	0.69	0.59	0.45
Decontamination factor in Th fraction	320 ± 120	80 ± 32	17 ± 7	20 ± 7	28 ± 10

Table 6.9.
 ^{210}Po decontamination in thorium fractions

6.4.3 Plutonium fractions

Plutonium-239 recoveries were high, achieving an average of $97.5\% \pm 5.4$. Plutonium recoveries achieved here are relatively high in comparison to other studies using similar separation techniques. Zapata-García and Wershofen (2017) attained recoveries of around 60% for Pu separation from concrete samples digested using a lithium borate/metaborate fusion technique. Wang et al., (2018) utilised a TEVA column to separate and purify Pu from a HF digest of concrete achieving Pu recoveries ranging between 56.5 – 92.9% (79.4% average). Both Wang et al., (2018) and Zapata-García and Wershofen (2017) utilised vacuum boxes to induce higher flow rates, however neither study states the flow rate achieved. Limit of detection for ^{239}Pu was calculated using Equation 4.6 and found to be 0.31 ± 0.10 mBq/g. This is much lower than The IAEA and UK's BEIS activity concentration for solid waste to be classed as radioactive with respect to its ^{239}Pu content (100 mBq) (Department for Business, Energy and Industrial Strategy, 2018; International Atomic Energy Agency, 2004). Analysis of ^{239}Pu precision yielded percentage deviation from expected activities between 3.48% and -2.33%. The accuracies of the ^{239}Pu measurements are sufficient, demonstrated by the ζ -scores (between 0.532 and -0.390), showing good alignment with expected activities for all five tests.

Alpha spectra show the presence of ^{241}Am in the Pu fractions. Around 9 Bq of ^{241}Am was added to each sample as a contaminant in the mixed gamma standard. Decontamination factors of ^{241}Am were calculated. The average decontamination factor of ^{241}Am in the plutonium fraction was found to be 2300 ± 720 . Americium's presence in the Pu fraction occurs as a result of Am's incomplete elution from the TEVA resin during the wash and Th elution phases. Americium-241's alpha decay peak energy is 5485 keV, which is significantly

Chapter 6

far enough away from the Pu peaks detected in these tests. Because of the decontamination of ^{241}Am and the distance between the emission energies of the Pu isotopes and ^{241}Am , accurate measurement of Pu content in the sample is achieved.

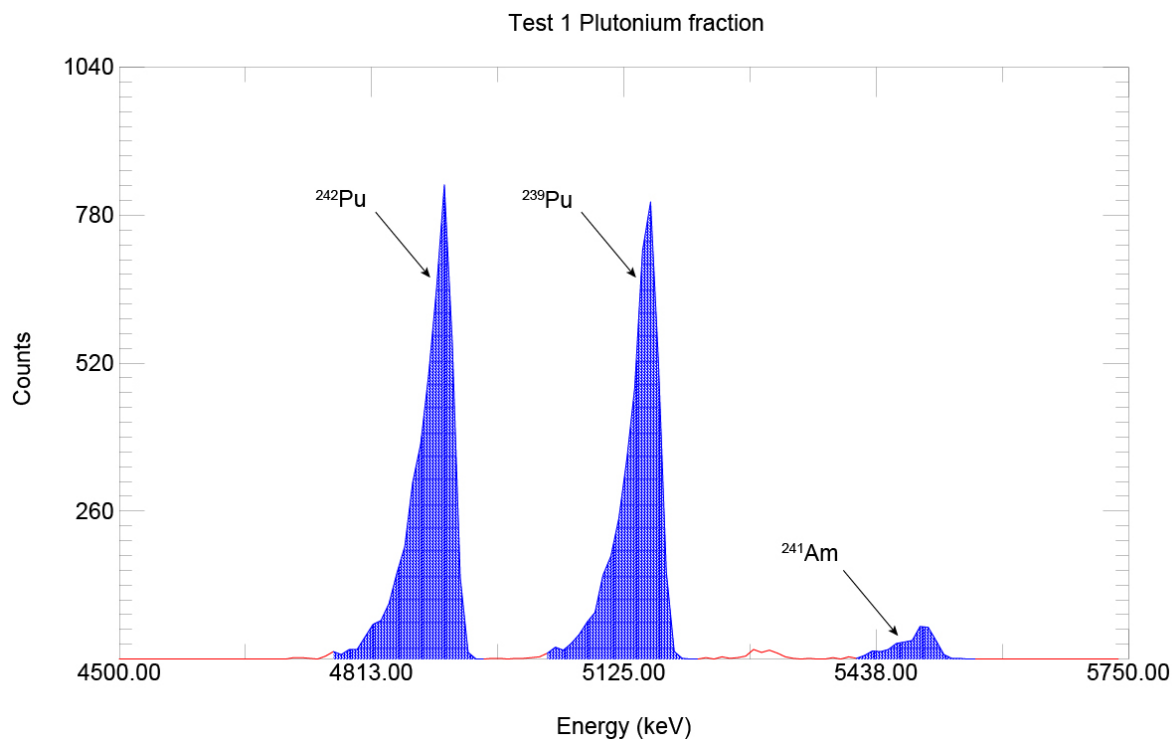


Figure 6.11.
Alpha spectrum of plutonium fraction

	Test 1	Test 2	Test 3	Test 4	Test 5
^{241}Am added (Bq)	9	8.6	8.9	8.5	8.7
^{241}Am present in Pu fraction (Bq)	0.00397	0.00497	0.00349	0.00379	0.00328
Decontamination factor in Pu fraction	2277 ± 493	1728 ± 341	2546 ± 514	2256 ± 442	2657 ± 575

Table 6.10.
 ^{241}Am decontamination in plutonium fractions

6.4.4 Strontium fractions

Measurement of ^{90}Sr by Cherenkov counting of the daughter isotope ^{90}Y was completed for all the samples. Strontium yields were on average $83.6\% \pm 1.2$. These Sr yields are greater than that achieved by Maxwell et al., (2016) who utilised a vacuum box system to induce 1-2 mL/min flow rate through a Sr column when separating Sr from a concrete digest. Kim et al., (2017) used gravimetric flow through a Sr column to separate ^{90}Sr from concrete and soil matrices, achieving average recoveries of 75.7%.

Fully corrected measured activities yielded accurate results, with ζ -scores ranging from 0.931 to -0.774 (Table 6.5), showing good alignment with the expected activities. Calculated percentage deviation from the expected activities ranged from 7.14% to -5.57%. Limit of detection for the separation technique was 0.055 ± 0.001 Bq/g, significantly lower than the 1 Bq/g required for classification as solid bulk waste (Department for Business, Energy and Industrial Strategy, 2018; International Atomic Energy Agency, 2004). As the Sr fraction is eluted from the Sr-spec column using 0.05 M HNO_3 , and the load and wash solutions used consist of 8 M HNO_3 , the eluate will consist of a nitric acid solution of a concentration of at least 0.05 M. Due to the apparent sensitivity of Cherenkov counting with regard to sample quench, a blank sample was produced from a Sr column, treated with 20 mL 8 M HNO_3 to simulate the load and wash phases (5 mL and 15 mL respectively). The column was then treated with 20 mL 0.05 M HNO_3 which was collected as a simulated eluate. A known activity of ^{90}Sr (in equilibrium with ^{90}Y) was added to the eluate simulant and counted multiple times. An average quench factor was established and applied to the Sr fractions.

An additional consideration is that of other beta-emitters producing Cherenkov radiation within the Sr fraction. As ^{90}Y reaches secular equilibrium with ^{90}Sr after about 19 days, the relationship between the two is expressed as:

$$A_2 = A_1(e^{-\lambda_2 t})$$

Equation 6.1.

Secular equilibrium equation

Where A_2 is the activity of ^{90}Y and A_1 is the activity of ^{90}Sr at time 0

Chapter 6

If A_2 at time period t is plotted against $e^{-\lambda t}$, a straight line should result where the gradient is equal to the activity of ^{90}Sr at $t = 0$. If other radionuclides are present, the plot will not follow a linear regression. The y-intercept is the ^{90}Y counts at $t = 0$. Figure 6.12 shows the plot for test 1 as a demonstration of the ^{90}Y counts for all Sr fractions counted. The r^2 value of 0.9966 shows a linear relationship and 314.08 was the ^{90}Sr counts used in the calculation of ^{90}Sr activity in Test 1. Additionally, the linear regression extended to the y-intercept shows almost 0 counts for $t = 0$. The variation in the y-intercept value is most likely due to a combination of background counts and slight inaccuracies in the recording of the time of Sr separation.

In addition, fully corrected ^{90}Sr measurements aligned closely with the expected activities. If the ^{90}Y Cherenkov count were supported by another Cherenkov emitter, fully corrected activity measurements for ^{90}Sr would be in excess of the activity added.

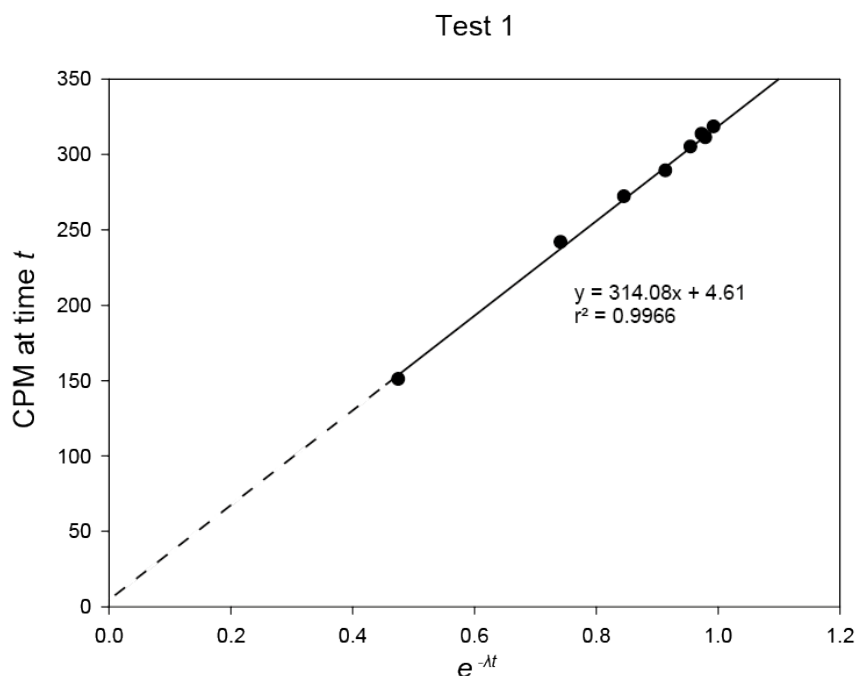


Figure 6.12.
 ^{90}Y ingrowth to secular equilibrium for Test 1
Representative of all tests conducted

6.5 Conclusions

Research undertaken in this chapter has demonstrated the applicability of an expedited separation system to the separation and purification of multiple radionuclides from a single sample of concrete digest. The analysis of each eluate fraction shows sufficient separation of Pu, Th, U and Sr. Recoveries of the target radionuclides were more than adequate to permit accurate measurement comparative to or higher than that of separation systems reported using lower flow rates (Kim et al., 2017; Maxwell et al., 2016; Wang et al., 2018; Zapata-García and Wershofen, 2017). This also indicates that the Fe hydroxide precipitations were sufficient for Sr separation and the calcium oxalate precipitation was effective at concentrating the Sr from the iron hydroxide supernatant. Decontamination of the fractions were sufficient, however Th fractions may benefit from larger wash volumes to increase decontamination of U even further. This may be necessary in high U samples. As is seen by the spectra and indicated by work in Chapter 5, higher flow rates did not cause premature elution of Th or Pu.

Fully corrected measurements for all four target radionuclides yielded good accuracy and precise results. Limits of detection calculated for all four radionuclides demonstrated that the expedited separation system is more than adequate for determining the radioactive status of a solid waste packet by IAEA or UK exemption criteria.

The main advantage of this separation system is one of time saving. The system examined in this chapter has proven accuracy and precision in the measurement of ^{239}Pu , ^{232}Th , ^{238}U and ^{90}Sr . However, in order to be of benefit, time saving must be demonstrated. Gravimetric flow rates through the columns used in this experiment were 0.6 ± 0.14 mL/min. For a conventional, gravimetric separation system using the same procedure described in 6.3.3 the total separation time (not including sample preparation) would be at least 2 hours 40 mins. For the expedited separation system, the procedure took 25 minutes. This represents a significant time saving in the preparation of samples for measurement. In addition, the procedure described did not use significantly larger volumes of reagent in order to achieve expedited separation.

The for the chromatographic separation is a constituent of the overall method described in 6.3. The time taken for the overall analysis of a single sample is roughly 54 hours with the time saved from the expedited separation. This includes time for preparation of sample

Chapter 6

and analysis. Without the expedited separation the overall time is around 56 hours. This represents a time saving for the entire technique of 3.5 %. Although the time saving made by the expedited chromatographic separation is small in comparison to the overall method, this study has shown the application for expedited separation within analytical methods. Use of an automated separator like the ASRS used in this study can also allow for simultaneous expedited separations, further reducing times and costs in comparison to conventional techniques using gravity flow columns.

Further research building on this could focus on other bottlenecks in the method. The method described in section 6.3 could be expedited, specifically in the cooling times for the metaborate fusion, ignition times for the CaC_2O_4 precipitate and the analysis times. U and Th fractions should also be investigated with respect to how the plating step is affected by organic compounds present in the eluate. Better understanding of this may aid in the further reduction of LODs. Further research into separations from other commonly found materials during nuclear decommissioning such as stainless steel, Inconel and aluminium would also be required.

Chapter 7 Conclusions and future work

The research presented in this thesis builds upon previous work produced within the department on the topic of expediting nuclear decommissioning processes. The use of an automated separation system has many benefits over gravimetric flow systems and other forced flow systems. However, due to the componentry involved, they are often a more expensive option. Use of these systems in emergency situations has been reported, but it is proposed that use of the systems more regularly can help to offset the costs associated with initial purchase. One such regular application would be the separation of radionuclides from nuclear waste materials during decommissioning, in order for the development of scaling factors. This study has examined the behaviour of separation systems at the flow rates a commercially available automated separation system is capable of.

Strontium separation using Sr resin was found to be highly effective due to the fast uptake kinetics of the resin. The crown ether active site was highly selective and strontium fractions produced had high decontamination factors for commonly found contaminants. Separation and purification of Sr from an acid digest of concrete yielded good results with limits of detection well below the activity concentration required for classification of bulk waste according to the IAEA and UK government. Measurement of ^{90}Sr using strontium yield tracer (^{85}Sr) yielded accurate and precise results. The time saving using the expedited technique was around 1 hour 20 minutes (from 1 hour 34 minutes to under 15 minutes). Analysis of Sr isotopic fractionation completed in this thesis has shown that over the flowrates tested there is no notable trend in the fractionation of strontium isotopes.

Study into the expedited separation of selected actinides (^{239}Pu , ^{238}U and ^{232}Th) analysed their behaviour on three different chromatographic materials. Here, two methods of active site bonding to the polymer could be compared using anion exchange resin and TEVA resin. This was enabled due to the similarities in their active sites (both quaternary amines). The uptake kinetics of TEVA resin were far superior to that of anion exchange resin. It was posited that the difference in uptake was because the active site molecules of the TEVA resin are able to move more freely in comparison to those of anion exchange resin. Uptake kinetics of actinides on UTEVA are similarly fast. Analysis of the isocratic elution of Th and U from anion exchange resin allowed for further discussion of the relationship between sorption of species to the chromatographic material and uptake kinetics. An effective

Chapter 7

system for the separation and purification of these three actinides would most effectively be done using TEVA and UTEVA columns in series.

From the work on Sr and actinide separations a rapid sample preparation technique was devised utilising a borate fusion on a non-active concrete sample. Separation of U, Pu, Th and Sr from the same sample was completed and repeat experiments conducted to assess precision. The matrix solution produced simulated that of a concrete sample being completely opened out and total dissolution of refractory radionuclide compounds to which target radionuclides and their tracers were added. The entire separation system was assessed and purified radionuclide fractions were produced. Analysis of the fractions was performed by alpha spectrometry for the actinide fractions and gamma and Cherenkov counting for the strontium fractions. The data attained shows adequate yields for all target radionuclides, and accurate and precise fully corrected measurements for all fractions. The LODs calculated from the multi-separation technique were more than adequate for assessment of bulk concrete for classification by IAEA guidelines. By use of an expedited separation system the time taken for the separation of multiple elements from a single concrete matrix sample was reduced from 2 hours 40 minutes to 25 minutes, a time saving of 2 hours and 15 minutes.

These multi-separation experiments showed some inefficiencies in the plating of U and, to some extent, Th from the purified fractions produced by the chromatographic separations. Study into the issues seen may further improve LODs for these fractions as the chemical yield would be increased.

The time saving facilitated by automated systems has a knock-on effect on subsequent procedures. Expedited separation can allow for faster report times and larger sample throughput of a laboratory. For laboratory managers this may be an attractive prospect. The versatility of automated systems allows for use in a wide variety of research contexts. In regards to the nuclear waste characterisation, an automated radionuclide separator can be integrated into a completely automated sample preparation system. This has the additional benefit of reducing operator exposure when working with high activities. Figure 7.1 shows a schematic for general sample analysis, from sampling to disposal. For a fully shielded method, remote handling techniques (which are commonly used on nuclear sites) are required. These allow for operators to control equipment from a safe area. Robotic

remote handling equipment has been shown to be very useful in decommissioning activities and can withstand high radiation fields (Borchardt et al., 2011; Zhang et al., 2020). Remote handling would be required to collect and move the sample between each stage in the analysis method. Sample pre-treatment methods include cutting or crushing or ignition of sample before digestion of the solid. Methods currently used for sample pre-treatment such as these are automated currently. For example, furnaces used for sample ignition currently have the ability to be heated to a defined temperature for a set period before cooling. It is also common for these heating and cooling rates to be controlled as well. Preparative chemistry is more difficult to automate as the actions for preparation of samples is often extremely specific and can vary widely, dependent on the material being analysed. This represents the biggest gap in the automation of the entire process and could benefit from additional research.

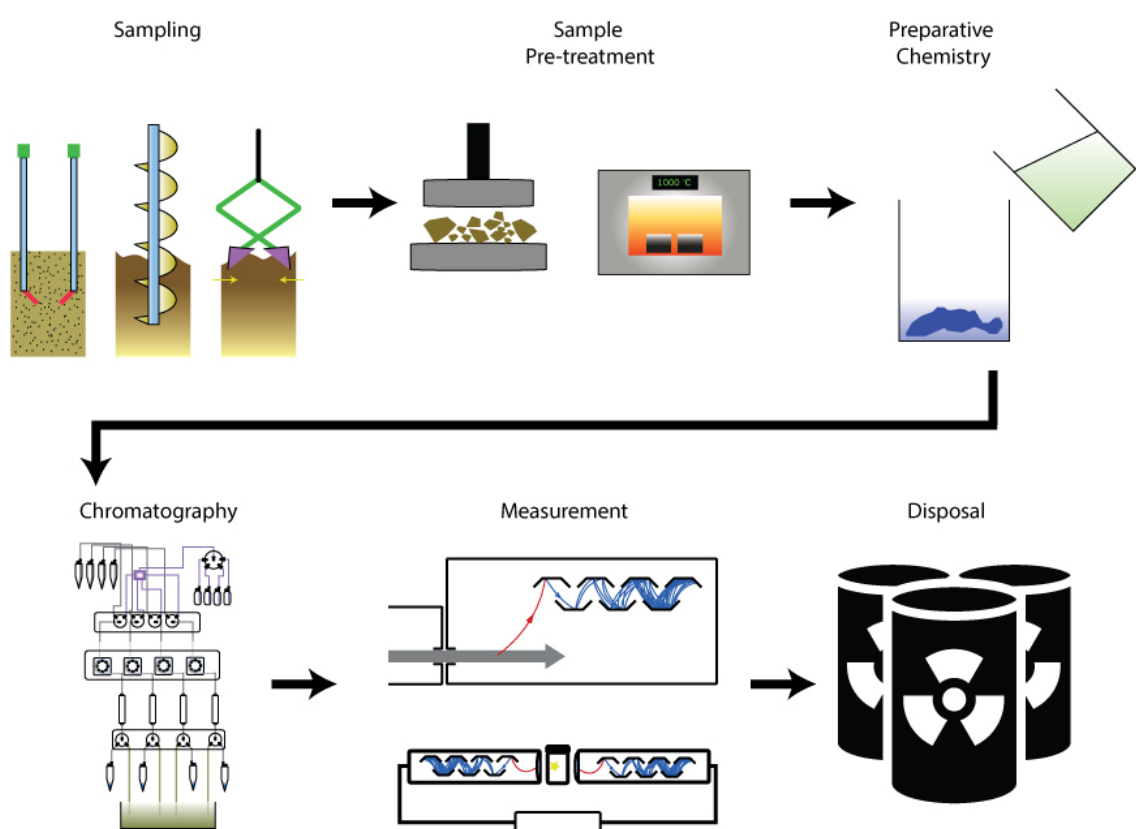


Figure 7.1 Sample analysis schematic

Chapter 7

As mentioned in section 2.4, online techniques have been developed, transferring sample straight to measurement technique. If a hyphenated system were to be employed, remote handling would be required to transfer sample between the automated chromatographic separator and the measurement. Remote handling would also be required for transfer of sample post-measurement to the desired disposal pathway.

General use of the Automated Sequential Radionuclide Separator (ASRS) (Hanjin Eni Co., LTD., Daejeon, Republic of Korea) was relatively simple, given the clear and concise design of the LabVIEW program used to control the device. The changing of the chromatographic columns was also simple as they had screw connectors at the top and bottom. The glass columns available were sturdy and made column packing easy. However, throughout the research some issues with the hardware did occur and these should be considered when designing systems to be used for chromatographic separations. A small number of the plastic componentry which had direct contact with the reagents were not made of PTFE, which lead to them being rapidly degraded. These were then replaced with PTFE equivalents. Additionally, ASRS seemed to produce different flow rates when in analysis mode compared to when in calibration mode. This was negated by measuring the mass of each fraction and calculating the flowrate produced gravimetrically. Another factor affecting the performance of the ASRS was the degradation of the tubing used in the peristaltic pumps. This is more difficult to avoid given the material requirements for the tubing and can be combatted by regular flow rate calibration and replacement of the tubing during routine maintenance.

For use in automated radionuclide analysis in shielded systems, an autosampler would be a better solution than the sample reagent bottle setup as it would eliminate the dead volume of the system. This would also help the flowrate disparity between analysis and calibration modes as the tubing diameter from the reagent bottles used in calibration mode was different to the tubing diameter from the sample bottles.

Study of nuclide behaviour on chromatographic materials at increased flowrates can have a theoretical basis in the concepts discussed here, especially with regards to the nature of active site bonding and uptake kinetics. These can provide the basis of future research into expedited separation systems and can aid in the selection of the most appropriate material.

Future research should focus on other radionuclides important for the decommissioning of nuclear facilities. Activation products such as ^{63}Ni , ^{59}Ni , ^{55}Fe , and ^{41}Ca , fission products such as ^{99}Tc , ^{94}Nb and ^{129}I and high mass neutron capture products such as ^{241}Am , ^{243}Cm and ^{237}Np are some of the nuclides of key interest (Hou, 2007). Materials for the separation and purification are available for many of these radionuclides, for example DGA resin is commonly used for Am separation and purification, Ni resin can separate Ni from other fission products and TK201 resin can be used to separate Tc in low acidic conditions (Triskem International, 2021a). The resins described have similar active site bonding methods to the polymer support than that of TEVA, UTEVA and Sr resins. However, the separation mechanisms differ depending on the nature of the active site used. Ni resin in particular works by on-column precipitation of Ni with the dimethylglyoxime at pH 8-9 (Triskem International, 2022).

A new resin produced by Triskem International called TK221 has active sites similar to that of both TRU and DGA resins (Vajda, 2021). It has a mixture of diglocylamide (DGA) and a phosphine oxide (similar to TRU active site). This resolves the partial adsorption of Am on TRU and of U on DGA in HNO_3 , as the diglocylamide is able to strongly retain AM and the TRU active site is able to strongly retain U from the same solution (Vajda, 2021). Further to this a wide range of lanthanides can be retained as well as Y and Sc. The technical documentation outlines a simple two column separation system for the separation and isolation of Pu, Th, U and Am from a single sample using stacked columns of TEVA above TK221 (Triskem International, 2021b). Investigation of how this system performs in comparison to the separation procedure detailed in Chapter 6 would be of interest.

Appendix A Determination of counting uncertainty

Single measurement uncertainties for radiometric analysis were calculated using the following equations

$$\sigma_c = \sqrt{C}$$

Where C is the counts detected

Combining uncertainties

$$\sigma_{(A+B)} = \sqrt{\sigma_A^2 + \sigma_B^2}$$

$$\sigma_{(A-B)} = \sqrt{\sigma_A^2 + \sigma_B^2}$$

$$\sigma_{(AB)} = AB \times \sqrt{\left(\frac{\sigma_A}{A}\right)^2 + \left(\frac{\sigma_B}{B}\right)^2}$$

$$\sigma_{(A/B)} = \left(\frac{A}{B}\right) \times \sqrt{\left(\frac{\sigma_A}{A}\right)^2 + \left(\frac{\sigma_B}{B}\right)^2}$$

Quoted uncertainties were $\pm 2\sigma$ in order to have 95% coverage

ICP-MS uncertainties were calculated from the standard deviation of repeat measurements of the same sample. Subsequent combination of uncertainties with uncertainties from calibration and internal standard measurement used the above equations.

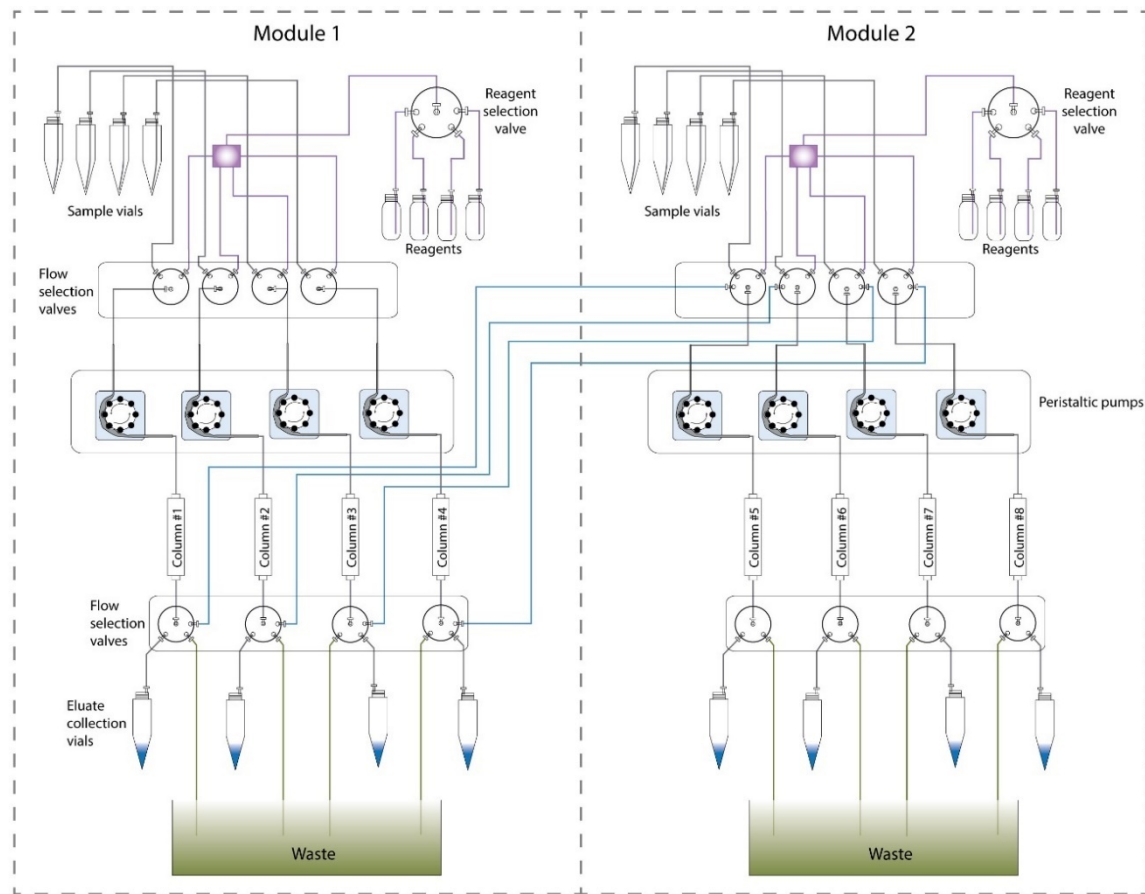
Appendix B Zeta-score calculation

From Analytical Methods Committee (2016):

$$\zeta = \frac{x_m - x_e}{\sqrt{\sigma_m^2 + \sigma_e^2}}$$

Where x_m is the measured value, x_e is the expected value (activity added) σ_m is the uncertainty on the measured value and σ_e is the uncertainty on the expected value.

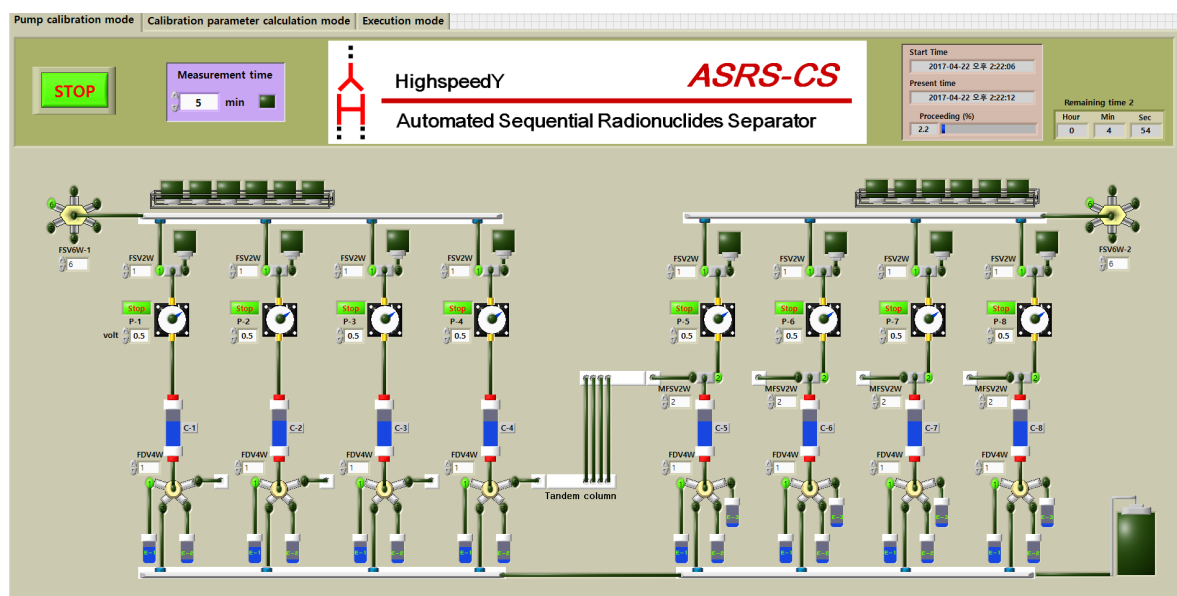
Appendix C ASRS configuration and control



Appendix Figure 1 Diagram of the ASRS

Showing the columns from Module 1 having connections to the flow selection valves at the top of the columns in Module 2. This allows for in-series separations using 2 different chromatographic materials. Each module has its own bank of sample vials and reagent bottles for single column set-up. In single column set-up 8 samples can simultaneously be separated.

Appendix C



Appendix Figure 2 LabVIEW™ control panel in analysis mode

List of References

Abe, T., Asakura, K., 2012. Uranium Oxide and MOX Production, in: Comprehensive Nuclear Materials. Elsevier, pp. 393–422. <https://doi.org/10.1016/B978-0-08-056033-5.00036-7>

Ageyev, V.A., Odintsov, O.O., Sajeniouk, A.D., 2005. Routine radiochemical method for the determination of ^{90}Sr , ^{238}Pu , $^{239+240}\text{Pu}$, ^{241}Am and ^{244}Cm in environmental samples. *J Radioanal Nucl Chem* 264, 337–342. <https://doi.org/10.1007/s10967-005-0718-5>

Agilent Technologies Inc., 2015. Agilent 8800 Triple Quadrupole ICP-MS.

Altenhein-Haese, C., Bischoff, H., Fu, L., Mao, J., Marx, G., 1994. Adsorption of actinides on cement compounds. *Journal of Alloys and Compounds* 213–214, 554–556. [https://doi.org/10.1016/0925-8388\(94\)90986-5](https://doi.org/10.1016/0925-8388(94)90986-5)

Analytical Methods Committee, 2016. z-Scores and other scores in chemical proficiency testing—their meanings, and some common misconceptions. *Anal. Methods* 8, 5553–5555. <https://doi.org/10.1039/C6AY90078J>

Andrews, H.L., 1955. Radioactive fallout from bomb clouds. *Science* 122, 453–456.

Andrieu, C., Olivier Dehaye, C., Tardy, F., Boisserie, T., Desnoyers, Y., Thierfeldt, S., Martin, N., Henrik Efraimsson, Haakansson, L., Larsson, A., Dunlop, A.A., Jarman, S., Orr, P., Abu-Eid, B., 2013. Radiological Characterisation for Decommissioning of Nuclear Installations - Final Report of the Task Group on Radiological Characterisation and Decommissioning (RCD) of the Working Party on Decommissioning and Dismantling (WPDD) - Final Report, September 2013. Nuclear Energy Agency of the OECD (NEA).

Attendorn, H.-G., Bowen, R.N.C., 2012. Radioactive and Stable Isotope Geology. Springer Netherlands, Dordrecht.

Bajpai, P., 2018. Miscellaneous Topics, in: Biermann's Handbook of Pulp and Paper. Elsevier, pp. 493–516. <https://doi.org/10.1016/B978-0-12-814238-7.00025-8>

Bauman, W.C., Robert, M., 1952. Anion exchange resins. US2614099A.

Be, M.M., Chiste, V., Dulieu, C., Browne, E., Chechev, V., Kuzmenko, N., Helmer, R., Nichols, A., Schonfeld, E., Dersch, R., 2004. Table of radionuclides (Vol 1 - A = 1 to 150). Bureau International des Poids et Mesures - BIPM, France.

Bio-Rad Laboratories, 2021. AG® 1, AG MP-1 and AG 2 Strong Anion Exchange Resin Instruction Manual.

BIS, 2013. The UK's Nuclear Future (No. BIS/12/627). Her Majesty's Government.

Blasius, E., Klein, W., Schön, U., 1985. Separation of strontium from nuclear waste solutions by solvent extraction with crown ethers. *Journal of Radioanalytical and Nuclear Chemistry Articles* 89, 389–398. <https://doi.org/10.1007/BF02040603>

List of References

Bock, R., 1979. Decomposition methods in analytical chemistry. The Blackie Group, Edinburgh.

Bond, A., Palerm, J., Haigh, P., 2004. Public participation in EIA of nuclear power plant decommissioning projects: a case study analysis. *Environmental Impact Assessment Review* 24, 617–641. <https://doi.org/10.1016/j.eiar.2004.02.002>

Bonnesen, P.V., Brown, G.M., Alexandratos, S.D., Bavoux, L.B., Presley, D.J., Patel, V., Ober, R., Moyer, B.A., 2000. Development of Bifunctional Anion-Exchange Resins with Improved Selectivity and Sorptive Kinetics for Pertechnetate: Batch-Equilibrium Experiments. *Environ. Sci. Technol.* 34, 3761–3766. <https://doi.org/10.1021/es990858s>

Borchardt, R., Denissen, L., Desbats, P., Jeanjacques, M., Nokhamzon, J.-G., Valentin, P., Slater, S., Valencia, L., Wittenauer, S., Yamauchi, T., Burton, B., 2011. Remote handling techniques in decommissioning - A report of the NEA Co-operative Programme on Decommissioning (CPD) project. Nuclear Energy Agency of the OECD (NEA).

Bowen, V., 1970. Analyses of sea-water for strontium and strontium-90. Reference methods for marine radioactivity studies. IAEA 93–119.

Brannon, J.C., Podosek, F.A., McLimans, R.K., 1992. Alleghenian age of the Upper Mississippi Valley zinc-lead deposit determined by Rb–Sr dating of sphalerite. *Nature* 356, 509–511. <https://doi.org/10.1038/356509a0>

Braysher, E., Russell, B., Woods, S., García-Miranda, M., Ivanov, P., Bouchard, B., Read, D., 2019. Complete dissolution of solid matrices using automated borate fusion in support of nuclear decommissioning and production of reference materials. *J Radioanal Nucl Chem* 321, 183–196. <https://doi.org/10.1007/s10967-019-06572-z>

Broekmans, M.A.T.M., Jansen, J.B.H., 1998. Silica dissolution in impure sandstone: application to concrete. *Journal of Geochemical Exploration* 62, 311–318. [https://doi.org/10.1016/S0375-6742\(97\)00034-4](https://doi.org/10.1016/S0375-6742(97)00034-4)

Brown, N.R., Powers, J.J., Feng, B., Heidet, F., Stauff, N.E., Zhang, G., Todosow, M., Worrall, A., Gehin, J.C., Kim, T.K., Taiwo, T.A., 2015. Sustainable thorium nuclear fuel cycles: A comparison of intermediate and fast neutron spectrum systems. *Nuclear Engineering and Design* 289, 252–265. <https://doi.org/10.1016/j.nucengdes.2015.04.015>

Bu, W., Zheng, J., Liu, X., Long, K., Hu, S., Uchida, S., 2016. Mass spectrometry for the determination of fission products ^{135}Cs , ^{137}Cs and ^{90}Sr : A review of methodology and applications. *Spectrochimica Acta Part B: Atomic Spectroscopy* 119, 65–75. <https://doi.org/10.1016/j.sab.2016.03.008>

Budd, P.M., 1989. Polyelectrolytes, in: *Comprehensive Polymer Science and Supplements*. Elsevier, pp. 215–230. <https://doi.org/10.1016/B978-0-08-096701-1.00011-2>

Budnitz, R., 1974. Strontium-90 and strontium-89: a review of measurement techniques in environmental media. California Univ.

Buesseler, K.O., Casso, S.A., Hartman, M.C., Livingston, H.D., 1990. Determination of fission-products and actinides in the Black Sea following the Chernobyl accident. *Journal of Radioanalytical and Nuclear Chemistry, Articles* 138, 33–47. <https://doi.org/10.1007/BF02049345>

Burrows, A., 2013. Chemistry³: introducing inorganic, organic and physical chemistry, Second edition. ed. Oxford University Press, Oxford.

Butler, F.E., 1963. Separation of Calcium and Strontium by Liquid Ion Exchange. Determination of Total Radiostrontium in Milk. *Analytical Chemistry* 35, 2069–2071. <https://doi.org/10.1021/ac60206a026>

Carey, J.M., Caruso, J.A., 1992. Electrothermal Vaporization for Sample Introduction in Plasma Source Spectrometry. *Critical Reviews in Analytical Chemistry* 23, 397–439. <https://doi.org/10.1080/10408349208051652>

Carignan, J., Machado, N., Gariépy, C., 1995. U-Pb isotopic geochemistry of komatiites and pyroxenes from the southern Abitibi greenstone belt, Canada. *Chemical Geology* 126, 17–27. [https://doi.org/10.1016/0009-2541\(95\)00100-8](https://doi.org/10.1016/0009-2541(95)00100-8)

Carroll, L.R., 2001. Predicting long-lived, neutron-induced activation of concrete in a cyclotron vault, in: AIP Conference Proceedings. Presented at the The CAARI 2000: Sixteenth international conference on the application of accelerators in research and industry, AIP, Denton, Texas (USA), pp. 301–304. <https://doi.org/10.1063/1.1395309>

Carswell, D.J., 1957. Separation of thorium and uranium nitrates by anion exchange. *Journal of Inorganic and Nuclear Chemistry* 3, 384–387. [https://doi.org/10.1016/0022-1902\(57\)80046-3](https://doi.org/10.1016/0022-1902(57)80046-3)

Chapon, A., Pigrée, G., Putmans, V., Rogel, G., 2016. Optimization of liquid scintillation measurements applied to smears and aqueous samples collected in industrial environments. *Results in Physics* 6, 50–58. <https://doi.org/10.1016/j.rinp.2016.01.018>

Chen, Q., Hou, X., Yu, Y., Dahlgaard, H., Nielsen, S.P., 2002. Separation of Sr from Ca, Ba and Ra by means of Ca(OH)2 and Ba(Ra)Cl2 or Ba(Ra)SO4 for the determination of radiostrontium. *Analytica Chimica Acta* 466, 109–116. [https://doi.org/10.1016/S0003-2670\(02\)00571-8](https://doi.org/10.1016/S0003-2670(02)00571-8)

Chenoweth, W.L., Pool, T.C., 2003. Uranium, in: *Encyclopedia of Physical Science and Technology*. Elsevier, pp. 351–357. <https://doi.org/10.1016/B0-12-227410-5/00802-4>

Chung, K.H., Choi, S.D., Choi, G.S., Kang, M.J., 2013. Design and performance of an automated radionuclide separator: Its application on the determination of 99Tc in groundwater. *Applied Radiation and Isotopes* 81, 57–61. <https://doi.org/10.1016/j.apradiso.2013.03.080>

Chung, K.H., Kim, H., Lim, J.M., Ji, Y.-Y., Choi, G.-S., Kang, M.J., 2015. Rapid determination of radiostrontium in milk using automated radionuclides separator and liquid scintillation counter. *Journal of Radioanalytical and Nuclear Chemistry* 304, 293–300. <https://doi.org/10.1007/s10967-014-3594-z>

List of References

Cook, M., 2021. Agile fusion method for the determination of Pu isotopes in diverse sediments. *Applied Radiation and Isotopes* 176, 109878. <https://doi.org/10.1016/j.apradiso.2021.109878>

Creaser, R.A., Grütter, H., Carlson, J., Crawford, B., 2004. Macrocrystal phlogopite Rb–Sr dates for the Ekati property kimberlites, Slave Province, Canada: evidence for multiple intrusive episodes in the Paleocene and Eocene. *Lithos* 76, 399–414. <https://doi.org/10.1016/j.lithos.2004.03.039>

Crocker, G., 1963. Estimates of fission product yields of a thermonuclear explosion. Northwestern University Technological Institute, Evanston IL.

Croudace, I., Warwick, P., Taylor, R., Dee, S., 1998. Rapid procedure for plutonium and uranium determination in soils using a borate fusion followed by ion-exchange and extraction chromatography. *Analytica Chimica Acta* 371, 217–225. [https://doi.org/10.1016/S0003-2670\(98\)00353-5](https://doi.org/10.1016/S0003-2670(98)00353-5)

Croudace, I.W., 2012. Height Correction when using well-type HPGe detectors. (Validation of methodology. No. 1). GAU, Southampton, United Kingdom.

Croudace, I.W., Russell, B.C., Warwick, P.W., 2017. Plasma source mass spectrometry for radioactive waste characterisation in support of nuclear decommissioning: a review. *J. Anal. At. Spectrom.* 32, 494–526. <https://doi.org/10.1039/C6JA00334F>

Croudace, I.W., Warwick, P.E., Reading, D.G., Russell, B.C., 2016. Recent contributions to the rapid screening of radionuclides in emergency responses and nuclear forensics. *TrAC Trends in Analytical Chemistry* 85, 120–129. <https://doi.org/10.1016/j.trac.2016.05.007>

D'Alelio, G.F., 1944. Production of synthetic polymeric compositions comprising sulphonated polymerizes of poly-vinyl aryl compounds and treatment of liquid media therewith. US2366007A.

DEFRA, 2002. Radioactive Wastes in the UK: A Summary of the 2001 Inventory (No. N/041), NIREX Report. Department for Environment, Food and Rural Affairs.

Department for Business, Energy and Industrial Strategy, 2019. 2019 UK Radioactive Waste Inventory. Department for Business, Energy & Industrial Strategy.

Department for Business, Energy and Industrial Strategy, 2018. SCOPE OF AND EXEMPTIONS FROM THE RADIOACTIVE SUBSTANCES LEGISLATION IN ENGLAND, WALES AND NORTHERN IRELAND (Guidance Document).

Dong, L., Wan, B., Yang, W., Deng, C., Chen, Z., Yang, L., Cai, K., Xiao, W., 2018. Rb-Sr geochronology of single gold-bearing pyrite grains from the Katbasu gold deposit in the South Tianshan, China and its geological significance. *Ore Geology Reviews* 100, 99–110. <https://doi.org/10.1016/j.oregeorev.2016.10.030>

EDF Energy, 2017. Generating energy [WWW Document]. EDF Energy. URL <https://www.edfenergy.com/energy> (accessed 11.14.17).

Edward, J.B., Benfer, R.A., Morris, J.S., 1990. The effects of dry ashing on the composition of human and animal bone. *Biological Trace Element Research* 25, 219–231. <https://doi.org/10.1007/BF02990417>

Eichrom Technologies, LLC, 2006. Eichrom method ACW17 VBS.

Emerson, H.S., Young, A.K., 1995. Method development for the extraction of naturally occurring radionuclides in marine sediments. *Science of The Total Environment* 173–174, 313–322. [https://doi.org/10.1016/0048-9697\(95\)04778-6](https://doi.org/10.1016/0048-9697(95)04778-6)

Ettre, L.S., 1993. Nomenclature for chromatography (IUPAC Recommendations 1993). *Pure and Applied Chemistry* 65, 819–872. <https://doi.org/10.1351/pac199365040819>

European Commission, 2018. COMMISSION IMPLEMENTING DECISION on the financing of indirect actions within the framework of Council Regulation (Euratom) No 2018/1563 and on the adoption of the work programme for 2019-2020.

Evans, J., Lepel, E., Sanders, R., Wilkerson, C., Silker, W., Thomas, C., Abel, K., Robertson, D., 1984. Long-lived activation products in reactor materials. Pacific Northwest Lab.

Ewing, R., Weber, W., Clinard Jr, F., 1995. Radiation effects in nuclear waste forms for high-level radioactive waste. *Progress in nuclear energy* 29, 63–127.

Faris, J., Buchanan, R., 1964. Anion Exchange Characteristics of the Elements in Nitric Acid and Nitrate Solutions and Application in Trace Element Analysis (No. ANL-6811, 4012440). <https://doi.org/10.2172/4012440>

Faye, G., Sutarno, R., 1976. Certified compositional reference materials for the earth sciences. *The Canadian Mineralogist* 14, 164–171.

Fedorowich, J.S., Richards, J.P., Jain, J.C., Kerrich, R., Fan, J., 1993. A rapid method for REE and trace-element analysis using laser sampling ICP-MS on direct fusion whole-rock glasses. *Chemical Geology* 106, 229–249. [https://doi.org/10.1016/0009-2541\(93\)90029-I](https://doi.org/10.1016/0009-2541(93)90029-I)

Feuerstein, J., Boulyga, S.F., Galler, P., Stingededer, G., Prohaska, T., 2008. Determination of ⁹⁰Sr in soil samples using inductively coupled plasma mass spectrometry equipped with dynamic reaction cell (ICP-DRC-MS). *Journal of Environmental Radioactivity* 99, 1764–1769. <https://doi.org/10.1016/j.jenvrad.2008.07.002>

Firestone, R.B., Baglin, C.M., 1999. Table of isotopes, 8th ed., 1999 update with CD-ROM. ed. Wiley, New York.

Fisher, Sallie., Kunin, Robert., 1957. Use of Ion Exchange Resins for Determination of Uranium in Ores and Solutions. *Anal. Chem.* 29, 400–402. <https://doi.org/10.1021/ac60123a021>

Fourie, H.O., Ghijssels, J.P., 1969. Radiostrontium in Biological Material: a Precipitation and Extraction Procedure Eliminating the Use of Fuming Nitric Acid. *Health Physics* 17, 685–689. <https://doi.org/10.1097/00004032-196911000-00005>

List of References

Franklin, B.H., Knauss, J.A., 1992. Standard and reference materials for marine science (NOAA Technical Memorandum No. NOS ORCA 68). National Oceanic and Atmospheric Administration, Rockville, Maryland USA.

Freiling, E., 1961. Radionuclide fractionation in bomb debris. *Science* 133, 1991–1998.

Gad, S.C., 2014. Thorium and Thorium Dioxide, in: *Encyclopedia of Toxicology*. Elsevier, pp. 560–561. <https://doi.org/10.1016/B978-0-12-386454-3.00940-4>

Galindo, C., Mougin, L., Nourreddine, A., 2007. An improved radiochemical separation of uranium and thorium in environmental samples involving peroxide fusion. *Applied Radiation and Isotopes* 65, 9–16. <https://doi.org/10.1016/j.apradiso.2006.05.012>

Ghaedi, M., Hossainian, H., Montazerzohori, M., Shokrollahi, A., Shojaipour, F., Soylak, M., Purkait, M.K., 2011. A novel acorn based adsorbent for the removal of brilliant green. *Desalination* 281, 226–233. <https://doi.org/10.1016/j.desal.2011.07.068>

Gilmore, G., 2008. *Practical gamma-ray spectrometry*, 2nd ed. ed. Wiley, Chichester, England ; Hoboken, NJ.

Gin, S., Abdelouas, A., Criscenti, L.J., Ebert, W.L., Ferrand, K., Geisler, T., Harrison, M.T., Inagaki, Y., Mitsui, S., Mueller, K.T., Marra, J.C., Pantano, C.G., Pierce, E.M., Ryan, J.V., Schofield, J.M., Steefel, C.I., Vienna, J.D., 2013. An international initiative on long-term behavior of high-level nuclear waste glass. *Materials Today* 16, 243–248. <https://doi.org/10.1016/j.mattod.2013.06.008>

Gječi, E., 1996. Analysis of ⁹⁰Sr in environmental and biological samples by extraction chromatography using a crown ether. *Journal of Radioanalytical and Nuclear Chemistry Letters* 213, 165–174. <https://doi.org/10.1007/BF02165687>

Goldin, A.S., Velten, R.J., Frishkorn, G.W., 1959. Determination of Radioactive Strontium. *Anal. Chem.* 31, 1490–1492. <https://doi.org/10.1021/ac60153a023>

Grahek, Ž., Dulanská, S., Karanović, G., Coha, I., Tucaković, I., Nodilo, M., Mátel, Ľ., 2018. Comparison of different methodologies for the ⁹⁰ Sr determination in environmental samples. *Journal of Environmental Radioactivity* 181, 18–31. <https://doi.org/10.1016/j.jenvrad.2017.10.012>

Grahek, Ž., Košutić, K., Rožmarić-Mačefat, M., 2006. Strontium isolation from natural samples with Sr resin and subsequent determination of ⁹⁰Sr. *J Radioanal Nucl Chem* 268, 179–190. <https://doi.org/10.1007/s10967-006-0152-3>

Grate, J.W., Strebini, R., Janata, J., Egorov, O., Ruzicka, J., 1996. Automated Analysis of Radionuclides in Nuclear Waste: Rapid Determination of ⁹⁰ Sr by Sequential Injection Analysis. *Analytical Chemistry* 68, 333–340. <https://doi.org/10.1021/ac950561m>

Gray, A.L., 1985. Solid sample introduction by laser ablation for inductively coupled plasma source mass spectrometry. *Analyst* 110, 551. <https://doi.org/10.1039/an9851000551>

Gu, B., Brown, G.M., Bonnesen, P.V., Liang, L., Moyer, B.A., Ober, R., Alexandratos, S.D., 2000. Development of Novel Bifunctional Anion-Exchange Resins with Improved

Selectivity for Pertechnetate Sorption from Contaminated Groundwater. *Environ. Sci. Technol.* 34, 1075–1080. <https://doi.org/10.1021/es990951g>

Guérin, N., Nadeau, K., Potvin, S., Hardy, J.-M., Larivière, D., 2013. Automated pressurized injection system for the separation of actinides by extraction chromatography. *J Radioanal Nucl Chem* 295, 1803–1811. <https://doi.org/10.1007/s10967-012-2102-6>

Habibi, A., Cariou, N., Boulet, B., Cossonnet, C., Gurriaran, R., Gleizes, M., Cote, G., Larivière, D., 2017. Automated chromatographic separation coupled on-line to ICP-MS measurements for the quantification of actinides and radiostrontium in soil samples. *Journal of Radioanalytical and Nuclear Chemistry* 314, 127–139. <https://doi.org/10.1007/s10967-017-5360-5>

Hamlin, A.G., Roberts, B.J., Loughlin, W., Walker, S.G., 1961. Separation of Uranium by Reversed-Phase Partition Chromatography on a Kel-F Column. *Anal. Chem.* 33, 1547–1552. <https://doi.org/10.1021/ac60179a027>

Hanrahan, G., 2012. Surface/Groundwater Quality and Monitoring, in: Key Concepts in Environmental Chemistry. Elsevier, pp. 109–152. <https://doi.org/10.1016/B978-0-12-374993-2.10004-4>

Harding, P., 2016. Uranium enrichment, in: Uranium for Nuclear Power. Elsevier, pp. 321–351. <https://doi.org/10.1016/B978-0-08-100307-7.00012-0>

Harms, A., Gilligan, C., 2010. Development of a neutron-activated concrete powder reference material. *Applied Radiation and Isotopes* 68, 1471–1476. <https://doi.org/10.1016/j.apradiso.2009.11.031>

Ho, Y.S., Ng, J.C.Y., McKay, G., 2000. Kinetics of Pollutant Sorption by Biosorbents: Review. *Separation and Purification Methods* 29, 189–232. <https://doi.org/10.1081/SPM-100100009>

Hohmann, B.P., Esselman, T.C., Wall, J.J., 2012. Irradiated Concrete in Nuclear Power Plants: Bridging the Gap in Operational Experience. International Atomic Energy Agency (IAEA).

Holmes, L., 2001. Determination of Thorium by ICP-MS and ICP-OES. *Radiation Protection Dosimetry* 97, 117–122. <https://doi.org/10.1093/oxfordjournals.rpd.a006647>

Horwitz, E.P., Bloomquist, C.A.A., 1974. High-Speed Radiochemical Separations by Liquid-Liquid Chromatography Using a CSP Support. II. Separation of Metal Ions Using Tricaprylmethylammonium Chloride on Zipax. *Journal of Chromatographic Science* 12, 200–205. <https://doi.org/10.1093/chromsci/12.4.200>

Horwitz, E.P., Chiarizia, R., Dietz, M.L., 1992a. A NOVEL STRONTIUM-SELECTIVE EXTRACTION CHROMATOGRAPHIC RESIN. *Solvent Extraction and Ion Exchange* 10, 313–336. <https://doi.org/10.1080/07366299208918107>

Horwitz, E.P., Chiarizia, R., Dietz, M.L., Diamond, H., Nelson, D.M., 1993. Separation and preconcentration of actinides from acidic media by extraction chromatography. *Analytica Chimica Acta* 281, 361–372. [https://doi.org/10.1016/0003-2670\(93\)85194-O](https://doi.org/10.1016/0003-2670(93)85194-O)

List of References

Horwitz, E.P., Dietz, M.L., Chiarizia, R., Diamond, H., Essling, A.M., Graczyk, D., 1992b. Separation and preconcentration of uranium from acidic media by extraction chromatography. *Analytica Chimica Acta* 266, 25–37. [https://doi.org/10.1016/0003-2670\(92\)85276-C](https://doi.org/10.1016/0003-2670(92)85276-C)

Horwitz, E.P., Dietz, M.L., Chiarizia, R., Diamond, H., Maxwell, S.L., Nelson, M.R., 1995. Separation and preconcentration of actinides by extraction chromatography using a supported liquid anion exchanger: application to the characterization of high-level nuclear waste solutions. *Analytica Chimica Acta* 310, 63–78. [https://doi.org/10.1016/0003-2670\(95\)00144-O](https://doi.org/10.1016/0003-2670(95)00144-O)

Horwitz, E.P., Dietz, M.L., Fisher, D.E., 1991. Separation and preconcentration of strontium from biological, environmental, and nuclear waste samples by extraction chromatography using a crown ether. *Analytical Chemistry* 63, 522–525.

Horwitz, E.P., Dietz, M.L., Nelson, D.M., LaRosa, J.J., Fairman, W.D., 1990. Concentration and separation of actinides from urine using a supported bifunctional organophosphorus extractant. *Analytica Chimica Acta* 238, 263–271. [https://doi.org/10.1016/S0003-2670\(00\)80546-2](https://doi.org/10.1016/S0003-2670(00)80546-2)

Horwitz, E.P., McAlister, D.R., Bond, A.H., Barrans, R.E., 2005. Novel Extraction of Chromatographic Resins Based on Tetraalkyldiglycolamides: Characterization and Potential Applications. *Solvent Extraction and Ion Exchange* 23, 319–344. <https://doi.org/10.1081/SEI-200049898>

Hou, X., 2007. Radiochemical analysis of radionuclides difficult to measure for waste characterization in decommissioning of nuclear facilities. *J Radioanal Nucl Chem* 273, 43–48. <https://doi.org/10.1007/s10967-007-0708-x>

Hou, X., Roos, P., 2008. Critical comparison of radiometric and mass spectrometric methods for the determination of radionuclides in environmental, biological and nuclear waste samples. *Analytica Chimica Acta* 608, 105–139. <https://doi.org/10.1016/j.aca.2007.12.012>

Hristovski, K.D., Markovski, J., 2017. Engineering metal (hydr)oxide sorbents for removal of arsenate and similar weak-acid oxyanion contaminants: A critical review with emphasis on factors governing sorption processes. *Science of The Total Environment* 598, 258–271. <https://doi.org/10.1016/j.scitotenv.2017.04.108>

Huang, W.J., Wang, M., Kondev, F.G., Audi, G., Naimi, S., 2021. The AME 2020 atomic mass evaluation (I). Evaluation of input data, and adjustment procedures*. *Chinese Phys. C* 45, 030002. <https://doi.org/10.1088/1674-1137/abddb0>

Huff, E.A., 1965. Trace Impurity Analysis of Thorium-Uranium and Plutonium-Thorium-Uranium Alloys by Anion Exchange-Partition Chromatography. *Anal. Chem.* 37, 533–536. <https://doi.org/10.1021/ac60223a023>

Hurtado-Bermudez, S., Mas, J.L., Villa-Alfageme, M., 2017. A sequential determination of 90 Sr and 210 Po in food samples. *Food Chemistry* 229, 159–164. <https://doi.org/10.1016/j.foodchem.2017.02.077>

Hurtgen, C., Jerome, S., Woods, M., 2000. Revisiting Currie — how low can you go? *Applied Radiation and Isotopes* 53, 45–50. [https://doi.org/10.1016/S0969-8043\(00\)00171-8](https://doi.org/10.1016/S0969-8043(00)00171-8)

IAEA, 2011. Focus on Low and Intermediate Level Waste. International Atomic Energy Agency, Vienna, Austria.

IAEA, 2001. The International Nuclear Event Scale (INES) User's Manual 2001 Edition.

IAEA PRIS, 2019. PRIS - Reactor status reports - Permanent Shutdown - By Country [WWW Document]. URL <https://pris.iaea.org/PRIS/WorldStatistics/ShutdownReactorsByCountry.aspx> (accessed 6.22.19).

International Atomic Energy Agency, 2021. Lesson 8: Gamma and Alpha Spectrometry for Workplace Monitoring.

International Atomic Energy Agency, 2017. Application of the Concepts of Exclusion, Exemption and Clearance [WWW Document]. URL <https://www.iaea.org/publications/7118/application-of-the-concepts-of-exclusion-exemption-and-clearance> (accessed 9.22.21).

International Atomic Energy Agency, 2012. Monitoring for compliance with exemption and clearance levels. IAEA, Vienna.

International Atomic Energy Agency, 2009. Determination and use of scaling factors for waste characterization in nuclear power plants. International Atomic Energy Agency, Vienna.

International Atomic Energy Agency, 2007. Strategy and methodology for radioactive waste characterization. International Atomic Energy Agency, Vienna.

International Atomic Energy Agency, 2004. Application of the concepts of exclusion, exemption and clearance (No. No. RS-G-1.7). International Atomic Energy Agency.

International Atomic Energy Agency (Ed.), 2000. Organization and management for decommissioning of large nuclear facilities, Technical reports series. International Atomic Energy Agency, Vienna.

International Atomic Energy Agency (Ed.), 1989. Measurement of radionuclides in food and the environment: a guidebook, Technical reports series / International Atomic Energy Agency. Internat. Atomic Energy Agency, Vienna.

Internationale Atomenergie-Organisation (Ed.), 2005. Derivation of activity concentration values for exclusion, exemption and clearance, Safety reports series. Vienna.

ISO Technical Committee: Nuclear installations, processes and technologies, 2007. ISO 21238:2007 [WWW Document]. ISO. URL <https://www.iso.org/cms/render/live/en/sites/isoorg/contents/data/standard/04/00/40081.html> (accessed 10.18.21).

List of References

Jäggi, M.E., Rüthi, M., Eikenberg, J., 2019. Fusion and chemical separation of Am, Pu and Sr from barite-concrete. *J Radioanal Nucl Chem* 322, 1279–1285.
<https://doi.org/10.1007/s10967-019-06854-6>

Jia, G., Testa, C., Desideri, D., Meli, M.A., 1989. Extraction-chromatographic method for the determination of plutonium-239,240 and plutonium-238 in soils with high natural radioactivity. *Analytica Chimica Acta* 220, 103–110.
[https://doi.org/10.1016/S0003-2670\(00\)80254-8](https://doi.org/10.1016/S0003-2670(00)80254-8)

Johansson, M.L.Y., 2008. Determination of Pb-210 and Po-210 in aqueous environmental samples. Hannover.

Joyce, M., 2018. The Actinides and Related Isotopes, in: Nuclear Engineering. Elsevier, pp. 87–110. <https://doi.org/10.1016/B978-0-08-100962-8.00005-6>

Kashiwagi, M., Masui, H., Denda, Y., James, D., Lante's, B., Müller, W., Garamszeghy, M., Leganes, J.L., Maxeiner, H., van Velzen, L., 2007. ISO Standardization of the Scaling Factor Method for Low- and Intermediate Level Radioactive Wastes Generated at Nuclear Power Plants, in: 11th International Conference on Environmental Remediation and Radioactive Waste Management, Parts A and B. Presented at the The 11th International Conference on Environmental Remediation and Radioactive Waste Management, ASMEDC, Bruges, Belgium, pp. 625–629.
<https://doi.org/10.1115/ICEM2007-7015>

Kim, H., Chung, K.H., Jung, Y., Jang, M., Kang, M. ja, Choi, G.-S., 2015. A rapid and efficient automated method for the sequential separation of plutonium and radiostrontium in seawater. *Journal of Radioanalytical and Nuclear Chemistry* 304, 321–327.
<https://doi.org/10.1007/s10967-014-3595-y>

Kim, H., Lim, J.M., Jung, Y., Chung, K.H., 2017. Determination of 90Sr and 99Tc from concrete and soil. *Korean Nuclear Society, Transactions of the Korean Nuclear Society Autumn Meeting*.

Kimura, T., Iwashima, K., Ishimori, T., Hamaguchi, H., 1977. Separation of Strontium Ion from a Large Amount of Calcium Ion by the use of a Macroyclic Ether. *Chemistry Letters* 6, 563–564. <https://doi.org/10.1246/cl.1977.563>

Kimura, Toshimasa., Iwashima, Kiyoshi., Ishimori, Tatsujiro., Hamada, Tatsuji., 1979. Separation of strontium-89 and -90 from calcium in milk with a macrocyclic ether. *Analytical Chemistry* 51, 1113–1116. <https://doi.org/10.1021/ac50044a005>

Kirk, R.E., Othmer, D.F., Grayson, M., Eckroth, D. (Eds.), 1978. *Encyclopedia of chemical technology*, 3rd ed. Wiley, New York.

Kołacińska, K., Chajduk, E., Dudek, J., Samczyński, Z., Łokas, E., Bojanowska-Czajka, A., Trojanowicz, M., 2017. Automation of sample processing for ICP-MS determination of 90 Sr radionuclide at ppq level for nuclear technology and environmental purposes. *Talanta* 169, 216–226.
<https://doi.org/10.1016/j.talanta.2016.10.051>

Kondev, F.G., Wang, M., Huang, W.J., Naimi, S., Audi, G., 2021. The NUBASE2020 evaluation of nuclear physics properties *. *Chinese Phys. C* 45, 030001.
<https://doi.org/10.1088/1674-1137/abddae>

Koning, A., OECD Nuclear Energy Agency, 2006. The JEFF-3.1 nuclear data library: JEFF report 21.

Kooi, Jacob., 1958. Quantitative Determination of Strontium-89 and Strontium-90 in Water. *Analytical Chemistry* 30, 532–535. <https://doi.org/10.1021/ac60136a025>

Korkisch, Johann., Tera, Fouad., 1961. Separation of Thorium by Anion Exchange. *Analytical Chemistry* 33, 1264–1266. <https://doi.org/10.1021/ac60177a041>

Kramar, U., 2017. X-Ray Fluorescence Spectrometers ☆, in: *Encyclopedia of Spectroscopy and Spectrometry*. Elsevier, pp. 695–706. <https://doi.org/10.1016/B978-0-12-409547-2.05068-X>

Kunin, R., Myers, R.J., 1949. Exchange equilibria in anion-exchange resins: porous exchangers. *Discuss. Faraday Soc.* 7, 114. <https://doi.org/10.1039/df9490700114>

Lagergren, S., 1907. Zur Theorie der sogenannten Adsorption gelöster Stoffe. *Zeitschr f Chem und Ind der Kolloide* 2, 15–15. <https://doi.org/10.1007/BF01501332>

L'Annunziata, M.F., 2003. Cherenkov Counting, in: *Handbook of Radioactivity Analysis*. Elsevier, pp. 719–797. <https://doi.org/10.1016/B978-012436603-9/50014-4>

LaRosa, J.J., Cooper, E.L., Ghods-Espahani, A., Jansta, V., Makarewicz, M., Shawky, S., Vajda, N., 1992. Radiochemical methods used by the IAEA's laboratories at Seibersdorf for the determination of 90Sr, 144Ce and Pu radionuclides in environmental samples collected for the International Chernobyl project. *Journal of Environmental Radioactivity* 17, 183–209. [https://doi.org/10.1016/0265-931X\(92\)90025-O](https://doi.org/10.1016/0265-931X(92)90025-O)

Larsen, R.P., Oldham, R.D., 1975. Anion-exchange separation of plutonium in hydrochloric-hydrobromic acid media. *Talanta* 22, 577–580. [https://doi.org/10.1016/0039-9140\(75\)80025-7](https://doi.org/10.1016/0039-9140(75)80025-7)

Lee, Y.K., Bakhtiar, S.N., Akbarzadeh, M., Lee, J.S., 2000. Sequential isotopic determination of strontium, thorium, plutonium, uranium, and americium in bioassay samples. *Journal of Radioanalytical and Nuclear Chemistry* 243, 525–533. <https://doi.org/10.1023/A:1016019307857>

Li, S., Wang, X.-C., Li, C.-F., Wilde, S.A., Zhang, Youyu, Golding, S.D., Liu, K., Zhang, Yuxiang, 2019. Direct Rubidium-Strontium Dating of Hydrocarbon Charge Using Small Authigenic Illitic Clay Aliquots from the Silurian Bituminous Sandstone in the Tarim Basin, NW China. *Sci Rep* 9, 12565. <https://doi.org/10.1038/s41598-019-48988-3>

Li, T.K., Kitagawa, O., Kuno, Y., Kurosawa, A., 1995. Feasibility study of plutonium and uranium measurements in input dissolver solutions (No. LA-UR-95-3380; CONF-950923-11). Los Alamos National Lab. (LANL), Los Alamos, NM (United States).

Li, W., Liu, X., Godfrey, L.V., 2019. Optimisation of Lithium Chromatography for Isotopic Analysis in Geological Reference Materials by MC - ICP - MS. *Geostand Geoanal Res* 43, 261–276. <https://doi.org/10.1111/ggr.12254>

Litaiem, Y., Dhahbi, M., 2015. Physicochemical Properties of an Hydrophobic Ionic Liquid (Aliquat 336) in a Polar Protic Solvent (Formamide) at Different Temperatures.

List of References

Journal of Dispersion Science and Technology 36, 641–651.
<https://doi.org/10.1080/01932691.2013.862170>

Longbottom, J.E., Martin, T.D., Edgell, K.W., Long, S.E., Plantz, M.R., Warden, B.E., 1994. Determination of Trace Elements in Water by Inductively Coupled Plasma–Mass Spectrometry: Collaborative Study. *Journal of AOAC INTERNATIONAL* 77, 1004–1023. <https://doi.org/10.1093/jaoac/77.4.1004>

Martin, A.J.P., Synge, R.L.M., 1941. A new form of chromatogram employing two liquid phases. *Biochemical Journal* 35, 1358–1368. <https://doi.org/10.1042/bj0351358>

Martin, V., 2021. DUKES chapter 5: statistics on electricity from generation through to sales, *Digest of UK Energy Statistics (DUKES)*. Department for Business, Energy & Industrial Strategy, UK.

Mason, G.W., Griffin, H.E., 1980. Demonstration of the Potential for Designing Extractants with Preselected Extraction Properties: Possible Application to Reactor Fuel Reprocessing, in: Navratil, J.D., Schulz, W.W. (Eds.), *Actinide Separations, ACS Symposium Series*. AMERICAN CHEMICAL SOCIETY, WASHINGTON, D. C.
<https://doi.org/10.1021/bk-1980-0117>

Mateos, J.J., Gómez, E., Garcias, F., Casas, M., Cerdà, V., 2000. Rapid determination in water samples using a sequential injection method. *Applied Radiation and Isotopes* 53, 139–144. [https://doi.org/10.1016/S0969-8043\(00\)00125-1](https://doi.org/10.1016/S0969-8043(00)00125-1)

Maxwell, I.I.I., Nichols, S., 1998. Actinide Recovery Method for Large Soil Samples (No. WSRC-MS-98-00647; CONF-981133-). Savannah River Site (SRS), Aiken, SC (United States).

Maxwell III, S.L., Culligan, B.K., 2006. Rapid column extraction method for actinides in soil. *J Radioanal Nucl Chem* 270, 699–704. <https://doi.org/10.1007/s10967-006-0449-2>

Maxwell, S.L., Culligan, B., Hutchison, J.B., Utsey, R.C., Sudowe, R., McAlister, D.R., 2017. Rapid method to determine 89/90Sr in steel samples. *Journal of Radioanalytical and Nuclear Chemistry* 314, 439–450. <https://doi.org/10.1007/s10967-017-5402-z>

Maxwell, S.L., Culligan, B., Hutchison, J.B., Utsey, R.C., Sudowe, R., McAlister, D.R., 2016. Rapid method to determine 89Sr/90Sr in large concrete samples. *Journal of Radioanalytical and Nuclear Chemistry* 310, 399–411.
<https://doi.org/10.1007/s10967-016-4787-4>

Maxwell, S.L., Culligan, B.K., Hutchison, J.B., Utsey, R.C., McAlister, D.R., 2014. Rapid determination of actinides in seawater samples. *J Radioanal Nucl Chem* 300, 1175–1189. <https://doi.org/10.1007/s10967-014-3079-0>

Maxwell, S.L., Culligan, B.K., Kelsey-Wall, A., Shaw, P.J., 2011a. Rapid radiochemical method for determination of actinides in emergency concrete and brick samples. *Analytica Chimica Acta* 701, 112–118. <https://doi.org/10.1016/j.aca.2011.06.011>

Maxwell, S.L., Culligan, B.K., Noyes, G.W., 2011b. Rapid separation method for ^{237}Np and Pu isotopes in large soil samples. *Applied Radiation and Isotopes* 69, 917–923.
<https://doi.org/10.1016/j.apradiso.2011.01.021>

Maxwell, S.L., Culligan, B.K., Noyes, G.W., 2010. Rapid separation of actinides and radiostrontium in vegetation samples. *J Radioanal Nucl Chem* 286, 273–282. <https://doi.org/10.1007/s10967-010-0653-y>

Maxwell, S.L., Hutchison, J.B., McAlister, D.R., 2015. Rapid fusion method for the determination of refractory thorium and uranium isotopes in soil samples. *J Radioanal Nucl Chem* 305, 631–641. <https://doi.org/10.1007/s10967-015-3972-1>

Mcburney, C.H., 1952. Resinous insoluble reaction products of tertiary amines with haloalkylated vinyl aromatic hydrocarbon copolymers. *US2591573A*.

Metzger, S.C., Rogers, K.T., Bostick, D.A., McBay, E.H., Ticknor, B.W., Manard, B.T., Hexel, C.R., 2019. Optimization of uranium and plutonium separations using TEVA and UTEVA cartridges for MC-ICP-MS analysis of environmental swipe samples. *Talanta* 198, 257–262. <https://doi.org/10.1016/j.talanta.2019.02.034>

Mirion Technologies, 2021. Gamma-Ray Absorption in Matter (Basic) [WWW Document]. URL <https://www.mirion.com/learning-center/lab-experiments/gamma-ray-absorption-in-matter-basic> (accessed 11.5.21).

Misra, S., Froelich, P.N., 2009. Measurement of lithium isotope ratios by quadrupole-ICP-MS: application to seawater and natural carbonates. *J. Anal. At. Spectrom.* 24, 1524. <https://doi.org/10.1039/b907122a>

Mitra, S. (Ed.), 2003. Sample preparation techniques in analytical chemistry, Chemical analysis. J. Wiley, Hoboken, N.J.

Moeller, T., Bailar, J.C., Kleinberg, J., Guss, C.O., Castellion, M.E., Metz, C., 1980. CHEMICAL KINETICS, in: Chemistry. Elsevier, pp. 420–443. <https://doi.org/10.1016/B978-0-12-503350-3.50020-2>

Mohite, B., Khopkar, S., 1987. Solvent extraction separation of strontium as 18-crown-6 complex with picrate ion. *Analytical Chemistry* 59, 1200–1203.

Nakai, S., Halliday, A.N., Kesler, S.E., Jones, H.D., Kyle, J.R., Lane, T.E., 1993. Rb-Sr dating of sphalerites from Mississippi Valley-type (MVT) ore deposits. *Geochimica et Cosmochimica Acta* 57, 417–427. [https://doi.org/10.1016/0016-7037\(93\)90440-8](https://doi.org/10.1016/0016-7037(93)90440-8)

National Research Council (US), 1999. Natural Radioactivity and Radiation, Evaluation of Guidelines for Exposures to Technologically Enhanced Naturally Occurring Radioactive Materials. National Academies Press (US).

Naushad, Mu., ALOthman, Z.A., Khan, M.R., Wabaidur, S.M., 2013. Removal of Bromate from Water Using De-Acidite FF-IP Resin and Determination by Ultra-Performance Liquid Chromatography-Tandem Mass Spectrometry. *Clean Soil Air Water* 41, 528–533. <https://doi.org/10.1002/clen.201200461>

Navratil, J.D., 1978. Evaluation of anion exchange resins for plutonium-uranium separations in nitric acid. *J. Radioanal. Chem.* 43, 31–35. <https://doi.org/10.1007/BF02519438>

List of References

Nebel, O., 2014. Rb–Sr Dating, in: Rink, W.J., Thompson, J. (Eds.), *Encyclopedia of Scientific Dating Methods*. Springer Netherlands, Dordrecht, pp. 1–19. https://doi.org/10.1007/978-94-007-6326-5_116-1

Nicoud, R.-M., 2015. *Chromatographic Processes: Modeling, Simulation, and Design*. Cambridge University Press.

Normand, C., Pfennig, G., Magill, J., Dreher, R., 2009. Mapping the nuclear landscape: 50 years of the Karlsruher Nuklidkarte. *J Radioanal Nucl Chem* 282, 395–400. <https://doi.org/10.1007/s10967-009-0334-x>

Noshkin, V.E., Mott, N.S., 1967. Separation of strontium from large amounts of calcium, with application to radiostrontium analysis. *Talanta* 14, 45–51. [https://doi.org/10.1016/0039-9140\(67\)80045-6](https://doi.org/10.1016/0039-9140(67)80045-6)

Nuclear Decommissioning Authority, 2021. NDA Annual Report and Accounts 2020 to 2021. Nuclear Decommissioning authority, UK.

Nuclear Decommissioning Authority, 2017. Nuclear Provision: the cost of cleaning up Britain's historic nuclear sites - GOV.UK.

Nuclear Decommissioning Authority, 2016. Strategy: effective from April 2016.

O'Donnell, R.G., Mitchell, P.I., Priest, N.D., Strange, L., Fox, A., Henshaw, D.L., Long, S.C., 1997. Variations in the concentration of plutonium, strontium-90 and total alpha-emitters in human teeth collected within the British Isles. *Science of The Total Environment* 201, 235–243. [https://doi.org/10.1016/S0048-9697\(97\)84060-0](https://doi.org/10.1016/S0048-9697(97)84060-0)

O'Hara, M.J., Burge, S.R., Grate, J.W., 2009. Automated Radioanalytical System for the Determination of Sr-90 in Environmental Water Samples by Y-90 Cherenkov Radiation Counting. *Analytical Chemistry* 81, 1228–1237. <https://doi.org/10.1021/ac8021407>

Parry, S.A., O'Brien, L., Fellerman, A.S., Eaves, C.J., Milestone, N.B., Bryan, N.D., Livens, F.R., 2011. Plutonium behaviour in nuclear fuel storage pond effluents. *Energy & Environmental Science* 4, 1457. <https://doi.org/10.1039/c0ee00390e>

Parsa, B., 1992. A sequential radiochemical procedure for isotopic analysis of uranium and thorium in soil. *Journal of Radioanalytical and Nuclear Chemistry, Articles* 157, 65–73. <https://doi.org/10.1007/BF02039778>

Pin, C., Bassin, C., 1992. Evaluation of a strontium-specific extraction chromatographic method for isotopic analysis in geological materials. *Analytica Chimica Acta* 269, 249–255. [https://doi.org/10.1016/0003-2670\(92\)85409-Y](https://doi.org/10.1016/0003-2670(92)85409-Y)

Poole, C.F., 2000. Chromatography, in: *Encyclopedia of Separation Science*. Elsevier, pp. 40–64. <https://doi.org/10.1016/B0-12-226770-2/00021-1>

Porter, C.R., Kahn, Bernd., 1964. Improved Determination of Strontium-90 in Milk by an Ion Exchange Method. *Analytical Chemistry* 36, 676–678. <https://doi.org/10.1021/ac60209a032>

Porter, C.Richard., Kahn, Bernd., Carter, M.Whitehead., Rehnberg, G.L., Pepper, E.W., 1967. Determination of radiostrontium in food and other environmental samples. *Environmental Science & Technology* 1, 745–750. <https://doi.org/10.1021/es60009a003>

Qiao, J., 2011. Rapid and automated determination of plutonium and neptunium in environmental samples.

Qiao, J., Hou, X., Miró, M., Roos, P., 2009. Determination of plutonium isotopes in waters and environmental solids: A review. *Analytica Chimica Acta* 652, 66–84. <https://doi.org/10.1016/j.aca.2009.03.010>

Reading, D.G., Croudace, I.W., Warwick, P.E., 2017. Fusion Bead Procedure for Nuclear Forensics Employing Synthetic Enstatite to Dissolve Uraniferous and Other Challenging Materials Prior to Laser Ablation Inductively Coupled Plasma Mass Spectrometry. *Anal. Chem.* 89, 6006–6014. <https://doi.org/10.1021/acs.analchem.7b00558>

Reichardt, K., Bacchi, O.O.S., 2005. Isotopes in Soil and Plant Investigations, in: *Encyclopedia of Soils in the Environment*. Elsevier, pp. 280–284. <https://doi.org/10.1016/B0-12-348530-4/00101-6>

Roberts, J., 2017. UK Nuclear Workforce Demand.

Rodriguez, Y.R., 2014. Plutonium, in: *Encyclopedia of Toxicology*. Elsevier, pp. 982–985. <https://doi.org/10.1016/B978-0-12-386454-3.00049-X>

Rožmarić, M., Ivšić, A.G., Grahek, Ž., 2009. Determination of uranium and thorium in complex samples using chromatographic separation, ICP-MS and spectrophotometric detection. *Talanta* 80, 352–362. <https://doi.org/10.1016/j.talanta.2009.06.078>

Russell, B., García-Miranda, M., Ivanov, P., 2017. Development of an optimised method for analysis of 90 Sr in decommissioning wastes by triple quadrupole inductively coupled plasma mass spectrometry. *Applied Radiation and Isotopes* 126, 35–39. <https://doi.org/10.1016/j.apradiso.2017.01.025>

Russell, W.A., Papanastassiou, D.A., 1978. Calcium isotope fractionation in ion-exchange chromatography. *Anal. Chem.* 50, 1151–1154. <https://doi.org/10.1021/ac50030a036>

Ryan, J.L., Wheelwright, E.J., 1959. Recovery and Purification of Plutonium by Anion Exchange. *Ind. Eng. Chem.* 51, 60–65. <https://doi.org/10.1021/ie50589a038>

Sadi, B.B., Rinaldo, C., Spencer, N., Li, C., 2018. An ion chromatographic separation method for the sequential determination of 90Sr, 241Am and Pu isotopes in a urine sample. *Journal of Radioanalytical and Nuclear Chemistry* 316, 179–189. <https://doi.org/10.1007/s10967-018-5758-8>

Sáez-Muñoz, M., Ortiz, J., Martorell, S., Gómez-Arozamena, J., Cearreta, A., 2020. Sequential determination of uranium and plutonium in soil and sediment samples by borate salts fusion. *J Radioanal Nucl Chem* 323, 1167–1177. <https://doi.org/10.1007/s10967-020-07028-5>

List of References

Sahoo, T.R., Prelot, B., 2020. Adsorption processes for the removal of contaminants from wastewater, in: Nanomaterials for the Detection and Removal of Wastewater Pollutants. Elsevier, pp. 161–222. <https://doi.org/10.1016/B978-0-12-818489-9.00007-4>

Saito, N., 1984. Selected data on ion exchange separations in radioanalytical chemistry. *Pure and Applied Chemistry* 56, 523–539. <https://doi.org/10.1351/pac198456040523>

Schneider, J., Melcher, F., Brauns, M., 2007. Concordant ages for the giant Kipushi base metal deposit (DR Congo) from direct Rb–Sr and Re–Os dating of sulfides. *Miner Deposita* 42, 791–797. <https://doi.org/10.1007/s00126-007-0158-y>

Schramel, P., Wendler, I., Roth, P., Werner, E., 1997. Method for the determination of thorium and uranium in urine by ICP-MS. *Mikrochim Acta* 126, 263–266. <https://doi.org/10.1007/BF01242331>

Schubert, J., Nachod, F.C., 1956. Ion Exchange Technology: Introduction, in: Ion Exchange Technology. Elsevier, pp. 1–6. <https://doi.org/10.1016/B978-1-4832-3202-7.50005-5>

Shannon, R.D., 1976. Revised effective ionic radii and systematic studies of interatomic distances in halides and chalcogenides. *Acta Crystallographica Section A* 32, 751–767. <https://doi.org/10.1107/S0567739476001551>

Shi, Y., Collins, R., Broome, C., 2013. Determination of uranium, thorium and plutonium isotopes by ICP-MS. *J Radioanal Nucl Chem* 296, 509–515. <https://doi.org/10.1007/s10967-012-2128-9>

Shin, K.-Y., Kim, S.-B., Kim, J.-H., Chung, M., Jung, P.-S., 2002. Thermo-physical properties and transient heat transfer of concrete at elevated temperatures. *Nuclear Engineering and Design* 212, 233–241. [https://doi.org/10.1016/S0029-5493\(01\)00487-3](https://doi.org/10.1016/S0029-5493(01)00487-3)

Sill, C.W., Puphal, K.W., Hindman, F.D., 1974. Simultaneous Determination of Alpha-Emitting Nuclides of Radium through Californium in Soil. *Analytical Chemistry* 46, 1725.

Sillanpää, M., Shestakova, M., 2017. Emerging and Combined Electrochemical Methods, in: Electrochemical Water Treatment Methods. Elsevier, pp. 131–225. <https://doi.org/10.1016/B978-0-12-811462-9.00003-7>

Smith, D.H., Turner, M.L., McBay, E.H., Lewis, B.E., Hobson, D.E., Ehinger, M.H., 1995. Independent verification of reprocessing input and process volumes. Progress report (No. ORNL/TM-12979). Oak Ridge National Lab. (ORNL), Oak Ridge, TN (United States). <https://doi.org/10.2172/90206>

Smith, L.L., Crain, J.S., Yaeger, J.S., Horwitz, E.P., Diamond, H., Chiarizia, R., 1995. Improved separation method for determining actinides in soil samples. *Journal of Radioanalytical and Nuclear Chemistry Articles* 194, 151–156. <https://doi.org/10.1007/BF02037621>

Smułek, W., Łada, W.A., 1979. Separation of alkali and alkaline earth metals by polyethers using extraction chromatography. Effect of diluent. *Journal of Radioanalytical Chemistry* 50, 169–178. <https://doi.org/10.1007/BF02519954>

Sober, H.A., Peterson, E.A., 1954. CHROMATOGRAPHY OF PROTEINS ON CELLULOSE ION-EXCHANGERS. *J. Am. Chem. Soc.* 76, 1711–1712. <https://doi.org/10.1021/ja01635a087>

Solatie, D., Carbol, P., Hrnecek, E., Jaakkola, T., Betti, M., 2002. Sample preparation methods for the determination of plutonium and strontium in environmental samples by low level liquid scintillation counting and α -spectrometry. *Radiochimica Acta* 90, 447–454. https://doi.org/10.1524/ract.2002.90.8_2002.447

Somogyi, Á., 2008. Mass spectrometry instrumentation and techniques, in: *Medical Applications of Mass Spectrometry*. Elsevier, pp. 93–140. <https://doi.org/10.1016/B978-044451980-1.50008-2>

Sonoda, A., Makita, Y., Hirotsu, T., 2008. Boron Isotope Fractionation in Column Chromatography with Glucamine Type Fibers. *Journal of Nuclear Science and Technology* 45, 117–121. <https://doi.org/10.1080/00223131.2008.10875991>

Stauffer, E., Dolan, J.A., Newman, R., 2008. Gas Chromatography and Gas Chromatography—Mass Spectrometry, in: *Fire Debris Analysis*. Elsevier, pp. 235–293. <https://doi.org/10.1016/B978-012663971-1.50012-9>

Suran, J., Kovar, P., Smoldasova, J., Solc, J., Van Ammel, R., Garcia Miranda, M., Russell, B., Arnold, D., Zapata-García, D., Boden, S., Rogiers, B., Sand, J., Peräjärvi, K., Holm, P., Hay, B., Failleau, G., Plumeri, S., Laurent Beck, Y., Grisa, T., 2018. Metrology for decommissioning nuclear facilities: Partial outcomes of joint research project within the European Metrology Research Program. *Applied Radiation and Isotopes* 134, 351–357. <https://doi.org/10.1016/j.apradiso.2017.08.032>

Surman, J.J., Pates, J.M., Zhang, H., Happel, S., 2014. Development and characterisation of a new Sr selective resin for the rapid determination of 90Sr in environmental water samples. *Talanta* 129, 623–628. <https://doi.org/10.1016/j.talanta.2014.06.041>

Suslova, K.G., Romanov, S.A., Efimov, A.V., Sokolova, A.B., S涅ve, M., Smith, G., 2015. Dynamics of body burdens and doses due to internal irradiation from intakes of long-lived radionuclides by residents of Ozyorsk situated near Mayak PA. *J. Radiol. Prot.* 35, 789–818. <https://doi.org/10.1088/0952-4746/35/4/789>

Suzuki, N., Fukaya, T., Imura, H., 1987. Substoichiometric isotope-dilution analysis for strontium by liquid-liquid extraction with a macrocyclic crown ether or cryptand. *Analytica Chimica Acta* 194, 261–268. [https://doi.org/10.1016/S0003-2670\(00\)84778-9](https://doi.org/10.1016/S0003-2670(00)84778-9)

Takács, M.P., Kossert, K., Nähle, O.J., 2019. Standardisation of 85Sr with digital anticoincidence counting and half-life determination of the 514 keV level of 85Rb. *Applied Radiation and Isotopes* 153, 108799. <https://doi.org/10.1016/j.apradiso.2019.07.004>

List of References

Takagai, Y., Furukawa, M., Kameo, Y., Suzuki, K., 2014. Sequential inductively coupled plasma quadrupole mass-spectrometric quantification of radioactive strontium-90 incorporating cascade separation steps for radioactive contamination rapid survey. *Anal. Methods* 6, 355–362. <https://doi.org/10.1039/C3AY41067F>

Talvitie, N.A., 1972. Electrodeposition of actinides for alpha spectrometric determination. *Anal. Chem.* 44, 280–283. <https://doi.org/10.1021/ac60310a013>

Talvitie, N.A., Demint, R.J., 1965. Radiochemical Determination of Strontium-90 in Water Using Ion Exchange. *Analytical Chemistry* 37, 1605–1607. <https://doi.org/10.1021/ac60231a050>

Taylor, V.F., Evans, R.D., Cornett, R.J., 2006. Determination of 90Sr in contaminated environmental samples by tuneable bandpass dynamic reaction cell ICP–MS. *Analytical and Bioanalytical Chemistry* 387, 343–350. <https://doi.org/10.1007/s00216-006-0938-8>

Thakur, P., 2017. Radiochemical Methods | Food and Environmental Applications ☆, in: Reference Module in Chemistry, Molecular Sciences and Chemical Engineering. Elsevier, p. B9780124095472142000. <https://doi.org/10.1016/B978-0-12-409547-2.14223-4>

Thomas, R., 2004. Practical guide to ICP-MS, Practical spectroscopy. M. Dekker, New York, NY.

Thompson, H.S., 1850. On the Absorbent Power of Soils. *Journal of the Royal Agricultural Society of England* 68.

Tooper, E.B., Wirth, L.F., 1956. Ion Exchange Technology: Elsevier.

Triskem International, 2022. Ni Resin Product Sheet.

Triskem International, 2021a. Extraction Chromatography Technical Documentation - All Resins.

Triskem International, 2021b. TK221 Resin Product Sheet.

Triskem International, 2019a. Analytical Procedure: Americium, Neptunium, Plutonium, Thorium, Curium, and Uranium in Water.

Triskem International, 2019b. Analytical Procedure: Americium, Neptunium, Plutonium, Thorium, Curium, Uranium and Strontium in Water.

Triskem International, 2015a. Sr Resin Product Sheet.

Triskem International, 2015b. TK100 Resin Product Sheet.

Triskem International, 2015c. Product Sheet DGA Resin.

Triskem International, 2014. Analytical Procedure: Radium-226/228 in Water.

Trojanowicz, M., Kołacińska, K., 2016. Recent advances in flow injection analysis. *Analyst* 141, 2085–2139. <https://doi.org/10.1039/C5AN02522B>

Tumey, S.J., Brown, T.A., Hamilton, T.E., Hillegonds, D.J., 2008. Accelerator mass spectrometry of strontium-90 for homeland security, environmental monitoring and human health. *Nuclear Instruments and Methods in Physics Research Section B: Beam Interactions with Materials and Atoms* 266, 2242–2245. <https://doi.org/10.1016/j.nimb.2008.03.088>

U.S. Environmental Protection Agency, 2014. Rapid Method for Sodium Hydroxide Fusion of Concrete and Brick Matrices Prior to Americium, Plutonium, Strontium, Radium, and Uranium Analyses for Environmental Remediation Following Radiological Incidents (No. EPA 402-R-14-004).

Vajda, N., 2021. Rapid Determination of Actinides in Water Samples Using TEVA and TK221 Resin Cartridges.

Vajda, N., Kim, C.-K., 2010. Determination of radiostrontium isotopes: A review of analytical methodology. *Applied Radiation and Isotopes* 68, 2306–2326. <https://doi.org/10.1016/j.apradiso.2010.05.013>

Vesterlund, A., Tovedal, A., Nygren, U., Ramebäck, H., 2009. Uncertainty assessment of methods for chemical yield determination in measurement of radioactive strontium. *J Radioanal Nucl Chem* 282, 951–955. <https://doi.org/10.1007/s10967-009-0184-6>

Vitkus, T.J., King, D.A., Altic, N.A., Ivey, W.P., 2021. Instrumentation and Practices for Radiological Assessments, in: *Encyclopedia of Nuclear Energy*. Elsevier, pp. 803–827. <https://doi.org/10.1016/B978-0-12-819725-7.00090-8>

Wai, C.M., Du, H., 1990. Separation of yttrium-90 and strontium-90 on papers impregnated with ionizable crown ethers. *Analytical Chemistry* 62, 2412–2414.

Wallace, S.H., Shaw, S., Morris, K., Small, J.S., Fuller, A.J., Burke, I.T., 2012. Effect of groundwater pH and ionic strength on strontium sorption in aquifer sediments: Implications for ⁹⁰Sr mobility at contaminated nuclear sites. *Applied Geochemistry* 27, 1482–1491. <https://doi.org/10.1016/j.apgeochem.2012.04.007>

Wang, Z., Wen, W., Quan, W., Du, L., Wang, P., Lin, J., Xie, Y., Tan, Z., 2018. Rapid determination of Pu isotopes for decommission concrete samples by inductively coupled plasma mass spectrometry. *J Radioanal Nucl Chem* 316, 411–417. <https://doi.org/10.1007/s10967-018-5756-x>

Warf, J.C., 1949. Extraction of Cerium(IV) Nitrate by Butyl Phosphate. *J. Am. Chem. Soc.* 71, 3257–3258. <https://doi.org/10.1021/ja01177a528>

Warshawsky, A., Patchornik, A., 1978. Impregnated Resins: Metal-Ion Complexing Agents Incorporated Physically In Polymeric Matrices. *Isr. J. Chem.* 17, 307–315. <https://doi.org/10.1002/ijch.197800056>

Warwick, P.E., Croudace, I.W., Dale, A.A., 1999. An optimised and robust method for the determination of uranium and plutonium in aqueous samples. *Applied Radiation and Isotopes* 50, 579–583. [https://doi.org/10.1016/S0969-8043\(98\)00064-5](https://doi.org/10.1016/S0969-8043(98)00064-5)

Warwick, P.E., Croudace, I.W., Hillegonds, D.J., 2009. Effective Determination of the Long-lived Nuclide ⁴¹Ca in Nuclear Reactor Bioshield Concretes: Comparison of Liquid

List of References

Scintillation Counting and Accelerator Mass Spectrometry. *Analytical Chemistry* 81, 1901–1906. <https://doi.org/10.1021/ac802225a>

Warwick, P.E., Russell, B.C., Croudace, I.W., Zacharauskas, Ž., 2019. Evaluation of inductively coupled plasma tandem mass spectrometry for radionuclide assay in nuclear waste characterisation. *J. Anal. At. Spectrom.* 34, 1810–1821. <https://doi.org/10.1039/C8JA00411K>

Way, J.T., 1850. On the power of soils to absorb manure. *Journal of the Royal Agricultural Society of England* 313.

Webb, G.A.M., Anderson, R.W., Gaffney, M.J.S., 2006. Classification of events with an off-site radiological impact at the Sellafield site between 1950 and 2000, using the International Nuclear Event Scale. *Journal of Radiological Protection* 26, 33–49. <https://doi.org/10.1088/0952-4746/26/1/002>

Weiss, H.V., Shipman, W.H., 1957. Separation of Strontium from Calcium with Potassium Rhodizonate...Application to Radiochemistry. *Analytical Chemistry* 29, 1764–1766. <https://doi.org/10.1021/ac60132a027>

Wellman, D.M., Mattigod, S.V., Arey, B.W., Wood, M.I., Forrester, S.W., 2007. Experimental limitations regarding the formation and characterization of uranium-mineral phases in concrete waste forms. *Cement and Concrete Research* 37, 151–160. <https://doi.org/10.1016/j.cemconres.2006.11.004>

Wheatley, S., Sovacool, B., Sornette, D., 2017. Of Disasters and Dragon Kings: A Statistical Analysis of Nuclear Power Incidents and Accidents: Statistical Analysis of Nuclear Power Incidents and Accidents. *Risk Analysis* 37, 99–115. <https://doi.org/10.1111/risa.12587>

Wheaton, R.M., Harrington, D.F., 1953. Process for making anionexchange resins. US2642417A.

Wickleder, M.S., Fourest, B., Dorhout, P.K., 2006. Thorium, in: Morss, L.R., Edelstein, N.M., Fuger, J. (Eds.), *The Chemistry of the Actinide and Transactinide Elements*. Springer Netherlands, Dordrecht, pp. 52–160. https://doi.org/10.1007/1-4020-3598-5_3

Yalkowsky, S.H., Dannenfelser, R.M., 1992. Aquasol database of aqueous solubility. College of Pharmacy, University of Arizona, Tucson, AZ 189.

Yalkowsky, S.H., He, Y., Jain, P., 2019. *Handbook of Aqueous Solubility Data*. CRC Press, Place of publication not identified.

Yang, Y., Song, L., Luo, M., Dai, X., Guo, X., 2017. A rapid method for determining 90Sr in leaching solution from cement solidification of low and intermediate level radioactive wastes. *Journal of Radioanalytical and Nuclear Chemistry* 314, 477–482. <https://doi.org/10.1007/s10967-017-5380-1>

Zack, T., Hogmalm, K.J., 2016. Laser ablation Rb/Sr dating by online chemical separation of Rb and Sr in an oxygen-filled reaction cell. *Chemical Geology* 437, 120–133. <https://doi.org/10.1016/j.chemgeo.2016.05.027>

Zapata-García, D., Wershofen, H., 2017. Development of radiochemical analysis strategies for decommissioning activities. *Applied Radiation and Isotopes* 126, 204–207. <https://doi.org/10.1016/j.apradiso.2017.02.038>

Zhang, A., Wang, W., Chai, Z., Kumagai, M., 2008. Separation of strontium ions from a simulated highly active liquid waste using a composite of silica-crown ether in a polymer. *J. Sep. Sci.* 31, 3148–3155. <https://doi.org/10.1002/jssc.200800358>

Zhang, K., Hutson, C., Knighton, J., Herrmann, G., Scott, T., 2020. Radiation Tolerance Testing Methodology of Robotic Manipulator Prior to Nuclear Waste Handling. *Front. Robot. AI* 7, 6. <https://doi.org/10.3389/frobt.2020.00006>

Zheng, J., Yamada, M., 2006. Inductively coupled plasma-sector field mass spectrometry with a high-efficiency sample introduction system for the determination of Pu isotopes in settling particles at femtogram levels. *Talanta* 69, 1246–1253. <https://doi.org/10.1016/j.talanta.2005.12.047>